

# Vapour-solid interactions for SMSB and asymmetric amplification of pyrimidine and pyridine aldehydes

Dissertation for the degree of *Philosophiae Doctor*

**Giuseppe Rotunno**



Department of Chemistry  
Faculty of Mathematics and Natural Sciences  
University of Oslo

2022

© **Giuseppe Rotunno, 2022**

*Series of dissertations submitted to the  
Faculty of Mathematics and Natural Sciences, University of Oslo  
No. 2553*

ISSN 1501-7710

All rights reserved. No part of this publication may be  
reproduced or transmitted, in any form or by any means, without permission.

Print production: Graphics Center, University of Oslo.

*L'asimmetria è il profumo della vita!*

*Asymmetry is the scent of life!*

*(Emer. Prof. Saverio Florio – Department of Pharmacy – University of Bari, Italy)*





# Acknowledgements

---

The work presented in this thesis has been carried out at the Department of Chemistry, University of Oslo in the period 2016 – 2020. The Research Council of Norway is acknowledged for the financial support during this period.

I would like to thank my supervisor, Prof. Dr. Mohamed Amedjkouh, for providing me with the opportunity to participate on his scientific work both during my Master Thesis and my PhD research, for his excellent guidance and support through the years and for always placing his trust on me. Under your supervision I had the chance to present my scientific work in different conferences around the world and to meet in person Prof. Kenso Soai, moments I will always keep with me. I will never forget as well the never-ending discussions on any possible topic of the human knowledge, the mandarins on your desk and your fine taste in whiskeys.

I would like to extend my thanks to all the members of the CONFINE project for the great collaboration that was established between members with such different backgrounds.

A big thanks goes to all the Catalysis group members that have collaborated with me during my researches: Dr. Gurpreet Kaur for providing the MOF materials employed in my experiments and proofreading a part of this thesis; Dr. Andrea Lazzarini for the IR analyses; Dr. Carlo Buono for DFT calculations; Dr. Georgios Kalantzopoulos and Dr. Sigurd Øien-Ødegaard for introducing me in the world of XRD analyses; Dr. David Wragg for SC-XRD analyses; Dirk Petersen and Dr. Frode Rise for providing the NMR service and Osamu Sekiguchi for the MS service. A special thank goes to Elijah Jeremiah Aller for the design of the glass supports that have played a central part in my researches.

Furthermore, I am also very grateful to all the members of the Homogenous Catalysis group I have shared my research years with, and especially to Carlo Romagnoli and Matias Funes-Maldonado for introducing me in the world of the Soai reaction, and Isabelle Gerz and Jakob Wåhlander who managed the proofreading of this thesis.

I extend my thanks to all my friends in Oslo for making my stay in Norway such a memorable one and making me feel at home. Gurpreet, Andrea, Cristiano, Mariella, Carlo, Irene, Alessia, Giulia, Enrico, Martin, Eikik, Jakob, Alessandra, Maddie, S'ama, Olesia, Vladimir, Javier, Sebastiano, Jeroen, Karolina (I will definitely forget someone, please forgive me) thanks for all the drinks/lunches/dinners/trips/hikes/saunas and many more things we have done together!

A special thanks to my family for their continuous support, motivation and having taught me to never settle, and to Irena for the two beautiful years we have spent together.

A final thank goes to Carmine because I cannot get rid of him even in Norway.

Giuseppe

Oslo, September 2022

# List of publications

---

**Paper I:** *Symmetry Breaking and Autocatalytic Amplification in Soai Reaction Confined within UiO-MOFs under Heterogeneous Conditions.* Giuseppe Rotunno, Gurpreet Kaur, Dr. Andrea Lazzarini, Dr. Carlo Buono, Prof. Dr. Mohamed Amedjkouh. *Chem Asian J.* **2021**, 16, 2361–2369

DOI: [doi.org/10.1002/asia.202100419](https://doi.org/10.1002/asia.202100419)

**Paper II:** *Absolute Autocatalytic Amplification under Heterogeneous Phase Conditions Involving Subsequent Hydride Transfer and a Hemiacetal Intermediate.* Giuseppe Rotunno, Dirk Petersen, Prof. Dr. Mohamed Amedjkouh, *ChemSystemsChem* **2020**, 2, e1900060,

DOI: <https://doi.org/10.1002/syst.201900060>

**Manuscript:** *Validation of a hemiacetal intermediate during absolute Soai autocatalytic amplification under heterogenous phase.* Giuseppe Rotunno, Prof. Dr. Mohamed Amedjkouh

<https://chemrxiv.org/engage/chemrxiv/article/details/6103ea4e8f6bf6461771f4ea>



# Abstract

---

In the last 25 years, the addition of diisopropylzinc to pyrimidine carbaldehydes, known nowadays as the Soai reaction, has drawn the attention of many research groups, not only as it is to date the only chemical reaction offering the chance to study the phenomenon of asymmetric autocatalysis in conjunction with high amplification of enantiomeric excess, but also for the remarkable property to give rise to high ee% even under absolute conditions. Absolute asymmetric synthesis produces chiral molecules in absence of any chiral polarization and is often speculated as possible explanation for the origin of homochirality.

This thesis work deepens the knowledge of the Soai reaction performed under absolute conditions and under the less explored heterogeneous vapour-solid reaction conditions. In order to gain information on the long-specified Soai reaction mechanism, the reactions were performed on both pristine materials and on Soai reagent encapsulated in UiO Metal-Organic Frameworks (MOFs).

In **Chapter 2**, a procedure to introduce the Soai reagents inside the pores of the UiO MOFs is presented. A variety of techniques (DFT calculations, NMR, HPLC and IR analyses) are used to predict the position of the aldehyde in the framework and understand how the amount of allocated aldehyde is influenced varying the pore size of the crystalline material.

Subsequent reaction of encapsulated Soai aldehyde with  $\text{Zn}(\text{i-Pr})_2$  vapours and the absolute asymmetric synthesis of the corresponding alkanol are reported in **Chapter 3**. Despite the confinement, the Soai reaction exhibits significant activity and autocatalytic amplification. Comparative catalytic studies with various UiO-MOFs indicate different outcomes in terms of enantiomeric excess, reaction rate and conversion. The work performed in these two chapters is also reported in **Paper I**.

In addition, when reaction was performed on pristine Soai aldehyde, in a parallel amplification process, some unreported side products were observed, in particular a chiral ester. This observation provides evidence for some recent debated transient intermediates,

and opens new perspectives in the elucidation of the mechanism of amplification of chirality in the Soai reaction. This section of the Chapter is reported in the **Manuscript**.

The same reaction approach of Chapter 3 has been performed in **Chapter 4** on pyridine aldehydes. The reaction of  $\text{Zn}(\text{i-Pr})_2$  vapours on a solid pyridine substrate induced autocatalytic amplification of chirality providing the alkanol product with an enantiopurity up to 90% ee, an unreported result for this class of compounds. Also in this study, side products similar to the ones reported for pyrimidine aldehydes were identified. In both reactions, their formation was traced back to redox pathways involving hydride transfer and a disproportionation following a Claisen-Tishchenko mechanism. The work performed in this chapters is also reported in **Paper II**.

Finally, conclusions and possible future works to be performed starting from the final outcomes of this Thesis work are reported in **Chapter 5**.

# Table of contents

---

<b>Acknowledgements</b> .....	<b>iv</b>
<b>List of publications</b> .....	<b>vi</b>
<b>Abstract</b> .....	<b>vii</b>
<b>Graphical abstract</b> .....	<b>xii</b>
<b>Abbreviations and units</b> .....	<b>xiv</b>

<b>Introduction</b> .....	<b>- 1 -</b>
1.1 The Soai reaction .....	- 1 -
1.1.1 Chirality.....	- 1 -
1.1.2 Chemical properties of enantiomers and their importance in biology .....	- 2 -
1.1.3 Asymmetric catalysis .....	- 3 -
1.1.4 Asymmetric autocatalysis.....	- 4 -
1.1.5 Asymmetric autocatalysis with amplification of ee: the Soai Reaction .....	- 6 -
1.1.6 The Frank model.....	- 8 -
1.1.7 Nonlinear effects .....	- 9 -
1.1.7.1 The Kagan model .....	- 10 -
1.1.7.2 The Noyori model.....	- 12 -
1.1.8 The mechanism of the Soai reaction .....	- 14 -
1.1.8.1 The Blackmond/Brown model: equimolar substrate concentration .....	- 14 -
1.1.8.2 The Blackmond/Brown model: non-equimolar substrate concentrations .....	- 16 -
1.1.8.3 Identification of solution species .....	- 17 -
1.1.8.4 Identification of crystal structures .....	- 19 -
1.1.8.5 Hemiacetal intermediates in the Soai reaction.....	- 21 -
1.1.9 Synthetic applications of the Soai reaction .....	- 24 -
1.2 Absolute Asymmetric Synthesis .....	- 26 -
1.2.1 Absolute Asymmetric Synthesis with Circularly Polarized Light .....	- 27 -
1.2.2 Amplification of Homochirality by Autocatalytic Crystallization.....	- 31 -
1.2.3 Absolute Asymmetric Synthesis via Enantiomorphous Crystals .....	- 36 -
1.2.4 Amplification of Asymmetry by Chirally Autocatalytic Systems.....	- 36 -
1.3 Metal-Organic Frameworks.....	- 39 -
1.3.1 Historical background.....	- 39 -

1.3.2 UiO-type MOFs .....	- 41 -
1.3.3 MOFs as molecular sponges .....	- 43 -
<b>Inclusion of Soai aldehyde in UiO-MOFs .....</b>	<b>- 47 -</b>
2.1 Introduction.....	- 47 -
2.2 Preliminary DFT analysis.....	- 47 -
2.3 The inclusion method .....	- 1 -
2.4 Infrared Spectroscopy analysis on the materials .....	- 3 -
2.5 Quantification of the Soai aldehyde in the materials.....	- 6 -
2.6 Conclusions.....	- 9 -
<b>The use of UiO-MOFs for vapour phase Soai reactions .....</b>	<b>- 10 -</b>
3.1 Introduction.....	- 10 -
3.2 Reaction setup and concept of reactivity .....	- 10 -
3.3 Preliminary results and screening of different UiO MOFs .....	- 13 -
3.4 Kinetic plots of the vapour phase reactions.....	- 16 -
3.5 Attempts to optimize the reaction parameters .....	- 19 -
3.6 Analyses on the materials .....	- 22 -
3.7 Focus on the vapour phase reaction on pristine Soai aldehyde .....	- 27 -
3.8 Conclusions.....	- 33 -
<b>Vapour-solid interactions for SMSB and asymmetric amplification of pyridine aldehydes.....</b>	<b>- 34 -</b>
4.1 Introduction.....	- 34 -
4.2 Analyses on the reaction crude .....	- 37 -
4.3 Kinetic analyses on the vapour phase reaction at different temperatures .....	- 39 -
4.4 Analyses varying the equivalents of Zn( <i>i</i> Pr) <sub>2</sub> .....	- 42 -
4.5 Proposed mechanism for the vapour phase reaction .....	- 45 -
4.6 Preliminary experiments to validate the proposed reaction mechanism.....	- 48 -
4.7 Influence of chiral triggers on the vapour phase reaction .....	- 51 -
4.8 Screening of other zincorganil reagents and pyridine aldehydes .....	- 52 -
4.9 A possible explanation for the amplification of <i>ee</i> in the vapour phase reaction .....	- 53 -
4.10 Conclusions.....	- 55 -

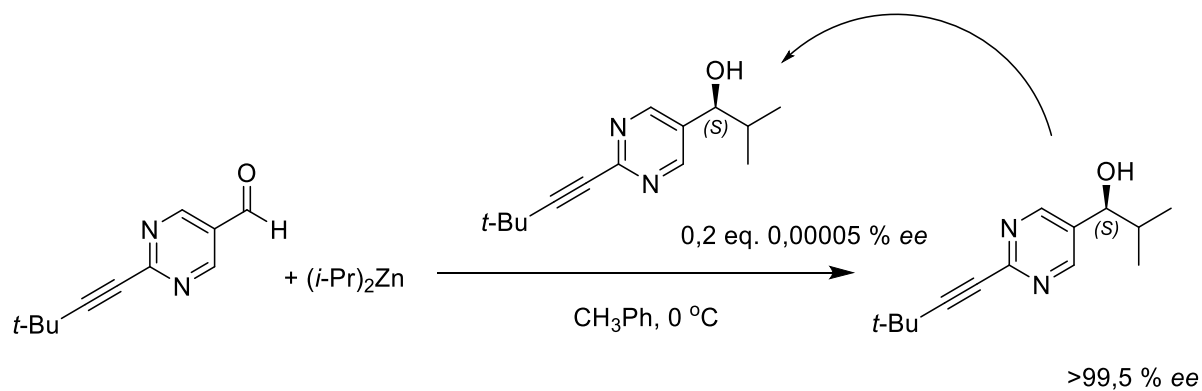


<b>Conclusions and future prospects .....</b>	<b>56</b>
5.1 Different MOFs for Soai aldehyde inclusion.....	56
5.2 Different reaction setups .....	57
5.3 Different material analyses .....	57
5.4 Different experiments to validate the reaction mechanism .....	57
5.5 Different reaction substrates .....	58
<b>Paper I .....</b>	<b>59</b>
<b>Paper II .....</b>	<b>- 119 -</b>
<b>Manuscript.....</b>	<b>- 125 -</b>
<b>Appendix I.....</b>	<b>- 136 -</b>
<b>Appendix II.....</b>	<b>- 142 -</b>
<b>Appendix III.....</b>	<b>- 147 -</b>
<b>Appendix IV .....</b>	<b>- 143 -</b>

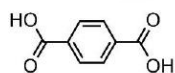
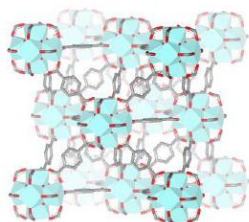


# Graphical abstract

## Chapter 1 Introduction

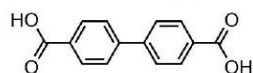
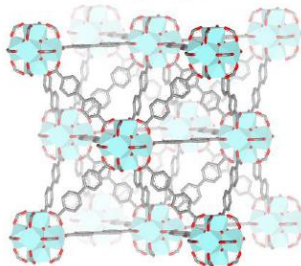


**UiO-66**



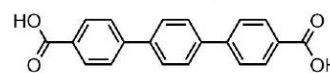
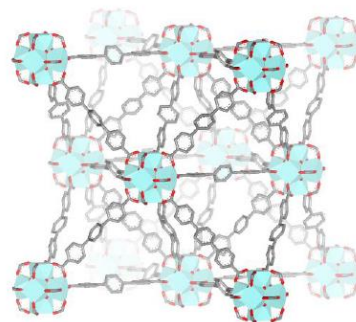
H<sub>2</sub>bdc

**UiO-67**



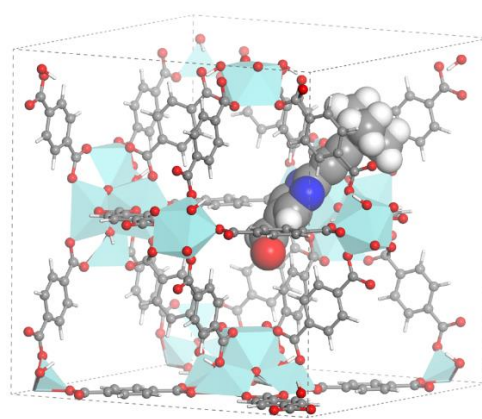
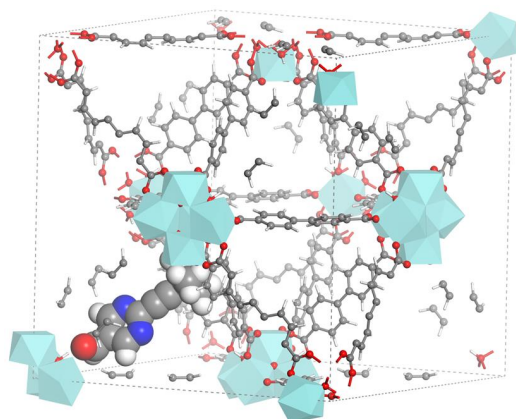
H<sub>2</sub>bpdc

**UiO-68**

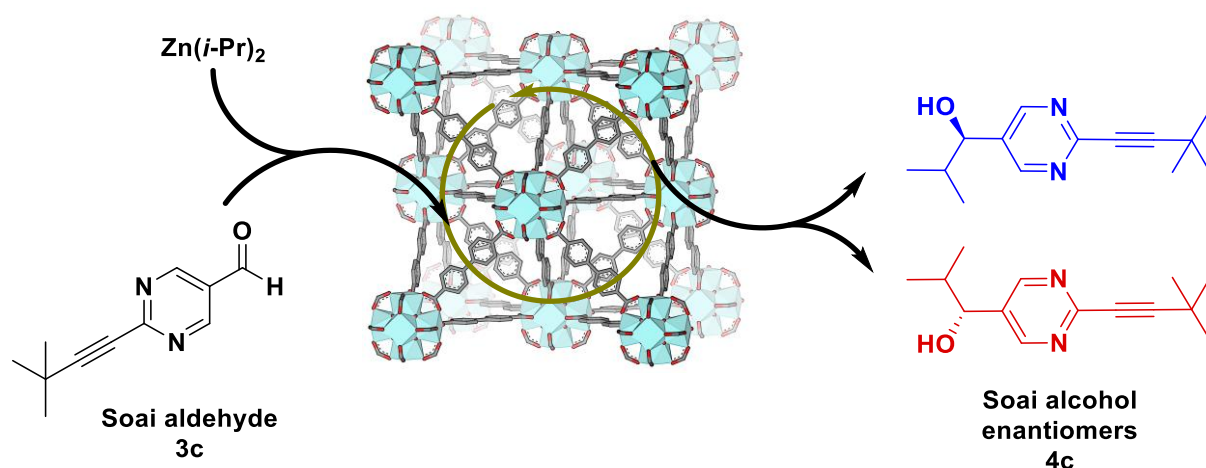


H<sub>2</sub>tpdc

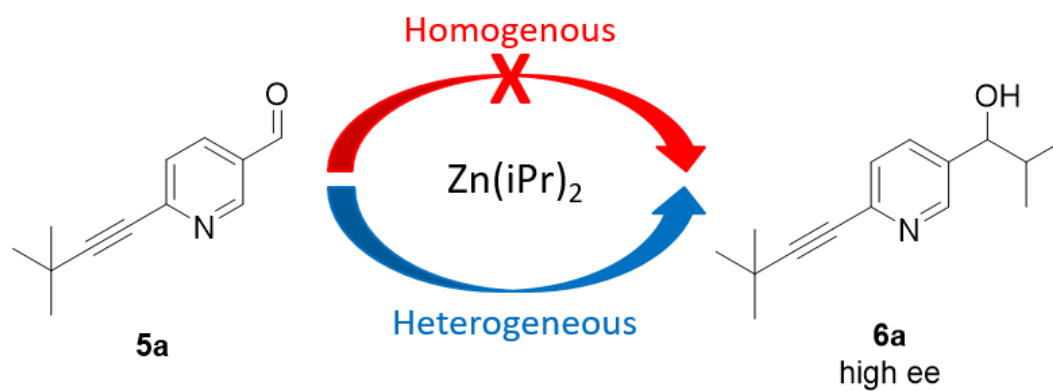
## Chapter 2 Inclusion of the Soai aldehyde in the UiO-MOFs



### Chapter 3 The use of UiO-MOFs for vapour phase Soai reactions



### Chapter 4 Vapour-solid interactions for SMSB and asymmetric amplification of pyridine aldehydes



# Abbreviations and units

---

AAS	absolute asymmetric synthesis
Ar	aryl
ATR-IR	Infrared Spectroscopy by Attenuated Total Reflectance
bpy	bipyridine
ca.	circa
calcd.	calculated
conc.	Concentration
CT	Claisen-Tishchenko disproportionation
$\delta$	delta, ppm (chemical shift)
d	doublet (NMR)
dd	doublet of doublets (NMR)
DFT	density functional theory
DMSO	dimethylsulfoxide
<i>ee</i>	enantiomeric excess
<i>ent</i>	enantiopure
Eq.	equation
equiv.	equivalents
ESI	electrospray (MS)
Et	ethyl
<i>et al.</i>	<i>et alii</i>
EtOAc	ethyl acetate
g	gram
$^1\text{H}$	proton
H <sub>2</sub> bdc	terephthalic acid
H <sub>2</sub> bpdc	biphenyl-4,4'-dicarboxylic acid
HPLC	high-pressure liquid chromatography
HRMS	high resolution mass spectroscopy
Hz	hertz

<i>i</i> Pr	isopropyl
IR	infrared spectroscopy
J	coupling constant
m	multiplet
m/z	mass per charge (MS)
Me	methyl
mg	milligram
MHz	mega Hertz
min	minute
mL	milliliter
mmol	millimole
MOF	Metal-Organic Framework
MPV	Meerwein–Ponndorf–Verley rearrangement
MS	mass spectroscopy
NLE	non linear effect
NMR	nuclear magnetic resonance
Ph	phenyl
Pr	propyl
ppm	part per million
PXRD	powder X-ray diffraction
q	quartet
<i>R</i>	rectus
Rac.	racemic
r.t.	room temperature
s	singlet
<i>S</i>	sinister
SBU	secondary building unit
SMS	square-macrocycle-square
SMSB	spontaneous mirror symmetry breaking
t	triplet
<i>t</i> -Bu	<i>tert</i> -butyl
THF	tetrahydrofuran

TMS	trimethylsilyl
XRD	X-Ray Diffraction
Zn( <i>i</i> Pr) <sub>2</sub>	diisopropylzinc
Å	angstrom





# Introduction

---

## 1.1 The Soai reaction

This section will introduce the Soai reaction, the first and only example to date of an asymmetric autocatalysis combined with amplification of the enantiomeric excess (*ee*) of the product <sup>[1]</sup>. It will briefly review the key experiments that led to the discovery of the reaction, its most important features and the relevant studies on its reaction mechanism.

### 1.1.1 Chirality

Chirality is the property of any object which is non-superimposable with its mirror image. This concept can be commonly found in our everyday life, for example considering our hands: the left one is the mirror image of the right one, but it is impossible to superimpose one on the other; thus, they are chiral. This example can seem trivial, but the word *chiral* itself comes from χειρ (kheir), the ancient Greek word for “hand”. Conversely, if an object is superimposable with its mirror image, it is called *achiral* <sup>[2]</sup>.

In chemistry, a molecule must possess a *stereogenic unit* to be chiral. The most common case is the presence of a *chiral centre*, an atom (in most of the cases a carbon) with four different substituents attached. The atom is then termed an *asymmetric atom*.

The most common way to describe a chiral centre is represented by the Cahn-Ingold-Prelog priority rules [3]. The atoms directly bonded to the asymmetric atom are numbered in order of decreasing atomic weight. After the assignment the molecule is rotated in order to have the lowest ranked ligand pointing away from the observer. If the priority of the other three ligands decreases clockwise, the chiral centre has an *R* configuration; if the decreasing is anticlockwise, the centre will have an *S* configuration. (Figure 1.1).

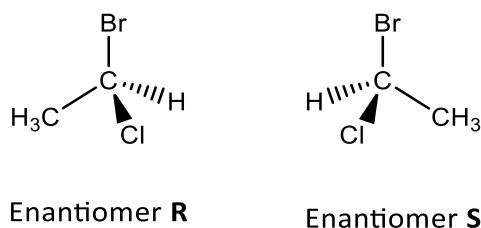


**Figure 1.1** In the *R* enantiomer going from Br to Cl to CH<sub>3</sub> implies a rotatory movement, whereas in the *S* enantiomer the movement is antirotatory.

Two molecules that share the same structure and connectivity and are non-superimposable are called *enantiomers*. If the enantiomers are present in equal amount, the resulting mixture is called *racemate*. If one of the enantiomers is present in a larger amount compared to its mirror image, it is possible to define an *enantiomeric excess* (*ee*). It is defined as the difference in mole fraction between the two enantiomers.

### 1.1.2 Chemical properties of enantiomers and their importance in biology

The enantiomers of a molecule share the same chemical and physical properties in an achiral environment, i.e. solubility, boiling point, melting point will be the same. Conversely, in presence of a chiral environment, the two enantiomers can behave differently.

Every biological system is a chiral environment: proteins are formed by 20 aminoacids, 19 of which are chiral, and nucleic acids contain chiral carbohydrates. Therefore, the interactions of a pair of enantiomers can lead to different responses in our body. These responses can imply a difference in the way we feel the taste or smell of the compounds, i.e. (*R*)- and (*S*)-limonene (orange/lemon smell) [4], (*L*)- and (*D*)-aspartame (sweet taste/tasteless) [5]. In other cases, especially with racemic drugs, the differences in behaviour can have severe consequences. The ADME profiles of the enantiomers can vary drastically as well as the pharmacodynamics and toxicity. For instance, L-penicillamine is used for the treatment of rheumatoid arthritis,

while D-penicillamine is toxic. In 1992 the Food and Drug Administration (FDA) stated that each enantiomer of a racemic mixture had to be fully characterized in its pharmacokinetic and pharmacodynamic properties to be approved, and this policy statement encouraged the pharmaceutical companies to move from the development of drugs as racemates to single-enantiomers [6].

### 1.1.3 Asymmetric catalysis

The most classic synthetic procedure to obtain a single enantiomer is by separation from a racemic mixture. Nevertheless these procedures are time-consuming and expensive. In the last decades, several research groups have explored new strategies to obtain a single enantiomer through organic synthesis. One of the most useful procedures involve a *chiral pool*. In this method the synthesis of a complex molecule starts from a simpler and cheap chiral compound available in nature (i.e. aminoacids, alkaloids, sugars) with the desired chirality. In other cases the cheap chiral molecule is not used as a building block. A *chiral auxiliary* can only be temporarily incorporated in a synthetic intermediate to control the stereochemistry in subsequent reaction steps, and finally be removed and recovered [7].

*Asymmetric catalysis*, schematized in Figure 1.2, differs from the aforementioned methods because it involves the use of a chiral *catalyst*. A catalyst is a substance which can increase the rate of the reaction without modifying the overall standard Gibbs energy. It interacts with the substrate, creates a new reaction pathway compared to the non-catalysed reaction and lowers the activation barrier of the rate determining step. As already stated, the enantiomers behave differently in a chiral environment, and the addition of a chiral catalyst may lower the activation energy stereospecifically, leading to the preferential synthesis of one enantiomer over the other.

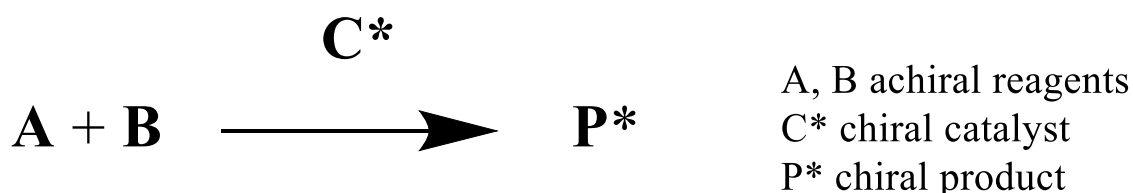


**Figure 1.2** The concept of asymmetric catalysis.

### 1.1.4 Asymmetric autocatalysis

*Autocatalysis* is a process in which the product acts as a catalyst for its own production. If the product is chiral, in certain cases it may act as a chiral catalyst [8]. (Figure 1.3). The process has some advantages over usual asymmetric catalysis. Atom-economy is an important feature, and there are no issues connected to the deterioration of the catalyst or its separation from the product after reaction.

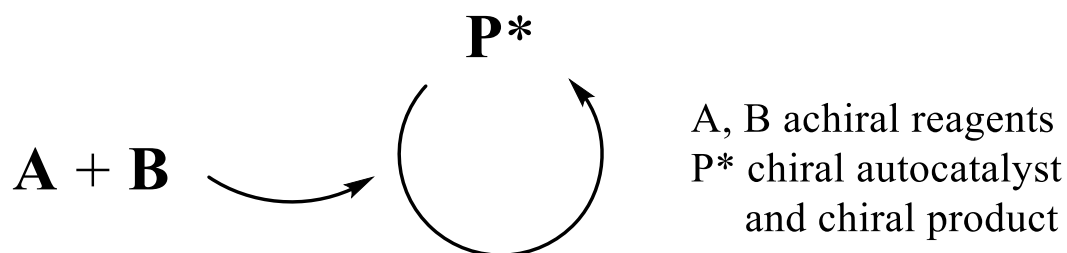


**Figure 1.3** The concept of asymmetric autocatalysis.

The reaction profiles of autocatalytic processes are complex, because the concentration of the catalyst is not constant and increases through time. An autocatalysis can be demonstrated kinetically considering two features: a sigmoidal (exponential in cases of high efficiency, parabolic in case of limited efficiency) product/time curve and a linear correlation between initial product concentration and reaction rate (Figure 1.4).

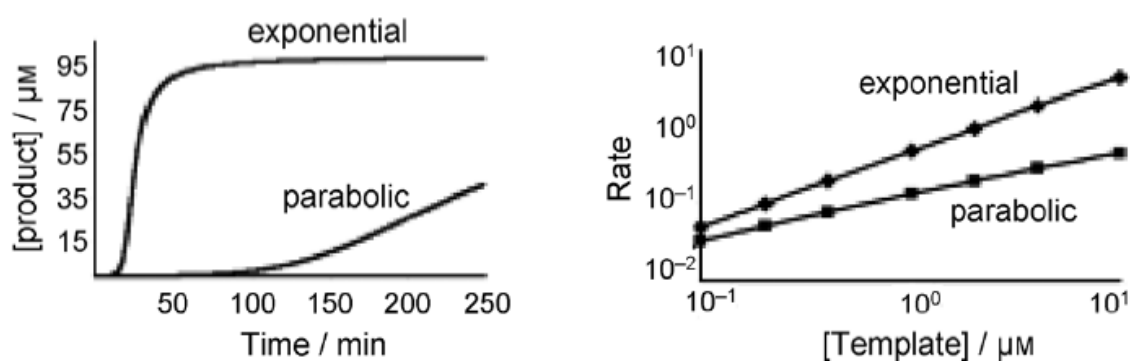


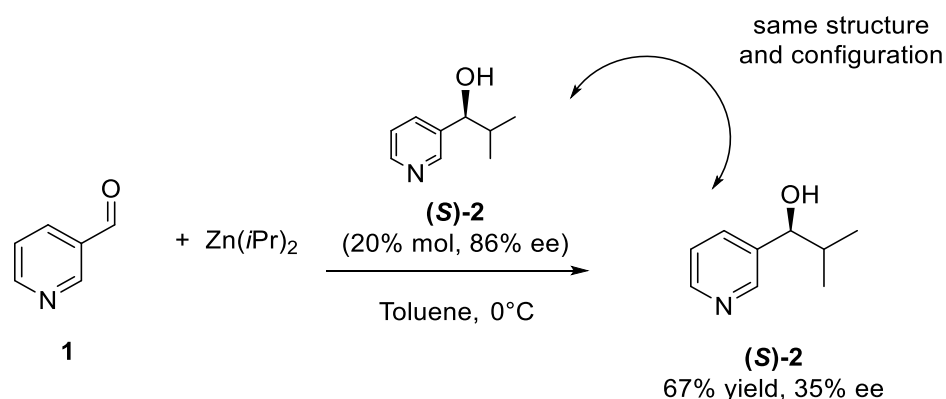
**Figure 1.4** Kinetic features of an autocatalytic reaction [8].

Autocatalytic reactions have been studied for over a century [9]. Autocatalysis has been observed in crystals growth [10], peptide chemistry [11], decomposition processes [12], and the most famous chemical reaction is probably the formose reaction [13], in which formaldehyde

condensates unselectively to form mixtures of various sugars which differ in carbon atoms and stereochemistry. All these process work with different mechanisms.

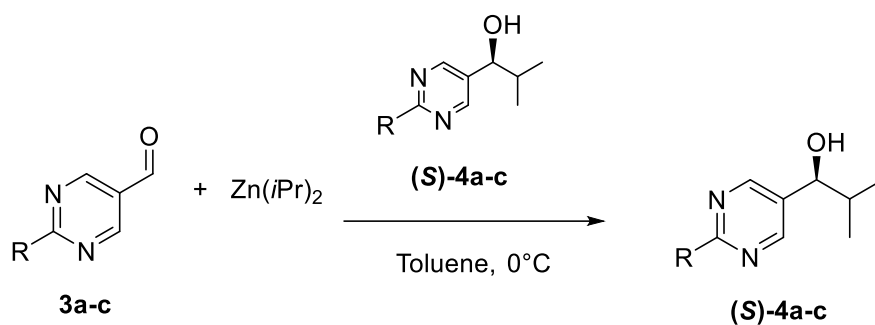
While asymmetric autocatalysis was well known in crystals (Section 1.2.2), the first example in organic chemistry was only reported in 1990.

Since the early 80's the research groups of Mukaiyama, Oguni, Noyori and Soai had explored the synthetic strategy of aminoalcohol catalysts for the enantioselective alkylation of aromatic aldehydes in presence of organozinc compounds <sup>[14]</sup>. Modifying the structure of the starting material, in order to form a product which incorporated an aminoalcohol moiety as well, seemed an interesting approach to perform an autocatalytic reaction. Indeed Soai showed that the addition of diisopropylzinc to pyridine-3-carbaldehyde **1** could behave autocatalytically <sup>[15]</sup> (Scheme 1.1). (*S*)-pyridyl alcohol **2** with 86% *ee* was used as a 20% chiral autocatalyst for the enantioselective alkylation of **1**. The product was obtained in 67% yield and 35% *ee*. Despite the erosion of *ee*, the predominant configuration of the product was the same as that of the catalyst.



**Scheme 1.1** Asymmetric autocatalytic isopropylation of 3-pyridine aldehyde.

After this first seminal discovery, other molecular scaffolds were shown to be substrates for asymmetric autocatalysis <sup>[16]</sup> under the same reaction conditions and among them 5-pyrimidine aldehydes were able to give higher enantioselective autocatalysis compared to the other substrates <sup>[17]</sup>. (Scheme 1.2)



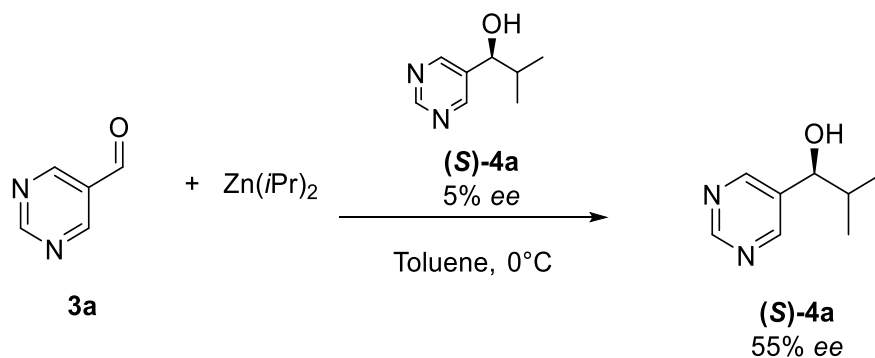
R	Initial ee	Final ee
a: H	93%	90%
b: Me	>99,5	98,2%
c: <i>t</i> Bu-C≡C	>99,5	>99,5

**Scheme 1.2** Asymmetric autocatalytic isopropylation of 5-pyrimidine aldehydes.

The substituent at the 2-position seemed to play an important role for the efficiency of the asymmetric autocatalysis and to prevent the erosion of the final *ee*. In particular, **(S)-4c** was found to be a perfect autocatalyst <sup>[17b]</sup>. Recycling the alcohol formed from a reaction as catalyst for a subsequent reaction, no decrease of *ee* was found even after 10 cycles.

### 1.1.5 Asymmetric autocatalysis with amplification of ee: the Soai Reaction

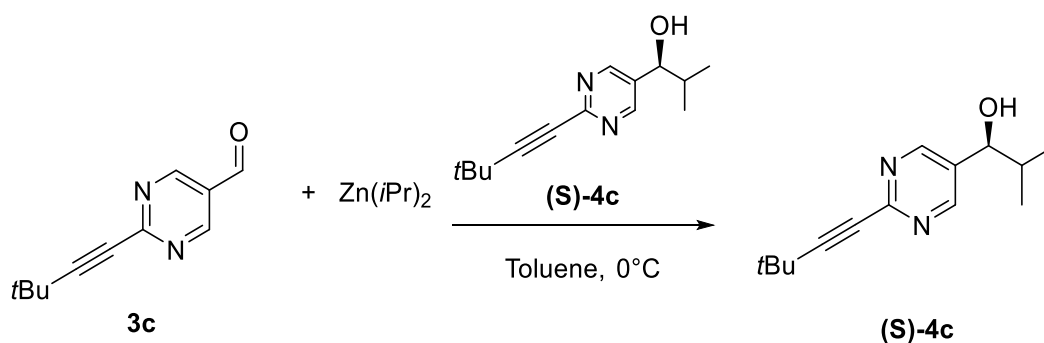
In the reactions showed in the previous section, the final *ee* of the product was always found lower or comparable to the *ee* of the chiral autocatalyst. In 1995, Soai found that in the addition of diisopropylzinc to 5-pyrimidine aldehydes asymmetric autocatalysis could be coupled with an improvement of the *ee* of the product. This phenomenon is defined as *asymmetric amplification* or *positive non-linear effect* ((+)-NLE, see Section 1.6 for more details). This reaction has since then been defined "the Soai Reaction" (Scheme 1.3) <sup>[1]</sup>.



**Scheme 1.3** Asymmetric autocatalysis with amplification of *ee*.

Soai also demonstrated that the product of one reaction could be recycled as catalyst for a subsequent reaction: starting from **(S)-4a** with 2% *ee*, through four reaction cycles the product enantioenriched to 88% *ee*.

In the same way as for the asymmetric autocatalysis, the substituent on the 2-position of the pyrimidine ring was crucial for the rate of amplification: alkyl <sup>[18]</sup> and, to a greater extent, alkynyl substituents were found to be better substrates for the reaction. A stunning amplification was reported using **4c** as substrate: in three consecutive reaction cycles the product amplified from 0,00005% *ee* to >99,5% *ee*. The (*S*)-enantiomer multiplied throughout the 3 cycles by a factor of 630000 while the (*R*)-enantiomer only by a factor of 950 (Scheme 1.4) <sup>[19]</sup>.



Cycles	Initial <i>ee</i>	Final <i>ee</i>	Yield
1	0,00005%	57%	96%
2	57%	99%	96%
3	99%	>99.5%	90%

**Scheme 1.4** Practically perfect asymmetric autocatalysis with amplification of *ee*.

The stunning asymmetric autocatalysis combined with the asymmetric amplification of the Soai reaction has some strict requirements to occur, i.e. the structure of the substrate, the organozinc reagent and the solvent. Only small changes in these parameters are allowed.

#### a) The aldehyde structure

All the substrates of the Soai reaction share a rigid  $\gamma$ -aminoaldehyde scaffold (red line in Figure 1.5). Depending on the substituents, the reaction shows differences in the non-linear effect. As already stated, 2-substituted-pyrimidine-5-carbaldehydes are the best performing

substrates both for the asymmetric autocatalysis and for the asymmetric autocatalysis with amplification of  $ee$  <sup>[20]</sup>. In general, the asymmetric amplification increases with size and rigidity of the R group.

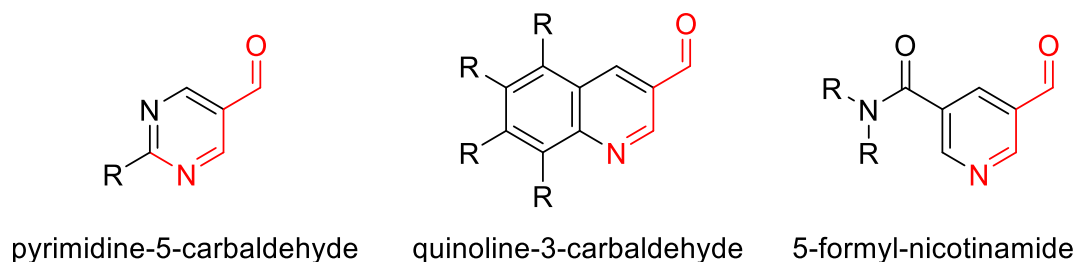


**Figure 1.5** Substrates of the Soai reaction.

#### b) The zincorganil source

Zincorganil compounds are known to produce (+)-NLEs when added to aromatic aldehydes (Section 1.1.6.2). In the case of the Soai reaction  $Zn(iPr)_2$  is the only zincorganil source capable to give rise to the asymmetric amplification. Smaller (Me, Et, Pr) or bulkier (cyclopropyl, tert-butyl and cyclopentyl) <sup>[21]</sup> substituents are not suitable for the reaction.

#### c) The solvent

Toluene is the most used solvent, but benzene, cumene, tert-butylbenzene, methylcyclohexane and diethylether can be employed, by themselves or in mixtures. In contrast, tetrahydrofuran (THF) is not a suitable solvent, showing a (-)-NLE. This effect was attributed to the high coordinative properties of the solvent <sup>[20]</sup>.

### 1.1.6 The Frank model

The Soai reaction is the first experimental demonstration of Frank's model <sup>[22]</sup>. In 1953, Frank proposed a mathematical model for the arising of homochirality. He postulated an autocatalytic reaction in which an achiral substrate forms two different chemical species (i.e. two enantiomers). Each of the enantiomers can catalyse its own formation and at the same time be an anti-catalyst for the opposite enantiomer, a property called *mutual antagonism*. In such system tiny imbalances of  $ee$ , that can arise stochastically or from a variety of physical sources, can be amplified to reach enantiopurity (Figure 1.6). In the closing remark of his article, Frank stated that "*a laboratory demonstration may not be impossible*", indeed realized 40 years later by Soai.



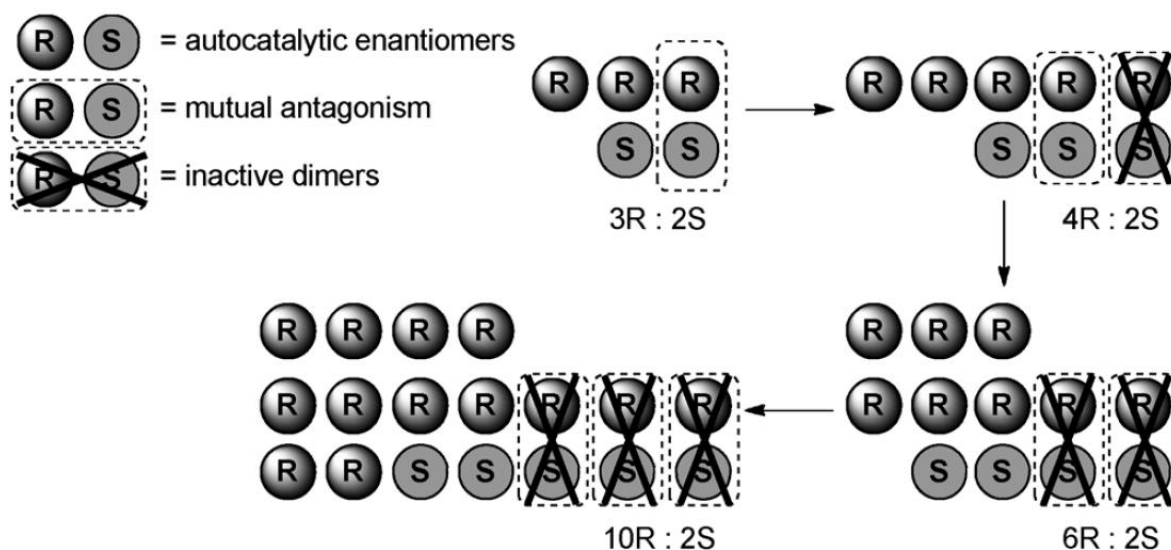


**Figure 1.6** The Frank model <sup>[8]</sup>.

In conventional asymmetric catalysis and asymmetric autocatalysis both enantiomers of the catalyst are active and will reproduce their configuration. However, at the end of the reaction, the *ee* of the product can never go beyond the one of the catalyst. This is mainly due to the fact that the asymmetric induction could not be perfect, or that racemic background reactions can take place. Through consecutive cycles the *ee* will constantly reduce and in the end a racemic product is the only possible final state. In the Soai reaction instead, one enantiomer is not only a catalyst for itself but serves also as an anti-catalyst for the opposite enantiomer. Even when recycling the catalyst, a near-racemic species can be amplified almost to enantiopurity.

### 1.1.7 Nonlinear effects

For years it was thought that only a linear relationship between the *ee* of the product ( $ee_{prod}$ ) and the *ee* of the chiral auxiliary/catalyst ( $ee_{aux}$ ) was achievable, represented in Eq.1.1 and illustrated in Figure 1.7 line A <sup>[23]</sup>.

$$ee_{prod}(\%) = ee_{max} * ee_{aux} \quad (1.1)$$

( $ee_{max}$  = enantiomeric excess of the product for an enantiopure auxiliary)

In 1986 Kagan reported for the first time a study on deviations from linearity in an organic reaction <sup>[24]</sup>. The study was focused on the Sharpless epoxidation of geraniol with (R,R)-(+)-diethyl tartrate (DET). The *ee* values of the epoxidic product were higher than those calculated for a linear correlation based on the *ee* values of the DET. Such a deviation was called *positive non-linear effect* [(+)-NLE] or *asymmetric amplification* (line B in Figure 1.7). In the same study, the sulphide oxidation by a water-modified Sharpless reagent in presence of (R,R)-(+)-DET resulted in lower *ee* of the product in regard to the linear correlation. The effect was called *negative non-linear effect* [(-)-NLE] or *asymmetric depletion* (line C in Figure 1.7). Generally, Eq.1.1 is not obeyed when autoassociation or formation of multiligand catalysts take place. Since the first report, many examples of non-linear effects have been reported <sup>[25]</sup>. In the next sections two models for (+)-NLE relevant for the discussion of the mechanism of the Soai reaction will be presented.

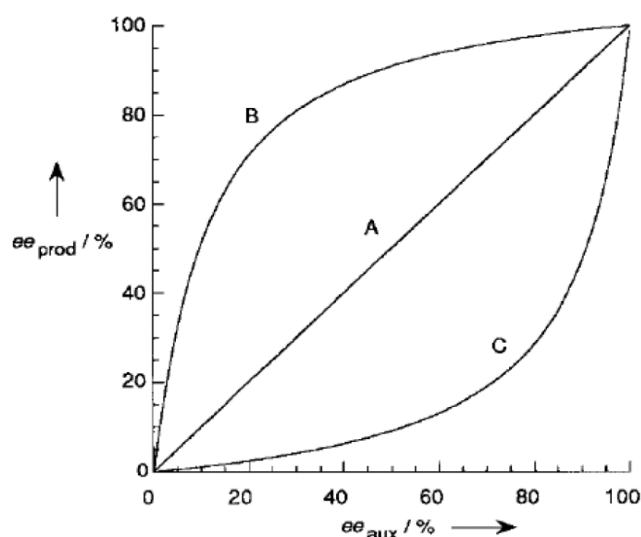
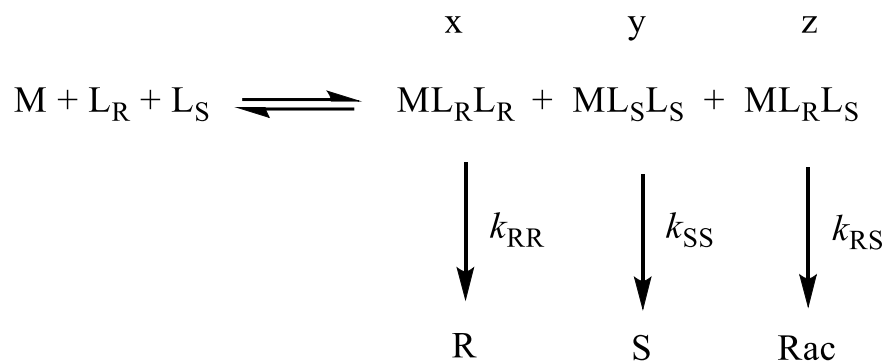


**Figure 1.7** Typical curves for positive (B) and negative (C) non-linear effects.

### 1.1.7.1 The Kagan model

The Kagan model <sup>[26]</sup>, also called  $ML_2$  model, is based on a system in which one metal atom M and two chiral ligands, in particular two enantiomers of a chiral species,  $L_R$  and  $L_S$ , can form three different complexes. The complexes, represented in Scheme 1.5, are two homochiral complex  $ML_RL_R$  and  $ML_SL_S$  and a *meso* heterochiral complex  $ML_RL_S$ . Each homochiral complex can catalyse the formation of its enantiomer, whereas the *meso* complex yields a racemic product. The rates of these reactions are represented by the first order constants  $k_{RR}$ ,  $k_{SS}$  and  $k_{RS}$ , with  $k_{RR} = k_{SS} \neq k_{RS}$ . At equilibrium, the concentration of the three complexes will be

respectively x,y and z. Two important parameters for the characterization of the complexes are their relative reactivity  $g = k_{RS}/k_{RR}$  and their relative concentrations  $\beta = z/(x+y)$ .



**Scheme 1.5** The Kagan model.

Eq.1.1 can be modified adding a correcting factor which accounts for the NLE:

$$ee_{prod} = ee_{max} * ee_{aux} * \frac{1 + \beta}{1 + g\beta} \quad (1.2)$$

When  $g < 1$  the homochiral complexes are more reactive than the *meso* complex, and a (+)-NLE will be detected. When  $g > 1$  the *meso* complex is more reactive, and a (-)-NLE will take place. Finally, if  $\beta = 0$  (no *meso* complexes formed), or  $g = 1$  (same reactivity in homochiral and *meso* complexes) Eq.1.2 reduces to Eq.1.1 and a linear correlation will be detected. In order to calculate  $\beta$ , a new variable is defined.  $K = z^2/xy$  represents the interconversion between homochiral and *meso* dimers.

$$\beta = \frac{-Kee_{aux}^2 + \sqrt{-4Kee_{aux}^2 + K(4 + ee_{aux}^2)}}{4 + Kee_{aux}^2} \quad (1.3)$$

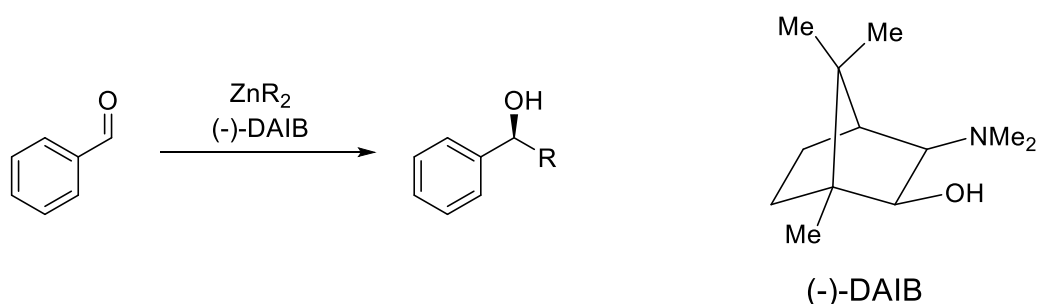
Another concept introduced by Kagan is *the reservoir effect*, which describes the case in which more unreactive complexes are formed, with only one catalytically active. For example, a non-enantiopure ligand can form a catalytically active  $ML_R$  complex and a stable inactive *meso* complex  $ML_RL_S$  at the same time. The *meso* complex will work as a trap for the racemic part of the non-enantiopure ligand, while the free enantio-enriched ligand will take part in the catalytic cycle. This can be represented mathematically defining  $\alpha$  as the part of ligand involved in the inactive complexes, with an enantiomeric excess indicated with  $ee_{res}$ . The term  $ee_{eff}$  will represent the *ee* of the active species involved in the catalytic process:

$$ee_{eff} = \frac{ee_{aux} - \alpha ee_{res}}{1 - \alpha} \quad (1.4)$$

The value of  $ee_{eff}$  can replace  $ee_{aux}$  in Eq.1.1 and fit the experimental data in a more accurate way. A reservoir effect does not exclude that the catalytically active species would follow a  $ML_2$  or any other NLE model, making the models not mutually exclusive.

### 1.1.7.2 The Noyori model

As already stated, after Kagan's report, many more non-linear effects were observed. In particular, a (+)-NLE was reported by Ogumi on the enantioselective addition of organozinc reagents to benzaldehyde using non-enantiopure  $\beta$ -aminoalcohols as catalysts [27]. The reaction was extensively studied and its mechanism rationalized by Noyori [28] (Scheme 1.6).



**Scheme 1.6** Asymmetric alkylation of benzaldehyde catalysed by (-)-DAIB.

As in Kagan's model, in the postulated reaction mechanism three dimers, represented in Figure 1.8, are formed. The two homochiral dimers are less stable than the heterochiral *meso* dimer: the alkyl groups of the organozinc reagent (in these cases two methyl groups) are arranged in a *syn* position, influencing negatively the stability of the complex compared to the *anti* position in the *meso* dimer.

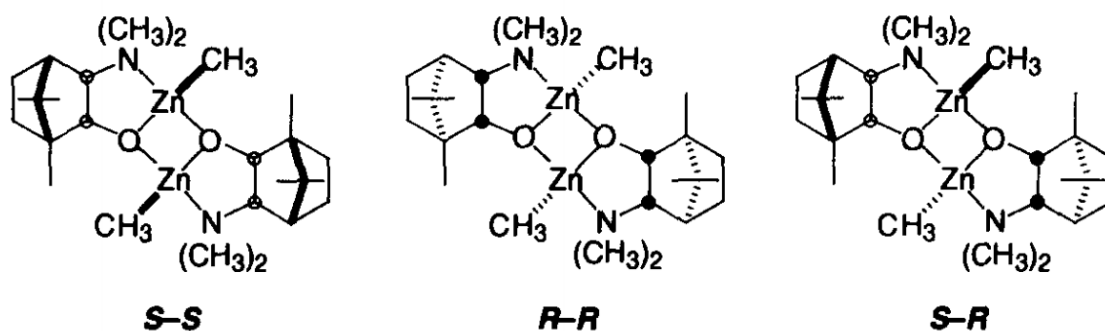
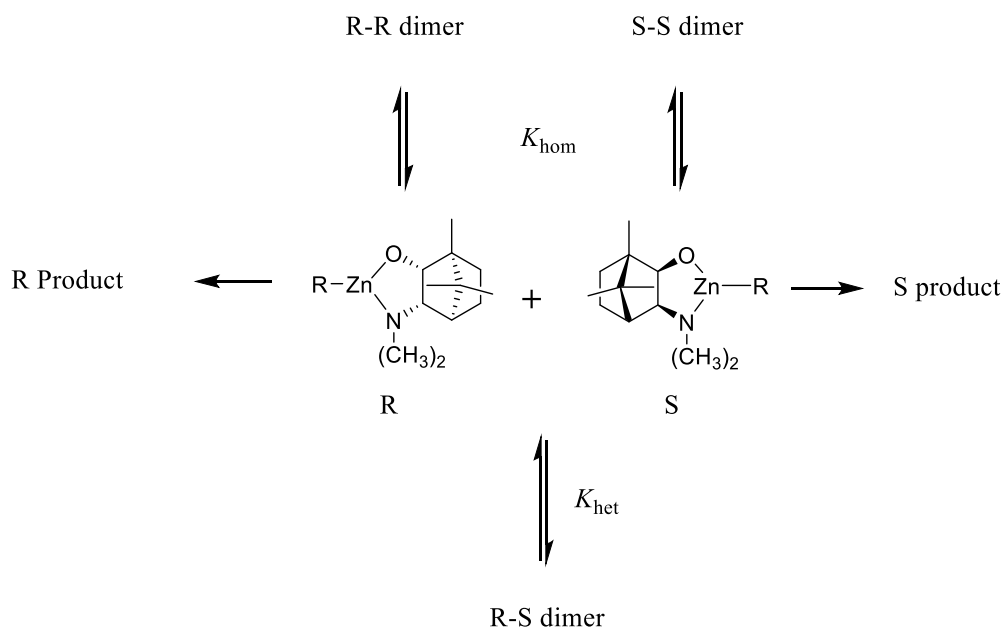


**Figure 1.8** Rationalization of the different stability of the dimers <sup>[27e]</sup>.

In contrast with Kagan's model, even if the catalytic assembly is dimeric in the ground state, the dimers are believed to be inactive, whereas the catalytically active species are monomers of (-)-DAIB and  $ZnR_2$ . The dimers are formed with equilibrium constants  $K_{hom}$  and  $K_{het}$  and the equilibrium between these species was found to be crucial for the (+)-NLE. If  $K_{het} = 2 K_{hom}$  a lineal behaviour would be observed. Nevertheless this would go in contrast with the observation, as already stated, that the homochiral dimers are less stable than the heterochiral,  $K_{het} \gg 2 K_{hom}$ . This implies that most of the minor enantiomer is trapped in the *meso* complex (reservoir effect). The remaining major enantiomer is free to catalyse the reaction and a (+)-NLE is originated (Scheme 1.7).



**Scheme 1.7** The Noyori model <sup>[28e]</sup>.

### 1.1.8 The mechanism of the Soai reaction

Even after almost 30 years, the exact mechanism of the Soai reaction is still under debating. Models have been proposed based on different techniques, such as microcalorimetry, kinetic studies, NMR analysis, X-ray diffraction and DFT calculations.

In this section a summary of the various studies performed and mechanisms proposed will be presented.

#### 1.1.8.1 The Blackmond/Brown model: equimolar substrate concentration

The first proposed reaction mechanism was published by Blackmond and Brown <sup>[29]</sup> in 2001 using reaction calorimetry as experimental technique. This was an ideal methodology for the study of autocatalytic reactions. The concentration of catalyst is directly proportional to the heat generated, and maximises and then decays through reagent depletion. A conventional catalytic reaction would show instead constant heat output or decay over time.

The report monitored the Soai reaction of **3b** using equimolar **3b**/ $\text{Zn}(i\text{Pr})_2$  ratios and 10% mol autocatalyst (**S**)-**4b** with three different *ee*: 97% (enantiopure), 43% and 0% (racemic).

In Figure 1.9a, the heat flow is plotted as a function of time, showing the classic autocatalytic shape. The normalized rate ( $\text{rate}(t)/\text{maximum rate}$ ) vs. fraction conversion is obtained in Figure 1.9b.

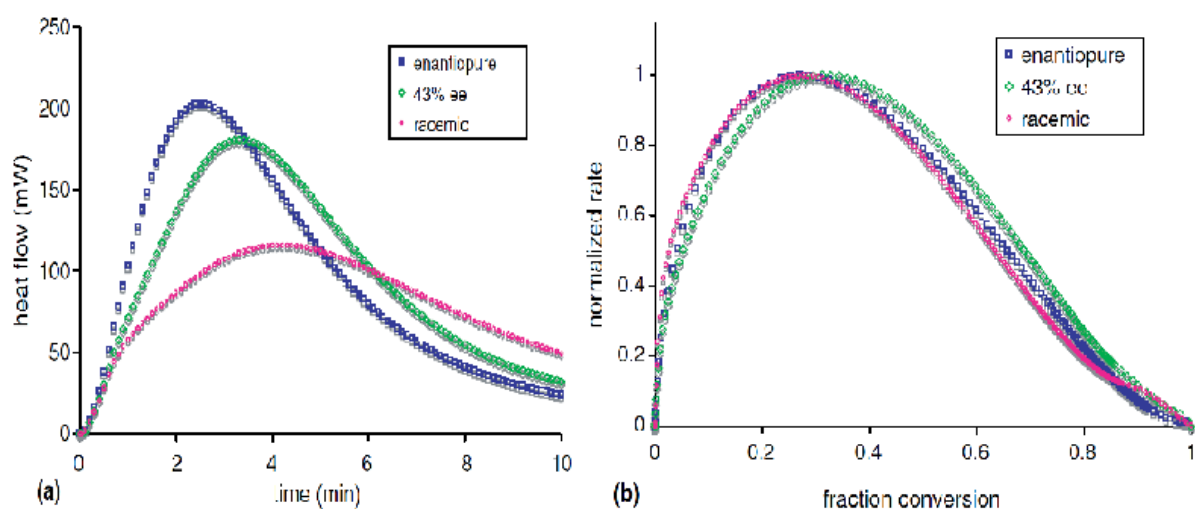


**Figure 1.9** Reaction calorimetry monitoring of the Soai reaction <sup>[30]</sup>.

The Noyori model was firstly considered as possible mechanism for the reaction. Figure 1.9b demonstrates how the data for enantiopure and racemic catalyst are superimposable, implying that the reaction rates in these two entries are proportional. Figure 1.9a indeed confirms that the rate for the racemic catalyst is approximately half that of the homochiral catalyst. This implies a nonselective formation of the heterochiral and homochiral dimers with equal stability ( $K_{het} = 2 K_{hom}$ ) which is in contrast with the requirement in the Noyori model for a (+)-NLE ( $K_{het} > 2 K_{hom}$ ). Moreover, the rigid  $\gamma$ -aminoalcohol scaffold of **4b** is not able to chelate zinc and form monomers which are the active catalysts in the Noyori model.

Blackmond and Brown proposed a model in which the system consisted predominantly of 2 homochiral dimers and a heterochiral dimer, equally thermodynamically stable and able to interconvert between each other. The homochiral dimers were thought to be active, while the heterochiral was supposed inactive. With these conditions, the model could be seen as a modified version of Kagan's model. A modification of Eq.1.2 gives the third-order reaction rate of Eq.1.5:

$$rate = k * [3b] * [Zn(iPr)_2] * [4b] * \frac{1 + g\beta}{1 + \beta} \quad (1.5)$$

When racemic catalyst is used  $\beta = 1$ , and when enantiopure catalyst is used  $\beta = 0$ . In both cases the rate will be the same through the course of the reaction, in agreement with Figure 1.10b. When an intermediate *ee* is used,  $\beta$  will change during the course of the reaction, explaining the shift of the green curve in Figure 1.9b. The scheme of the model and the structures of the proposed dimers are showed in Figure 1.10.

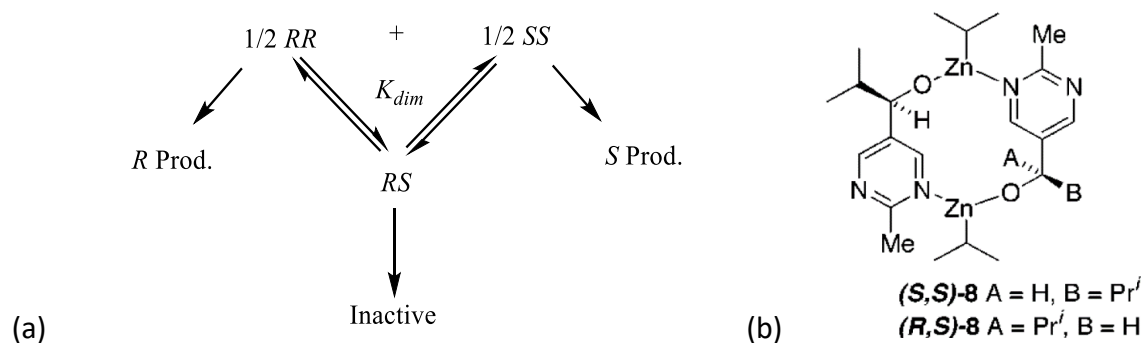


**Figure 1.10** The Blackmond/Brown model: (a) scheme (b): dimers.

### 1.1.8.2 The Blackmond/Brown model: non-equimolar substrate concentrations

The model described above fitted with the experimental data and could predict the evolution of the *ee* when equal amounts of **3b** and  $\text{Zn}(i\text{Pr})_2$  were employed but did not fit instead the experimental data points in case of non-stoichiometric ratios.

In Figure 1.11a, schemes showing fraction conversion vs. time in reactions carried out using 2 and 4 equiv. of  $\text{Zn}(i\text{Pr})_2$  are showed. The reaction model described in the previous paragraph predicted that the reaction rate should be sensitive to increasing  $[\text{Zn}(i\text{Pr})_2]$ , in contrast with the experimental data which does not seem to be sensible to changes of  $[\text{Zn}(i\text{Pr})_2]$ . This meant that the reaction was zero-order kinetic in this reagent. Figure 1.11b shows how the reaction profile keeps the same shape showed in Figure 1.9b and does not decrease from a third order kinetic to a second order kinetic, even if the reaction appears to lose its dependence on  $\text{Zn}(i\text{Pr})_2$  amount.

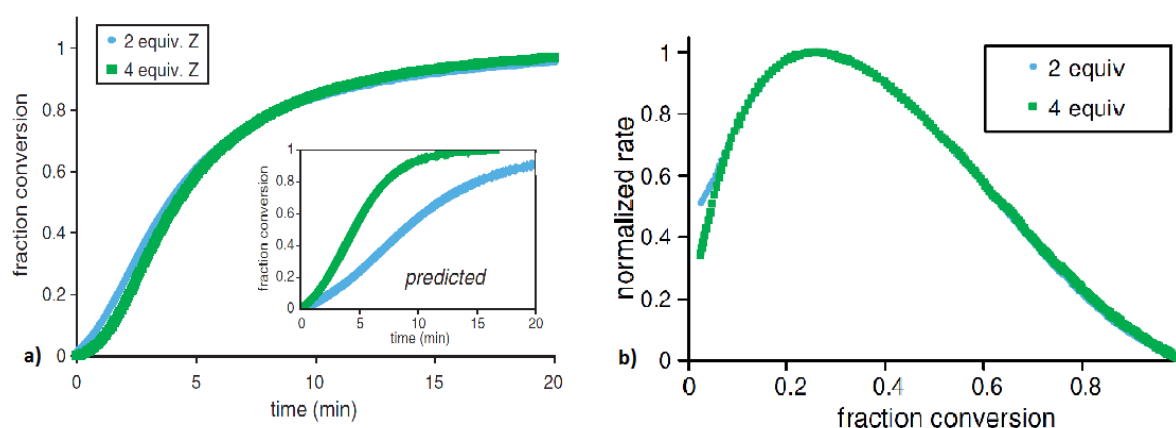
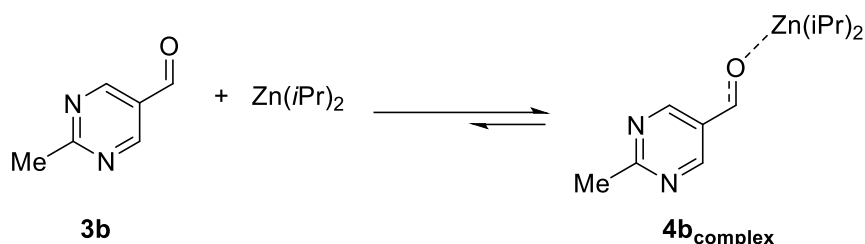


**Figure 1.11** Experimental kinetic profiles for the Soai reaction with excess of  $\text{Zn}(i\text{Pr})_2$  [30].

Blackmond and Brown rationalised this paradox suggesting the formation of a **3b**- $\text{Zn}(i\text{Pr})_2$  Lewis-acid complex prior to the alkyl transfer step (Scheme 1.8) [31]. The equilibrium was supposed to be in favour of the complex such that its concentration dominates over that of the free aldehyde.





**Scheme 1.8** Aldehyde- Zn(*i*Pr)<sub>2</sub> complex.

Two molecules of **4b<sub>complex</sub>** would then interact with the dimeric catalyst and form a tetrameric transition state. The rate law of this revisited model was then given by Eq.1.6.

$$rate = k' * [4b_{complex}]^2 * [dimer] \quad (1.6)$$

Although these studies were accurate in the case of the low reacting **3b**, the (+)-NLE reported by Soai on alkynyl-substituted pyrimidine aldehydes was greater than what could be explained by the model. Higher oligomeric species were then considered to be involved.

### 1.1.8.3 Identification of solution species

Several NMR studies by Brown have tried to elucidate the solution species involved in the Soai reaction. Working with the TMS-alkynyl-pyrimidine aldehyde, they found that the [ZnO]<sub>2</sub> square homochiral and heterochiral dimers of Figure 1.12 were the most promising structures for the resting state <sup>[32]</sup>. This was supported by DFT calculations, which found the two structures comparable in enthalpy, whereas the macrocycle structure shown in Figure 1.10b was found less favourable. Low temperature experiments with the same substrate showed dramatic signal broadening and increment in the complexity of the spectra, consistent with the presence of several higher oligomers, in which Zn-N association, not present in the dimers of Figure 1.12, became significant.

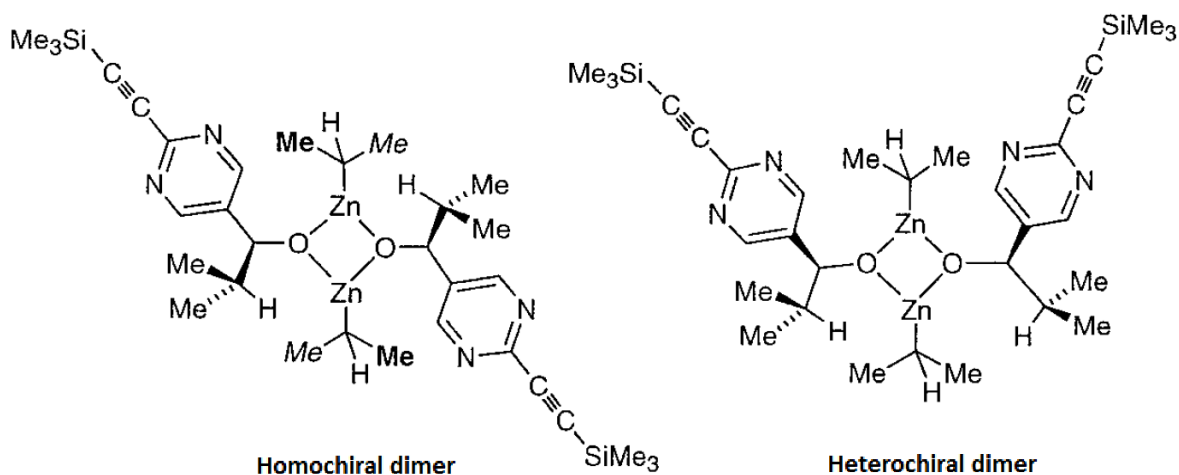
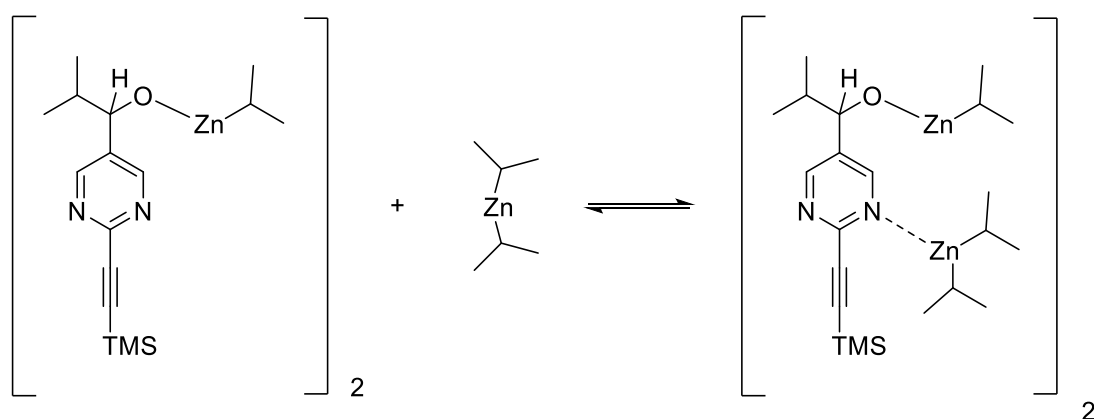


**Figure 1.12**  $[\text{ZnO}]_2$  square dimers proposed by Brown.

Studies focused on the binding of  $\text{Zn}(i\text{Pr})_2$  to the aldehyde showed that the binding site was the pyrimidine nitrogen, and not the carbonyl group, as proposed in Scheme 1.8. The same studies conducted on the Zn alkoxide dimers suggested that the dimer binds more strongly than the aldehyde to  $\text{Zn}(i\text{Pr})_2$  with a predominant N coordination (Scheme 1.9). There is also a rapid exchange between the  $i\text{Pr}$  of the Zn reagent and the alkoxide dimer, consistent with the trigonal coordinatively unsaturated zinc sites of Figure 1.12.



**Scheme 1.9** Dialkylzinc binding to aldehyde and Zn alkoxide.

It is known that alkylzinc alkoxides associate to form stable cubic tetramers<sup>[33]</sup>. Further DFT analysis were directed to predict possible tetrameric structures<sup>[21]</sup>. The most promising one was the square-macrocycle-square structure (SMS), in which the trigonal coordinatively unsaturated Zn geometry described above is retained (Figure 1.13). It could be formed by a dimer with addition of two aldehydes and two  $\text{Zn}(i\text{Pr})_2$  molecules. The  $i\text{Pr}$  groups play a

fundamental role in the assembly of these type of macrostructures. This could be a possible explanation to the fact that only these substituents are able to be reagents in the Soai reaction.

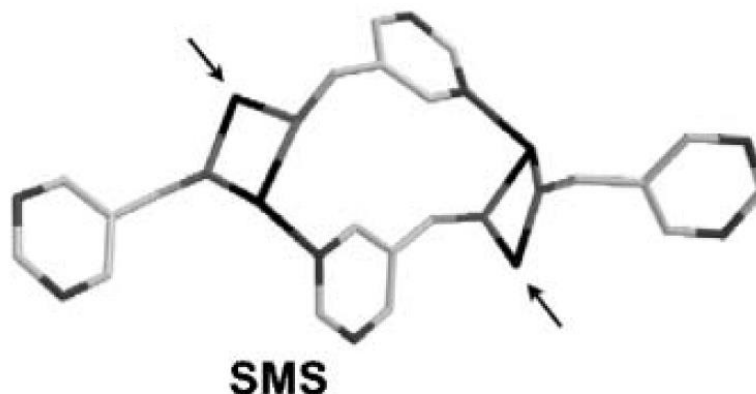


**Figure 1.13** The SMS tetramer <sup>[21]</sup>. The arrows indicate coordinatively unsaturated trigonal zinc sites.

It is known that bulky ligands can modulate dimer-tetramer equilibria <sup>[34]</sup>. As already stated, the dimer model is not able to explain the high (+)-NLE of the pyrimidine aldehydes with bulky ligands. If the higher oligomers proposed by the low temperature experiments are the species involved in the mechanism, then the SMS tetramer would become a possible reaction intermediate. Further kinetic, NMR <sup>[35]</sup> and DFT analysis <sup>[36]</sup> have pointed towards the presence of tetrameric species or even higher oligomers.

#### 1.1.8.4 Identification of crystal structures

In 2015, the Soai group was able to obtain crystal structures of isopropylzinc alkoxides <sup>[37]</sup>. Although crystal structures are not directly connected to solution structures, these findings suggest that various aggregation statuses should be present during the reaction.

A first set of crystals were obtained using an excess of  $\text{Zn}(i\text{Pr})_2$ . They are composed by an enantiopure and racemic tetramer made of respectively homochiral and heterochiral dimers (Figure 1.14). In accordance with previous reports, they are characterized by two square  $[\text{ZnO}]_2$  tetrameric structure, bridged one another by Zn-N coordination to afford a 12-membered macrocyclic structure. In the crystal of the enantiopure tetramer the two Zn atoms that do not form part of the macrocyclic structure remain in a coordinatively unsaturated 3-coordination state. The structures are closely resembling the SMS macrocycle described in the previous paragraph. The different conformation around the 12-membered macrocycle makes the racemic tetrameric crystal more stable than the enantiopure.

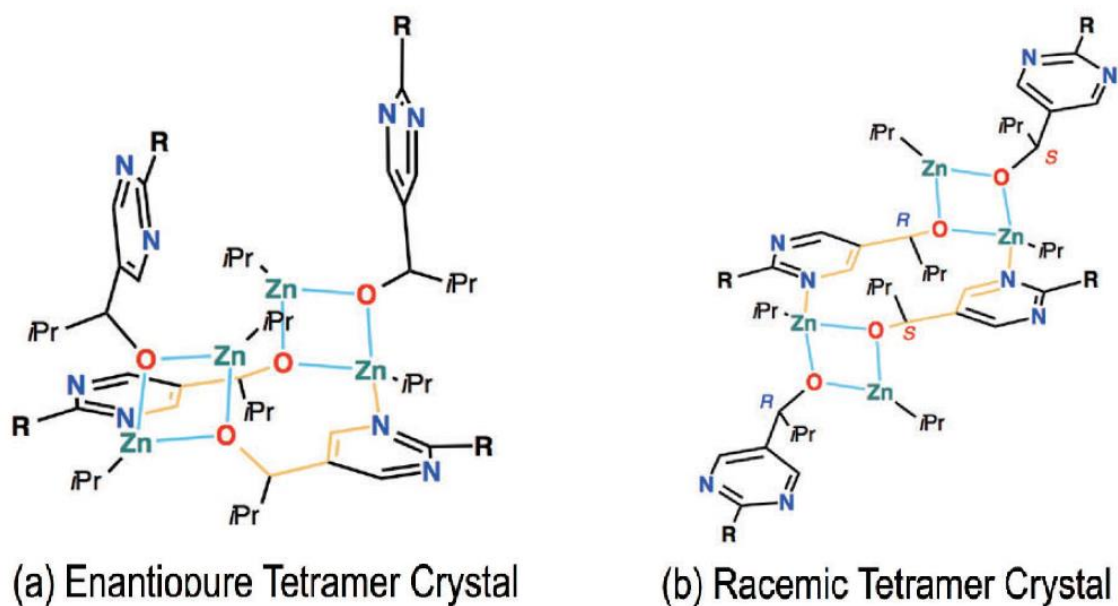


**Figure 1.14** Tetrameric structures of the alkoxides <sup>[37]</sup>.

When the amount of  $\text{Zn}(\text{iPr})_2$  is reduced to near-stoichiometric, there is no coordinative  $\text{Zn}(\text{iPr})_2$  anymore. Pyrimidine nitrogens can only coordinate zinc atoms of other tetramers, forming higher oligomeric structures. (Figure 1.15). The alkoxide forms a  $[\text{ZnO}]_2$  tetrameric structure and the dimers are again connected to form 12-membered macrocycles. The remaining nitrogen atom forms another 12-membered macrocycle with another dimer, giving a 1D oligomer in which  $[\text{ZnO}]_2$  squares and 12-membered macrocycles are alternated. The structure of the enantiopure and racemic oligomers are almost superimposable.

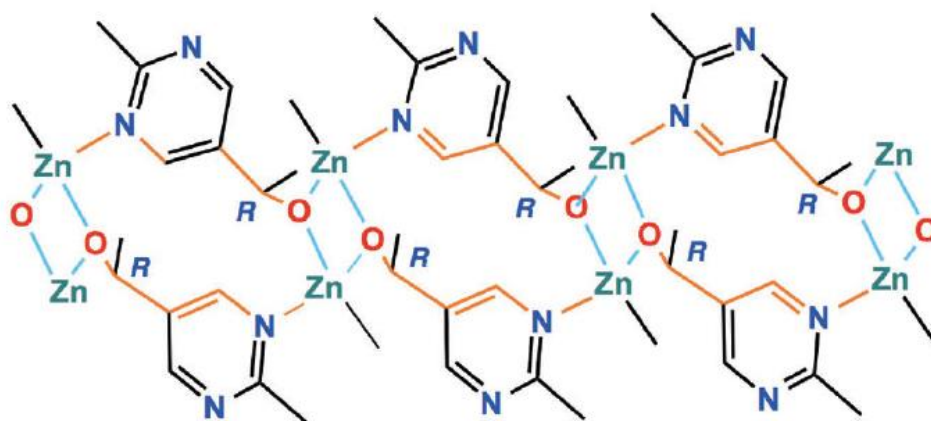


**Figure 1.15** Oligomeric structure of the alkoxide (enantiopure) <sup>[37]</sup>.

### 1.1.8.5 Hemiacetal intermediates in the Soai reaction

In 2012, Brown and Blackmond reported the observation of a transient acetal intermediate in solution. The intermediate was forming in presence of high concentrations of aldehyde and at low temperatures (below 0 °C).

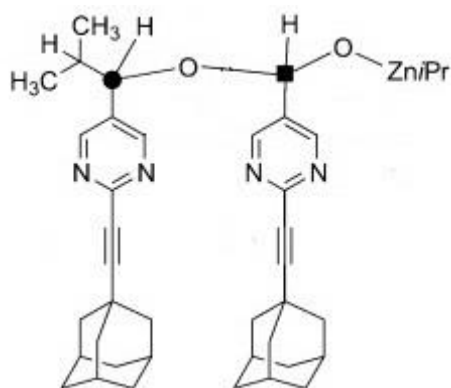
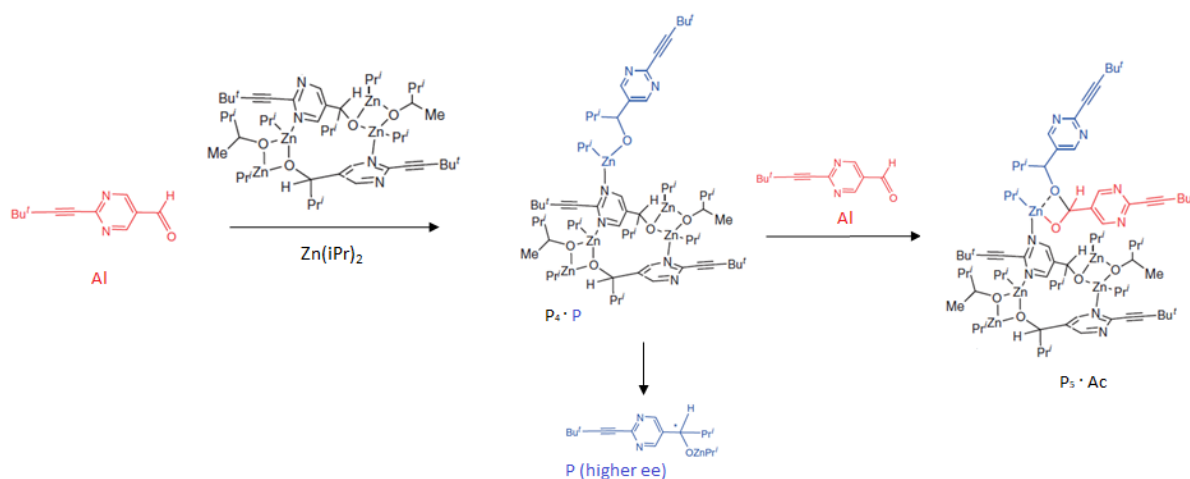


**Figure 1.16:** Structure of the acetal intermediate

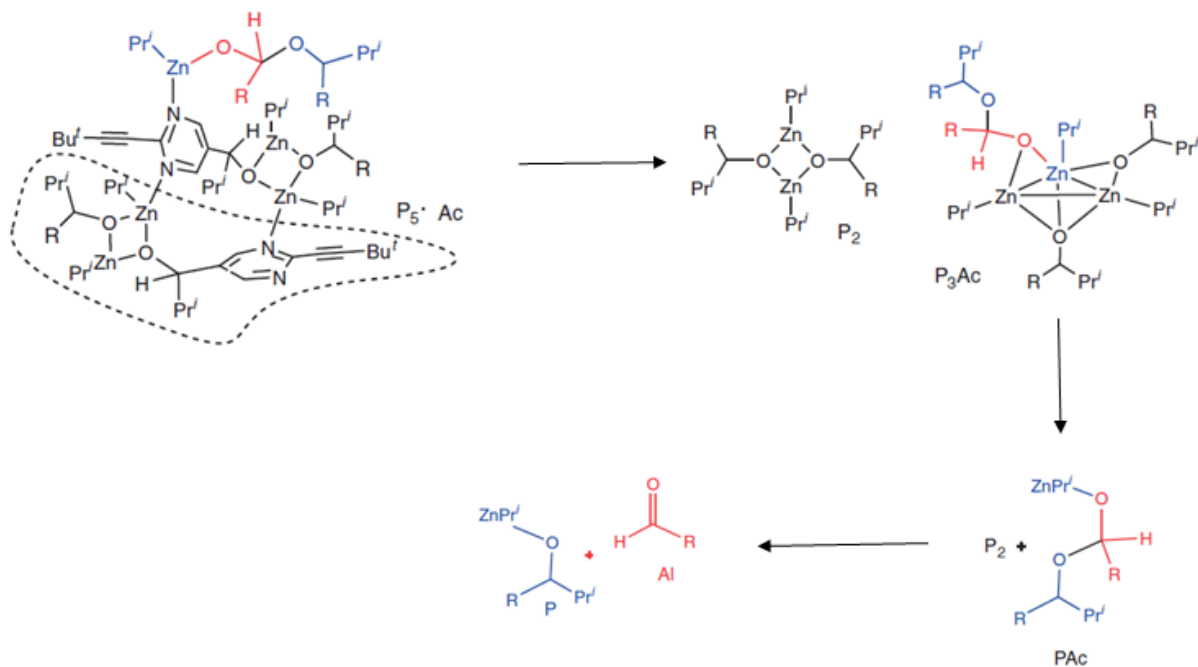
Further DFT analysis by Gridnev demonstrated how the acetal was not an important intermediate in the amplifying cycle of the Soai reaction. In the proposed mechanism the acetal is obtained from the same intermediate as the reaction product (P<sub>4</sub>P in Scheme 1.10. In presence of excess of aldehyde, adduct P<sub>5</sub>Ac is obtained).



**Scheme 1.10** Proposed formation of acetal in solution.

The unstable P<sub>5</sub>Ac would then immediately dissociate in P<sub>3</sub>Ac and P<sub>2</sub> (the latter is known to be the most stable species existing in the reaction pool of the Soai reaction). Further dissociations

would lead to the formation of PAc and finally product P and recovered aldehyde A (Scheme 1.11). To sum up, the acetal intermediate is supposed to form in a off-loop of the catalytic cycle and it yields the reaction product after decay.



**Scheme 1.11:** Degradation of transient P<sub>5</sub>Ac

Recently, Trapp and co-workers have reported the formation of hemiacetal complexes employing HRMS during liquid phase Soai reactions <sup>[38]</sup>. The group identified a variety of intermediates and transient intermediates formed by coordination of monomeric units of **3c/4c** and Zn(iPr)<sub>2</sub> and Zn-hemiacetalate complexes with **3c**.

It was found out, as shown in Figure 1.17 that the apex of the concentration of the most important transient intermediate coincides with the end of the induction period of the reaction. This means that the intermediate is built up during the induction period, and then rapidly depleted.

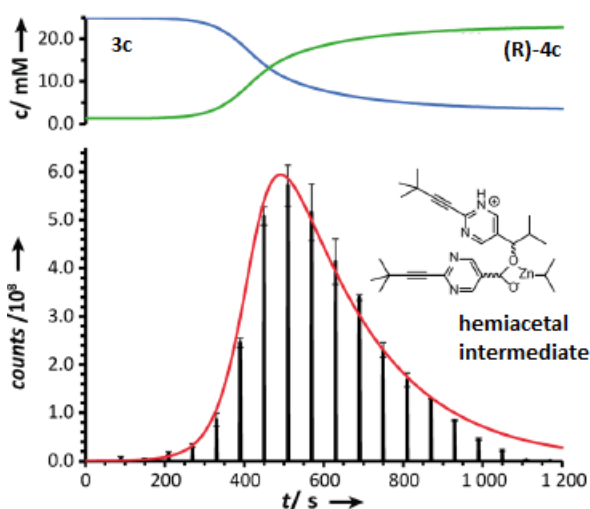


**Figure 1.17** Amount of transient intermediate vs. time during the Soai reaction [38].

On the basis of spectrometric and kinetic observations, Trapp proposed his reaction mechanism for the Soai reaction (Figure 1.18)

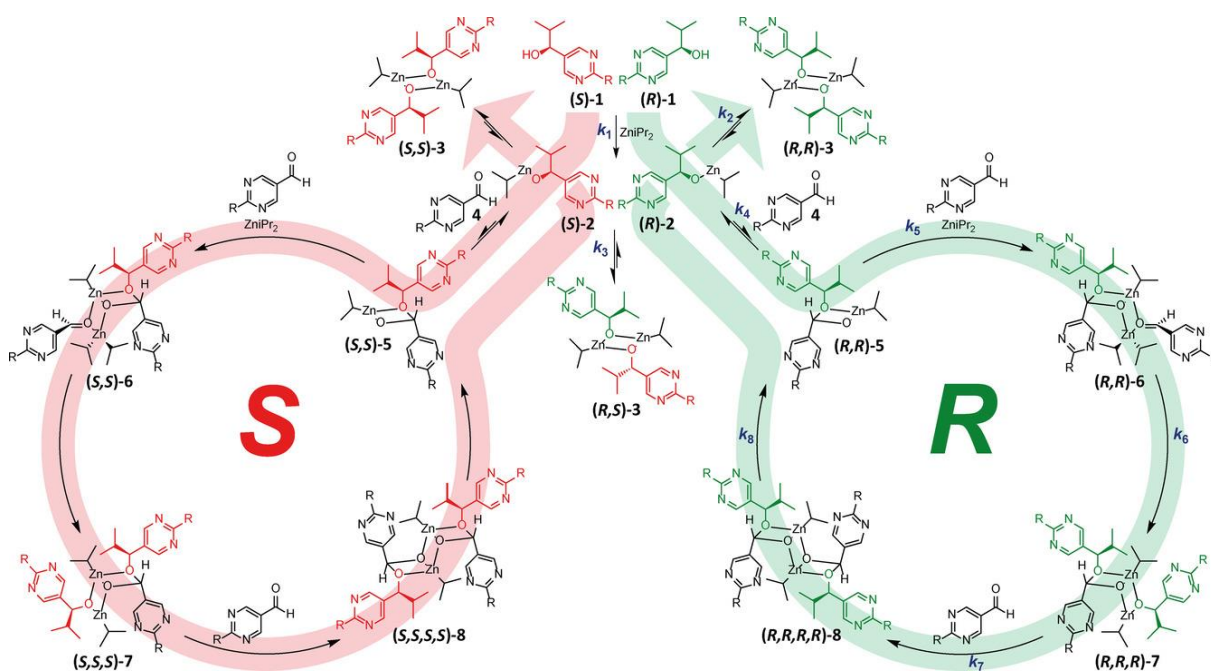


**Figure 1.18:** Proposed mechanism for the Soai reaction, formation of Zn-hemiacetalate (5 in the picture) is the key step intermediate [38].

The starting point is the reaction of **3c** with  $\text{Zn}(\text{iPr})_2$  to form the pyrimidyl alkoxides, which are in equilibrium with the homochiral complexes and heterochiral dimer. The insertion of another aldehyde molecule gives rise to the hemiacetal catalyst which is the key step of the reaction mechanism. The catalytic cycle is completed with the coordination of another

aldehyde molecule and  $\text{Zn}(\text{iPr})_2$ , spatial alignment and transfer of  $\text{iPr}$  from Zinc to the alkoxide, insertion of another aldehyde molecule to form a dimeric hemiacetal that splits in two monomers. The splitting of the dimeric hemiacetal could explain the rapid increase of the hemiacetal catalyst in the induction period.

The Soai reaction model proposed by Trapp is the last one in chronological order, and is of particular relevance for the results and the discussion presented in Chapter 3 and Chapter 4.

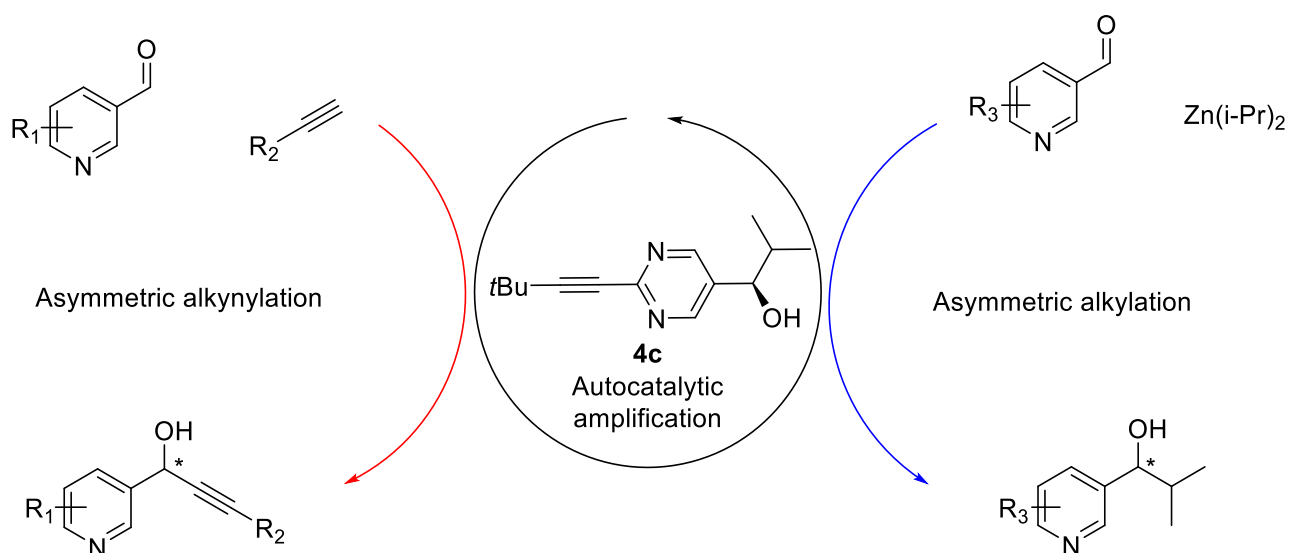
### 1.1.9 Synthetic applications of the Soai reaction

Many efforts have been put in in trying to understand the mechanism of the Soai reaction but, due to the fact that the reaction is restricted to a limited number of substrates, the chances to use the autocatalytic system of the reaction as a synthetic tool are almost unexplored.

In 2001 <sup>[39]</sup> Soai has showed how the asymmetric alkylation of various aza-aryl aldehydes could be catalysed by the Soai alcohol **4c** in an elegant one-pot sequence of asymmetric autocatalysis and asymmetric catalysis. The system was able to afford *sec*-alcohols with high yields and high *ees*. Interestingly, two of the substrates employed for the catalytic step were quinoline-3-carbaldehyde and 5-(diisopropylcarbamoil)pyridine-3-carbaldehyde, two of the Soai-type molecular scaffolds (Figure 1.5). Therefore, it was unclear if the final *ee* arose from the effect of the catalyst **4c** or from the autocatalytic effect of the alcohol products.

Based on the paper, our research group has explored the synthetic strategy of exploiting Soai alcohol **4c** as a chiral catalyst for asymmetric alkylation and alkynylation of various aza-aryl aldehydes (Scheme 1.12).

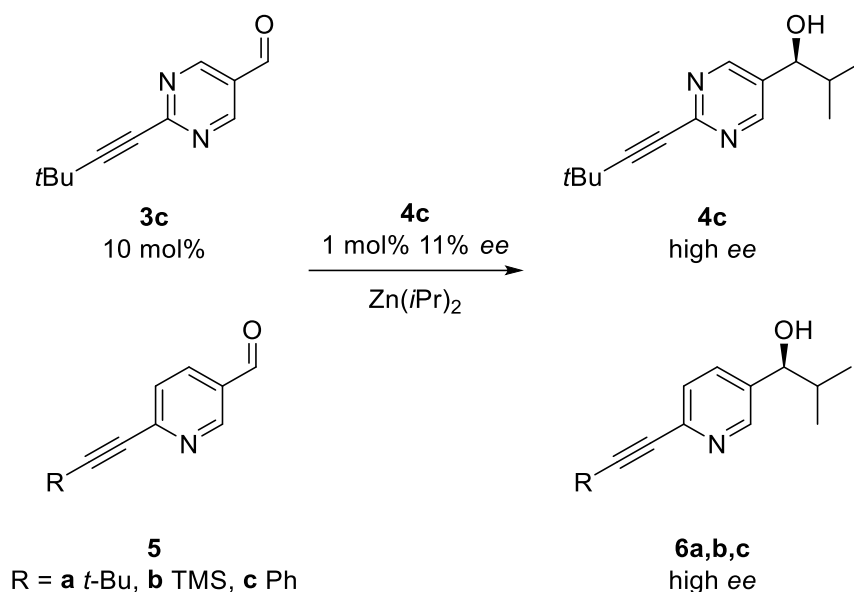




**Scheme 1.12** Reaction system overview.

The asymmetric alkylation of various substituted aza-aryl aldehydes <sup>[40]</sup> provided enantioenriched propargylic alcohols, valuable building blocks for a series of chiral targets. High *ees* (up to 86%) and good yields were obtained using **4c** as chiral catalyst (99% *ee*, 20 mol%). The propargylic alcohols showed no autocatalytic behaviour, therefore **4c** was the only species responsible for the asymmetric induction. A (+)-NLE was observed in the reactions, attributed to aggregates of **4c**-Zn or even synergistic interactions between catalyst, Zn and product. A one-pot procedure of autocatalysis-catalysis without isolation of catalyst **4c** afforded the product in 65% *ee*, thus good asymmetric induction was achieved also in this case.

The asymmetric alkylation of various substituted aza-aryl aldehydes <sup>[41]</sup> with Zn(*i*Pr)<sub>2</sub> showed to be sensitive to the substitution on the ring. The best results were obtained when 2-alkynylpyridine aldehydes with bulky ligands were employed, structures that showed an enhanced similarity with the best performing Soai alcohols. Also in this case, the pyridine alcohols formed were not able to give amplification of *ee*. The one pot asymmetric autocatalysis of **3c** and enantioselective addition of Zn(*i*Pr)<sub>2</sub> to substrates **5** using low *ee* **4c** as catalyst (Scheme 1.13) afforded both products **4c** and **6** with high yields and *ees* (>90%), indicating that **4c** is not working only as an autocatalyst but could be part of an improved catalytic system.



**Scheme 1.13** Reaction scheme for the one-pot autocatalysis-asymmetric alkylation system.

Kinetic studies performed on the system depicted in Scheme 1.11 showed a fast increase of the *ee* already in the first minutes. It would be rational to think that the *ee* of **6** would follow the amplification of **4c**, but conversely the *ees* of substrates **6** were found to increase even faster in comparison to the *ee* of **4c**, suggesting the presence of a cooperative system. Two strong and independent (+)-NLE were found for both reactions <sup>[42]</sup>.

## 1.2 Absolute Asymmetric Synthesis

Living molecules and their components in nature are homochiral rather than heterochiral. As already stated in Section 1.1.2, nucleic acids and proteins, the most vital macromolecules for life, are respectively composed by D-carbohydrates and L-aminoacids and their tertiary structures and functions depend on their homochirality. The emergence of homochirality on Earth has always intrigued scientists because it is strictly correlated with the evolution of life. At the moment the most supported theory is that homochirality evolved before life (abiotic theory) in three main steps: *spontaneous mirror-symmetry breaking* (SMSB, the spontaneous arise of a small *ee*), *chiral amplification* (enantiomeric enrichment occurs) and *chiral transmission* to other molecules <sup>[43]</sup> (Figure 1.19).

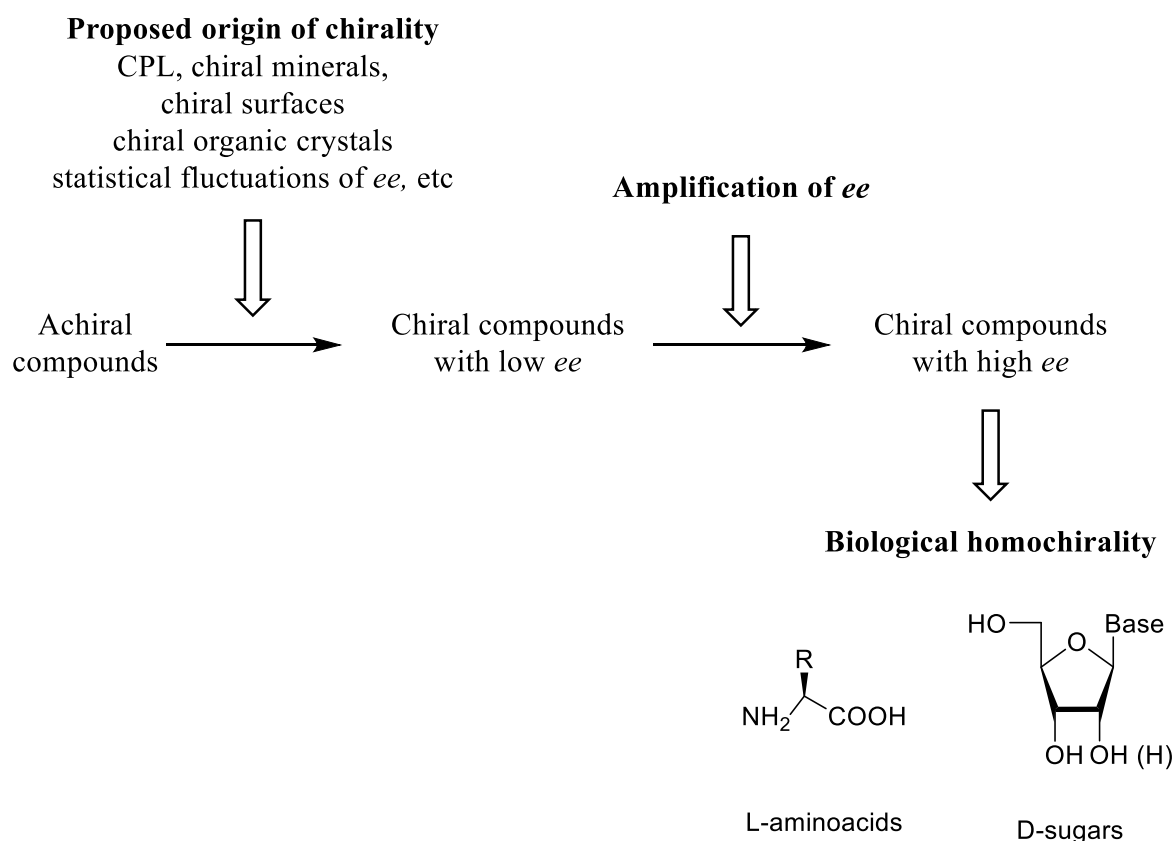


**Figure 1.19** Simplified scenario of chemical evolution of biological homochirality.

Many factors have been postulated for the mirror-symmetry breaking to have occurred: circularly polarized light (CPL) <sup>[44]</sup>, chiral minerals (quartz) <sup>[45]</sup>, chiral crystallization of achiral organic molecules <sup>[10, 46]</sup>, the electroweak interactions <sup>[44c]</sup>, the magnetic field of Earth <sup>[44c]</sup> and even extra-terrestrial origins (molecules with small *ees* have been found in meteorites).

Moreover, enantiomeric excesses have been obtained even in absence of any chiral physical force. Absolute asymmetric synthesis (AAS) is defined as asymmetric synthesis in absence of chiral chemical reagents <sup>[44c, 46b, 47]</sup>.

In the next sections, a selection of different approaches followed by different research groups through the years to archive absolute asymmetric synthesis is presented.

### 1.2.1 Absolute Asymmetric Synthesis with Circularly Polarized Light

Circularly Polarized Light (CPL) is a massless electromagnetic source and can be undoubtedly considered a chiral entity. Already in the end of the 19th century Le Bel <sup>[48]</sup> proposed the use of (*R*)- and (*L*)- CPL to induce an enantiomeric excess in a reaction, and the concept was further developed by van't Hoff <sup>[49]</sup>. The idea gained more relevance after the discovery of the isotropic circular dichroism (CD) by Cotton <sup>[50]</sup> *i.e.* absorption of CPL may be differ for the two

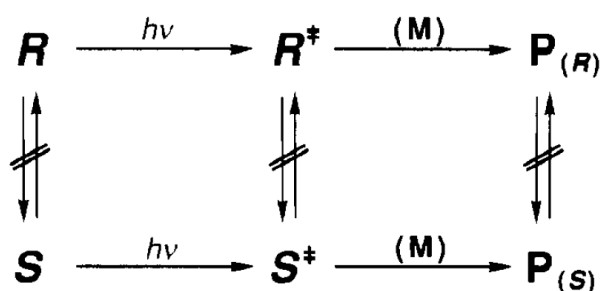
enantiomers. Moreover, irradiation of a prochiral molecule with CPL might in principle convert the ground state of the molecule to an excited state with a certain chirality and therefore lead to the preferential conversion in one or the other enantiomer.

The main factor for the optical purity of the product of these photochemical reactions is the anisotropy factor ( $g$ ), defined by Kuhn <sup>[51]</sup> as the relative difference of the molar extinction coefficients of an optically pure compound toward ( $R$ )- and ( $L$ )-CPL at a given wavelength. This value can in theory oscillate between  $0 \leq g < 2$  but in general for organic compounds  $g < 10^{-2}$ , therefore only low  $ee$  values can be expected.

Three different approaches to CPL-induced enantioselective conversions can be distinguished <sup>[52]</sup>.

(a) Asymmetric Photodestruction

In this approach, as shown in Scheme 1.14, the two enantiomers of a racemate are irreversibly consumed at different rates (depending on their  $g$  factor) and the system in consideration will therefore be enriched of one of the two species. The more-absorbing enantiomer can in theory be converted in chiral or achiral photoproducts, but except for some cases no photoproducts have ever been isolated, and preferential destruction of one of the two enantiomers is the major outcome of the reaction. The most important condition for this approach is that the two enantiomers are unable to interconvert in the opposite one.



**Scheme 1.14** Asymmetric Photodestruction <sup>[44b]</sup>.

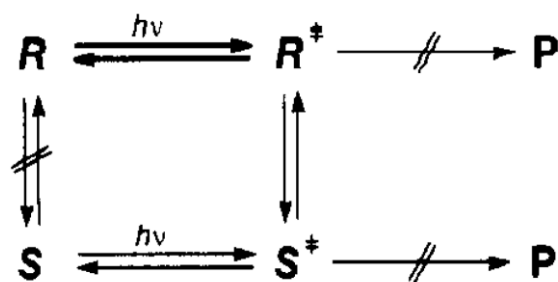
The best results to date were obtained by Kagan and co-workers, with 20% optical purity of camphor ( $g = 0,09$ ) and later 30% optical purity of trans-bicyclo[4.3.0]nonan-8-one ( $g = 0,24$ ). In both cases the photodestruction of the racemates was at 99%, leading to very low yields <sup>[53]</sup>. Since the  $g$  factor plays an important role in the optical purity of the product, a molecule with

a high  $g$  factor would be a suitable candidate for asymmetric photodecomposition, but so far the highest  $g$  factor observed has been  $g = 0,30$  for tricyclo[4.4.0.0]decan-2-one [54].

Conversely, the process of photodestruction plays a central role in the study of homochirality. CPL has been found in star forming regions [55], and L-enantioenriched aminoacids have been found in a series of meteorites and comet dusts [56]. Therefore, CPL is thought to be a highly plausible factor for the symmetry breaking in the universe and for the rise of homochirality on Earth [57].

(b) Partial photoresolution

The mechanism of this process is shown in Scheme 1.15: each enantiomer of a racemic mixture cannot interconvert in the ground state but becomes mutually interconvertible at different rates in the excited state upon irradiation with CPL. There is the formation of a photostationary phase ( $pss$ ) in which the enantiomeric ratio is different from the starting system. The  $pss$  can be archived not only from racemic mixtures but also from optically pure ( $R$ )- or ( $S$ )-compounds. Again, the  $g$  factor governs the enantioselectivity of the process, and only low  $ee\%$  can be expected. The major requirement is that the enantiomers should be able to interconvert photochemically without producing any side product. This is at the same time the major drawback, since it is difficult to find suitable candidate molecules with these features. The main difference between this method and asymmetric photodestruction is that the concentration of the starting material doesn't change during the process, which means, in theory, that no enantiomer should be destroyed.



**Scheme 1.15** Partial Photoresolution [44b].

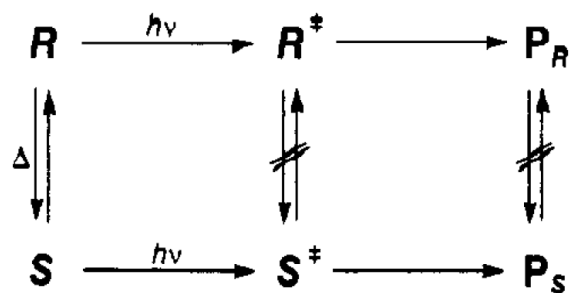
Early works on this approach have been published by Stevenson and Verdieck on CPL-induced irreversible deracemization of octahedral oxalate complexes of chromium(III) [58], while the

first successful approach on organic chiral compounds was reported by Hayashi and Irie on a 1,1'-binaphthyl racemic mixture <sup>[59]</sup>.

The discovery by Shuster <sup>[60]</sup> of a reversible photoderacemization of axially chiral bicyclic ketones has triggered an intense research in the field of supramolecular structures. The properties of liquid crystals can be driven by CPL through interaction with small guest molecules: an induction or modification of chirality of a guest molecule in a nematic achiral phase can induce a switch to a cholesteric chiral phase with a helical organization. This phenomenon has a wide impact especially on nanotechnological applications such as chiroptical molecular switching, optical storage and light driven devices.

(c) Asymmetric photosynthesis

This process leads to the enantioselective photochemical formation of an optical active compound from a prochiral starting material. The prochiral substrates should show a fast conversion between the enantiomeric conformations, one of which will be selectively excited by CPL. The racemization in the excited state should not take place or at least be slower than the conversion to the final product (Scheme 1.16). This approach to CPL-induced enantioselective conversion is the most appealing, requiring only a prochiral molecule, but again the low *g* factors limits the selectivity of the reactions.



**Scheme 1.16** Asymmetric Photosynthesis <sup>[44b]</sup>.

Kagan <sup>[61]</sup> and Calvin <sup>[62]</sup> independently showed a one-pot  $I_2$  mediated oxidative photocyclization of a range of diarylethylenes: the reaction involved an isomerization of the olefin from trans to cis configuration. Upon further photoabsorption a ring closing step occurred, followed by oxidation which gave the optical enriched hexa and octahelicenes, with *ee* values respectively of 0.35% and 2%, with the reduced *ee* for the former product rationalized by the lower *g* factor of the reagent.

### 1.2.2 Amplification of Homochirality by Autocatalytic Crystallization

The first example of a crystallization technique to separate enantiomers dates to 1848: Pasteur managed to separate the enantiomers of sodium ammonium tartrate by direct crystallization and hand-sorting <sup>[63]</sup>. Even if nowadays crystallization techniques could seem “out-of-date” or “low-tech”, they have the advantage of being widely applicable, simple and cost-efficient, requiring only easily available standard equipment. Moreover, the majority of enantiomers synthesized in food, pharmaceutical and agrochemical industry are still produced via the simplest crystallization technique, classical resolution.

Classical resolution involves a reaction between the racemate and a suitable enantiomerically pure resolving agent in order to form two diastomeric salts which have different solubilities and can be easily separated. The yield of this method would be limited to 50%, but when racemization of the unwanted enantiomer is feasible, yields can increase to more than 90%. Active pharmaceutical ingredients as (S)-Naproxen, Sertralin, Frovatriptan, Duloxetine, Eszopiclone are produced in thousands of tons scale per year through this method <sup>[64]</sup>.

In classical resolution chiral sources are required. Conversely, in the last 30 years, two different methods to obtain homochirality in the crystal state with no requirement of chiral sources have been discovered: Kondepudi’s total spontaneous resolution and Viedma’s attrition enhanced deracemization (or Viedma ripening). They are some of the most powerful tools to reach homochirality in a chemical laboratory. In addition to these two methods, chiral additives have also been found to direct the formation of one chiral solid state, with the use of the so called “tailor-made inhibitors”.

#### (a) Total Spontaneous Resolution

When a racemate crystallizes it may form: (1) in 90-95% of cases a racemic compound, in which both enantiomers are present in the same crystal, due to the higher affinity of one enantiomer for the opposite enantiomer in the crystal structure; (2) in 5-10% of cases a racemic conglomerate, in which each crystal contains only one single enantiomer, but the solid sample is racemic as a whole; in this case one enantiomer has a higher affinity for the same enantiomer than for the opposite one; (3) in less than 1% of cases a solid solution, which contains both enantiomers in a random arrangement. (Figure 1.20) <sup>[65]</sup>. Not only chiral, but also achiral molecules can crystallize into chiral crystals: in these cases the chirality of the crystal structure arises from a chiral packaging of the molecule.

Chiral discrimination in the solid state can only be archived with molecules that form conglomerate crystals, narrowing the suitable substrates for this technique.

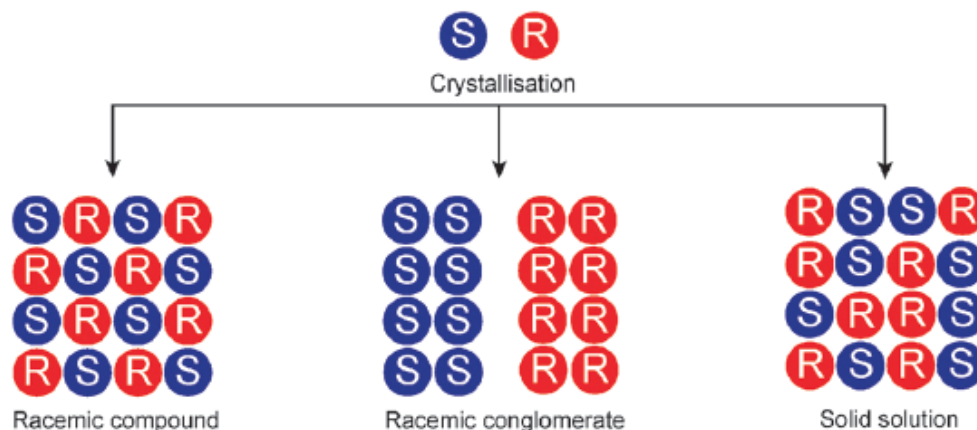


**Figure 1.20** Enantiomers crystallize either as a racemic compound, racemic conglomerate or a solid solution <sup>[66]</sup>.

Being able to form conglomerates is not the only requirement for the total spontaneous resolution, because, as already said, the *D*- and *L*- crystals of a conglomerate are enantiomeric, therefore they share same properties, including solubility. If a racemate solution of conglomerate forming molecules is left equilibrating, the same amount of *D*- and *L*- crystals will be formed. The crystallization will proceed giving a first crystal of a certain handedness (primary nucleation). The solution will then be enriched in the opposite enantiomer triggering its crystallization as well.

Total spontaneous resolution allows to obtain only one single enantiomeric form of crystals. In 1990 <sup>[67]</sup>, Kondepudi, following pioneering work by Havinga <sup>[68]</sup>, showed formation of conglomerates of nearly single chirality (99.7%) from a vigorously stirred solution of NaClO<sub>3</sub>. The molecule in this case was achiral (but forming chiral crystals). In repeated experiments, random distributions of both enantiomerically pure conglomerates were formed. This result was rationalized considering the dynamic of crystallization: the rate of primary nucleation is normally low, and was kept even lower by adding a stirrer. Stirring causes the crush of the primary nucleus, originating a higher number of smaller crystals of the same handedness (secondary nucleation). These second crystals would then grow rapidly, depleting the solution and preventing the formation of the primary nucleus of the opposite enantiomer, resulting in a single chiral solid state (Figure 1.21). This hypothesis was confirmed by repeating the experiments without stirring, in which only racemates were obtained.



Stirring and secondary nucleation are the key features of this method. Moreover, the production of second nuclei from the primary nucleus, and the suppression of the formation of the opposite crystal are in line with Frank's chiral amplification via autocatalysis model. This process has been successfully applied also to chiral molecules: an important feature for total spontaneous resolution in these cases is that the compound must be able to racemize in solution, spontaneously or aided by a racemizing agent, because it prevents the nucleation of the other enantiomer.

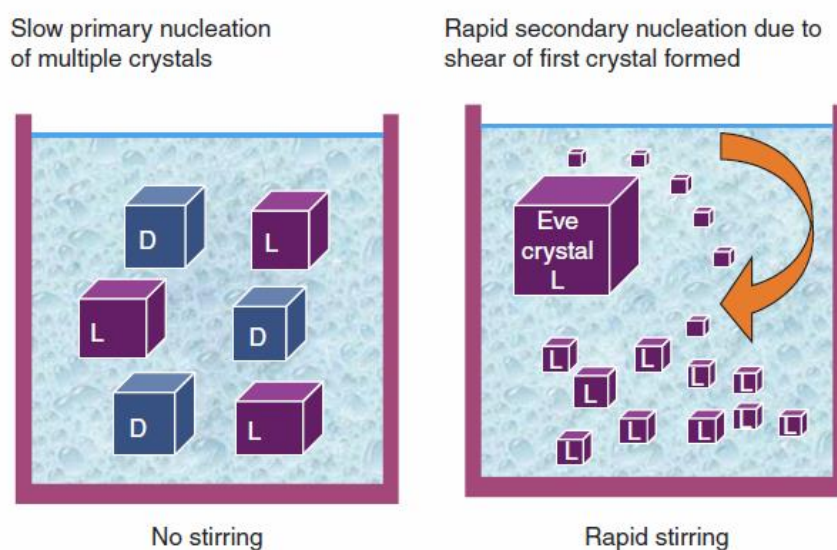


**Figure 1.21** Scheme of total spontaneous resolution <sup>[69]</sup>.

(b) Attrition-enhanced deracemization (or Viedma ripening)

In 2005 <sup>[70]</sup>, following Kondepudi's work, Viedma subjected a racemic solution of *L*- and *D*-conglomerates of NaClO<sub>3</sub> to abrasive grinding with glass beads in a closed system under isothermal conditions. After several days the racemic mixture was completely converted to a homochiral crystal state. As for total spontaneous resolution, there was equal probability for the handedness of the final crystals. This process can be described as a "solid-to-solid" deracemization, conversely to the "solution-to-solid" deracemization of total spontaneous resolution (Figure 1.22). Some years later Viedma's striking discovery, Vlieg and Blackmond showed the first example of Viedma ripening on an intrinsically chiral molecule, an amino acid derivative which was able to racemize in solution through a strong base <sup>[71]</sup>.

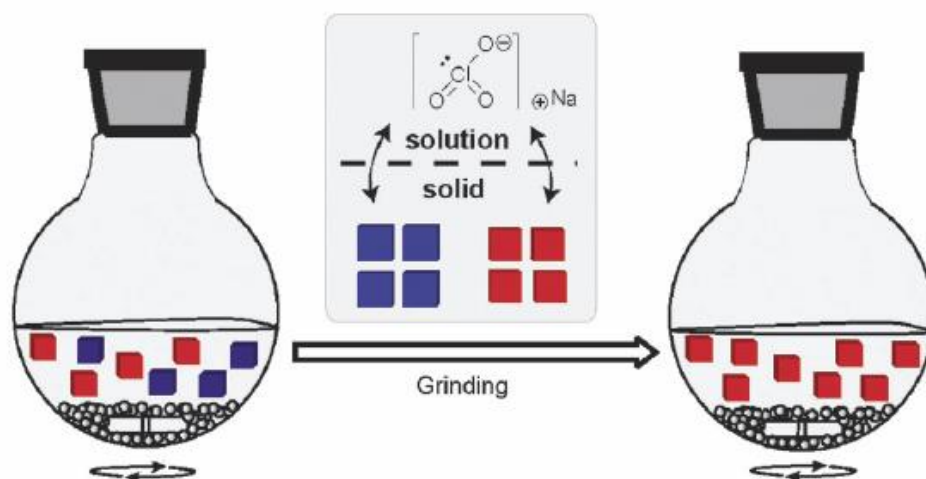


**Figure 1.22** Schematic representation of Viedma's experiment <sup>[66]</sup>.

Viedma ripening is not a crystallization, conversely its starting state is the end of a typical crystallization, with a racemic solution of crystals. During the experiment no primary nucleation takes place, and the only process is the simultaneously dissolution of crystals and recrystallization of molecules from the solution. The addition of the glass beads enhances the attrition in the system causing the formation of a large number of small crystals. These small crystals dissolve more rapidly than big crystals, causing a slight supersaturation of the solution. The supersaturation is not enough driving force however to trigger new primary nucleation. In fact, to balance the supersaturation, the system is then forced to increase the rate of growing of the existing crystals. Molecules will add to bigger crystals than small ones (Ostwald ripening), so if by chance there is a predominance of bigger crystals of one handedness, the amount of this enantiomeric solid will increase through time. The process is overall cyclical, with an autocatalytic feedback mechanism driven by the initial imbalance in size of *L*- vs *R*-crystals.

Further research showed how the deracemization could be archived via CPL irradiation and grinding <sup>[72]</sup> or replacing glass beads and stirring with temperature gradient cycles <sup>[73]</sup> and also through a High Pressure Homogenization, which combines grinding and temperature cycling in a single step <sup>[74]</sup>.

Many applications of total spontaneous resolution and Viedma ripening have appeared in literature in recent years, and some excellent reviews have covered the most important papers <sup>[66, 75]</sup>. The major drawback, as already highlighted, is the need of conglomerates

forming molecules. In order to find suitable candidates libraries of derivatives have to be synthesized and analyzed. It should be noticed that in many cases seeding the starting system with small amounts of pure chiral product can speed the reaction, and give the desired product more easily.

(c) Tailor-made inhibitors

Even if it seems intuitive that an additive of a certain handedness could induce the formation of crystals of the same handedness by positive autocatalytic feedback, several examples have reported that the final crystal state would be enriched of the opposite enantiomeric conglomerates, with the additives working instead as inhibitors. This process has been rationalized by virtue of the stereochemical similarity between the conglomerate crystals and the additive/chiral inhibitor. The additive could be integrated in the crystal structure of the conglomerate, blocking its growth. In this way a selective growth of conglomerates of the opposite handedness can be archived. This phenomenon is also none as the “rule of the reversal”. As represented in Figure 1.23, the tailor-made inhibitor can be a lattice-controlled product of one of the conglomerates (b), or a simple chiral additive (c).

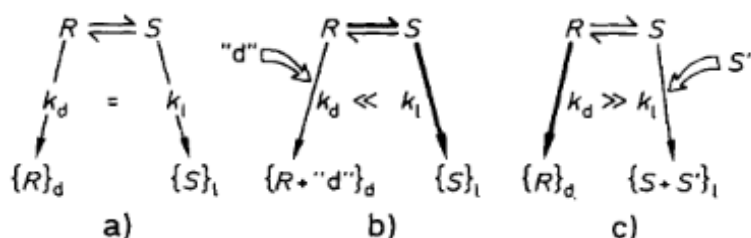


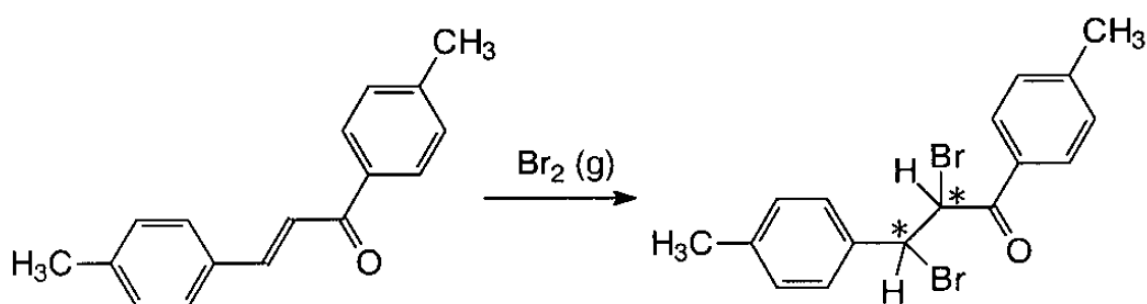
**Figure 1.23** (a) Spontaneous crystallization of a racemate (RS) to give  $\{R\}_d/\{S\}_l$  conglomerates; (b) crystallization in presence of the additive “d” (lattice-controlled product of the  $\{R\}_d$  phase); preferred crystallization of  $\{S\}_l$ ; (c) crystallization in presence of a chiral additive  $S'$  (with stereochemical similarity to S); delayed crystallization of  $\{S\}_l$  [76].

One of the first reports of this phenomenon was published by Purvis in 1957 [77]. Addition of (S)-Asparagine or (S)-Leucine to a conglomerate forming solution of Glutamate led to the preferential crystallization of (R)-Glutamate crystals. An example of lattice-controlled product as inhibitor was demonstrated by Green and Heller on the same system developed by Penzen and described in Section 1.2.3. The addition of the enantiopure dibromide product to conglomerate forming 4,4'-dimethylcalcone led to the crystallization of the reactant of opposite handedness [78].

### 1.2.3 Absolute Asymmetric Synthesis via Enantiomorphous Crystals

A different approach to perform absolute asymmetric reactions is exploiting the chirality of crystals in solid-state reactions. In crystals, molecules can pack into 230 space groups, 65 of which are enantiomorphs. While chiral molecules always pack into one of the latter 65 space groups, also achiral molecules can form in some cases chiral crystals. There are few approaches by which crystal chirality can be converted in molecular chirality. One approach is through photochemical conversion, while a second way is through heterogeneous catalysis in which the chiral surface of a crystal acts as a catalyst.

A third way, interesting for the scope of this thesis and firstly demonstrated by Penzien and Smith in 1969 <sup>[79]</sup>, is through an absolute asymmetric transformation in the solid state. An achiral 4,4'-dimethylcalcone was found to crystallize in the chiral space group  $P2_12_12_1$ . When single crystals were exposed to gaseous bromine, they underwent a gas/solid trans-bromination to yield a chiral dibromine product with *ee%* of random handedness in the range 6-25% (Scheme 1.17).



**Scheme 1.17** Absolute asymmetric synthesis exploiting the crystal environment of 4,4'- dimethylcalcone.

### 1.2.4 Amplification of Asymmetry by Chirally Autocatalytic Systems

The small but persistent energy difference between two enantiomers might be enough to induce a symmetry breaking, and enantiomerically enriched products can be obtained as a result of statistical fluctuations by stochastic processes. This phenomenon is much more common than what chemists usually believe. According to statistical theories, the number of enantiomers in a racemic mixture is rarely the same and there are always small fluctuations: considering  $n$  molecules, there will be a standard deviation from 50:50 of  $(n^{1/2})/2$ . These deviations normally lie below the detection level of the instruments i.e. the formation of a racemate. If the reaction system has a way to amplify these tiny imbalances, then an

asymmetric amplification will be observed. The Soai reaction, with its Frank-like asymmetric autocatalytic system, is a perfect example of this possibility.

Singleton and Soai have demonstrated how substrates **3b** and **3c** were able to yield enantioenriched **4b** and **4c** without the addition of any chiral substance in liquid phase reactions. In absence of the initial autocatalyst, the zinc alkoxide of pyrimidyl alkanol is formed *in situ* by reaction of starting aldehyde and  $\text{Zn}(i\text{Pr})_2$  with an infinitely small initial bias in *ee*. The tiny imbalance in one of the two enantiomers will subsequently catalyze the reaction and amplify the *ee*. The products were formed with an approximately stochastic distribution of the two enantiomers <sup>[80]</sup>.

Although not plausible for the actual mechanism of prebiotic homochirality (the reaction cannot happen in presence of water and oxygen), the Soai reaction shows a strong correlation between the source of chirality and the enantioenriched chirality of the products. It has extensively been employed as a model for the emergence of homochirality on Earth.

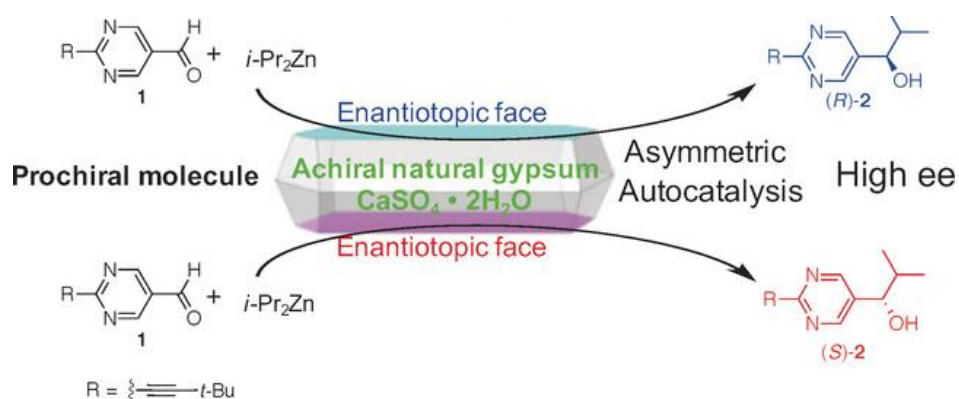
Irradiation of the racemic autocatalyst **4c** by (*l*)- or (*r*)-CPL <sup>[81]</sup>, and subsequent asymmetric catalysis afforded respectively (*S*)- and (*R*)-**4c** in high *ee*%. It is possible to assume that CPL induced photodestruction of one of the enantiomers of racemic **4c** (see Section 1.2.1) creating a small imbalance of *ee* subsequently amplified by the Soai reaction.

Chiral inorganic crystals exhibits enantiomorphic forms. d- and l-Quartz ( $\text{SiO}_2$ ), d- and l- $\text{NaClO}_3$ , and M- and P- crystals of Cinnabar ( $\text{HgS}$ ) were successfully employed as catalyst for the Soai reaction <sup>[45b, 82]</sup>. The chirality of the crystals directed the preferential formation of the two enantiomers of **4c**. The same result was obtained with chiral organic crystals of achiral compounds as triggers (adenine, serine, cytosine) <sup>[83]</sup>.

Even isotope chirality has shown to be discriminated by asymmetric autocatalysis. Achiral compounds were made chiral through the substitution of one or more atoms through isotope substitution ( $\text{D}/^1\text{H}$ ,  $^{13}\text{C}/^{12}\text{C}$ ,  $^{18}\text{O}/^{16}\text{O}$ ,  $^{15}\text{N}/^{14}\text{N}$ ). Isotope enantiomers differ only in the number of neutrons and they have been rarely been employed as chiral auxiliaries. The chiral isotopomers were able to give the preferential formation of one of the two enantiomers of **4c** <sup>[84]</sup>.

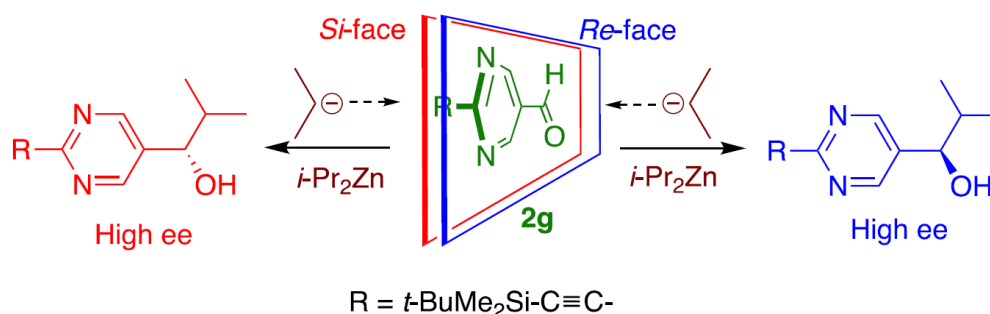
Interestingly for the scope of this thesis, some of these applications of the Soai reaction involved vapour/solid interactions between  $\text{Zn}(i\text{Pr})_2$  and Soai aldehyde.

Gypsum ( $\text{CaSO}_4 \cdot 2\text{H}_2\text{O}$ ) is an achiral inorganic molecule crystallizing in achiral crystals with  $C2/c$  space group. However, the large surfaces of the crystals are enantiotopic. Carefully slicing the crystal it was possible to obtain the two enantiotopic faces (010) and (0 $\bar{1}$ 0). Aldehyde **3c** rubbed on the crystal faces and exposed to vapours of  $\text{Zn}(i\text{Pr})_2$  afforded the preferential formation of one of the two enantiomers on each enantiotopic face (Scheme 1.18). The result was rationalized with a preferential orientation of the *Re/Si* prochiral aldehyde by interaction with the enantiotopic face of gypsum <sup>[85]</sup>.



**Scheme 1.18** Absolute asymmetric synthesis induced by 2D chirality of achiral crystals <sup>[85]</sup>.

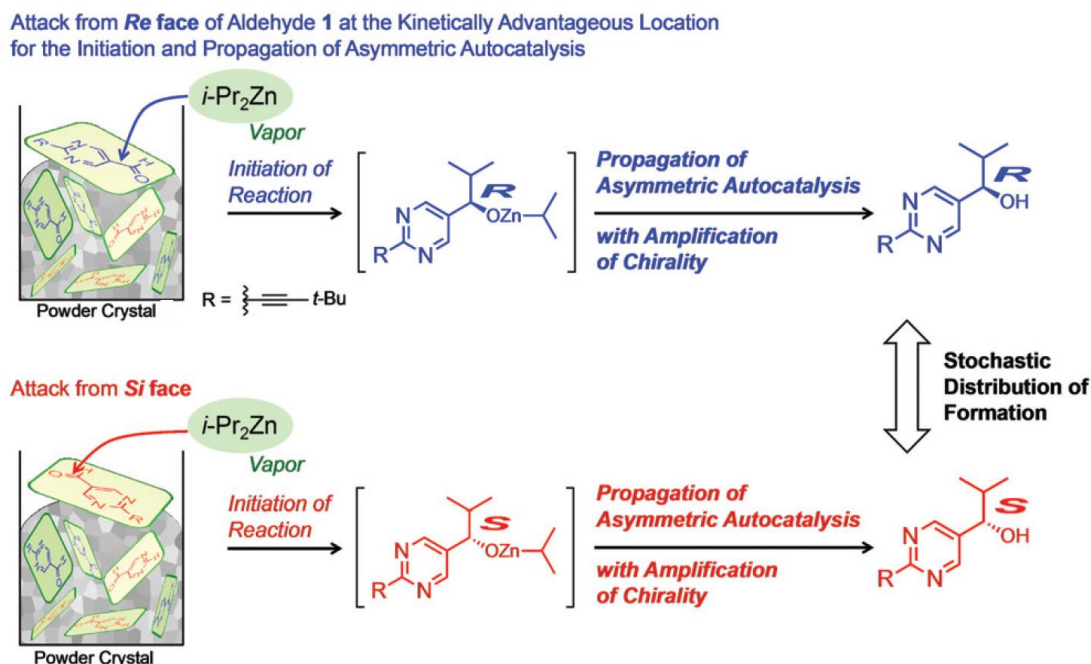
In a similar work, the reaction was performed between vapours of  $\text{Zn}(i\text{Pr})_2$  and crystals of aldehyde with no involvement of other materials. 2-TMS-pyrimidine aldehyde crystallizes in an achiral  $P\bar{1}$  space group with two enantiotopic faces. Treating of the two specific faces of a crystal with vapours of  $\text{Zn}(i\text{Pr})_2$  afforded also in this case the preferential formation of one of the two enantiomers on each enantiotopic face (Scheme 1.19) <sup>[86]</sup>.



**Scheme 1.19** Enantioselective addition of  $\text{Zn}(i\text{Pr})_2$  at the oriented surface of an achiral aldehyde <sup>[86]</sup>.

Soai has recently reported how absolute asymmetric synthesis can be archived also *via* a heterogeneous vapour-solid interaction with achiral crystals of **3c** oriented in a random

manner. Aldehyde **3c** crystallizes in achiral crystal with achiral  $P2_1/n$  space group. The first attack of  $Zn(iPr)_2$  on one or few molecules of **3c** forms alkoxides whose configuration is dictated by the random orientation of the aldehyde crystals and then amplified through asymmetric autocatalysis (Scheme 1.20). A stochastic distribution of the two enantiomers is yielded also in this case [87].



**Scheme 1.20** Kinetic heterogeneous absolute asymmetric synthesis of alcohol **4c** [87].

### 1.3 Metal-Organic Frameworks

Metal-Organic Frameworks (MOFs) are porous solid materials and can be considered the second main element of this thesis work. In the next paragraphs the most relevant aspects of MOFs for the scope of the thesis will be highlighted.

#### 1.3.1 Historical background

In the field of Chemistry there has always been an interest in the synthesis of inorganic/organic hybrid compounds [88]. Industrial motivations dictated the interest in expanding the chemical connectivity of these compounds from zero-dimensional to 3D materials. A milestone in the field was the discovery of purely inorganic silicious zeolites [89], whose high porosity and thermal stability made them suitable for high-temperature gas phase reactions like petrochemical processes. However, zeolites have some drawbacks; the

structures are fixed and hardly modifiable, they can accommodate in their pores only a limited amount of transition metals and they cannot be analysed by crystallographic techniques due to their amorphous walls.

Metal-Organic Frameworks instead are crystalline porous material of a 2D or 3D networks<sup>[90]</sup>. They are composed of organic *linkers* and, interconnected by them, inorganic *secondary building units* (SBUs, also referred as *nodes*) of single metal ions, oxide-sharing metal ions or metal clusters (Figure 1.24). Their easy preparation and the high degree of tunability of connectivity, bridging ligands and pore size makes them promising materials for heterogeneous catalysis.

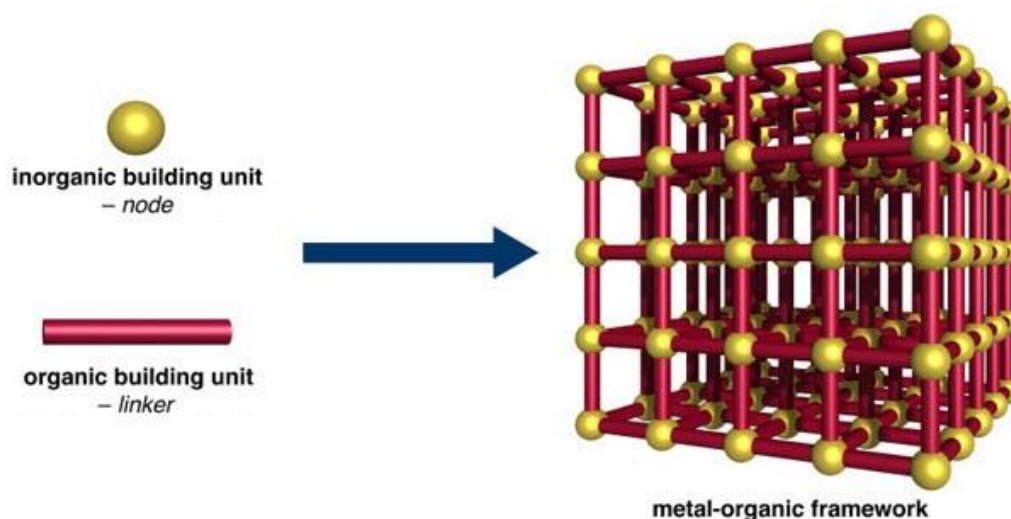


**Figure 1.24** Schematic figure showing the formation of a MOF.

The first MOFs were formed by metal cations and neutral ligands, making the resulting material cationic and requiring anions for charge balance. Moreover, the framework was very fragile and, after removal of solvent molecules present in the pores, the material was inevitably collapsing<sup>[91]</sup>.

A ground-breaking discovery was reported in 1999: more robust and porous MOFs were synthesized using dicarboxylate-based linkers<sup>[92]</sup>. These new linkers were anionic, forming stronger bonds with the cationic SBUs, and eliminating the need of charge-balancing anions. Since then, dicarboxylate-based MOFs have been studied most widely. Amongst them,



Zirconium-based MOFs have been demonstrated to be some of the most promising materials because of their enhanced chemical, thermal and mechanical stability.

### 1.3.2 UiO-type MOFs

In 2008, our research group reported the synthesis of the first MOF with Zirconium as SBU called UiO-66 and the UiO-isorecticular series of MOFs, UiO-67 and UiO-68 [93].

The SBU is composed by a cuboctahedral  $Zr_6O_4(OH)_4(CO_2)_{12}$  inorganic cluster. In the cluster, 6  $Zr^{4+}$  cations are arranged in an octahedron, and each of the 8 octahedron facets is alternatively capped by a ( $\mu_3$ -O) and ( $\mu_3$ -OH). Additionally, each neighbouring  $Zr^{4+}$  cation is bridged by a carboxylate group, for a total of 12 units. Each carboxylate is bidentate, bridging different clusters, allowing the formation of a face-centered cubic structure in which each cluster is linked to 12 others (Figure 1.25).

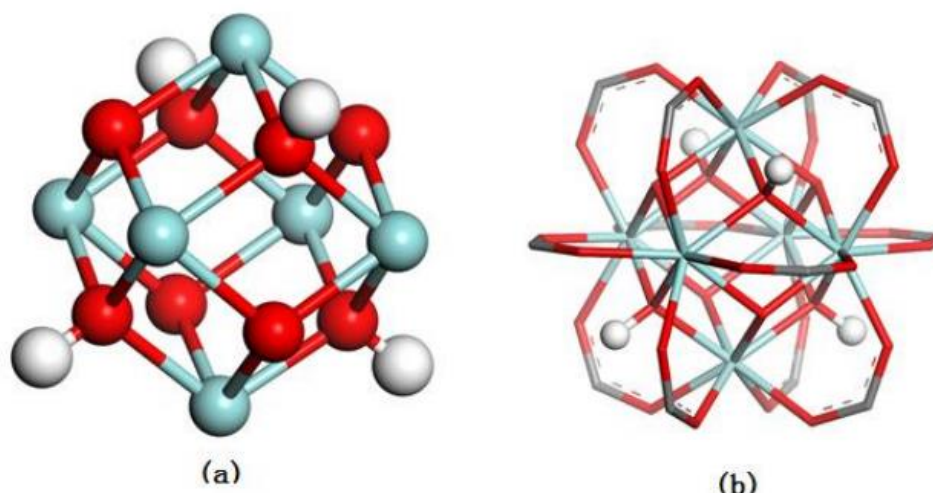


**Figure 1.25** (a) Inner core of the  $Zr_6$  cluster; (b) Cluster showing the carboxylates [93].

The MOFs differ in the dicarboxylates molecules: UiO-66, UiO-67 and UiO-68 have organic linkers terephthalic acid ( $H_2$ bdc), biphenyl-4,4'-dicarboxylic acid ( $H_2$ bpdc) and p-terphenyl-4,4''-dicarboxylic acid ( $H_2$ tpdc), respectively (Figure 1.26).

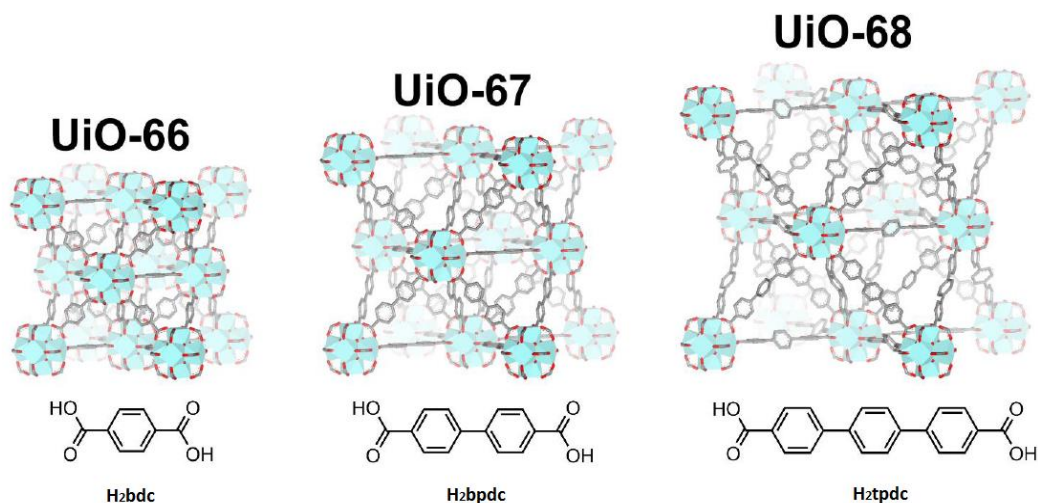


**Figure 1.26** The isoreticular series of UiO-MOFs and the corresponding linkers.

One of the advantages of UiO MOFs is that they can be functionalised and/or modified with other dicarboxylic acids (Figure 1.27). Different substitutions are achievable, and these new functionalities are exploited to tune the properties and applications of the resulting materials.

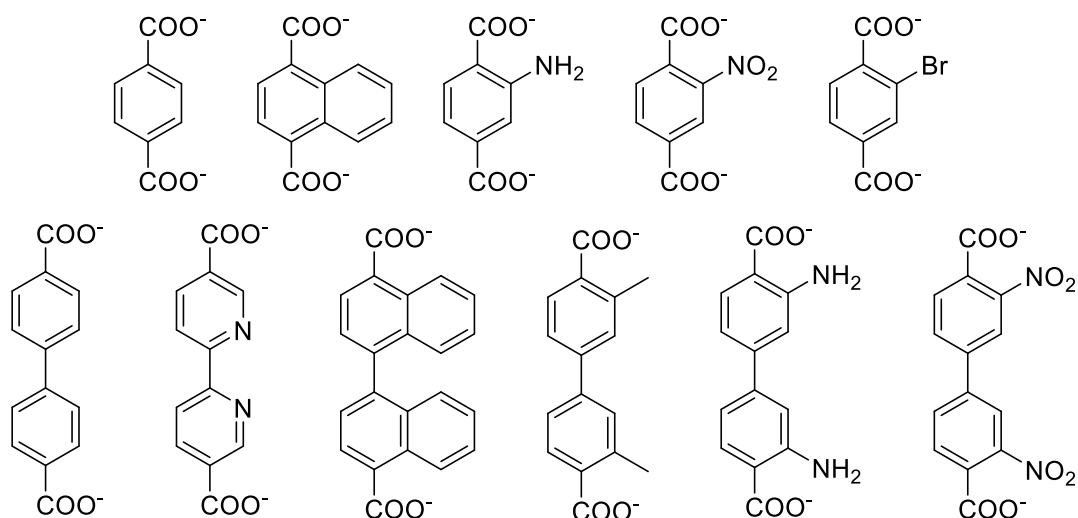


**Figure 1.27** Examples of dicarboxylate linkers used for the synthesis of UiO-66 and UiO-67.

The pore structure of the UiO-MOFs features two octahedral and a tetrahedral cage per cluster. The bigger octahedral cage shares its edges with other octahedral cages, while the smaller tetrahedral cage shares its facets with 4 different octahedral cages (Figure 1.28).

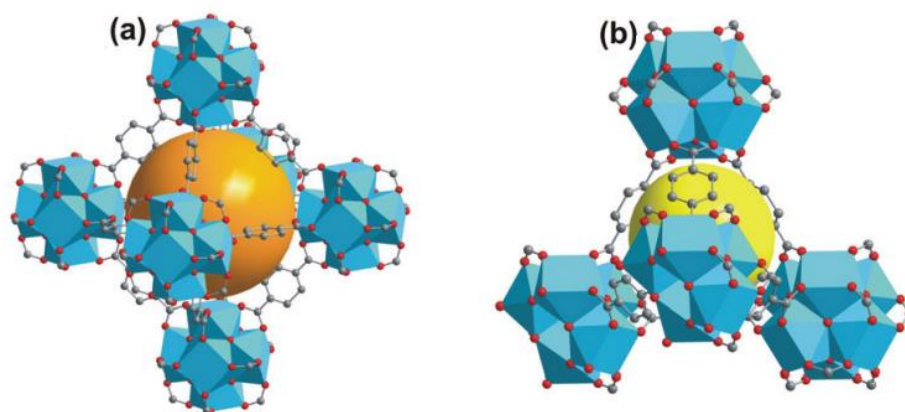


**Figure 1.28** The cages of UiO-MOFs: (a) octahedral; (b) tetrahedral <sup>[94]</sup>.

Thanks to its enhanced thermal (up to 540 °C under inert atmosphere) and water stability, UiO-66 has attracted the attentions of many research groups and is the most popular candidate for industrial applications of MOFs. UiO-67 has a reduced thermal stability (250-300 °C) but the porosity of the material increases from 1241 m<sup>2</sup>g<sup>-1</sup> to 3000 m<sup>2</sup>g<sup>-1</sup> <sup>[93]</sup>.

After the discovery of the UiO-MOFs, further Zr-MOFs have been characterized. The MIL-140 series is characterized by structures with one-dimensional porous channels instead of an open framework <sup>[95]</sup>, MOF-808 is based on 6-coordinated clusters and tricarboxylate linkers <sup>[96]</sup>, PCN-222 has 4-coordinated planar porphyrinic linkers <sup>[97]</sup>. Furthermore, Metal-Organic frameworks have been extensively studied for a wide range of applications like catalysis<sup>[98]</sup> gas storage <sup>[99]</sup>, separation <sup>[100]</sup>, electrical conductivity <sup>[101]</sup>, drug delivery <sup>[102]</sup> and fluorescence sensing <sup>[103]</sup>.

### 1.3.3 MOFs as molecular sponges

One of the many applications of MOFs exploits their high porosity as “molecular sponges”. Even if performed with different scopes and employing different MOF materials, some of the concepts of this application have been inspirational for the work performed in Chapter 2 and Chapter 3.

With the terms “molecular sponges” or “crystalline molecular flasks” the scientific community is referring to the ability of MOF frameworks to absorb molecules into their pores and arrange them in an ordered way in the crystal when soaked in a solution of a target molecule. The first

report of this application was published by Fujita in 2013 and was immediately recognized as a milestone for structure identification of molecules <sup>[104]</sup>.

X-Ray Single-Crystal Diffraction (SC-XRD) is the most reliable structure determination method. One of the limitations of the technique is the time-consuming trial-and-error procedure to find the most suitable crystal for the analysis. Moreover, powders or amorphous solids and even more liquid materials, oil or volatile matter, are not analyzable by SC-XRD. Conversely, the regular ordering of the molecules inside the framework can contribute to the Bragg peaks and a diffraction pattern. In this way this approach can overcome the limitations of SC-XRD and allow for the structure identification also of non-crystalline substrates.

The most employed MOFs for this application share a trigonal 2,4,6-tris(4-pyridyl)-1,3,5-triazine linker (tpt) coupled with  $ZnI_2$  or  $Co(NCS)_2$  metal salts (Figure 1.29). The linker has electron-poor heteroaromatic moieties that allow  $\pi$ - $\pi$  or CH- $\pi$  interactions and, when becoming part of the MOF framework, these properties are enhanced by the formation of “sticky” hydrophobic pores that absorb the target molecules via solvent-guest exchange.

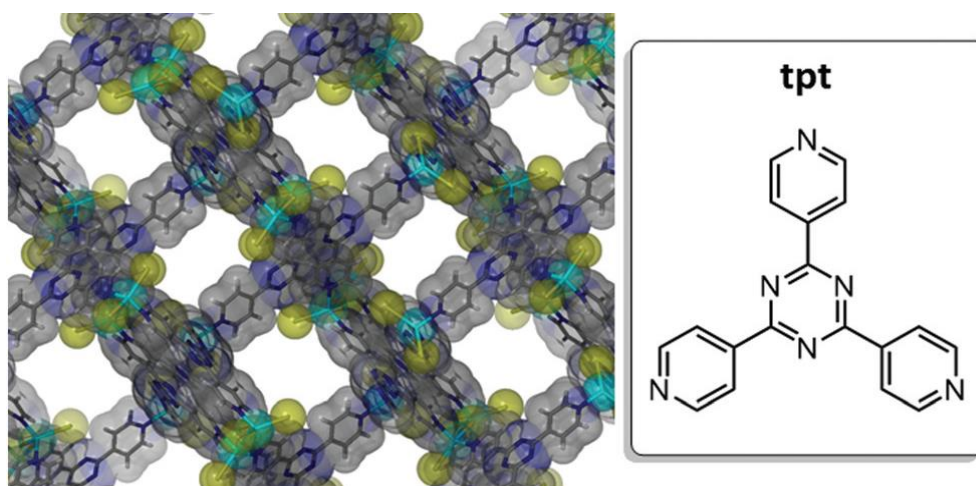


**Figure 1.29** On the left, representation of MOF  $[(ZnI_2)_3(tpt)_2] \cdot 6C_6H_5NO_2$ . On the right, structure of ligand tpt <sup>[105]</sup>.

The MOFs are synthesized in nitrobenzene, a toxic solvent with high affinity for the MOF framework. However, these MOFs showed high tolerance for structural deformation in response to the loss of solvent molecules, with no loss of crystallinity <sup>[106]</sup>. Solvent exchange with non-interacting cyclohexane yields a crystalline material which is ready for the guest soaking step. The easy exchange between cyclohexane and guest molecule enhances the uptake of the latter ones in an ordered way. As already stated, this method allows the

structure determination of a wide range of compounds as liquid materials, volatile matter and even complex natural products with challenging chiral structures.

The crystalline sponge method has even found applications in the chemical visualization of organic reactions. The crystallinity of the network facilitates the observation of reaction intermediates which are transient and non-isolable. This was also possible thanks to the advancements of time-resolved crystallography in which “snapshots” of a chemical process are taken with X-Ray diffraction experiments. Through this technique it was possible to observe processes on the femtosecond ( $10^{-15}$  s) timescale, like bond formations and changes of bond lengths.

In 2009 <sup>[107]</sup>, Fujita published a proof-of-concept of this approach in the simple liquid-phase reaction taking place inside a molecular sponge between an amine guest and an aldehyde reagent. Performing the reaction at low temperatures it was possible to have a crystallographic visualization of the hemiaminal intermediate (Figure 1.30).

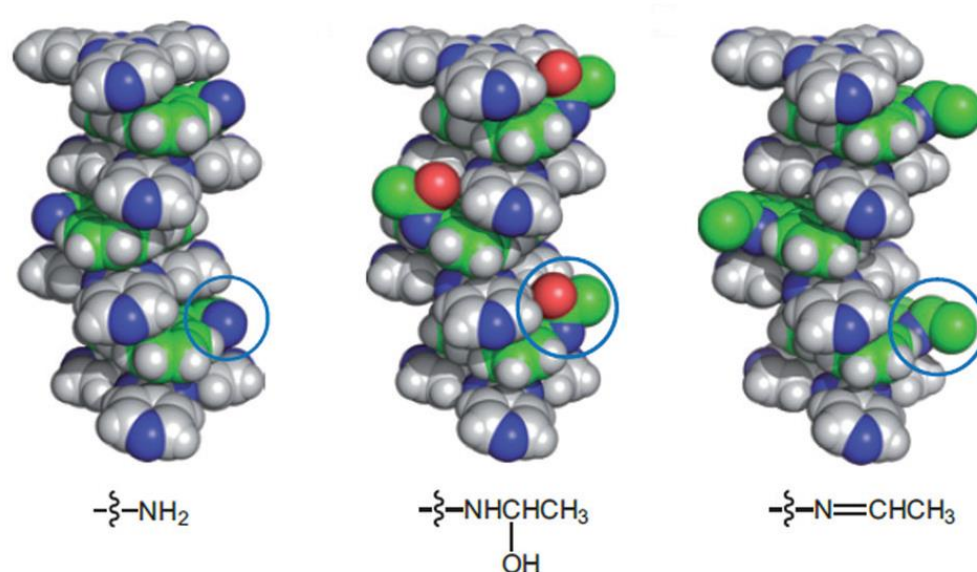
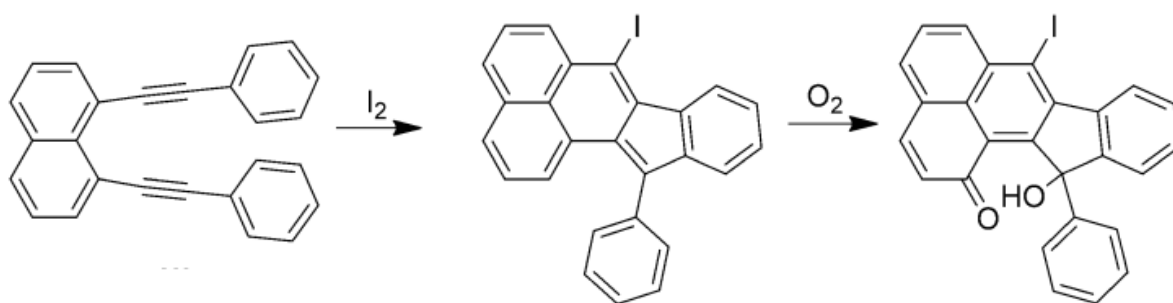


**Figure 1.30** X-Ray snapshots of the reaction between amine guest and aldehyde reagent <sup>[108]</sup>.

Even if MOFs have been largely exploited for gas phase processes, the use of gas-phase reagents by the crystalline sponge methods has been limited. Recently, a cyclisation reaction of a hosted dialkylnaphthalene guest catalyzed by iodine vapours has been reported <sup>[109]</sup>. The MOF with included guest molecule was put in a small glass vial and the vial inserted in a larger vial containing solid iodine crystals and sealed. A dramatic change in color of the MOF material from yellow to black was already observed after 12 hours, but only <5% conversion was

archived at that time. This could have been a sign that either  $I_2$  penetrated in the MOF before reacting, or that only the surface of the crystal had undergone reaction with  $I_2$ . The reaction was shown to reach completion after 7 days as proven by  $^1H$ -NMR analysis of the digested crystals. Through the SC-XRD of the MOF it was possible to identify the likely location of the cyclized product and assign its structure. Interestingly, a side-product was found by reaction of the cyclized main product and oxygen from air (Scheme 1.21). This result demonstrates the ability of the MOF to host not only the solvent-free cyclization of the starting material, but also consecutive gas-mediated reaction. The yield of the side product was higher compared to the yields reported in liquid-phase reactions.



**Scheme 1.21** Cyclization of the dialkylnaphthalene mediated by  $I_2$  and oxidation of the product mediated by  $O_2$ .

## Inclusion of Soai aldehyde in UiO-MOFs

### 2.1 Introduction

As discussed in Section 1.2.3, the confinement of reagents in the framework of a MOF has some advantages for organic reactions, such as protective effect and selectivity. It was envisioned that a different and innovative approach to gain insights into the Soai reaction mechanism would have been to exploit the confinement effect of a MOF (see Chapter 3 for a detailed motivation for the work).

In order to perform Soai reactions inside a MOF it was necessary to develop a method to include the substrate into the pores of the MOF and to exploit different analytical tools for the characterization of the resulting material.

This chapter will summarize the work performed on the inclusion of the Soai aldehyde in the UiO-MOFs and the obtained results.

### 2.2 Preliminary DFT analysis

Soai aldehyde **3c** was chosen as a substrate for the inclusion process. As stated in Section 1.1.5 and 1.1.8.1, aldehyde **3c** is considered by the scientific community the best performing substrate for the asymmetric autocatalysis with (+)-NLE, and the reaction can take place even under absolute conditions.

The size of aldehyde **3c** was found comparable to the size of the biphenyl dicarboxylate linker of UiO-67 and almost double in size compared to the terephthalic acid linker of UiO-66 (Figure



2.1). Moreover, the octahedral cages of the MOFs have been calculated being 16 Å for UiO-67 and 11 Å for UiO-66<sup>[93]</sup>: from these measurements the accommodation of **3c** in UiO-67 was believed to take place easily, while less space was available for **3c** in the smaller cage of UiO-66.

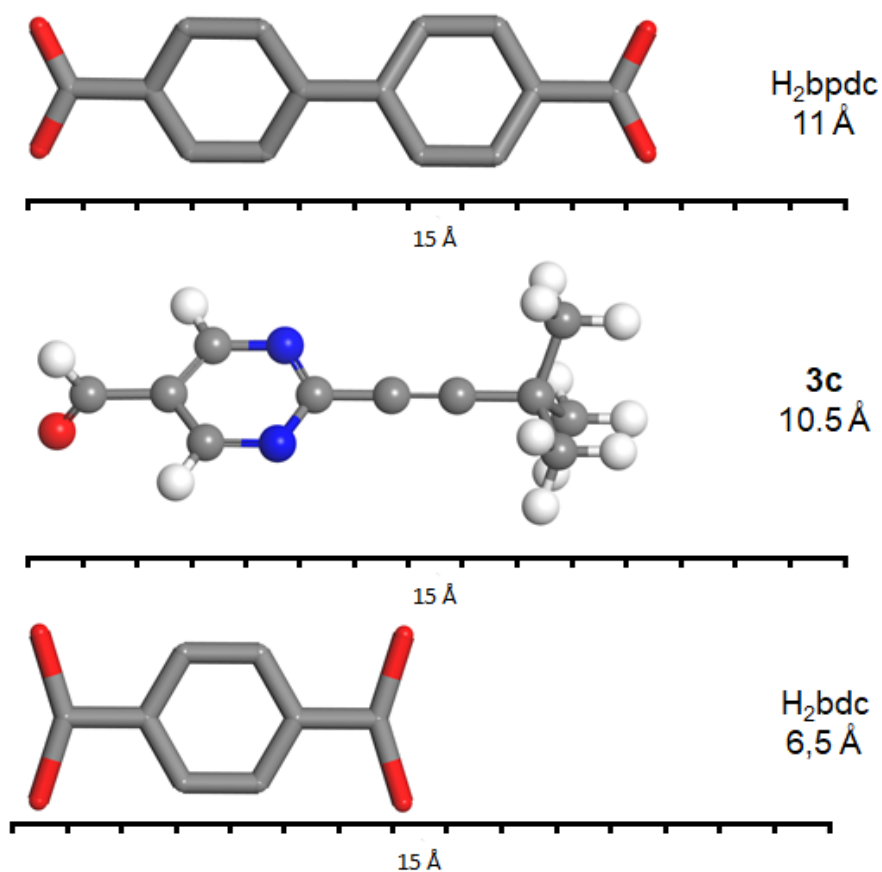


**Figure 2.1:** Size comparison between aldehyde **3c** (centre) and the linkers of UiO-67 (top) and UiO-66 (bottom)

To evaluate the feasibility of the inclusion process, periodic DFT calculations have been performed for predicting the position in which aldehyde **3c** would preferentially be located inside the unit cell of the MOFs. (Figure 2.2). For UiO-67, the optimized structure shows the aldehyde physisorbed in the octahedral cage of the framework. The interaction between aldehyde **3c** and the cluster is characterized by an H-bond between the hydrogen of the hydrated cornerstone of the MOF cluster and the oxygen of the carbonyl group of the aldehyde. The interatomic distance between H and O is of 2.161 Å, in line with the average distance in an H bond.



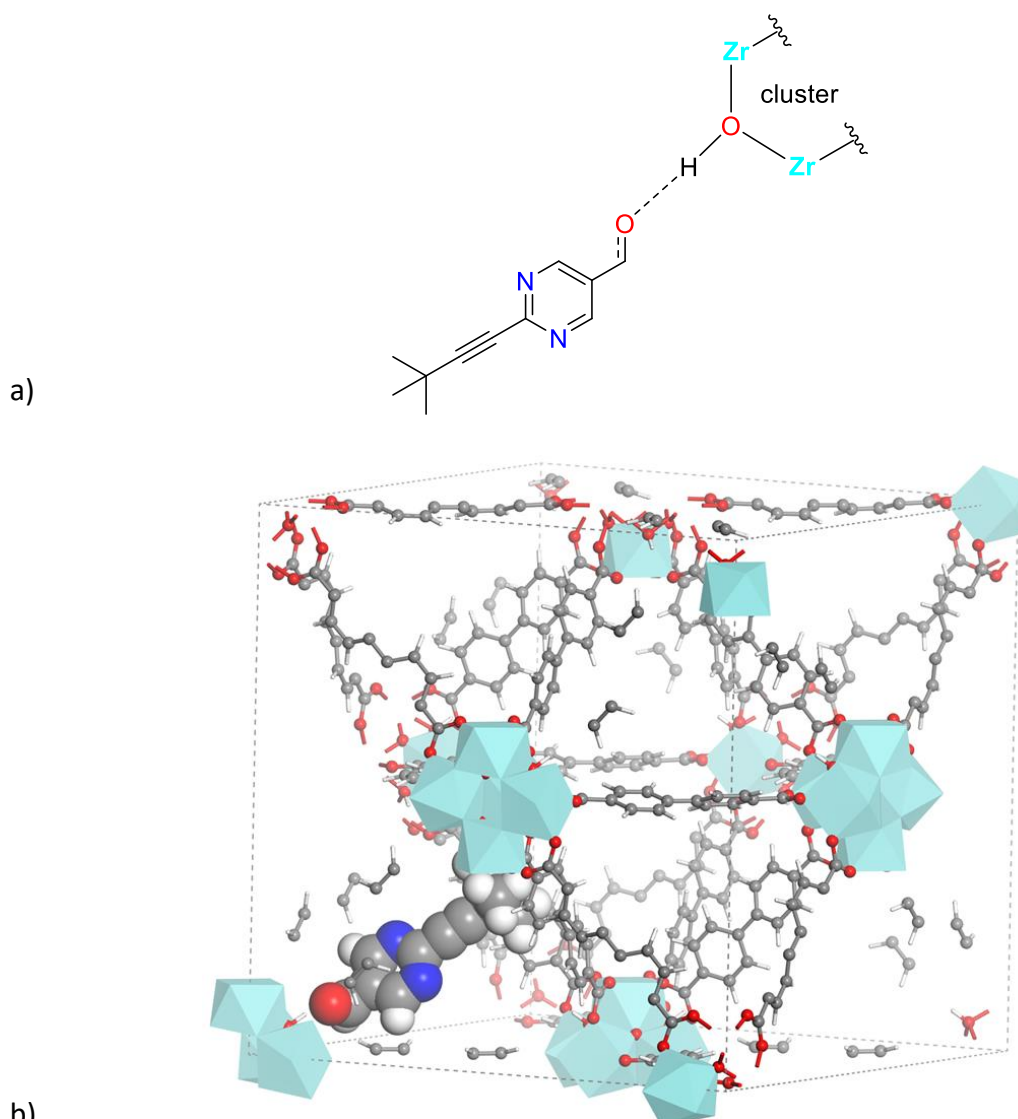


**Figure 2.2:** a) Simplified representation of the physisorption. b) Periodic DFT calculation of aldehyde **3c** inside UiO-67 MOF.

The same analysis has been performed on Soai aldehyde **3c** in UiO-66. As supposed, the DFT calculations show that the octahedral cages of this type of MOF is too small to accommodate the Soai aldehyde and high repulsions make the presence of aldehyde **3c** in the same position as in UiO-67 energetically disfavoured. In the most stable structure, the interactions between **3c** and the framework is mainly consisting of week van der Walls interactions with the organic linkers with no involvement of the clusters.

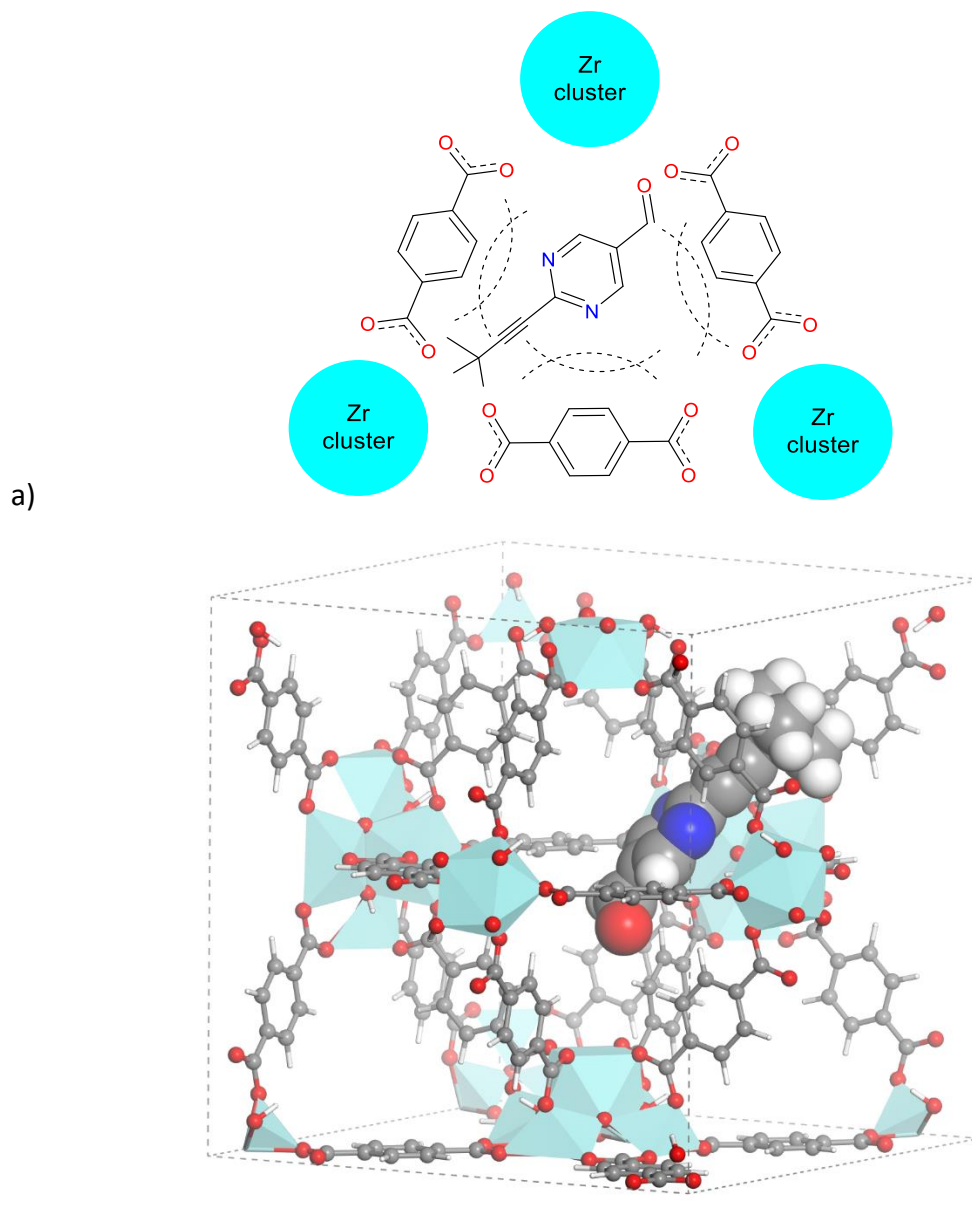


**Figure 2.3:** a) Simplified representation of the physisorption. b) Periodic DFT calculation of aldehyde **3c** inside the UiO-66.

### 2.3 The inclusion method

The inclusion of Soai aldehyde **3c** is performed soaking the MOF powder in a toluene solution of Soai aldehyde. Slow evaporation of solvent at room temperature gradually concentrates the guest molecule (aldehyde **3c**), which is forced to diffuse and crystallize inside the pores of the host (MOF).

After complete evaporation, the MOF powder is washed, filtered under vacuum and oven-dried (Figure 2.4).

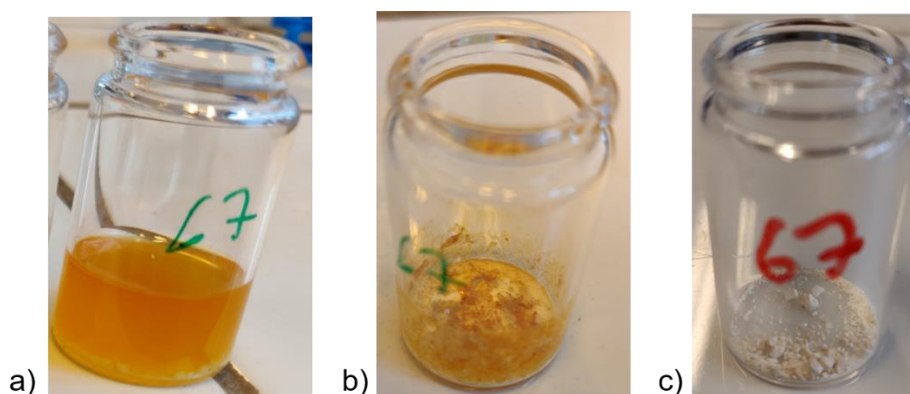


**Figure 2.4:** The inclusion steps: a) soaking MOF powder in aldehyde solution, b) MOF powder after evaporation of the solvent, c) MOF powder after washing and drying.

The washing process is a key step that removes the excess of aldehyde **3c** on the MOF surface, and not confined inside its pores. In order to confirm this, two samples respectively of washed and unwashed UiO-67 were soaked in an Ethyl Acetate solution and the leakage of aldehyde **3c** was monitored by HPLC (Figure 2.5). The presence of aldehyde **3c** in the solution of the unwashed MOF was already detected after few minutes and the concentration remained constant through the experiment. This can be attributed to the large excess of Soai aldehyde present on the surface of the MOF, unbound to the framework and immediately released into the solution. The concentration of aldehyde **3c** in the washed MOF, on the other hand, slowly increased throughout time, demonstrating a release and diffusion of Soai aldehyde from the inside of the MOF to the solution. Moreover, confronting the areas of the aldehyde peaks in the two experiments, the unwashed sample contains ca. 15 times more aldehyde than the

washed sample. This result is in line with a higher concentration of aldehyde **3c** in the unwashed MOF sample.

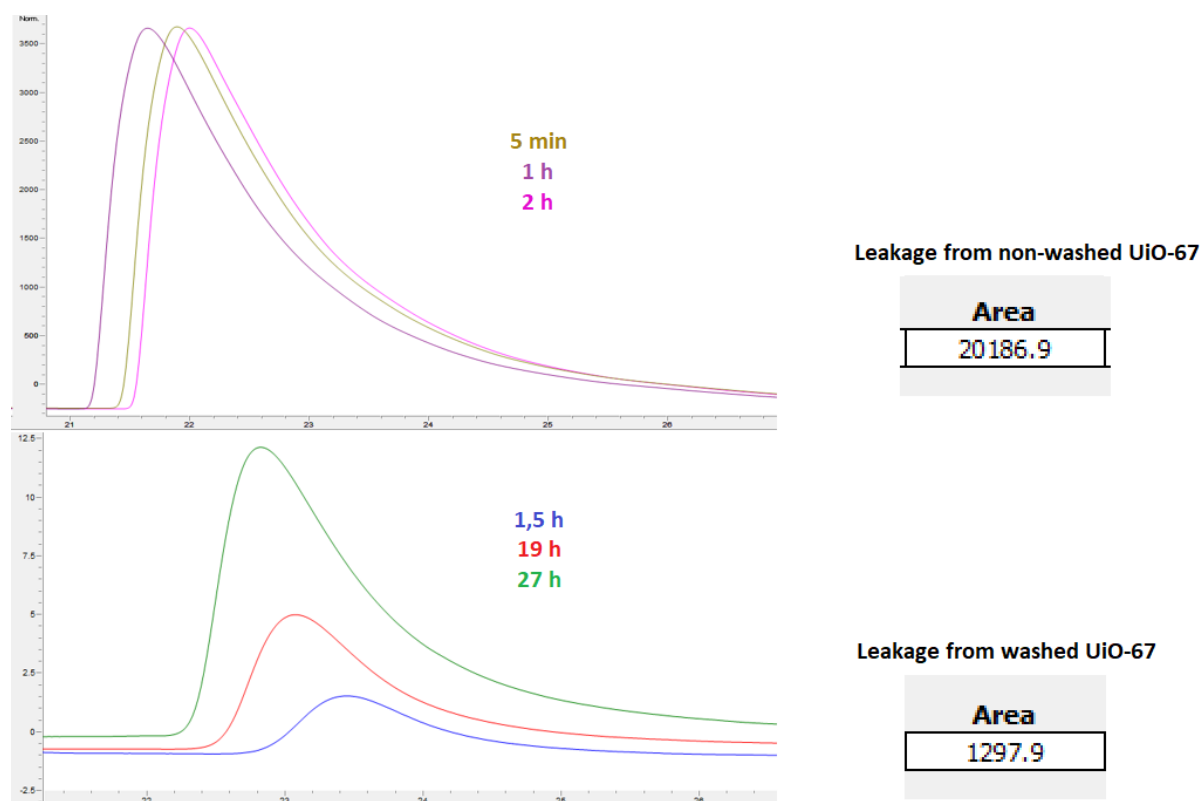


**Figure 2.5:** Leakage of aldehyde **3c** from unwashed and washed UiO-67.

PXRD analysis of the UiO-67 with included aldehyde **3c** showed no loss in crystallinity compared to the starting material (Figure 2.6). It was crucial to obtain a crystalline material after the inclusion step. In amorphous MOFs there is no long-range order within the structure; in such materials it would have been difficult to predict the position of aldehyde **3c**, and it is likely to believe that it probably have been located in only certain areas of the MOF framework. Consequently, in such a MOF it would have been difficult to exploit the confinement effect and to evaluate the influence of the framework on the reactions.

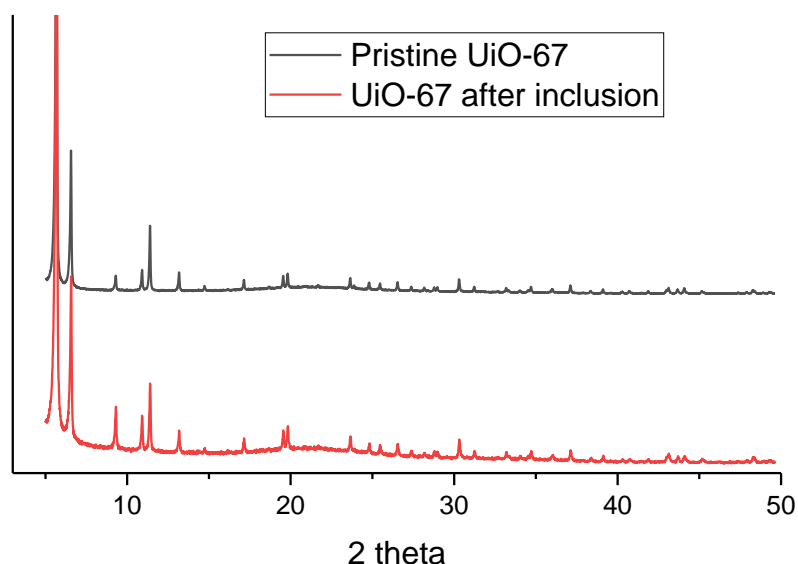


**Figure 2.6** PXRD before and after inclusion of aldehyde **3c**.

Unfortunately, it was not possible to resolve the structure of aldehyde **3c** inside the UiO MOFs through XRD analysis as performed with the MOF  $[(Zn)_3(tpt)_2] \cdot 6C_6H_5NO_2$  described in Section 1.3.3. Conversely for the crystalline sponge MOF, the structure of the UiO MOFs do not allow the guest molecules to be arranged in a regular and ordered way inside the framework, but rather in a random and disordered manner. In such materials, the XRD analysis would only allow to observe an average of all the possible positions in which aldehyde **3c** would be located in the framework.

#### 2.4 Infrared Spectroscopy analysis on the materials

The results of the leakage experiments were supporting the presence of the Soai aldehyde in UiO-67 after the inclusion and washing steps. In addition, ATR-IR analysis (Infrared Spectroscopy by Attenuated Total Reflectance) was performed on the materials. A series of diagnostic signals indicate the presence of aldehyde **3c** in the framework (red line of Figure 2.7). The signal at  $1700\text{ cm}^{-1}$  can be attributed to the stretching of the carbonyl group of Soai aldehyde **3c**, furthermore the peak around  $2200\text{ cm}^{-1}$  can be attributed to the C-N stretching of the aromatic ring while the C-H stretching of the terbutyl/isopropyl groups can be observed below  $3000\text{ cm}^{-1}$ . Interestingly, the O-H stretching of the hydroxyl groups of the clusters below  $3700\text{ cm}^{-1}$  in the pristine material are perturbed in the UiO-67 after inclusion. This behaviour of the material is in line with the interaction of Soai aldehyde **3c** with the MOF framework predicted by the DFT calculations.

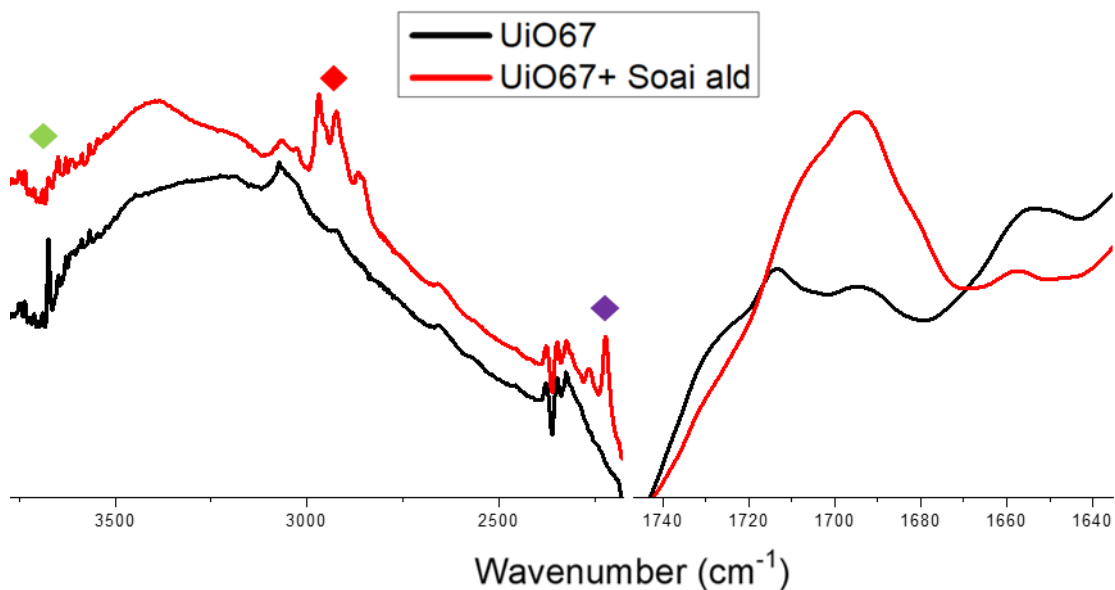


**Figure 2.7** IR analysis of UiO-67 and UiO-67 after inclusion of aldehyde **3c**. On the left, stretching of the hydroxyl groups (in green), stretching of the terbutyl/isopropyl groups (in red), stretching of the C-N of the ring (in purple). On the right, stretching of the carbonyl group.

The ATR-IR analyses have also been performed on a sample of UiO-66 before and after the inclusion (Figure 2.8). The previously discussed signals of the aldehyde in the framework are present in UiO-66 after the inclusion treatment (blue line). Moreover, aldehyde **3c** seems to be located in a different position in the framework of UiO-66 compared to UiO-67. This can be supported by the hydroxyl groups of the clusters not being perturbed in the sample after inclusion, meaning that they do not interact with aldehyde **3c**. Again, these observations are in agreement with the DFT calculations.

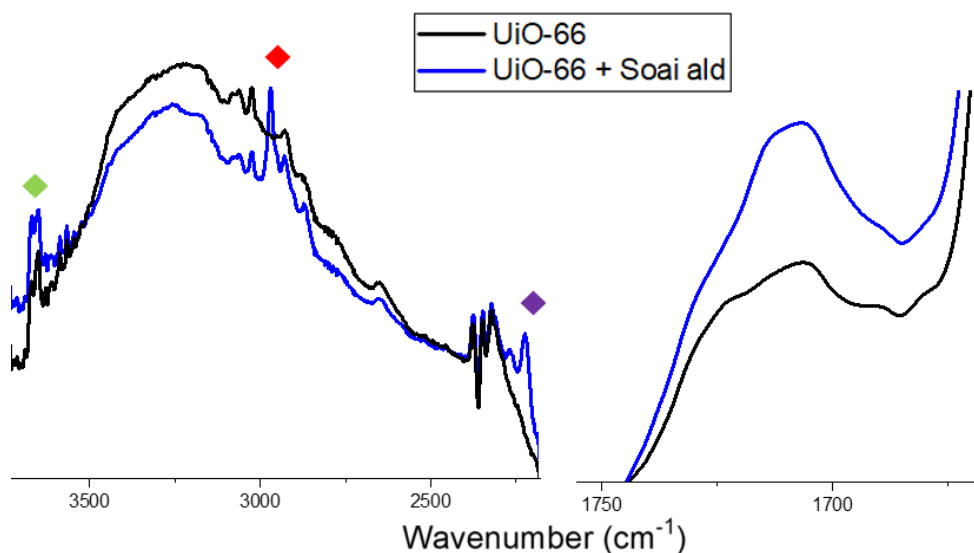


**Figure 2.8** IR analysis of UiO-66 and UiO-66 after inclusion of aldehyde **3c**. On the left, stretching of the hydroxyl groups (in green), stretching of the terbutyl/isopropyl groups (in red), stretching of the C-N of the ring (in purple). On the right, stretching of the carbonyl group.

Comparing the spectra of the two materials after inclusion (Figure 2.7 and 2.8, red and blue line), a slight shift to lower wavenumbers of the carbonyl stretching around  $1700\text{ cm}^{-1}$  in the UiO-67 is observed compared to UiO-66. Once again, this observation is in line with the hypothesis of an interaction of the carbonyl of the aldehyde with the clusters in UiO-67 not taking place instead in UiO-66.

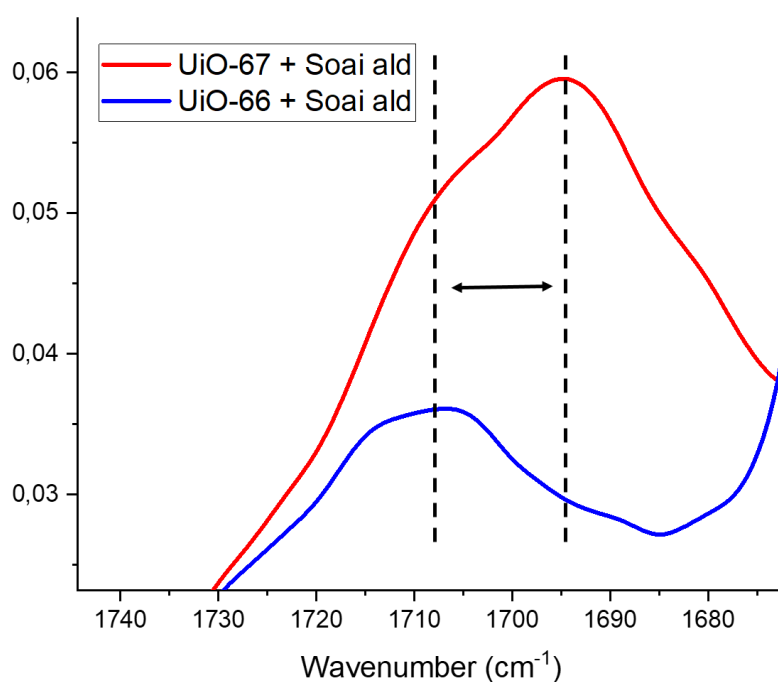


**Figure 2.9:** Carbonyl stretching in UiO-67 and UiO-66.

## 2.5 Quantification of the Soai aldehyde in the materials

In order to better understand the results of the reactions performed in the next chapter, it was essential to have an estimation of the quantity of Soai aldehyde **3c** included in the materials. Three methods were adopted for this purpose. These methods were not meant to find the real amount of included species in the material (which remains a debated issue even in the MOF community) but to find reliable methods to approximate the real value, and compare different MOFs. Of the three methods, only the third can be considered a direct method, while the first two do not analyse directly the material but rather other properties connected to it.

a) Soai aldehyde recovered after washing: In this method the amount of aldehyde **3c** recovered after the washing step is compared to the aldehyde **3c** employed for the inclusion step. Some of the aldehyde can be trapped in the filter pores, so this method can be employed only for a preliminary estimation of the inclusion.

b) Leakage experiment and HPLC analysis: The area of the aldehyde peak in the chromatogram is proportional to its concentration in the liquid sample and can therefore be used for a qualitative evaluation. However, it should be considered an indirect method because the concentration will only represent the fraction of aldehyde leaked from the MOF into the solution and not the real amount present in the powder sample. Depending on the material the leakage rate could vary, so the samples have been analysed various times over several weeks until a stable area was obtained and no further increase was observed.

c) MOF digestion and NMR analysis: The MOF with included Soai aldehyde **3c** is digested in a solution of  $D_3PO_4$  in  $DMSO-d_6$ . The acidic media dissolves the organic components of the MOF (linkers and aldehyde) while the inorganic portions precipitate as salts. NMR analysis allows to correlate the aldehyde signals with the signals coming from the linkers. This method can be considered a direct quantification of the amount of aldehyde in the material. Digestion processes are normally used in the MOF community to estimate a linker functionalization in the framework. In this case instead the estimation is made between the linkers and a molecule which is not part of the MOF, but rather a guest present inside the cavities, instead.



A first set of analyses was performed on three samples in which the inclusion of aldehyde **3c** had been performed with the same amount of UiO-67 powder and varied ratio of aldehyde, 2:1, 1:1 and 0,5:1 (in weight) respectively. The results obtained with the different methods are summed in Table 2.1.

**Table 2.1:** Comparison of quantification methods on UiO-67 and different amount of aldehyde **3c**

Entry	UiO-67 sample	Aldehyde recovered	Area of HPLC peak	Incorporation (NMR)
1	2:1 ratio	86%	25447	14%
2	1:1 ratio	88%	4013	3%
3	0,5:1 ratio	86%	1278	2%

The results indicate that the amount of aldehyde **3c** recovered does not give any valuable information on the amount of aldehyde in the material. The percentages are very similar and do not follow the trend of the other two methods. HPLC and NMR measurements are in agreement, even if the two methods evaluate different parameters. It is interesting to consider that Entry 2 is closer to Entry 3 in terms of amount of included aldehyde **3c** rather than being midway between the amounts incorporated using the ratios of Entries 1 and 3. The ratio of Entry 1 was chosen for all the following inclusions.

A second trial was performed with different UiO MOFs and a constant aldehyde/MOF weight ratio of 2:1. The UiO MOFs employed are UiO-67, UiO-67 bpy<sub>10%</sub>, UiO-67 binaphthyl and UiO-66. The UiO-67 bpy<sub>10%</sub> was of particular interest because the bpy linkers offered a possible second anchoring point to the Soai aldehyde in addition to the cluster. UiO-67 binaphthyl still shares the same pore size of UiO-67 type MOF but with a more hindered cavity, and it was interesting to investigate the amount of aldehyde **3c** it would be able to include compared to the much smaller cavity of the UiO-66 (Figure 2.10).

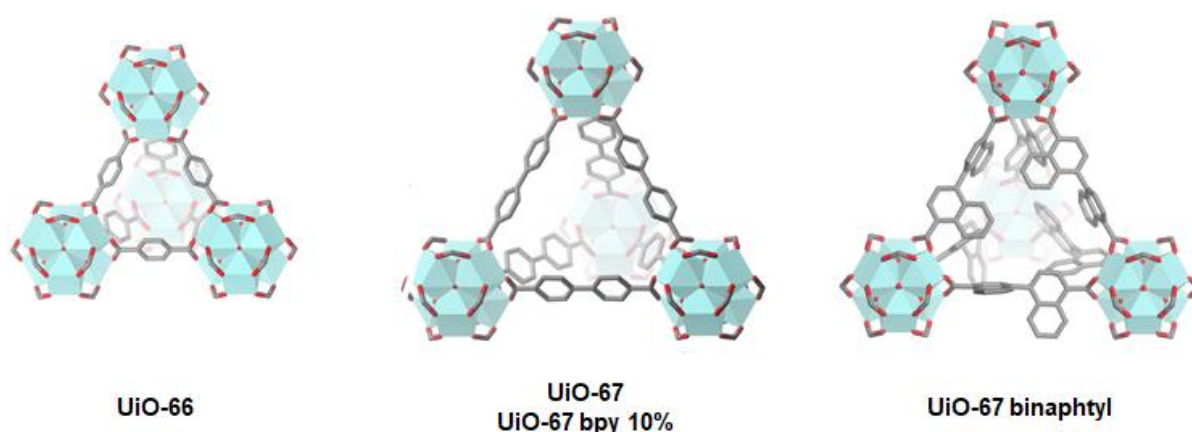


**Figure 2.10:** Comparison of the cavity of the four UiO-MOFs employed

**Table 2.2:** Comparison of quantification methods on different UiO MOFs and same amount of aldehyde **3c**

Entry	MOF sample	Aldehyde recovered	Area of HPLC peak	Incorporation (NMR)
1	UiO-67	83%	18846	19%
2	UiO-67 bpy <sub>10%</sub>	76%	31698	31%
3	UiO-67 binaphthyl	84%	22299	25%
4	UiO-66	89%	4370	14%

Table 2.2 summarizes the results obtained. In this investigation, once again, the recovered aldehyde does not follow the trend of the other two methods. In line with the hypothesis previously reported, UiO-67 bpy<sub>10%</sub> was the UiO-MOF in which the highest amount of aldehyde **3c** was located. On the other hand, UiO-66 was the one with the lowest amount of guest inclusion. Interestingly UiO-67 binaphthyl, characterized by a more hindered cage, is able to allocate a slightly higher amount of Soai aldehyde compared to UiO-67. This could be explained by  $\pi$ - $\pi$  interactions between the naphthyl rings of the linker and the pyrimidine rings of aldehyde **3c**.

It is important to point out that Entry 1 of Table 2.1 and Entry 1 of Table 2.2 refer to an inclusion made with the same batch of aldehyde **3c** and UiO-67 and at the same conditions, yet the results are different in all parameters. Apart from the examples reported in the chapter, repeated inclusion processes have shown a vast variability of results. In one case for instance, the amount of aldehyde **3c** in UiO-67 was found to be even lower than in UiO-66. The inclusion process seems to suffer from reproducibility issues, and analyses on the material had to be

repeated after every inclusion in order to select the MOF materials with the higher amount of **3c** to perform the reactions reported in Chapter 3.

## **2.6 Conclusions**

In this chapter, a method for the inclusion of Soai aldehyde **3c** in UiO-type MOFs is described. Despite the simplicity of the procedure, a high variability of results is archived. Anyhow, two reliable methods for the qualitative evaluation of the amount of included **3c** are presented (direct and indirect).

The work performed in this chapter has been published in **Paper I**. Additional supporting informations for unpublished experiments can be found in **Appendix II**.

# The use of UiO-MOFs for vapour phase Soai reactions

---

## 3.1 Introduction

The materials obtained and analyzed in Chapter 2 had the potential to be employed for a variety of reactions. A first approach envisioned was to perform liquid phase Soai reactions adding  $\text{Zn}(\text{iPr})_2$  to a suspension of solvent and MOF with included Soai aldehyde. Nevertheless, this approach had some drawbacks, the main one being the leaking of Soai aldehyde from the MOF to the solution. With this reaction procedure, it would have been impossible to discriminate whether the reaction had happened outside or inside the MOF.

In order to prevent the leakage problem, it was thought that a better solution would have been a reaction system in which MOF powder and solvent could not come in contact and lead to the leakage of the guest molecules. A vapour phase reaction setup has then been developed and employed for the reactions of this chapter.

## 3.2 Reaction setup and concept of reactivity

Two different experiment setups have been employed for the vapour phase reactions. In the one presented in Figure 3.1a, from now on called “the single cylinder setup”, the Soai reagent (pristine aldehyde **3c** or UiO MOFs containing aldehyde **3c**) is placed on the top of a cylindrical glass support, the support arranged inside a glass vial.  $\text{Zn}(\text{iPr})_2$  solution in Toluene is added on the bottom of the vial under inert atmosphere. The vial is immediately sealed after the addition. The experiments were firstly conducted inside a glove box to be sure that no oxygen

could be present in the vial after the sealing of the cap, but later it was found out that the inert atmosphere in the vials could be recreated also under a normal laboratory fume hood. In the second setup (Figure 3.1b), from now on the “three cylinders setup”, up to three cylindrical glass supports containing the reagents were located in a bigger vial. For this setup all experiments were conducted inside a glove box.

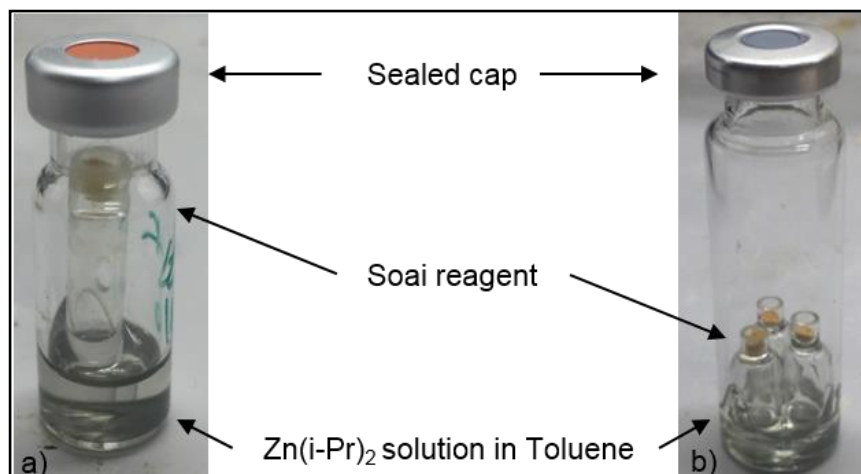


**Figure 3.1:** Vapour phase reactions setups

Soai had already demonstrated the feasibility of heterogeneous reactions employing solutions of Zn(*i*Pr)<sub>2</sub> in Toluene. A control experiment to test the volatility in our reaction vials was conducted with the single cylinder setup. The reaction was performed with **3c** as Soai reagent and Toluene-d<sub>8</sub> as solution on the bottom (without any Zn(*i*Pr)<sub>2</sub> added). After few hours the solid aldehyde **3c** had turned into an oil, and analysis of the crude revealed the presence of Toluene-d<sub>8</sub> in the mixture. At the same time, NMR analysis of the Toluene-d<sub>8</sub> solution on the bottom of the vial showed the presence of aldehyde **3c**. This experiment demonstrated how Toluene-d<sub>8</sub> and aldehyde **3c** had reached their vapour pressure and mixed through vapour diffusion. It confirmed the feasibility of these setups and surprisingly showed how even **3c** could pass from solid to the vapour phase and then to liquid phase (Figure 3.2).

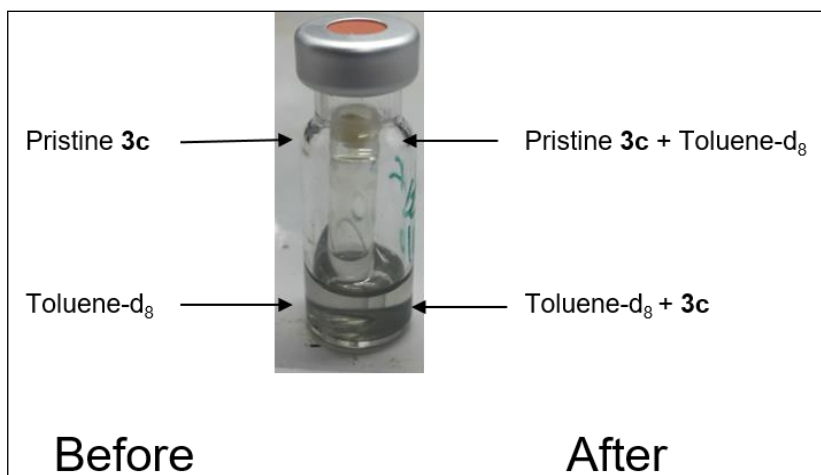


**Figure 3.2:** Scheme of the control experiment

The interesting aspect in this unusual approach to perform the Soai reaction lies in the confinement effect that the UiO-type MOFs imposes on the reactive complexes relevant for the propagation of chiral amplification. In a liquid phase reaction the dimers, tetramers or higher oligomers supposedly involved in the catalytic cycle of the Soai reaction are free to propagate in three dimensions without any hindrance. Inside a MOF instead, the diffusion of these species should be limited by the size of the cavities and compartmentalization, which could affect reactivity and reaction outcome. It is intuitive to think that the MOF cavities should not be able to allocate the catalytic species efficiently and be an obstacle to their propagation, especially in absence of solvent as in the vapour phase setup. These confinement effects could affect reactivity and reaction outcome. Also, the reaction takes place in absence of any chiral trigger. As already demonstrated (Section 1.1.8.1), Soai aldehyde **3c** is able to perform the asymmetric autocatalysis with (+)-NLE in absence of chiral triggers (absolute asymmetric catalysis) both in solution <sup>[80]</sup> and under the heterogeneous conditions of the vapour phase setup <sup>[87]</sup>.

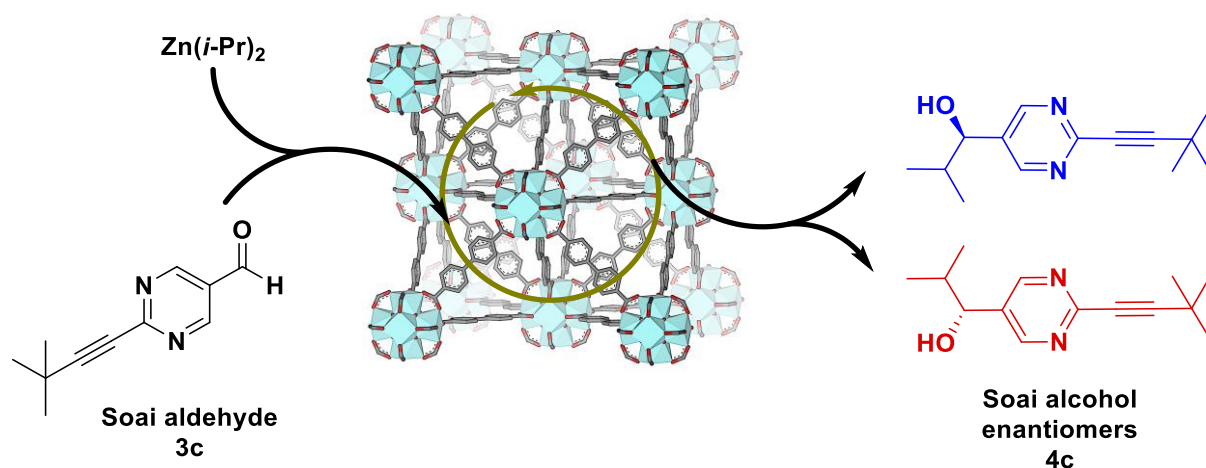


**Figure 3.3:** Scheme of the vapour phase Soai reaction performed inside the UiO MOFs

### 3.3 Preliminary results and screening of different UiO MOFs

In the reaction setups of Figure 3.1, the designed glass support can only fit a limited amount of material (maximum 6 mg). Unless otherwise stated, an excess of  $\text{Zn}(i\text{Pr})_2$  solution in Toluene has been employed in both setups (15-20 equiv.).

Firstly, the reactivity of the Soai aldehyde in three different materials has been studied. Pristine Soai aldehyde **3c**, unwashed UiO-67 with included aldehyde **3c** and washed UiO-67 with included aldehyde **3c** have been tested using the three cylinders setup. In terms of conversion, the washed MOF sample had a slightly lower conversion compared to the other two samples. However, the final ee% of the washed MOF was much lower (Table 3.1). The results complement the observations made on the leakage experiments in washed vs. unwashed UiO-67 (Section 2.3). In the latter material, the excess of loosely bound aldehyde **3c** on the surface of the unwashed sample reacts with  $\text{Zn}(i\text{Pr})_2$  in the same way as pristine Soai aldehyde powder. The final ee is similar to the reaction performed on pristine **3c** and making the presence of the MOF unimportant. In contrast, the washed UiO-67 features no aldehyde on the surface and the reaction to yield alcohol **4c** takes place only inside the pores of the MOF. The low ee% is a direct consequence of the reaction taking place in a confined space. The fact that the reaction takes place in absence of any chiral trigger is confirmed by the randomness of the preferred enantiomer obtained from the same batch of aldehyde **3c** and  $\text{Zn}(i\text{Pr})_2$  under the same reaction conditions.

**Table 3.1:** Vapour phase reactions on three different substrates

Entry	Substrate	Enantiomer	ee%	Conversion
1	Pristine Soai aldehyde	(R)	88%	99%
2	Non washed UiO-67	(S)	70%	98%
3	Washed UiO-67	(S)	38%	82%

Different MOFs in the UiO series were screened for the vapour phase reactions with the single cylinder setup. The amount of Soai aldehyde included in the materials had been evaluated beforehand through the leaking experiment and HPLC analysis, and is shown in Figure 3.4.

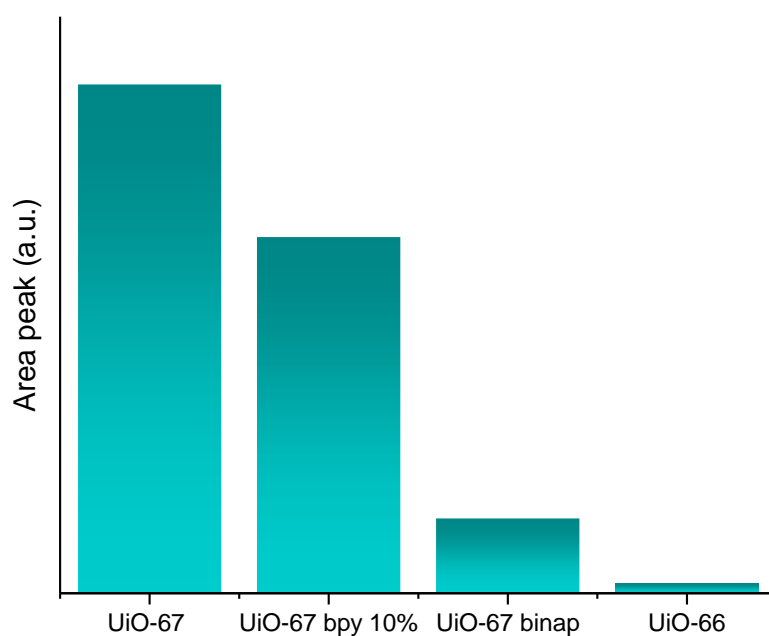


**Figure 3.4:** Amount of **3c** included in different UiO MOFs used for vapour phase reactions (determined by HPLC)

Three different  $\text{Zn}(i\text{Pr})_2$  batches were employed on the same starting materials. In parallel, the zinc solution of a same batch was added to each sample and all reactions were stopped after 7 days. The results are shown in Table 3.2.



**Table 3.2:** Screening of different UiO MOFs to the vapour phase reaction

Soai reagent	Zinc batch 1	Zinc batch 2	Zinc batch 3
Pristine	ee% = 93% conversion = 99%	ee% = 92% conversion = 99%	ee% = 94% conversion = 99%
UiO-67	ee% = 23% conversion = 93%	ee% = 30% conversion = 93%	ee% = 14% conversion = 92%
UiO-67 bpy <sub>10%</sub>	ee% = 18,5% conversion = 81%	ee% = 26% conversion = 86%	ee% = 48,5% conversion = 89%
UiO-67 binaphtyl	ee% = 21% conversion = 80%	ee% = 43,5% conversion = 71,5%	ee% = 28,5% conversion = 82%
UiO-66	ee% = 32% conversion = 55%	ee% = 35,5% conversion = 51%	ee% = 16,5% conversion = 43,5%

Legend: (R)-enantiomer / (S) – enantiomer obtained in higher percentage

The decrease of *ee* in the MOF samples compared to the pristine Soai aldehyde can be explained by the confinement effect of the framework of the MOF: the oligomeric species involved in the catalytic cycle are not free to propagate in a 3D fashion. Thus, autocatalysis is probably confined to several reaction compartments, and the final *ee*% is an average of the autocatalytic cycles happening in local portions of the MOF. The lower conversion of the UiO-66 samples could be explained by the even more difficult propagation of the catalytic species in the smaller cavities of the MOF. In contrast, all aldehyde molecules are in contact with each other in the pristine Soai aldehyde **3c** and part of the same catalytic cycle.

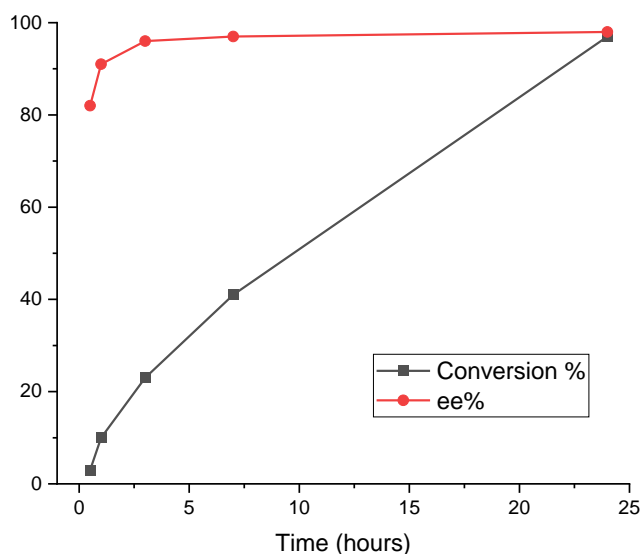
In absence of a chiral inductor, the UiO MOFs provide enantiomers of the Soai alcohol **4c** following a random distribution, a typical feature of an Absolute Asymmetric Synthesis. Moreover, the distribution of the final *ees* obtained from the reactions performed on the MOF materials seems to indicate the absence of any local chirality in UiO series. Considering the 15 reaction performed, (*R*)-**4c** was the enantiomer preferentially formed, but this could hardly reflect a *pro-R* orientation of the Soai aldehyde and be more probably just a stochastic result due to the small number of experiments performed. Disappointingly, even in the UiO-67

binaphtyl, a MOF characterized by a prochiral orientation in space of its linkers, no preferential formation of a specific enantiomer, or a higher ee%, was observed. Lastly, no influence of the three different Zn batches were observed.

### 3.4 Kinetic plots of the vapour phase reactions

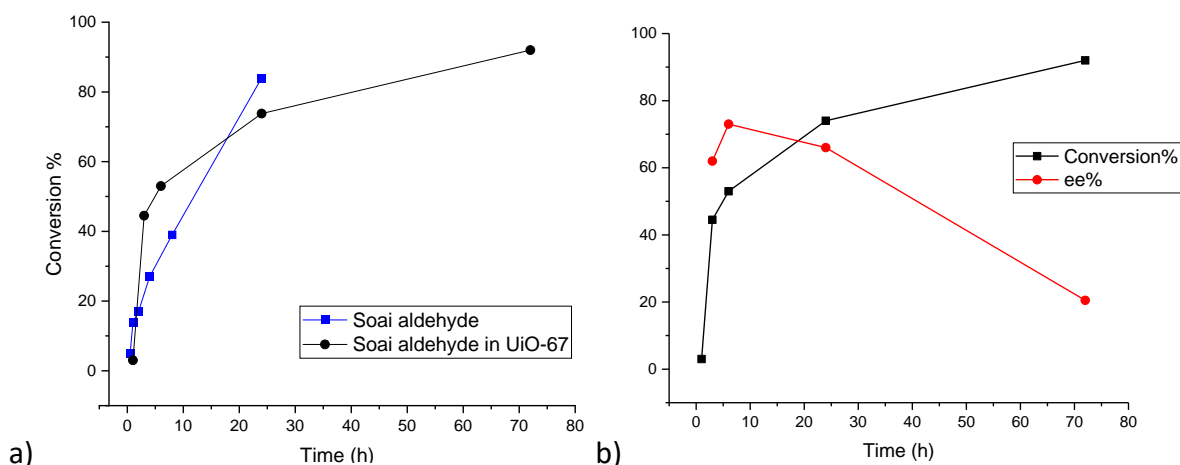
After having understood the behaviour of the different MOFs in the Soai reactions, the next step considered was to check the evolution of both conversion and ee% over time for the vapour phase reactions. However, the reaction setup employed did not allow to sample the reaction: the piercing of the sealed rubber cap would result in contamination of the inert atmosphere in the vial, with lowering of the vapour pressure of the reagents and decomposition of the  $\text{Zn}(i\text{Pr})_2$  in the solution due to oxygen and moisture. The only way to perform these analyses was starting simultaneously a number of reactions and stopping them at fixed time points. A drawback of this approach is that the results can show a high variability, especially for reactions with reproducibility issues like the Soai reaction.

At first, the analyses have been made using the single cylinder setup. Pristine Soai aldehyde **3c** was tested firstly and the analysis showed a rapid and almost linear conversion into alcohol **4c** starting from the first sample after 30 minutes, reaching 97% conversion after 24h (Figure 3.5). The ee values were found constantly high already from the first sample, with apparently no induction period.



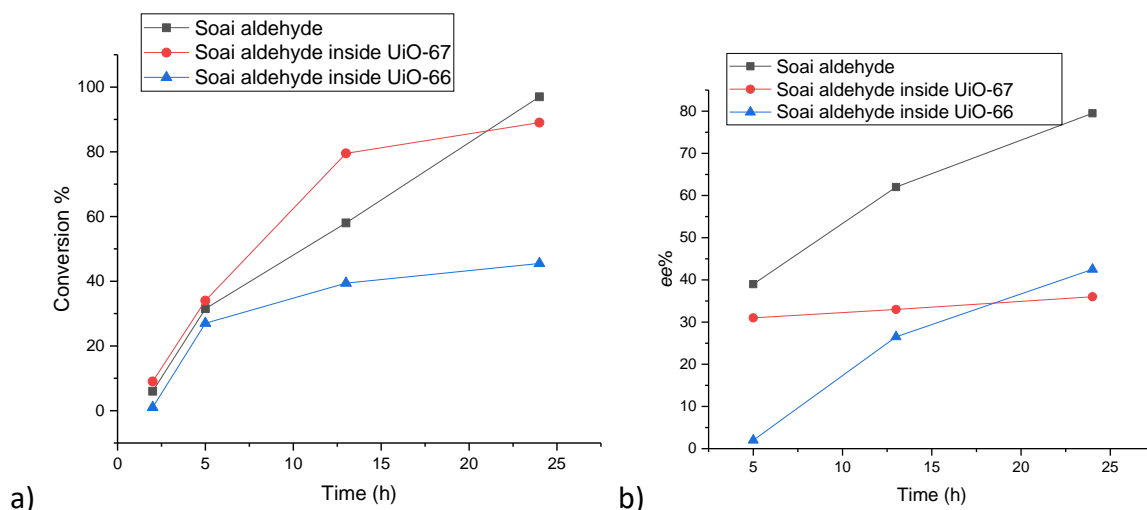
**Figure 3.5:** Kinetic plot of pristine Soai aldehyde **3c**.

Figure 3.6 shows the results for **3c** included in UiO-67. Plotting the data previously obtained in the pristine aldehyde **3c** (blue line in Figure 3.6a) against the ones in the MOF (black line in Figure 3.6a), the conversion seems to proceed at a faster rate in the MOF than in the pristine material in the first 20 hours. High *ee* values were found in the early samples, but the final *ee* (after 72 h) was around 20%, in line with the values reported in Table 3.2.



**Figure 3.6:** a) Conversion in pristine aldehyde **3c** vs. UiO-67 b) conversion and *ee*% in UiO-67.

The experiments have been repeated with the “three cylinders setup” with samples of pristine aldehyde **3c**, aldehyde **3c** included in UiO-67 and aldehyde **3c** included in UiO-66. This setup was used to improve reproducibility by ensuring identical reaction conditions for all materials placed in the single vial. The comparison of materials from different vials can still be affected by reproducibility issues and be less meaningful, but the results for the three materials in the same reaction setup are comparable. Conversion and *ee*% obtained in the three different samples have been plotted in Figure 3.7.



**Figure 3.7:** a) Conversion in the three materials b) ee% in the three materials

Even if performed with different setups, the conversion plot confirms the trend observed in the previous analysis. The conversion in the UiO-67 is faster than in the pristine material in the first 20 hours. This could be attributed to one of the properties that make MOFs such interesting materials for catalytic applications: the ability to store gasses. The  $\text{Zn}(i\text{Pr})_2$  in the vapour phase is efficiently trapped and concentrated by the MOF framework, allowing a more rapid conversion than in the pristine material. However, it is important to point out that there is no information at the moment about the physical phase in which  $\text{Zn}(i\text{Pr})_2$  is stored inside the MOF (gaseous, liquid or solid) and in which phase it reacts with the Soai substrate. The conversion in UiO-66, as already shown in Table 3.2, reaches a lower value compared to the other MOFs. The ee values for **3c** included in the MOF samples slowly increased through time, but were always found to be lower than in the pristine aldehyde **3c**. Unlike the results of Figure 3.5 in which the ee of aldehyde **3c** was found constantly higher than 80%, in these analyses it increased through time starting from 40%: in this case a possible explanation could be the different size of the reaction setup employed for the analyses.

After these analyses, the interest moved towards the reaction kinetic in UiO-67 bpy<sub>10%</sub>. Again, the three cylinders reaction setup was employed to compare the kinetic profile of the reactions in pristine aldehyde **3c**, aldehyde **3c** included in UiO-67 and aldehyde **3c** included in UiO-67 bpy<sub>10%</sub> (Figure 3.8).

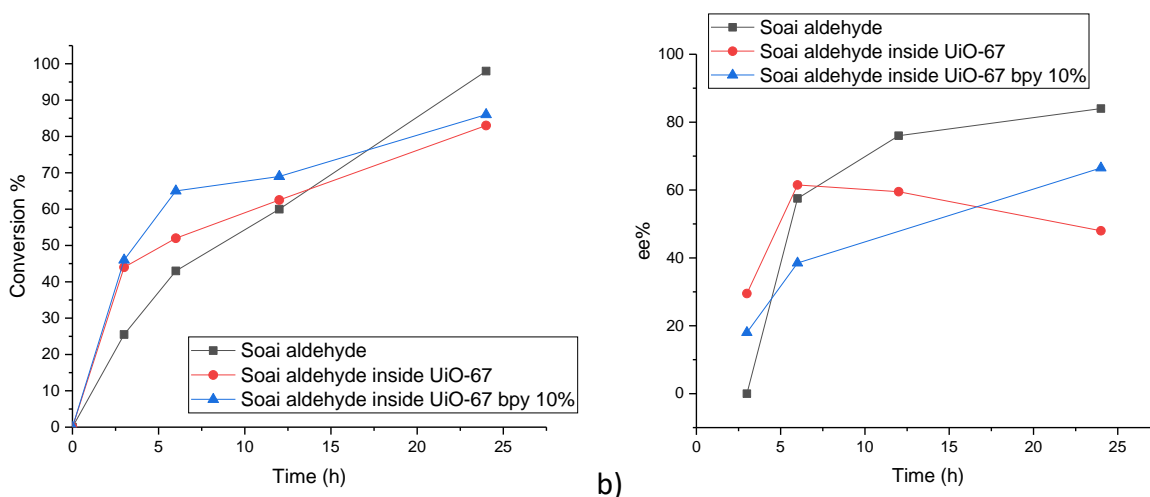


**Figure 3.8:** a) Conversion in the three materials b) *ee*% in the three materials

The kinetic plots of the conversion demonstrate a higher initial rate for the reaction confined in UiO-67 bpy<sub>10%</sub> compared to UiO-67. A possible explanation could be the additional coordination point for the zincorganil reagent offered by the bipyridine linkers that coordinate and help to store more Zn(*iPr*)<sub>2</sub> vapours. The *ee* values for **3c** confined in the MOFs were found constantly lower than in the pristine sample with few exceptions in the early samples.

In summary, the kinetic plots showed good accordance between the results obtained with different setups in terms of conversion, and a great variety in terms of *ee*%. The final *ees* from reactions in the MOF samples were almost constantly found lower than in the pristine **3c**.

### 3.5 Attempts to optimize the reaction parameters

As stated previously, low *ees* were observed in all vapour phase reactions performed inside the UiO MOFs. This could be explained by multiple autocatalytic cycles taking place in different compartments of the MOF and in different crystals.

As demonstrated by Soai in his work <sup>[80b]</sup>, in order to get high amplification of *ee*% in the Soai reactions performed in solution under absolute conditions, alcohol **4c** obtained from a first reaction is used as a seed (2-10 mol%) for another reaction, and after a variable number of reaction cycles high *ee*% is obtained. In a certain way, the seeding alcohol **4c** is “diluted” in larger and larger amounts of aldehyde **3c**, and the efficiency of the amplification improves accordingly. It was thought that, in a similar way, the amount of aldehyde **3c** was a crucial parameter that could lead to a higher improvement of the final *ee*% in the vapour phase

reactions performed inside the MOFs: the more aldehyde is present in the reaction, the more aldehyde enters in the catalytic cycle and the better the *ee*%. The following experiments tried to prove this concept. The three cylinders setup was employed in all the experiments of this section.

In a first attempt the reactions were performed employing different amounts of UiO-67 with included aldehyde **3c**. As shown in Table 3.2, the results in terms of conversion and *ee*% are similar in all samples. These results illustrate how, even if the amount of aldehyde **3c** surely increases in the three reactions proportionally to the amount of MOF, this is not affecting the reaction outcome. This could be due to the impossibility of the catalytic cycles in the different compartments of the MOF to communicate with each other, or even to “migrate” from one crystal to another, making the presence of more or less MOF, and consequently aldehyde **3c**, uninfluential.

**Table 3.2:** Vapour phase reaction on different amount of UiO-67

Amount of UiO-67	Enantiomer	ee%	Conversion
1,5 mg	(R)	43%	95%
3 mg	(R)	44%	91%
6 mg	(R)	46%	88%

On the basis of previous results, it was thought that probably it was not the amount of MOF powder, but instead the amount of Soai aldehyde in the MOF that could play a crucial role in the reaction. UiO-67 with different amounts of included aldehyde **3c** have been employed. The amount of aldehyde **3c** has been evaluated by HPLC and NMR analysis (Table 3.3). In these samples the load of aldehyde presents in the material seemed more widespread with the HPLC method, but instead not a great difference was found through NMR analysis between Sample 2 and 3.

**Table 3.3:** Amount of **3c** in three different samples of UiO-67

UiO-67 sample	Area of HPLC peak	Incorporation (NMR)
1	1540	3%
2	7438	10%
3	12960	12%

The results of the experiments in Table 3.4, show how the different materials performed again in a similar way. Even different amounts of aldehyde **3c** in the framework seem not to play a role in the final outcome of the reaction. A possible explanation would be that, even if the MOFs had different loading of aldehyde **3c**, this loading was not significantly different to play a role in the reaction outcome. Probably a similar experiment with, for instance, MOFs with 10%, 100% and 300% inclusion of aldehyde **3c** would give different results, but the difficulty to reach such high inclusion percentages makes it impossible at the moment to prove the assumption.

**Table 3.4:** Vapour phase reaction on UiO-67 with different load of **3c**

UiO-67 sample	Enantiomer	ee%	Conversion
1	(R)	28%	69%
2	(R)	22%	70%
3	(R)	24%	72%

Finally, the influence of the absolute configuration and enantiomeric purity of alcohol **4c** on the reaction outcome was explored. A mixture of aldehyde **3c** and three alcohols **4c**, which differed for handedness and enantiopurity, have been included in three samples of UiO-67. These experiments aimed to understand a possible influence of the alcohols **4c** on the catalytic cycles taking place inside the MOFs. In liquid phase Soai reactions, the *ee* of alcohol **4c** always increases throughout the reaction. In the vapour phase reactions described so far, there has always been a symmetry breaking followed by amplification of *ee* arising from an absence of chirality in the starting material. It was appealing to understand how the presence of a source of chirality in the system from the beginning of the reaction would have influenced the final result.

The initial solution for the inclusion had a ratio of aldehyde:alcohol 1:0,2, but in two out of three samples the ratio of the included species was found lower. The ratios of the initial materials have been evaluated only through HPLC analysis, because the amounts of alcohol were too small to be observed in the NMR spectra. The samples have then been tested to vapour phase reaction and the results are shown in Table 3.5.

**Table 3.5:** Vapour phase reaction on UiO-67 with aldehyde **3c** and alcohol **4c**

Entry	Ratio <b>3c:4c</b>	Initial Alcohol included	Alcohol yielded	Conversion
1	1:0,2	(R)- <b>4c</b> 15% ee	(R)- <b>4c</b> 50% ee	81%
2	1:0,07	(S)- <b>4c</b> 50% ee	(S)- <b>4c</b> 39% ee	80%
3	1:0,11	(R)- <b>4c</b> 96% ee	(R)- <b>4c</b> 69% ee	84%

The alcohols **4c** included were able to direct the handedness of the newly formed alcohol **4c**, but the amplification of *ee*% was observed only in the first entry. In the other two cases the *ee*% of the final alcohols **4c** was found lower than in the initial alcohol included.

All things considered, the experiments performed in this section were not conclusive to find a parameter that could play a role in terms of final conversion and *ee*% for the vapour phase reaction in the MOFs. However, the last experiments demonstrated that a source of chirality included in the MOF can influence the final handedness of the alcohol even if present just in traces.

### 3.6 Analyses on the materials

After the vapour phase reactions, the previously solid pristine Soai aldehyde **3c** was found as a brown/red oil, while some of the UiO MOFs experienced a change in color from yellow to brown or black (Figure 3.9).

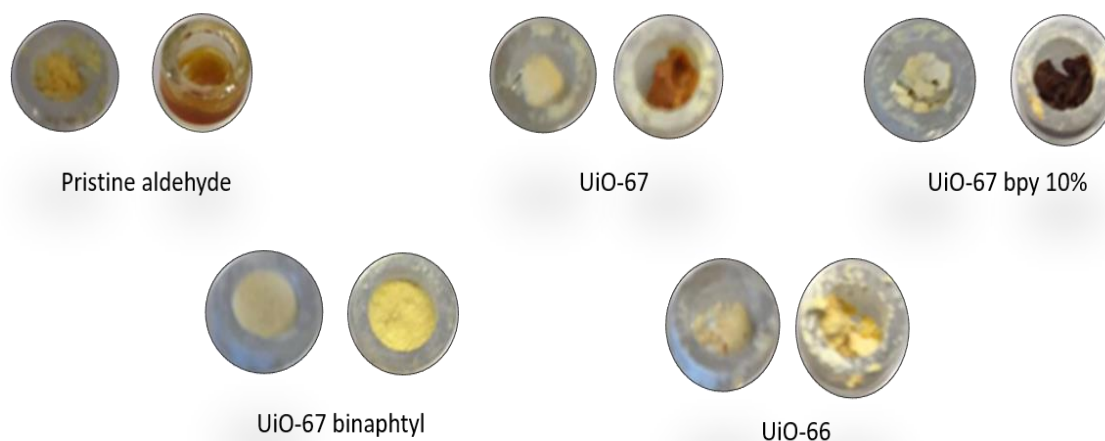


**Figure 3.9:** Appearance of the materials before and after vapour phase reaction.



Regarding the analyses on pristine **3c** after reaction, as shown in Figure 3.10,  $^1\text{H}$  NMR analysis on the crude material showed an almost quantitative conversion of **3c** and the unsurprising presence of toluene.

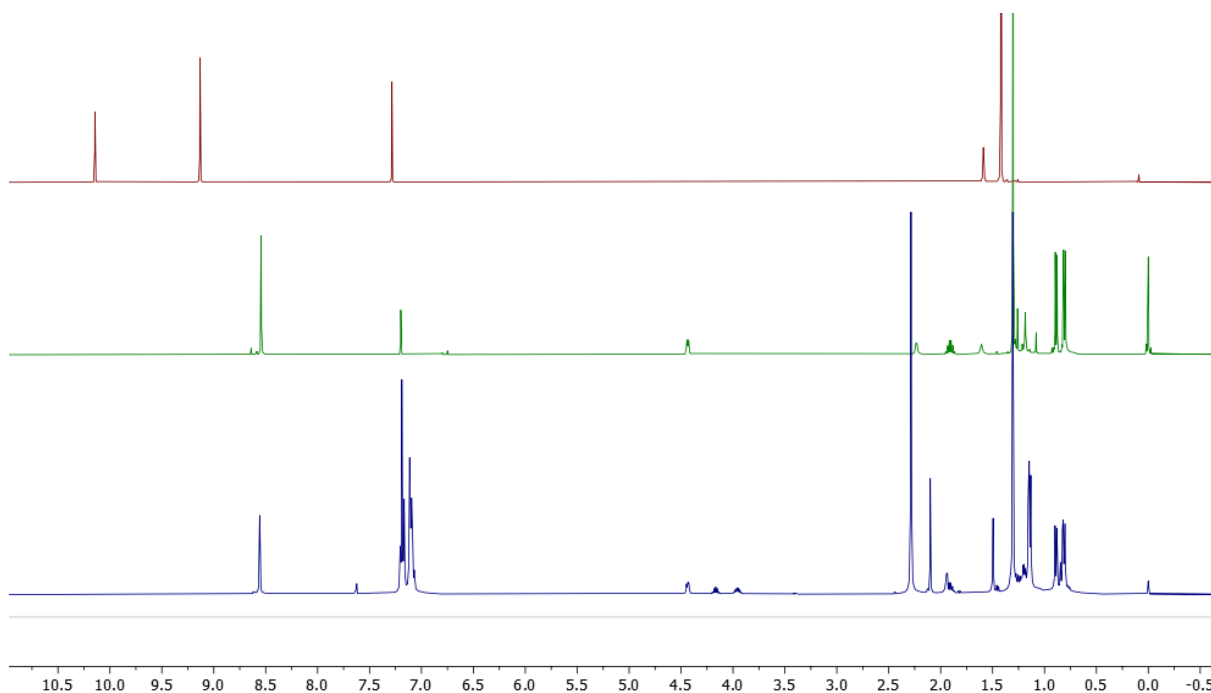


**Figure 3.10:** top to bottom: Soai aldehyde **3c**, Soai alcohol **4c**, crude of the vapour phase reaction.

A closer look onto the crude  $^1\text{H}$  NMR (Figure 3.11a) reveals the presence of other signals in addition to those arising from alcohol **4c**. The signal at 3.47 ppm has been attributed to the proton on the isopropyl group of ketone **8**, while the signal at 4.75 ppm was attributed to the vicinal protons of the alcohol group of alcohol **7**. Ketone **8** has always been observed in the crude  $^1\text{H}$  NMRs, while alcohol **7** was only present in some entries without any particular difference in reaction conditions between the experiments. The appearance of the signals of **4c** and **7** in the crude differ from the ones in the isolated materials (Figure 3.11b): while in the isolated materials they look respectively as a doublet and a singlet, they appeared as a quartet and a doublet in the crude spectrum. This could be possible due to coordination to Zn still present in the reaction crude. The multiplets at 4.00 and 4.15 ppm can be attributed to *iPr* groups of  $\text{Zn}(\text{iPr})_2$  still present in the reaction crude. The average yield of these side products was ca. 5% for alcohol **7** and ca. 12% for ketone **8**. It can be speculated that these side products

are also forming inside the MOFs, but none of them was detected, possibly due to the small amounts of material present in the framework. Alternatively, the MOF framework could suppress the side-product reactions leading to **7** and **8**.

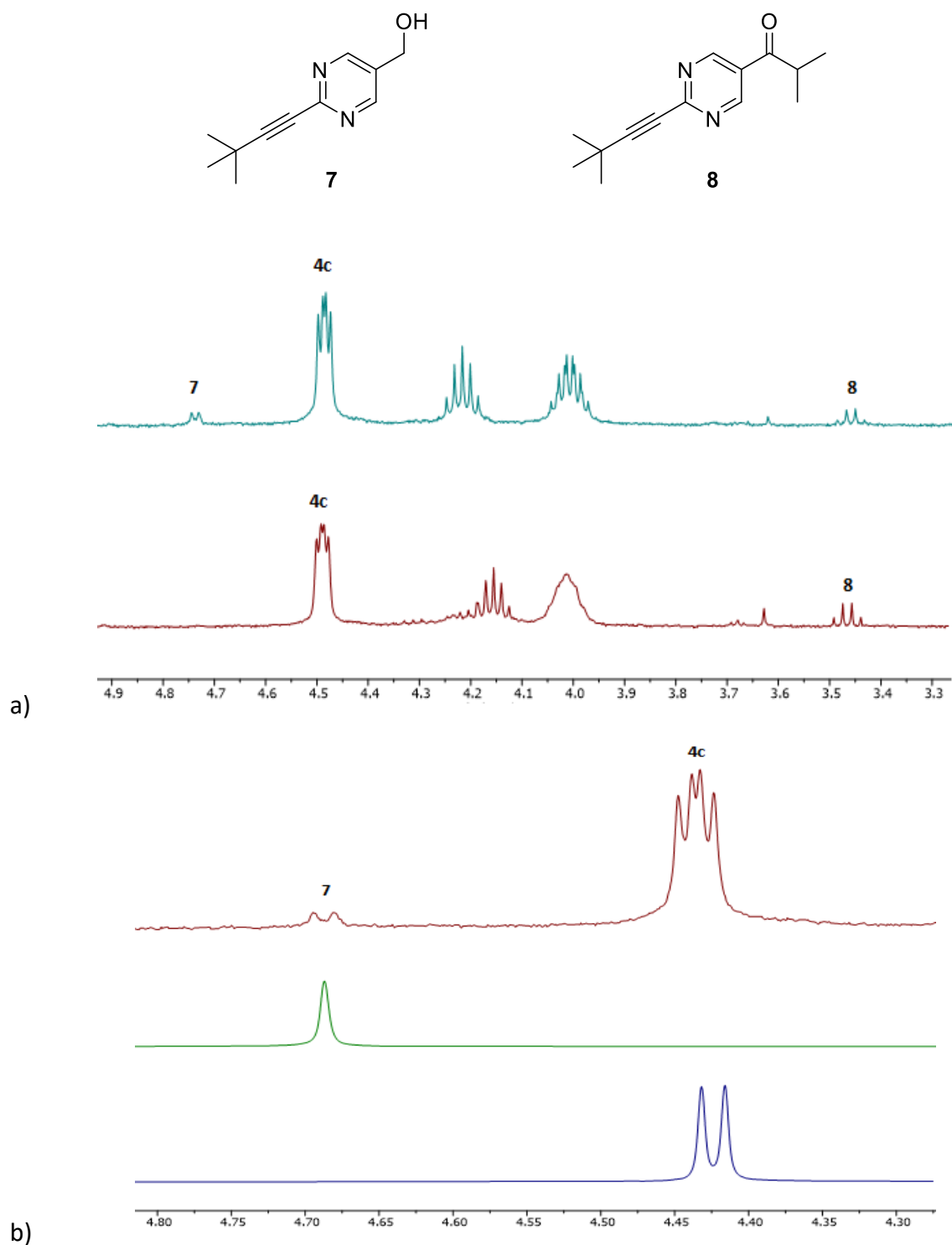


**Figure 3.11:** a) Part of the crude  $^1\text{H}$  NMR of two different vapour phase reactions on pristine **3c** b) Stacking of **4c** and **7** in the crude in respect with isolated materials.

Of the four MOF materials, two (UiO-66 and UiO-67 binaphthyl) had no change in color after reaction, while the remaining two (UiO-67 and UiO-67 bpy<sub>10%</sub>) showed a drastic change from yellow to dark brown/black. This could be due to a possible interaction of Zn(*i*Pr)<sub>2</sub> with the MOF cluster. The Zr cluster (Zr<sub>6</sub>O<sub>6</sub>(bpdc)<sub>6</sub>) contains μ<sub>3</sub>-OH. This site may provide an anchoring point for Zn(*i*Pr)<sub>2</sub> during the vapour phase reaction (Figure 3.12). In addition, as already explained, the bipyridine linkers of UiO-67 bpy<sub>10%</sub> could be an additional anchoring site.

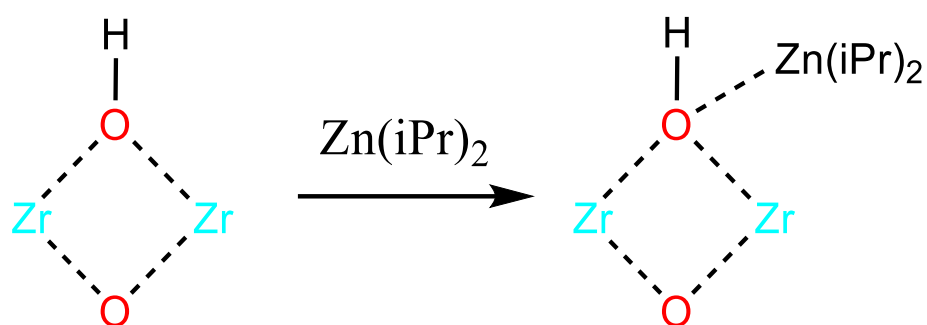


**Figure 3.12:** Possible interaction between Zn(*i*Pr)<sub>2</sub> and the Zr-O moiety of the MOF cluster

In order to investigate the color change, XRD analysis was employed. In particular, Capillary XRD was the chosen technique due to the small amount of MOF powder used for these reactions, not sufficient to perform a Powder XRD analysis (PXRD).

Two MOF samples, one of pristine UiO-67 bpy<sub>10%</sub> and one of UiO-67 bpy<sub>10%</sub> with included aldehyde **3c** were subjected to the vapour phase reaction. As shown in Figure 3.13, both materials retained crystallinity after reaction. A closer analysis of the XRD pattern showed no sign of interactions between Zn(*i*Pr)<sub>2</sub> and clusters or linkers. The same analyses on UiO-67 gave similar results.

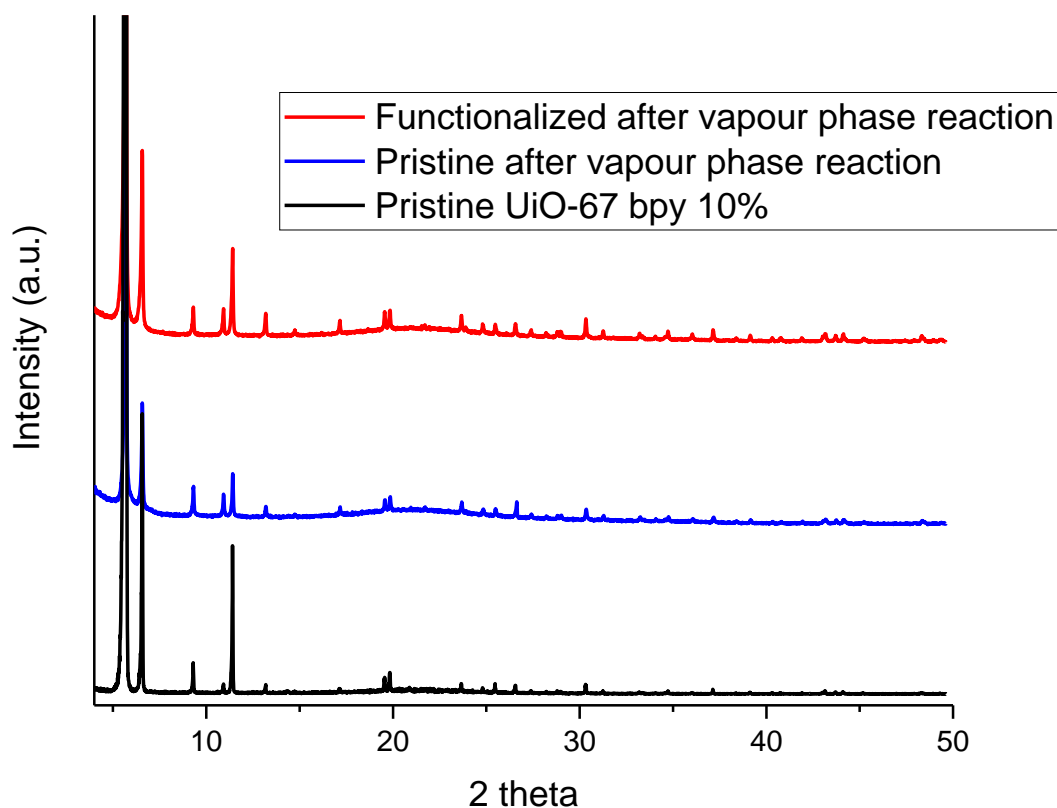


**Figure 3.13:** Capillary XRD analysis of UiO-67 bpy<sub>10%</sub>

IR analysis has also been carried out on the MOF samples after reaction. Comparing the spectra of the three materials in Figure 3.14, the C=O stretching of the carbonyl group of aldehyde **3c** at  $1700\text{ cm}^{-1}$ , not present in the pristine material, almost disappears in the UiO-67 after vapour phase reaction. Although diagnostic signals of the alcohol group of **4c** are not possible to detect (they overlap with peaks of the carboxylate linkers), other signals, common to both **3c** and **4c** are visible: the C-H stretching of the terbutyl/isopropyl groups below  $3000\text{ cm}^{-1}$  and the C-N stretching of the ring at  $2200\text{ cm}^{-1}$ . The stretching of the O-H groups above  $3500\text{ cm}^{-1}$ , present in the pristine material and perturbed in the material after the inclusion, is still perturbed after the vapour phase reaction. This hints that alcohol **4c** is still located on the cluster.

The IR analysis alone indicates that a similar molecule to aldehyde **3c** is present in the material, and they complement nicely the results obtained through other techniques and described above.

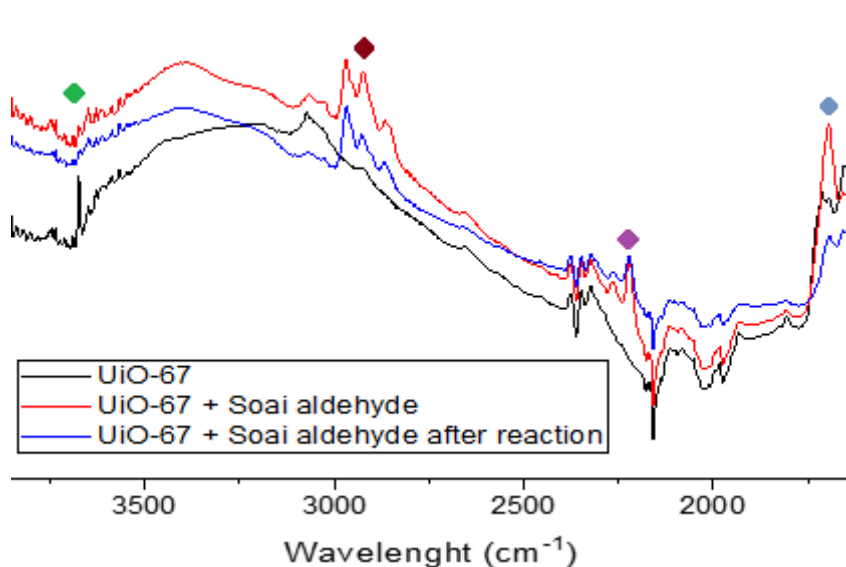


**Figure 3.14:** IR analysis on the UiO-67 after vapour phase reaction. Stretching of the hydroxyl groups (in green), stretching of the terbutyl group (in red), stretching of the C-N of the ring (in purple), stretching of the carbonyl group (in blue).

### 3.7 Focus on the vapour phase reaction on pristine Soai aldehyde

The results shown in Table 3.5 and the absence of a clear indication of amplification of *ee* for alcohol **4c** casted doubts whether the vapour phase Soai reactions analyzed so far were following the same mechanism and had the same properties as the liquid phase reactions.

The starting point was the analysis of the results in the experiments of Figure 3.4: the conversion slowly increased through time but the *ees* were found to be high already in the first sample taken after 30 minutes. A typical feature of autocatalysis a sigmoidal product/time curve and an induction period (Section 1.1.4). Additional experiments therefore focused on the early stages of the reaction. To do so, a set of reactions with the “single cylinder setup” were started simultaneously and stopped at fixed time points.

**Table 3.6:** Conversion and *ee*% in the early stages of the reaction

Time	<i>ee</i> %	Conversion
5 min	89%	2%
10 min	89%	2%
15 min	82%	4%
30 min	81%	3%
45 min	90%	5%

The results are summarized in Table 3.6. The results show a slow increase of conversion through time, while the *ee* values were constantly very high in all samples. Figure 3.15 combines the conversion and *ee* values obtained from the analysis on pristine aldehyde **3c** at early times (Table 3.6) and later times (Figure 3.5). The plot shows a typical parabolic shape with a slow induction period and a fast increase of the conversion after the first 60 minutes, proving that an autocatalytic reaction is taking place. Still, the surprisingly constant high *ee* values make this reaction intriguing.

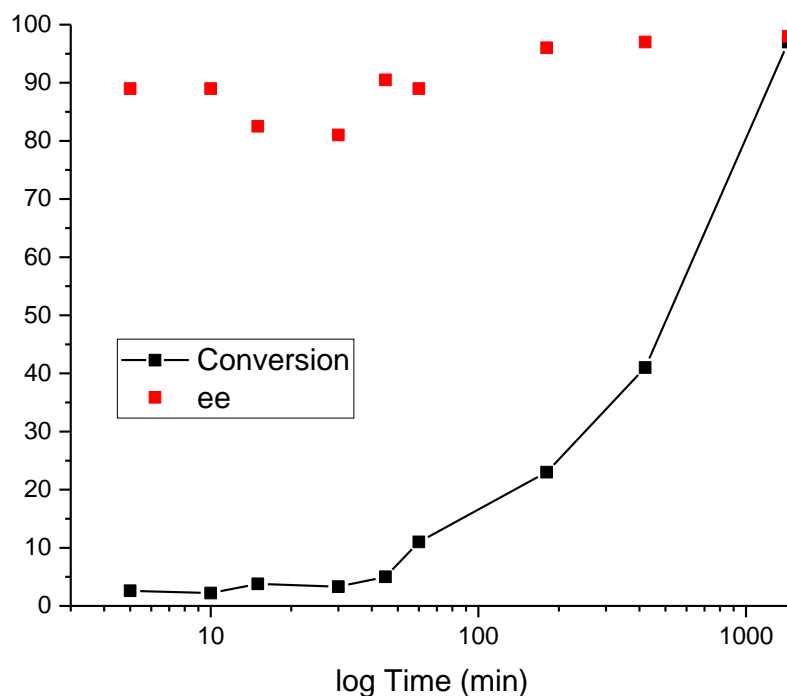


**Figure 3.15:** Conversion and *ee*% of vapour phase reaction on aldehyde **3c** between 5 minutes and 24 hours.

Furthermore, the role of the amount of  $\text{Zn}(\text{iPr})_2$  present in the reaction on the high *ee*% of alcohol **4c** was also tested. The reactions were performed with a scale-up of the “single cylinder reaction” setup. Instead of a small vial with few milligrams of starting material, a bigger vial with 50 mg of aldehyde **3c** was employed (Figure 3.16).

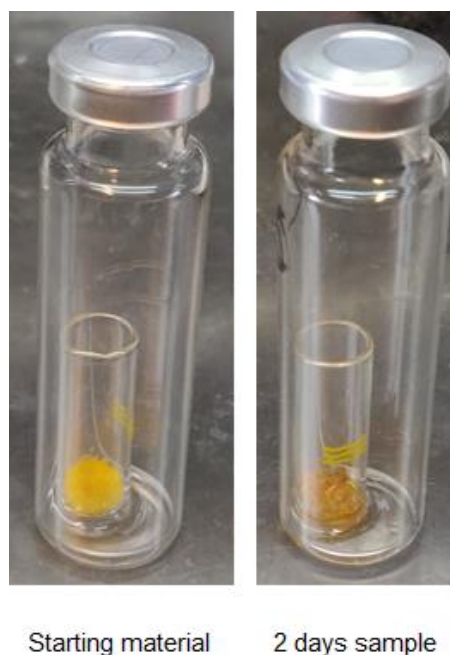


**Figure 3.16:** Reaction setup for the experiments with different equivalents of  $\text{Zn}(\text{iPr})_2$

The reactions were performed varying the equivalents of  $\text{Zn}(\text{iPr})_2$  compared to aldehyde **3c** and stopping the reaction after 72 hours. When the reaction was performed with an excess of  $\text{Zn}(\text{iPr})_2$  (Table 3.7, Entry 1), the already described side products **8** was detected. Surprisingly, when the reaction was performed lowering the amount of  $\text{Zn}(\text{iPr})_2$  to a 1:1 or 1:0.5 ratio with aldehyde **3c** (Table 3.7, Entry 2 and Entry 3) two new side products, esters **9** and traces of ester **10**, were detected. There was no substantial difference in the yields of the side products between Entries 2 and 3, and the only important change was the ratio between **3c** and **4c**. Table 3.7 shows the yields found in the reaction crude for the three reactions. A possible reaction mechanism for the formation of side products **7-10** will be given in Sections 4.5 and 4.6.

Despite the different amount of  $\text{Zn}(\text{iPr})_2$  employed in the three entries, the *ees* of **4c** were found identical. After hydrolysis of ester **9**, it was found out that it was forming with the same

absolute configuration of **4c**, and the *ee* values for (R)-**9** were found comparable to the ones for **4c**.

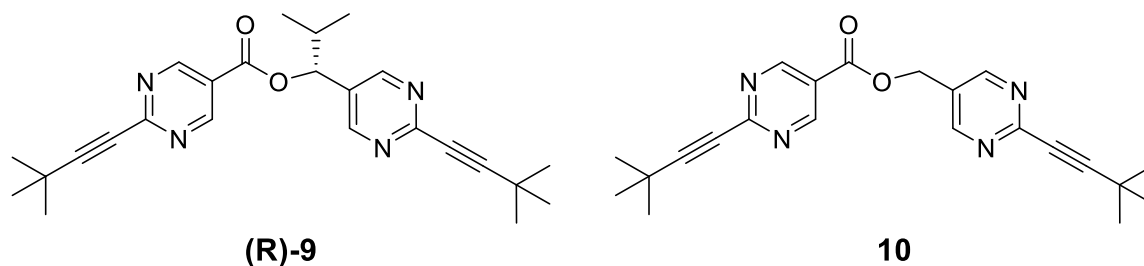


**Table 3.7:** Vapour phase reactions with different amount of Zn(*i*Pr)<sub>2</sub>

Entry	Ratio 3c:Zn( <i>i</i> Pr) <sub>2</sub>	Unreacted	Yield	Yield	Yield	Yield	Yield
		3c	4c	7	8	9	10
1	1:2	/	81%	/	19%	/	/
2	1:1	2%	65%	13%	13%	7%	/
3	1:0,5	17%	46%	11%	16%	8%	1%

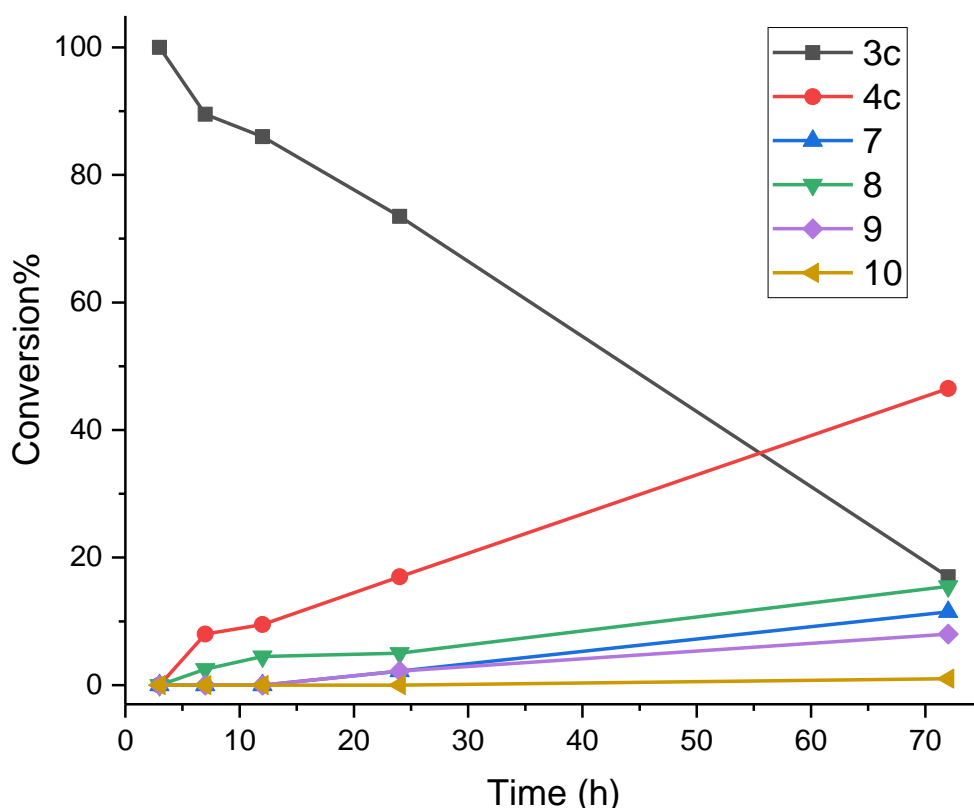
**Table 3.8:** *ee* values for **4c** and **9**

Entry	Ratio 3c:Zn( <i>i</i> Pr) <sub>2</sub>	<i>ee</i> %	<i>ee</i> %
		4c	9
1	1:2	94%	/
2	1:1	95%	94%
3	1:0,5	96%	98%

A kinetic analysis was performed in order to follow a vapour phase reaction with a 1:0,5 ratio 3c:Zn(*i*Pr)<sub>2</sub>. The experiment shows how the formation of **4c** and **8** is taking place already in the early stages of the reaction, while **7**, **9** and **10** were detected only after 24 hours. The *ee*% of **4c** steadily increased throughout the reaction (Table 3.9).



**Table 3.9:** Kinetic experiment on the vapour phase reaction with a 1:0,5 ratio of **3c** to Zn(iPr)<sub>2</sub>.



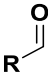
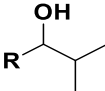
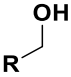
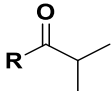
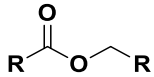
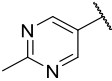
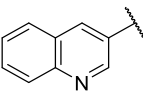
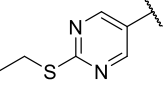
COMPOUND	3 h	7 h	12 h	24 h	72 h
<b>4c</b>	/	<i>ee</i> = 33%	<i>ee</i> = 42%	<i>ee</i> = 59%	<i>ee</i> = 96%

Different zincorganil compounds were also tested for the vapour phase reaction. Reactions with Zn(Me)<sub>2</sub> and Zn(Et)<sub>2</sub> afforded a quantitative conversion of **3c** and yielded the corresponding alcohols without presence of side products. The alcohols were obtained as racemic mixtures, similarly to the liquid phase Soai reaction with these same zincorgsnic compounds.

Lastly, an initial screening of other Soai substrates was performed (Table 3.10). The aldehydes on Entries 1 and 2 had been already tested for liquid phase Soai reactions in the past by various

research groups [18, 110], and they were found able to give asymmetric autocatalysis with amplification of *ee*% in presence of the corresponding alcohol/autocatalyst, even if to a lower extent compared to substrate **3c**. Aldehyde **3b** in Entry 1 was also found able to give asymmetric amplification in absence of alcohol **4b**<sup>[80a]</sup>, whereas Quinoline aldehyde in Entry 2 was not able to produce a (+)-NLE under absolute conditions. Under the conditions of the vapour phase reaction, both substrates yielded the corresponding chiral alcohol in good yields, but while the *ee*% of the Quinoline alcohol was found to be nearly racemic, Me-pyrimidine alcohol **4b** afforded a moderate *ee*%. The aldehyde in Entry 3 had never been tested previously for liquid or vapour phase Soai reactions. In liquid phase reactions, it showed to give a low amplification in presence of the corresponding chiral alcohol and no amplification under absolute conditions. The final *ee*% in the vapour phase reaction was low. Nevertheless, the result is promising as it shows that even substrates that do not show amplification under absolute conditions in solution can give positive results under the vapour phase absolute conditions. Some of the previously discussed side products were also found in the reaction crudes.

**Table 3.10:** Screening of other Soai-type substrates

Entry	R					
1		11%	61% <i>ee</i> = 12%	12%	12%	4%
2		7%	68,5% <i>ee</i> < 2%	10%	14%	/
3		1%	64% <i>ee</i> = 5-6%	11%	24%	/

### 3.8 Conclusions

Vapour phase reactions on **3c** included in UiO-MOFs have been performed. The results show how the reaction is faster in the MOFs than in the pristine materials, and how the confinement in different frameworks can contribute to the final conversion. **3c** amplifies under absolute conditions to yield **4c** in high *ee*% in the pristine material. When employing the UiO MOFs as confinement for **3c**, moderate *ee*% were found. Moreover, unreported side products have been detected and characterized in the reaction under specific conditions. Finally, it has been demonstrated that other substrates that do not show SMSB in solution are able to amplify under the heterogeneous conditions of the vapour-solid reaction.

The work performed in this chapter has been published in **Paper I**. Supporting information to unpublished experiments can be found in **Appendix III**

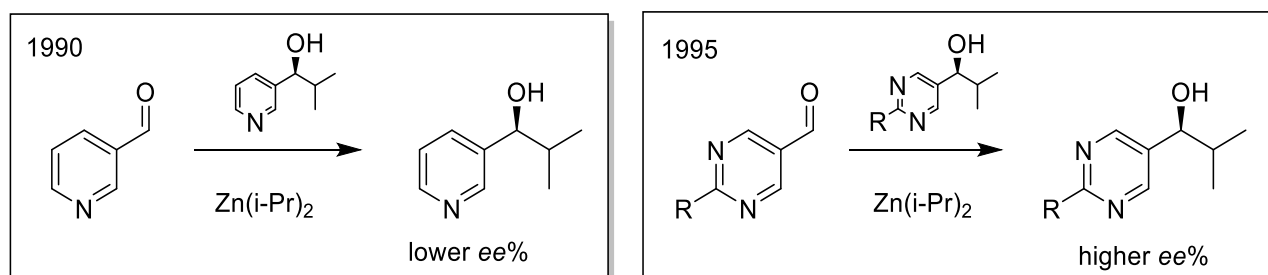
# 4

## Vapour-solid interactions for SMSB and asymmetric amplification of pyridine aldehydes

---

### 4.1 Introduction

As shown in Section 1.1.4, pyridine aldehydes have been the first substrates tested by Soai to demonstrate the feasibility to perform an asymmetric autocatalysis. Unlike the pyrimidine aldehydes (like **3c**) though, these molecular scaffolds did not show any (+)-NLE in homogenous conditions (solutions): in presence of a corresponding chiral alcohol that operates as autocatalyst, erosion of *ee*% was observed in the final product compared to the starting alcohol (Scheme 4.1). Previous work performed in our research group reported similar results <sup>[41]</sup>.



**Scheme 4.1:** Difference in amplification of the *ee*% between pyridine and pyrimidine aldehydes.

Recently, Denmark and co-workers have reported studies performed on 3-pyridinecarbaldehydes in solution <sup>[111]</sup> varying the functionalization of the Soai alkoxides and different zincorganil reagents. They reported a rationale, defined as “pyridine-assisted cube escape model”, to explain the formation of the SMS tetramer and to answer why the reaction performs best only when *iPr* is present on both the Zn center and the alkoxide. The nitrogen on the pyridine ring plays a crucial role in the disruption of the stable and unreactive cubic tetramer and the formation of the active SMS tetramer.

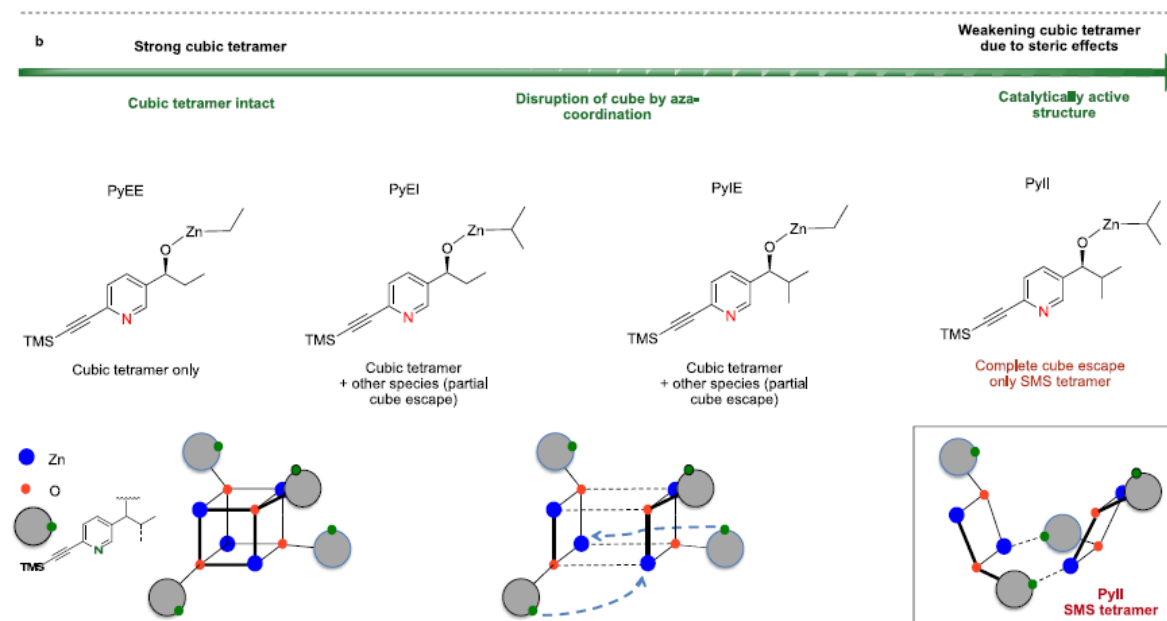


**Figure 4.1:** The pyridine-assisted cube escape model

Additionally, they proposed an alternative “floor-to-floor transition state model” that differs from the Gridnev model. Even if this proposal is based on pyridine aldehydes, the Authors suggest it could be valid also also for reactions of pyrimidine aldehydes.

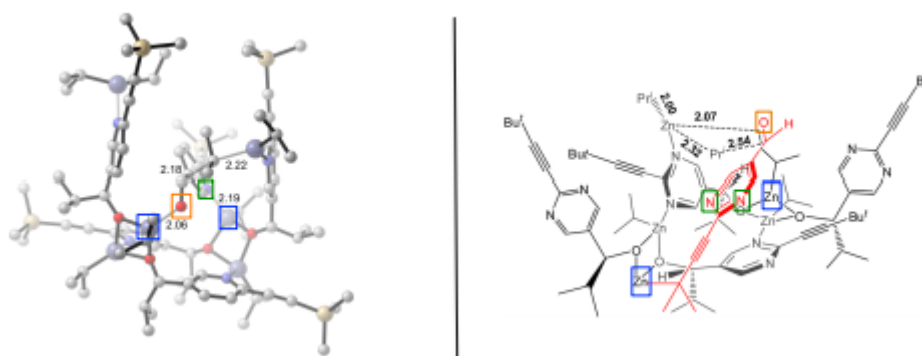
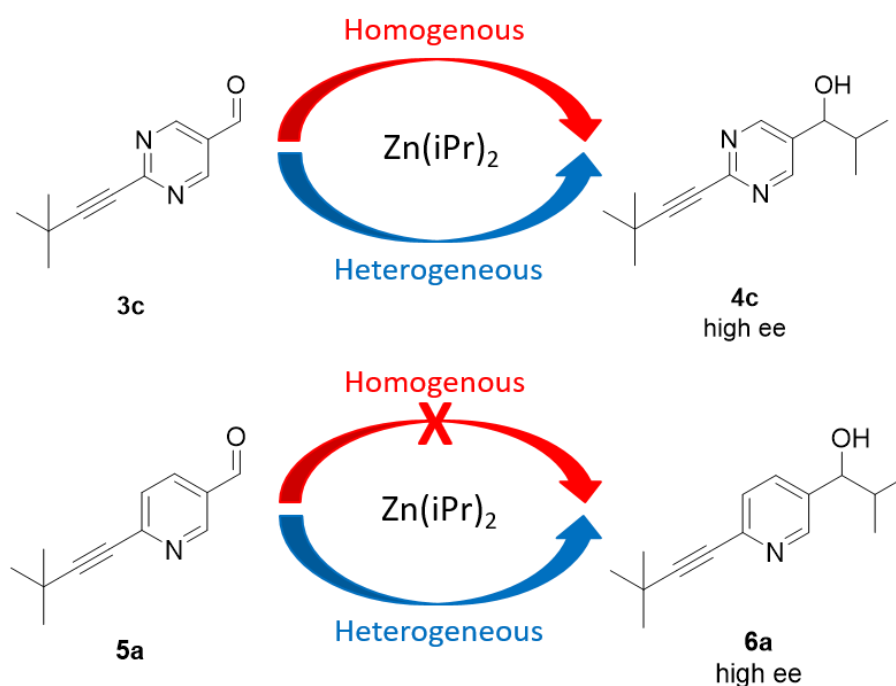


**Figure 4.2:** Floor-to-floor transition state model vs. Gridnev transition state model

As last point, the same group reported a new asymmetry-amplifying autocatalytic system based on pyridine aldehydes. This report was unexpected and surprising since it was in contrast with previous literature. In any case, in their reports, it was mentioned that when reaction was performed on pyridine aldehyde **5a** or similar substrates under absolute conditions no asymmetric amplification was observed.

While experimenting vapour-phase reactions with the standard Soai pyrimidine substrates, it was found that pyridine aldehyde **5a** was able to give amplification of *ee* under the same absolute heterogeneous vapour-solid conditions. This chapter describes the experiments focused on this unexpected reaction outcome.

Scheme 4.2 depicts the present situation about absolute reaction performed on pyrimidine and pyridine aldehydes with  $\text{Zn}(\text{iPr})_2$  under both homogenous and heterogeneous conditions.



**Scheme 4.2:** Difference between Soai aldehyde **3c** and the pyridine aldehyde **5a** under absolute conditions between homogenous (solutions) and heterogeneous (vapour phase reaction) conditions.

## 4.2 Analyses on the reaction crude

Single crystals analysis revealed that aldehyde **5a** crystallizes in an orthorhombic crystal system and in the achiral  $Pca2_1$  space group. This result establishes that **5a** is not the chiral source leading to symmetry breaking when used as starting material.

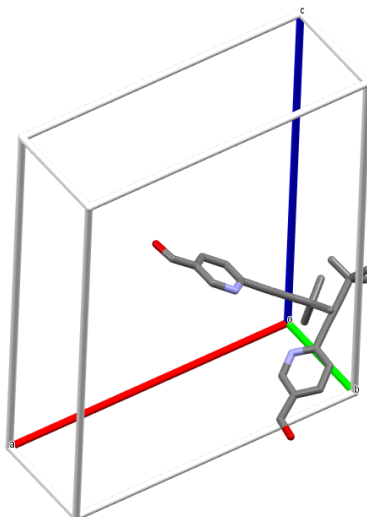
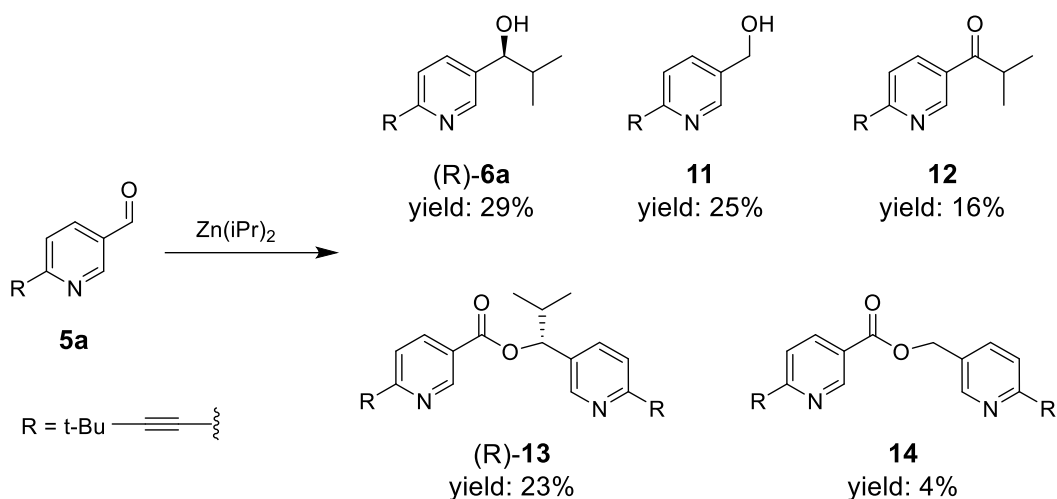


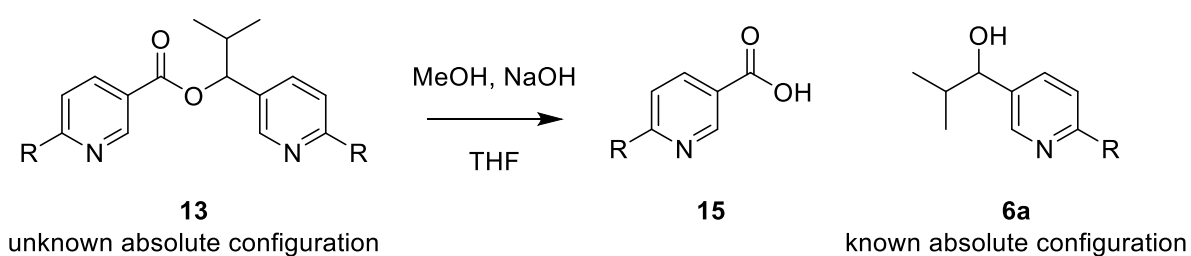
**Figure 4.3:** Single-crystal analysis of crystal of aldehyde **5a**.

The products formed in the reaction at r.t. and the respective yields are reported in Scheme 4.3. It was previously reported that in liquid phase reactions the primary alcohol **11** was forming as side product in considerable amount, in addition to the autocatalyst/product **6a** (the same behaviour was also described for pyrimidine aldehydes <sup>[112]</sup>). Moreover, in the vapour phase reactions, ketone **12** and two esters, chiral **13** and achiral **14** were found in the reaction mixture. The products of the reaction are the pyridine equivalent of compounds **7-10** described in the previous chapter. While compounds **7-10**, with the exception of ketone **8**, were found in low amount and only in particular conditions, the side products of Scheme 4.3 were found in comparable amounts to the main product **6a** and in almost every run.



**Scheme 4.3:** Products of the vapour phase reaction on **5a**.

It seemed clear that **6a** and **13**, as well as **11** and **14**, were related in the reaction mechanism. To prove this, the absolute stereochemistry of compound **13** was determined by hydrolysis of the ester to form carboxylic acid **15** and gain the alcohol **6a** responsible for the stereochemistry of **13** (Scheme 4.4). It was observed that invariably both **6a** and **13** were forming with the same absolute configuration. Moreover, both **6a** and **13** had been obtained with a random distribution of enantiomers. As for the vapour phase reactions of aldehyde **3c**, the (R) enantiomer has been obtained in a higher percentage.

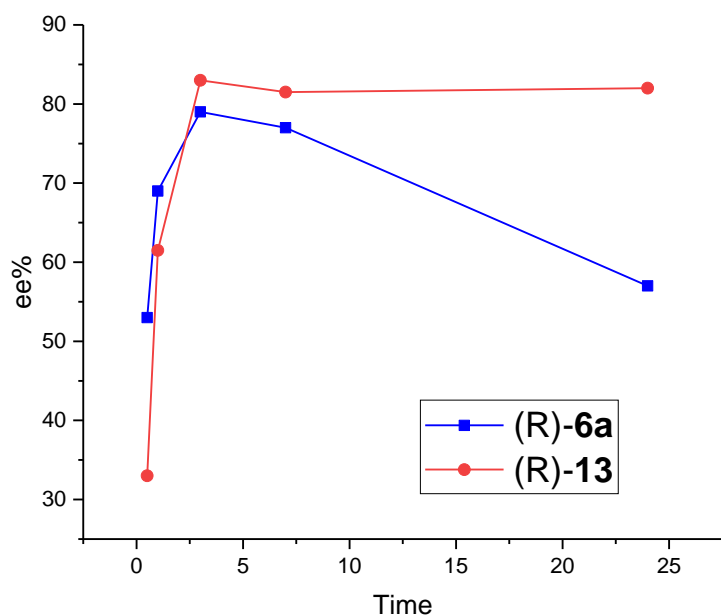


**Scheme 4.4:** Hydrolysis of **13**.

The progression in terms of enantiopurity of the two chiral compounds was followed through time with the “single cylinder reaction setup” (Figure 4.4). The *ee*% of (R)-**6a** was found higher than the one of (R)-**13** at first, but over time, while the *ee*% of (R)-**13** maintained consistently



high, the *ee%* of (R)-**6a**, after reaching a maximum, steadily decreased. A set of triplicate experiments with the “three cylinders setup” showed that, in almost all entries, (R)-**6a** was formed with *ee%* lower than (R)-**13** (Table 4.1).



Entry	<i>ee%</i> (R)- <b>6a</b>	<i>ee%</i> (R)- <b>13</b>
1	48	72
2	53	65
3	62	83
4	55	54
5	47	25
6	63	79
7	67	81
8	50	57
9	49	66

**Figure 4.4** (left): Evolution of the amplification of *ee%* of **6a** and **13**.

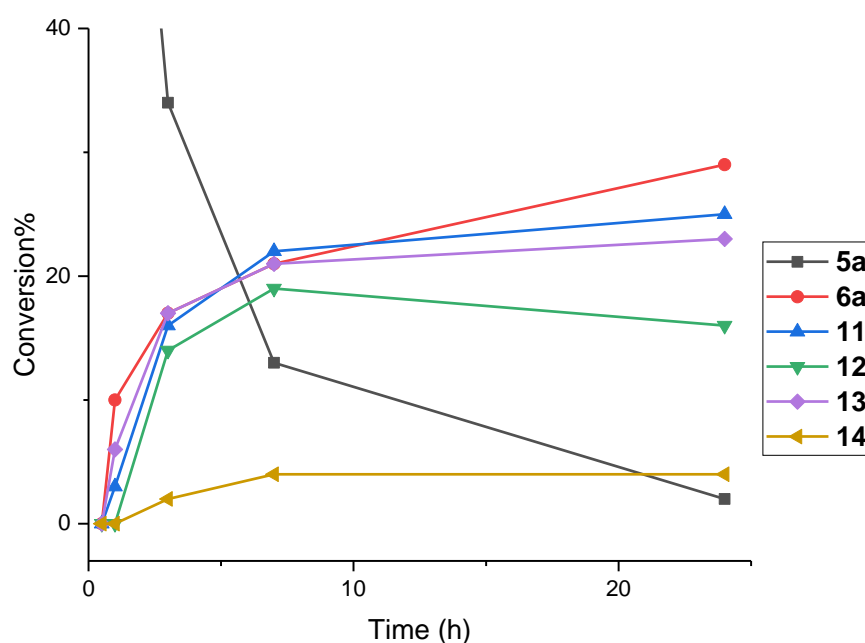
**Table 4.1** (right): Final *ee%* of **6a** and **13** in a series of vapour phase reactions.

### 4.3 Kinetic analyses on the vapour phase reaction at different temperatures

A deeper understanding of the reaction behavior came from kinetic analyses of the reaction at different temperatures with the setup previously established (“single cylinder setup”). Initially, the reaction was analysed at r.t. as summarized in Table 4.2. After 30 minutes no product was observed, while in the following samples the amount of **5a** decreased slowly with parallel increasing yield of the other reaction products, all following similar trends except for achiral ester **14**.

**Table 4.2:** NMR ratio of products over time at rt

COMPOUND	30 min	1 h	3 h	7 h	24 h
<b>5a</b>	≅ 100%	81%	34%	13%	2%
<b>6a</b>	/	10%	17%	21%	29%
<b>11</b>	/	3%	16%	22%	25%
<b>12</b>	/	/	14%	19%	16%
<b>13</b>	/	6%	17%	21%	23%
<b>14</b>	/	/	2%	4%	4%

**Figure 4.5:** Graphical representation of the progress of the reaction (cut over 40% conversion)

The experiment run at r.t. gave some indications about the reaction profile but no insight about the order in which products were forming in the early phases of the reaction. Since the vapour pressure of **a** is directly correlated with the temperature of the system, it was thought that performing the reaction at lower temperatures would have slowed down the passage of  $\text{Zn}(i\text{Pr})_2$  in the vapour phase and consequently the reaction kinetic (Figure 4.6). When performing the reaction at 0 °C the yield of **6a** was not different from the one observed in the 24 hours sample of the r.t. experiments. As a consequence of low temperature, decreasing vapour tension of  $\text{Zn}(i\text{Pr})_2$  resulted in a slower alkylation, as shown by the high amount of

recovered aldehyde **5a**. The formation of the other side products was also drastically slowed down. The same trend could be observed performing the reaction at  $-15^{\circ}\text{C}$ . In this case, after 24 hours, **6a** was the only product found in the reaction crude, and only when the reaction was left for 72 hours at the same temperature the other side products were detected. Also, the three reactions provided amplification with a slightly higher final *ee* than the average at r.t. with an almost similar enantiopurity for **6a** and **13**, probably due to the fact that the aldehyde **5a** was not depleted and the reaction not complete (Table 4.3).

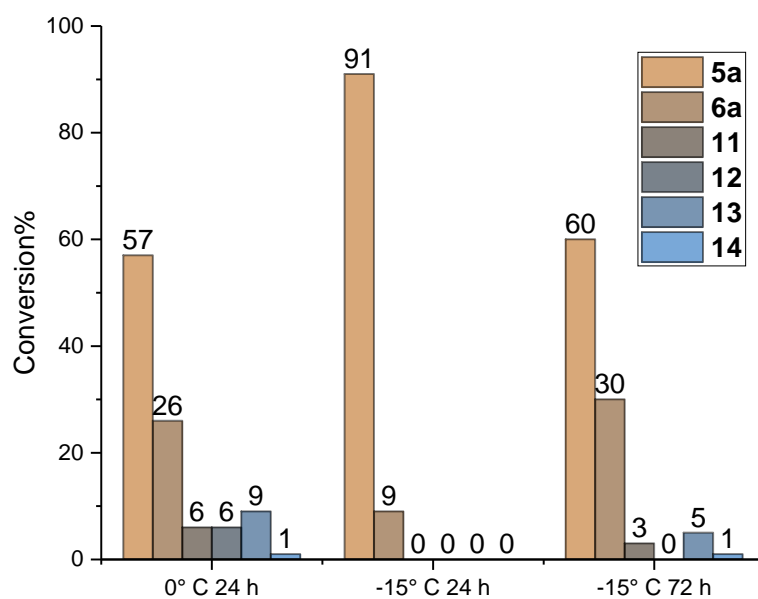


**Figure 4.6:** Conversion of the products at different time and temperatures

**Table 4.3:** *Ee*% of compounds **6a** and **13** at different time and temperatures

COMPOUND	0° C 24 h	-15° C 24 h	-15° C 72 h
<b>6a</b>	91% <i>ee</i>	60% <i>ee</i>	83% <i>ee</i>
<b>13</b>	86% <i>ee</i>	/	81% <i>ee</i>

These results suggest that **6a** was the starting product of the reaction, and only in a second step the other side products are formed. In addition, it can be concluded that esters **13** and **14** are forming from alcohols **6a** and **11**, and not the other way around.

Interestingly, a difference in behavior was observed for reactions performed at  $40^{\circ}\text{C}$ . Not surprisingly, in respect to the reaction performed at low temperatures and at r.t., the aldehyde consumption was faster. The final yields were comparable to the r.t. reaction, but with a lower *ee*% in **6a** and **13** (Table 4.4 and Figure 4.7). The results were rationalized considering the influence of temperature on the vapour tension of toluene: at higher temperatures, the partial

vapour of toluene would increase in the saturation vapour, re-establishing similar conditions to the homogenous liquid phase reactions. In the same way, the high ee% observed in the reactions at lower temperatures could be attributed to a less extent of Toluene in the reaction crude.

**Table 4.4:** NMR ratio of products through time at 40° C

COMPOUND	3 h	7 h	24 h	Final ee%
<b>5a</b>	20%	3%	2%	
<b>6a</b>	13%	23%	33%	2,5%
<b>11</b>	25%	26%	24%	
<b>12</b>	21%	24%	19%	
<b>13</b>	20%	22%	20%	15%
<b>14</b>	2%	3%	3%	

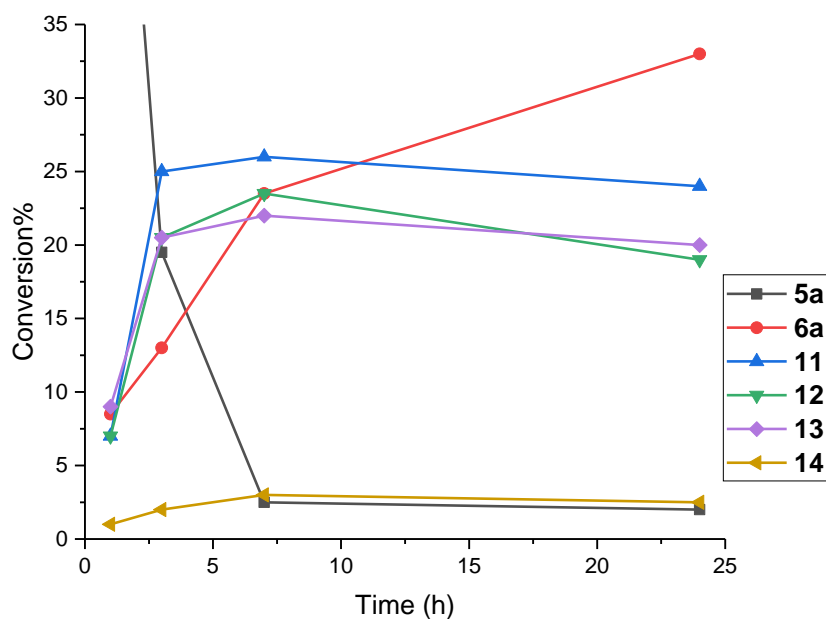


**Figure 4.7:** Graphical representation of the progress of the reaction (cut over 35% conversion)

#### 4.4 Analyses varying the equivalents of Zn(*i*Pr)<sub>2</sub>

The analyses have been performed lowering the loading of Zn(*i*Pr)<sub>2</sub> employed in the vapour phase reaction from 5 equivalents to 0,5 equivalents and stopped after 48 hours. As shown in Figure 4.8, the main difference between the 4 entries is the ratio between **5a** and **6a**. Indeed, more aldehyde **5a** was found unreacted and less alcohol **6a** was found in the reaction crude. Surprisingly, the formation of the other side products appears independent on the

concentration of  $\text{Zn}(i\text{Pr})_2$  in the vapour phase, with similar yields between experiments performed with excess as well as in depletion of  $\text{Zn}(i\text{Pr})_2$ .

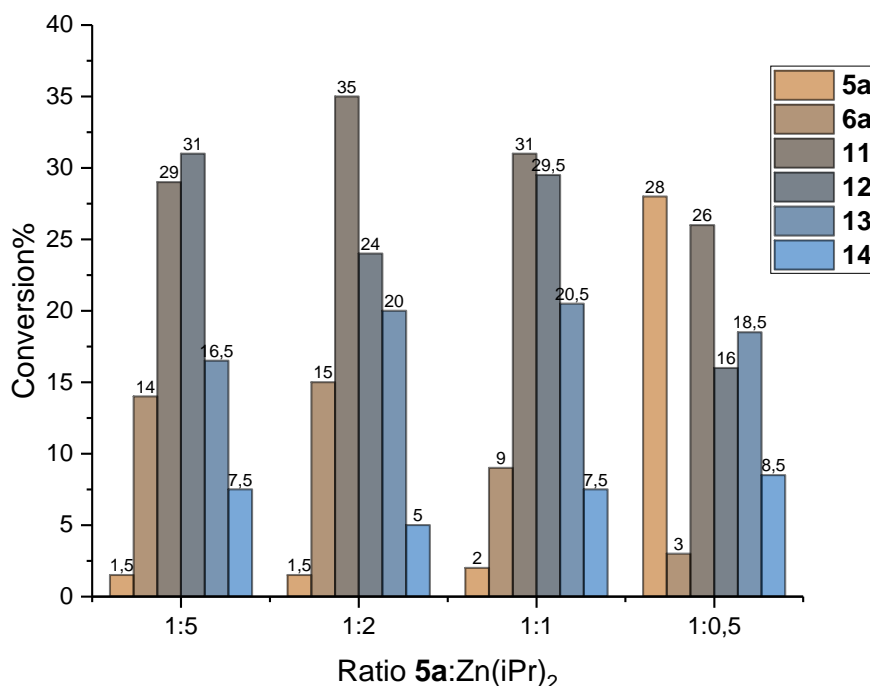
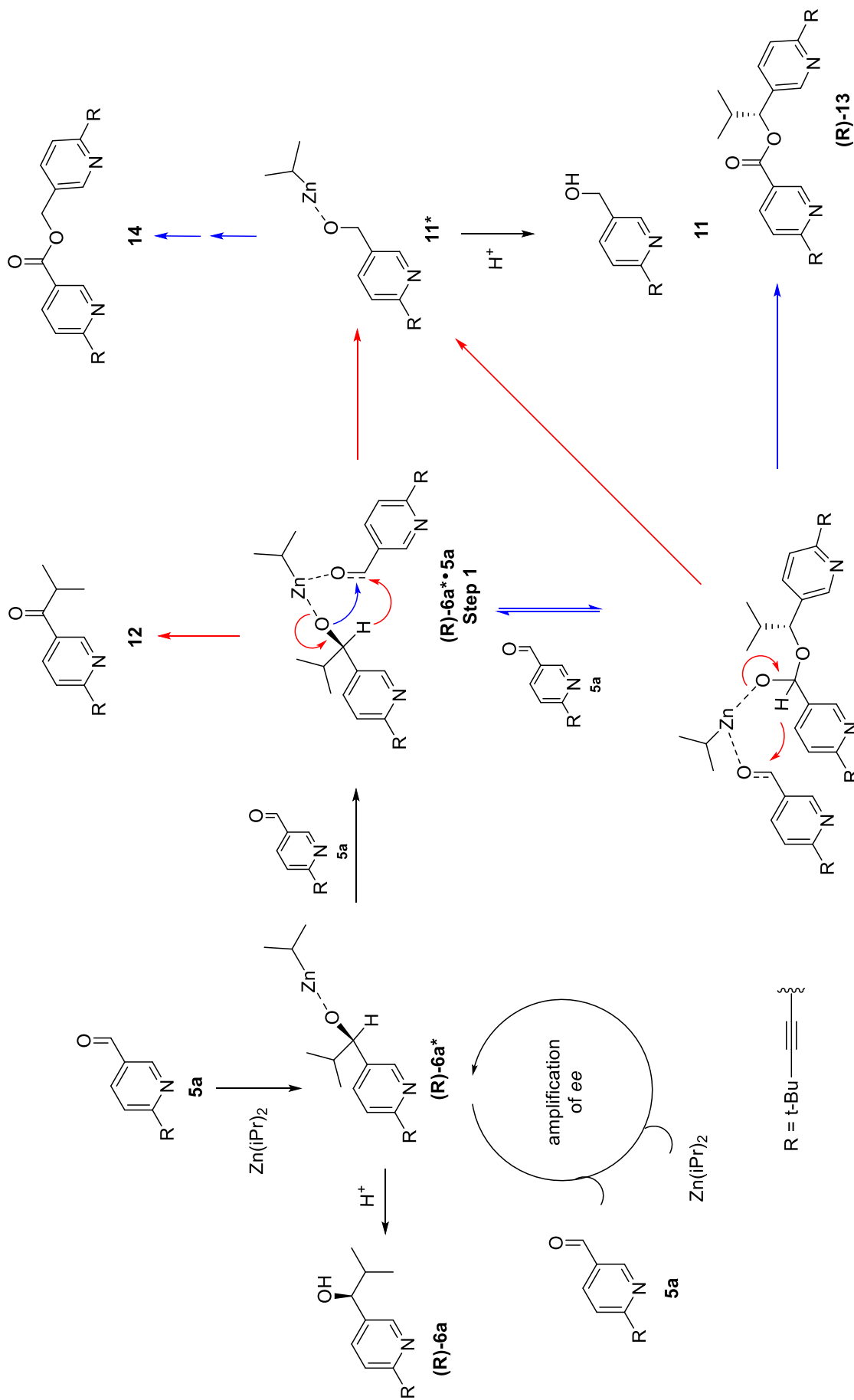


**Figure 4.8:** Conversion of the products with different equivalents of  $\text{Zn}(i\text{Pr})_2$

The *ee* values for **6a** and **13**, reported in Table 4.5, show how, even reducing the amount of  $\text{Zn}(i\text{Pr})_2$ , the asymmetric amplification for the two chiral products is not hindered. However, the results do not show a clear trend: while the final *ee*% of ester **13** has only some small fluctuations between the experiments, **6a** varies much more in terms of enantiopurity. These results are in contrast with the similar experiment discussed in Table 3.8 on the behavior of Soai alcohol **4c** and ester **11** in which similar high values of *ee*% were found for the two species.

**Table 4.5:** *Ee*% of **6a** and **13** varying the ratio 5a:Zn(*i*Pr)<sub>2</sub>

COMPOUND	1:5	1:2	1:1	1:0,5
<b>6a</b>	34%	22%	20%	53%
<b>13</b>	56%	70%	59%	63%



(R)-13\*•5a  
Step 2

→ MPV rearrangement  
→ CT disproportionation

Scheme 4.5: Mechanism for the vapour-phase reaction

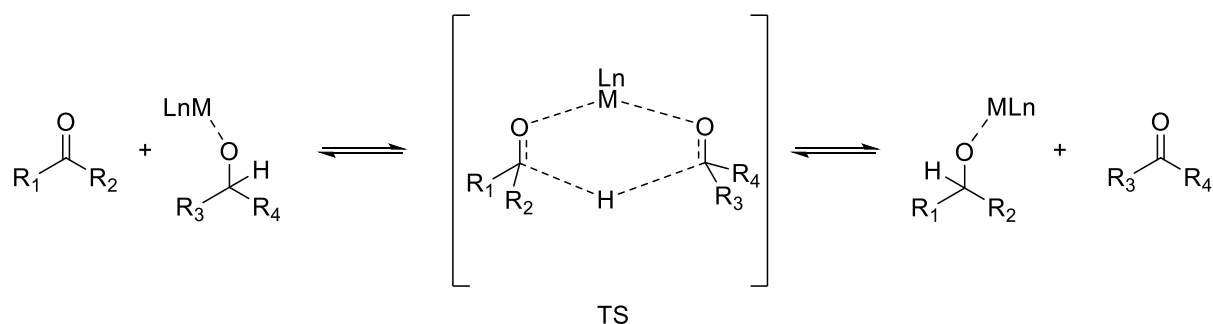
#### 4.5 Proposed mechanism for the vapour phase reaction

On the basis of the information gained in the previous sections, it is possible to delineate a mechanism for the transformation upon vapour-solid interaction of  $\text{Zn}(\text{iPr})_2$  and **5a** (Scheme 4.5). At least four different processes taking place at the same time were identified:

- SMSB in the interaction of  $\text{Zn}(\text{iPr})_2$  and **5a** and amplification of *ee%* of **6a**
- Formation of **11** and **12** through a Meerwein-Ponndorf-Verley mechanism
- Formation of **13** and **14** through a Claisen-Tishchenko disproportionation
- Amplification of *ee%* of **13**

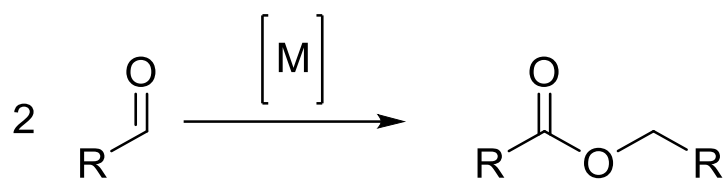
As proven by the low temperature experiments, the first step of the reaction mechanism is the interaction between  $\text{Zn}(\text{iPr})_2$  and aldehyde **5a** to form alkoxide **6a\***. As already explained by Soai in similar experiments<sup>[87]</sup>, the crystals of **5a** are distributed with a random orientation, so when Zinc vapours react with one or a small number of molecules of **5a**, the initial *ee%* of **6a\*** is dictated by the orientation of **5a** (kinetic control). The initial *ee%* is then amplified by the asymmetric autocatalytic process. It is tempting to assume that the amplification of alcohol **6a** would follow the same mechanism of the Soai reaction in vapour phase, but more experiments need to be designed to better understand how the amplification process occurs and what are the catalytic species involved in the reaction (a small discussion is given in the last paragraph of this section).

The Meerwein-Ponndorf-Verley (MPV) rearrangement involves a reversible hydride transfer from a secondary alcohol to a carbonyl substrate activated through coordination to a Lewis acidic metal center<sup>[113]</sup> (main group, in particular Al) (Scheme 4.6).



**Scheme 4.6:** Mechanism of the Meerwein-Ponndorf-Verley reduction

In the Claisen-Tishchenko (CT) reaction, a disproportionation occurs on an aldehyde in presence of an alkoxide and the product of the reaction is an ester <sup>[114]</sup> (Scheme 4.7). Unlike the more common ester synthesis obtained through reaction of carboxylic acids and alcohols, no side products are yielded. The recognized mechanism for the reaction is the Ogata–Kawasaki model <sup>[115]</sup>, on which the reaction pathways described in Scheme 4.5 are based. Recently Guanidinatozinc complexes <sup>[116]</sup> and achiral Metallic Zinc <sup>[117]</sup> has shown to be active for this type of rearrangement.



**Scheme 4.7:** The Claisen-Tishchenko disproportionation

In the vapour-phase reaction, alkoxide **6a\*** can react with **5a** in the autocatalytic system that allows the amplification of *ee*% of **6a**. Due to its large excess, other molecules of **5a** can enter in the coordination sphere of Zn(*i*Pr)<sub>2</sub> forming the intermediate complex (*R*)-**6a\***•**5a** (Step 1). Two possible pathways were envisioned after the coordination step and the formation of the intermediate. The red arrows in Step 1 represent the MPV pathway, with the hydride transfer from **6a\*** to **5a** and formation of **11\*** and **12**. A second possibility is the nucleophilic attack of **6a\*** on the carbonyl of **5a**, represented with blue lines. This pathway will result in Step 2, in which, through the coordination of another molecule of **5a**, a hemiacetal intermediate, (*R*)-**13\***•**5a** is formed. A second MPV rearrangement yields ester **13** and alkoxide **11\***. The CT disproportionation can also take place starting from alkoxide **11\***. The identical two-steps pathway leads to ester **14**.

Some confirmations to this mechanism can be found in the reaction conversions previously showed. For example, in the proposed reaction mechanism, ketone **12** can be formed only by the MPV rearrangement in Step I, while alcohol **11** can be formed by both MPV rearrangements in Steps I and II. This hypothesis is strengthened by the fact that, in the results of Section 4.3, alcohol **11** has always been found in higher proportions compared to **12**, and, taking a closer look to the 1 hour reaction of Table 4.2 or the 72 h reaction of Figure 4.5, compounds **6a**, **11** and **13**, the products of the CT rearrangement, were found in the reaction



crude, with no sign of **12**, meaning that the CT pathway was the only one taking place, and **11\*** was forming only through that mechanism.

The formation of ester **13** starts from alkoxide **6a\***, whose *ee* is constantly increasing through autocatalytic asymmetric amplification. The CT mechanism does not involve the chiral center of **6a\***, so through time (R)-**13** is obtained with a constantly higher *ee*% that is related to the improving *ee*% of (R)-**6a**. This explains how, following the first part of the graph representing the *ee*% of (R)-**6a** and (R)-**13** in Figure 4.4, they show a similar and almost parallel trend. It was observed from Table 4.1, that the final *ee*% of (R)-**13** remained constantly higher than the final *ee*% of (R)-**6a**. A possible explanation for this behaviour could be made by considering the formation of diastereomeric hemiacetal intermediates in Step II as a reversible process. The subsequent hydride transfer could ensue enantioselectively, with the preferential formation of (R)-**13**, while the opposite diastereomer could preferably revert back to Step I. In this way the amplification of (R)-**13** would happen at the expenses of (R)-**6a**. Taking in consideration again the results in Table 4.2, the formation of **6a** reached 21% in the first 7 hours, and increased of only 8% in the subsequent 17 hours. Figure 4.4 shows that the depletion of *ee*% of (R)-**6a** starts more or less after the first 4-5 hours of reaction. The amplification of *ee*% of (R)-**6a** is not affected by the formation of (R)-**13** in the first hours of reaction because new (R)-**6a** is synthesized from **5a** in continuously high *ee*. While this reaction slows down with the consuming of **5a**, the enantioselective formation of (R)-**13** keeps the same rate, maintaining high the *ee*% of **13** and depleting **6a** of the (R)-enantiomer.

The experiments of Section 4.4 provide additional information on the relationship between the different and simultaneous pathways in the reaction. It can be observed in Scheme 4.5 how no  $\text{Zn}(i\text{Pr})_2$  takes part in the MPV and CT mechanisms after the formation of alkoxide **6a\***. This is confirmed by the fact that all the side products form in almost the same proportions lowering the equivalents of  $\text{Zn}(i\text{Pr})_2$  employed. In the reaction performed in deficiency of  $\text{Zn}(i\text{Pr})_2$ , the lack of Zn reagent is affecting negatively only the autocatalytic cycle, and as a consequence **5a** is not completely converted. Therefore, less **6a** is formed, and most of it is converted into the other side products. This explains why the amount of **6a** was found much lower in the 1:0,5 experiment compared to the other entries.

As described in Section 3.8, similar side products to **11-14** have been found in the vapour phase reaction of **3c**, with the difference that **9** and **10** were found in the reaction crude only

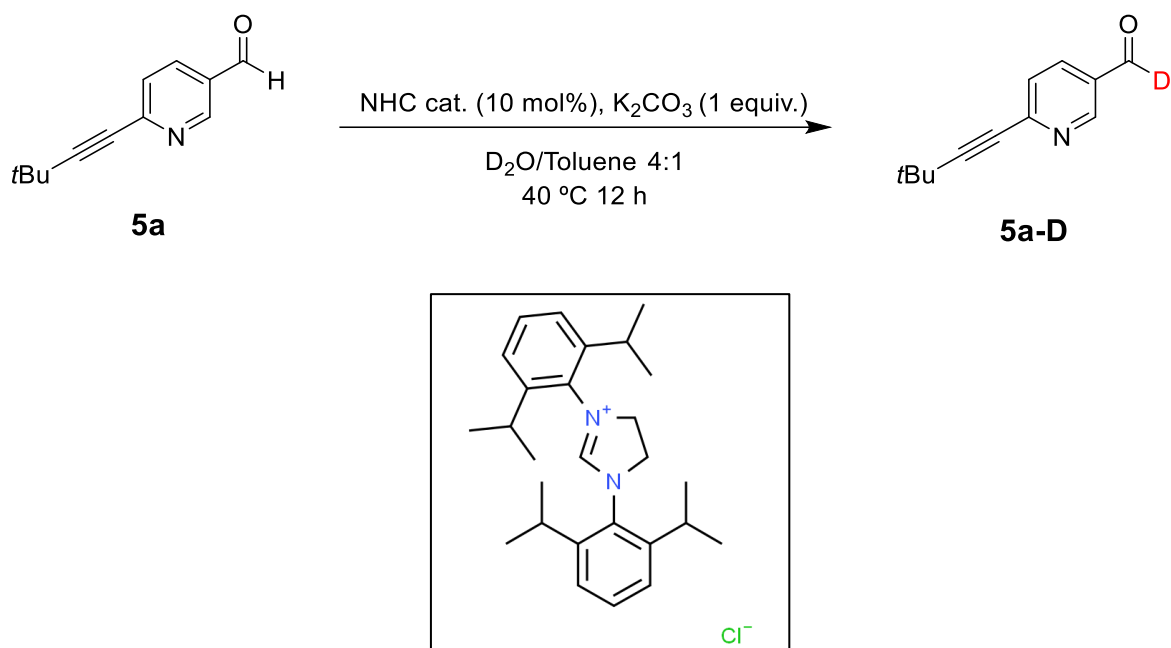
reducing the amount of  $\text{Zn}(i\text{Pr})_2$  employed. The formation of the esters is believed to follow the same reaction pathway previously described. It can be supposed that, if these side products are formed only with a lower amount of  $\text{Zn}(i\text{Pr})_2$ , it means that the autocatalytic cycle of **4c\*** in presence of enough amount of  $\text{Zn}(i\text{Pr})_2$  in the saturation vapour probably does not allow the CT rearrangement to occur. In any case, even in presence of a lack of  $\text{Zn}(i\text{Pr})_2$ , **9** and **10** form in lower amount compared to **13** and **14**. Further studies are needed to probe the role that the pyrimidine ring could play in this difference of behaviour. In those experiments ketone **8** has been found in the reaction crude as only side product. The MPV rearrangement could still be valid but probably also other mechanisms that lead to the preferential formation of **8** could take place during the reaction. One possibility could be the formation of **7** and its subsequent oxidation into **8**.

The mechanism reported in this Chapter has many affinities with the mechanism reported by Trapp (section 1.1.8.5). It must be noted that in Trapp's mechanism the hemiacetal was a key intermediate for the amplification of *ee* of alcohol **4c**, while in our case the hemiacetal intermediate is part of a parallel reaction pathway that leads to the formation of stable esters. Since a reaction mechanism for the amplification of *ee* of **4c** and **6a** was intentionally not provide in Scheme 4.5, it can be speculated that Trapp's mechanism is still valid under the heterogeneous conditions and is one of the reaction pathways taking place in the vapour-solid reaction mechanism.

#### 4.6 Preliminary experiments to validate the proposed reaction mechanism

The only moiety of the structure of **5a** involved in the chemical transformations of Scheme 4.5 is the carbonyl group, so it was thought, to gain more insights on the previously described reaction mechanism, to design experiments in order to follow the changes happening on this group during the reaction. The chosen strategy has been to synthesize a deuterated version of aldehyde **5a** and check the percentage of deuteration of the products formed at the end of the vapour phase reaction.

Deuterated aldehyde **5a** (**5a-D**) was synthesized following the procedure developed by Geng, Chen *et al.* <sup>[118]</sup> (Scheme 4.8). The product was obtained in 20% yield and 95% deuteration.



**Scheme 4.8:** Synthesis of **5a-D** and structure of the NHC catalyst employed

If the reaction was following the proposed reaction mechanism, a vapour phase reaction with **5a-D** as starting material would have resulted in all the products having deuterium instead of hydrogen in the structure, with the exception of ketone **12** in which the protons of the *iPr* group, coming from  $\text{Zn}(i\text{Pr})_2$ , would be hydrogens. Indeed, the crude  $^1\text{H-NMR}$  of the reaction in Figure 4.9 shows how all the diagnostic peaks between 6 ppm and 3 ppm were silenced by the deuteration, with the exception of the ketone signal at 3.45 ppm. Conversely, the aromatic signals (between 9.5 and 7 ppm) are not silenced and overlap perfectly with a typical vapour phase reaction of **5a**.

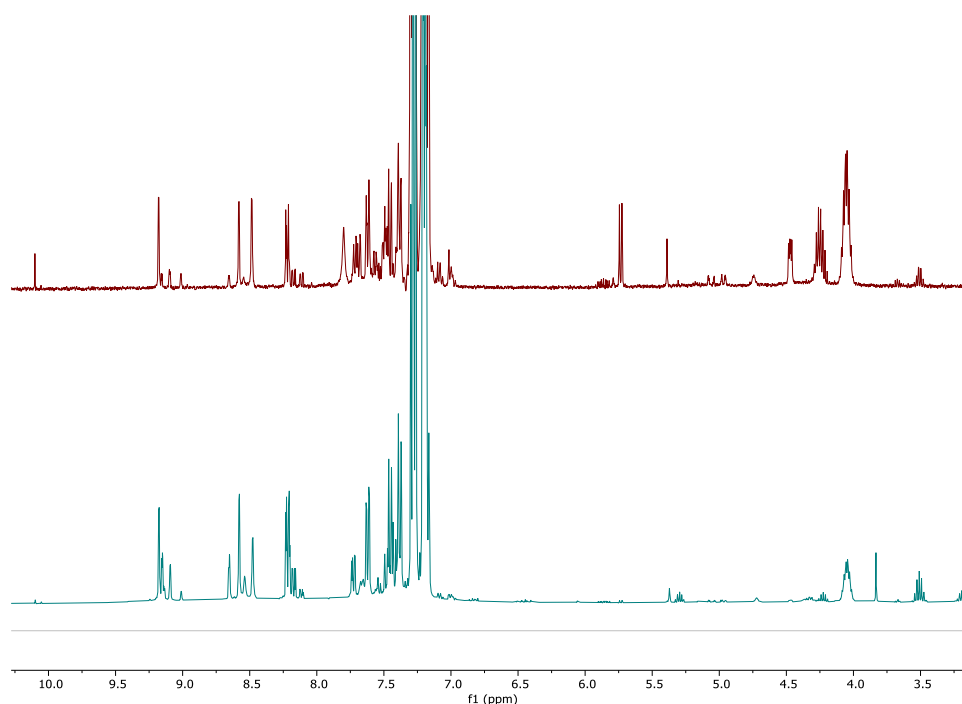


**Figure 4.9:** Top to bottom: crude  $^1\text{H-NMR}$  of vapour phase reaction of **5a** and crude  $^1\text{H-NMR}$  of vapour phase reaction of **5a-D**

In a second experiment, a 50/50 mixture of **5a** and **5a-D** was employed as substrate for the vapour phase reaction. In this case, it was not expected a complete disappearance of the mid-field signals of the products, but rather a decrease in their integral compared to the aromatic and alkylic signals. The  $^1\text{H-NMR}$  spectrum of the crude confirmed this hypothesis (Figure 4.10).

Confronting the peaks in the mid-field area with the peaks from the aromatic area it was also possible to evaluate the amount of deuteration in the products (Table 4.6): the deuteration levels were found quite similar for alcohol **6a** and chiral ester **13** but lower for achiral ester **14**. Again, this preliminary experiment agrees with the proposed reaction mechanism, but a larger set of repeated experiments are needed to have a statistically relevant percentage of deuteration in the products. Moreover, varying the amount of deuterated starting material in more rationally designed experiment will help to define the effect of deuteration on the reaction kinetics. Some minor new peaks were also observed, a sign that other reaction products could be present in the crude.

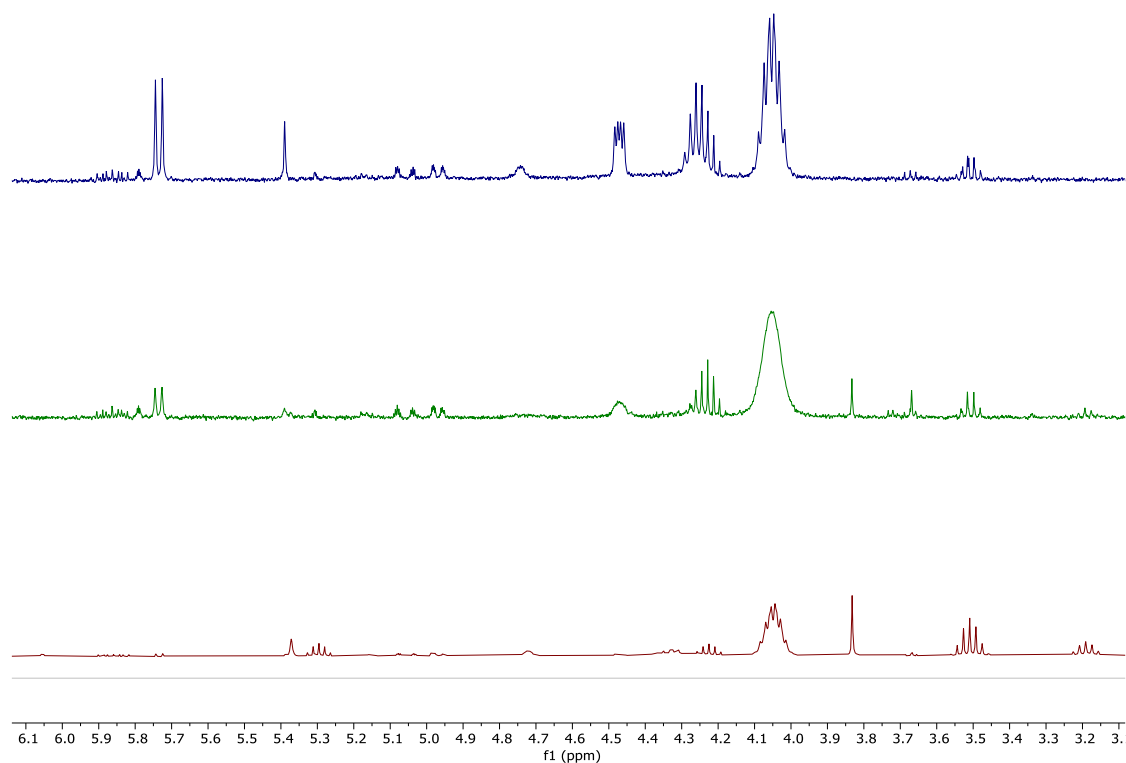


**Figure 4.10:**  $^1\text{H}$ -NMR spectra of vapour phase reactions of (top to bottom): **5a**, **5a** + **5a-D** in 50/50 mixture, **5a-D**.

**Table 4.6:** Deuteration of the products of the 50/50 mixture experiment (no reduction product **11** observed in the crude).

COMPOUND	DEUTERATION
<b>6a</b>	28%
<b>13</b>	38%
<b>14</b>	13%

#### 4.7 Influence of chiral triggers on the vapour phase reaction

I was thought that the addition of pyridine alcohol **6a** from the beginning in the reaction mixture could have helped to direct the reaction mainly to the autocatalytic reaction of **5a** in **6a** and the subsequent amplification of *ee* of **6a**, and reduce the amount of the “off-loop” side products formed. The starting mixture subjected to the vapour phase reaction was composed with 0,1 equiv. of (*R*)-**6a** with 15% *ee*. Despite the presence of **6a**, the side products formed in comparable proportions to the reaction performed under absolute conditions. The final *ees*

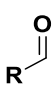
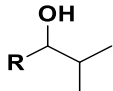
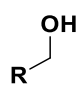
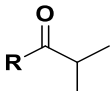
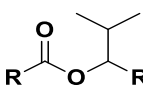
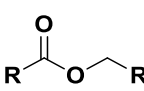
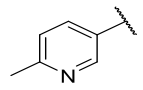
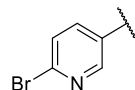
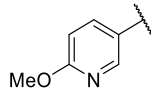
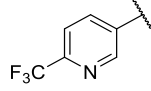
had no substantial difference from the previous reactions as well: (R)-**6a** was obtained in 39% *ee*, while (R)-**13** in 81% *ee*. When (S)-**6a** was employed in 0,1 equiv. in the reaction mixture, both (S)-**6a** and (S)-**13** were produced. This means that, as for the vapour phase reactions on Soai aldehyde **3c**, the reaction seems to be sensitive to the presence of chiral triggers, and it is possible to direct the preferential formation of one or the other enantiomer with an appropriate source of chirality.

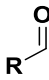
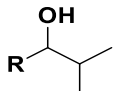
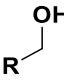
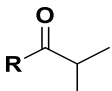
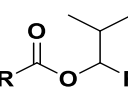
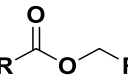
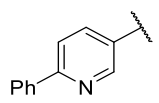
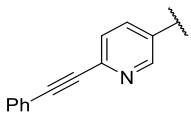
#### 4.8 Screening of other zincorganil reagents and pyridine aldehydes

The reaction was performed on aldehyde **5a** employing Zn(Me)<sub>2</sub> and Zn(Et)<sub>2</sub>. In both cases a quantitative conversion of **5a** to the corresponding alcohols was archived, interestingly with no side products formation. The alcohols were obtained as racemate solutions.

A preliminary screening of other pyridine aldehydes was performed. The substrates were 2-substituted pyridine aldehydes with R groups that differ for steric and electronic effects. The results are summarized in Table 4.6.

**Table 4.7:** Screening of different 2-substituted pyridine aldehydes

Entry	R						
1		19%	44% <i>ee</i> = rac	/	17%	14%	7%
2		/	73% <i>ee</i> = rac	6%	21%	/	/
3		/	76% <i>ee</i> = 2%	/	23%	/	/
4		/	43% <i>ee</i> = 12%	36%	15%	5%	/

Entry	R						
5		/	49% <i>ee</i> = rac	9%	26%	15%	/
6		/	59% <i>ee</i> = 84%	5%	29%	6%	/

In all the reactions the corresponding alcohol was obtained in higher yields compared to **6a**. In half of the cases the alcohol was found racemic, and considering the non-racemic alcohols, in Entries 3 and 4 the *ee* was found low and only in Entry 6, with the substrate more similar to **5a**, a high *ee*% was archived. It is interesting to notice the dramatic difference in final *ee* between the substrates in Entries 5 and 6, which differ only for the presence of an additional triple bond on the R group.

The number and amount of other side products formed differs from substrate to substrate, but in general they were found in lower amount compared to the side products obtained from **5a**. The corresponding ketones are the only substrates found in all entries (and in Entry 3 it is the only side product detected). As previously discussed for aldehyde **3c**, the formation of a ketone without the presence of the corresponding primary alcohol can be attributed to a different reaction mechanism than the MPV mechanism.

#### 4.9 A possible explanation for the amplification of *ee* in the vapour phase reaction

As described in the introduction of the chapter, no report on absolute asymmetric synthesis and (+)-NLE has ever been made on pyridine aldehydes in solution. On the other way around, the process is feasible under heterogeneous vapour-solid conditions.

When starting from a reactive achiral system leading to chiral products, the racemic mixture is the only thermodynamic stable state at equilibrium. Nevertheless, stable homochiral states can be obtained under particular conditions. In far-from-equilibrium systems, which are defined as systems unable to archive thermodynamic equilibrium, the rules of equilibrium thermodynamic are not applicable anymore: the racemic steady state may become

metastable and more stable non-racemic steady states will be reached by the system. Through a symmetry breaking transition, the conversion of starting achiral reactants to final chiral products will be obtained (absolute asymmetric synthesis).

When considering systems able to lead to SMSB, two issues must be considered. Firstly, the reaction network, the simplest possibility being an enantioselective autocatalytic reaction. The process itself is however not able to give a stable homochiral state if not coupled with a heterochiral reaction between product/catalysts. Frank's model (described in Section 1.1.5) has all the features to lead to SMSB. It involves an enantioselective autocatalysis and the mutual inhibition between the enantiomers is the heterochiral reaction required. The second issue is the thermodynamic system in which the above discussed reaction has to take place in order to lead to the SMSB. Examples of systems unable to reach equilibrium with its surroundings are open systems or closed systems with non-uniform distribution of matter or energy. Moreover, the system should be able to generate a flux between initial and final products. In the case of enantioselective cycles, the flux is directed only to some of the species of the reaction network.

It should not be surprising that the Soai reaction, the first and only experimental demonstration of Frank's model, has the features of a SMSB under certain conditions. In particular, SMSB takes place in solution when the product of a reaction is recycled as a catalyst for a subsequent reaction. This procedure is similar to an open flow system with constant inflow of reagents and outflow of products.



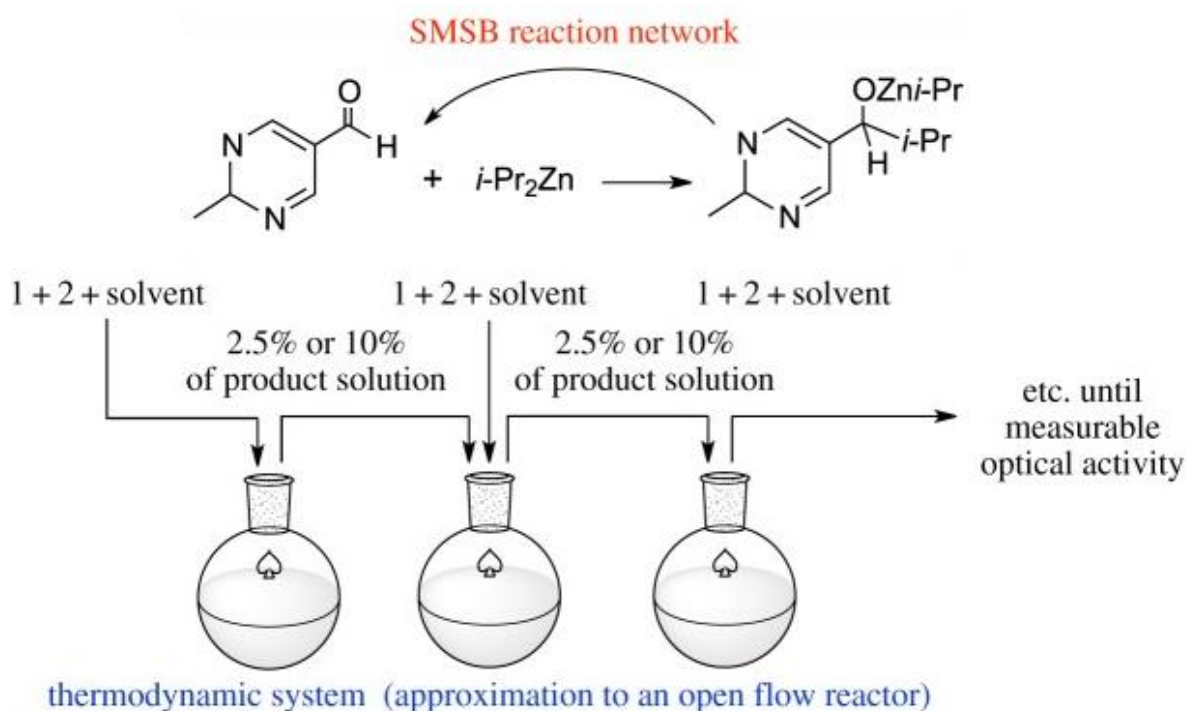


**Figure 4.11:** Reaction network and thermodynamic system for SMSB in the Soai reaction.

In the same way, the vapour phase reaction setup can be considered as well an approximation of an open flow system: vapours of  $\text{Zn}(\text{iPr})_2$  come from the gas phase and react in a kinetically-controlled way with solid aldehyde. It is possible to think that the reaction products segregate, for example, as separated solid phases, or that the off-loop formation of the side products is allowing the net flux to take place, creating conditions for the SMSB to occur.

#### 4.10 Conclusions

With the heterogeneous vapour-solid reaction setup SMSB and absolute asymmetric synthesis of alcohol **6a** is obtained, a reaction outcome not taking place under homogenous conditions. Moreover, unreported side products are obtained and a reaction mechanism for the formation of the side products is presented. The mechanism is not only important for the reaction of aldehyde **5a** but provides new insights into the mechanism elucidation of the Soai reaction itself.

The work presented in this chapter has been published in **Paper II**, additional supporting informations for unpublished results can be found in **Appendix IV**.

# 5

## Conclusions and future prospects

---

This thesis work has been focused on performing the Soai reaction in a different and less explored way compared to the standard liquid phase reactions. The heterogeneous vapour phase reactions have demonstrated to give high ee% for both the standard pyrimidine aldehyde of the Soai reaction **3c** but also for the less conventional pyridine aldehyde **5a**. Moreover, it gave the chance to isolate mechanistically relevant intermediates for the elucidation of the Soai reaction mechanism.

Still, the results presented in this thesis will require further confirmations in the future. This chapter will briefly recap the results of each previous chapter and suggest some further work worth attempting.

### 5.1 Different MOFs for Soai aldehyde inclusion

**Chapter 2** reported a method for the inclusion of Soai aldehyde **3c** in UiO-type MOF and two reliable methods for the qualitative evaluation of the amount of included **3c**. The inclusion of the Soai aldehyde was demonstrated through different techniques.

In order to further understand the reactions taking place inside the framework, different type of materials should be employed. As already explained, the UiO-MOFs are too symmetrical to be used for a regular arrangement of the aldehyde in the framework, and exploit the molecular sponge effect (see Section 1.3.3). With that effect, a chemical visualization of the reaction could be performed, a work that would give great results in the elucidation of the reaction mechanism not only when confined in the MOF.

One of the main drawback of the inclusion method was the low reproducibility of results and the low amount of aldehyde included in the material. Also in this case, exploring different MOFs could be beneficial for having a robust and reproducible inclusion procedure with high amount of Soai aldehyde included.

## 5.2 Different reaction setups

In **Chapter 3** vapour phase reactions on **3c** included in UiO-MOFs have been performed. The results show that aldehyde **3c** amplifies under absolute conditions to yield **4c** in high *ee*% in the pristine material, while moderate *ee*% were found when employing the UiO MOFs as confinement for **3c**, even if with a faster reaction kinetic. Moreover, unreported side products have been detected and characterized in the reaction under specific conditions.

One of the main improvements that could be beneficial for this field of research would be to find a new and better reaction setup to perform the vapour phase reactions. The system employed (Figure 3.1) does not allow to sample the MOF material and follow the reaction through time. A piercing of the sealed vial cap would result in a contamination from the outside (if the reaction is not performed in a glove box) and in the lowering of the vapour tension of  $\text{Zn}(i\text{Pr})_2$ . Moreover, to overcome this limitation, series of reactions were starting at the same time and stopped at fixed time points. Despite the fact that some clear trends were found in the reactions through this approach, reproducibility is always an issue when considering the Soai reaction, and these analyses will not always be 100% meaningful.

## 5.3 Different material analyses

A significant improvement in the analyses of the materials before and during the vapour phase reactions could come from different spectroscopic techniques. For example, for the determination of the amount of Soai aldehyde inside the MOF. The leakage experiments and the MOF digestion are still quite rudimental ways to gain information on the amount of substrate inside the framework. Different techniques could help to give the exact amount of physisorbed substrate in the framework without wasting MOF with destructive analyses.

Spectroscopic techniques could become useful also to follow the reaction: they could give an estimation of consumed reagent, converted products and *ee*% with no need of opening the reaction chamber and without the need to start more reactions at the same time.

## 5.4 Different experiments to validate the reaction mechanism

In **Chapter 4**, absolute asymmetric synthesis of alcohol **6a** is obtained under heterogeneous conditions, a reaction outcome recently reported under homogenous conditions. Moreover, unreported side products are obtained and a reaction mechanism for the formation of the side products is presented. The mechanism

is not only important for the reaction of aldehyde **5a** but provides new insights into the mechanism elucidation of the Soai reaction itself.

The mechanism proposed in Section 4.5 is based on the structures of the reaction products and on some insights gained performing the reactions at various temperatures and in different substrate/reagent ratios. Moreover, preliminary experiments to validate the reaction mechanism are presented.

The choice to perform the reaction with a deuterated version of pyridine aldehyde **5a** was considered the best choice to start the preliminary experiments. A wider set of experiments, employing for example deuterated  $\text{Zn}(i\text{Pr})_2$  and **5a-H** would give more information and complement the already performed experiments. Isolation of the reaction products would help to give a better estimation of the deuteration of the different species, and to follow the break and formation of bonds in the reaction. Also, the isotope effect could lead to isolate the reaction intermediates.

### **5.5 Different reaction substrates**

Previously to this thesis work, there has never been an observation of the reaction products found in the reactions described in the previous chapters. Esters **9**, **10**, **13** and **14** and ketones **8** and **11** have been found in the reaction mixture only performing the heterogeneous vapour phase reactions with the reaction setup developed in this thesis work. In addition, some different reaction substrates than **3c** and **5a** gave rise to some esters and ketones, something not found in their liquid phase reactions.

This gives the idea of how heterogeneous reactions can be a powerful and quite unexplored method for asymmetric reactions. It is possible that vapour-solid interactions can give rise to new reaction mechanisms like the one reported in this thesis work. The exploration of this methodology should not be limited only to the Soai reactions, but could find applications also in other fields of organocatalysis.

# Paper I

*Symmetry Breaking and Autocatalytic Amplification in Soai Reaction Confined within UiO-MOFs under Heterogeneous Conditions.*



# Symmetry Breaking and Autocatalytic Amplification in Soai Reaction Confined within UiO-MOFs under Heterogenous Conditions.

Giuseppe Rotunno,<sup>[a, b]</sup> Gurpreet Kaur,<sup>[a, b]</sup> Andrea Lazzarini,<sup>[a, b]</sup> Carlo Buono,<sup>[a, b]</sup> and Mohamed Amedjkouh\*<sup>[a, b]</sup>

**Abstract:** Symmetry breaking is observed in the Soai reaction in a the Soai reaction exhibits significant activity and autocatalytic confinement environment provided by zirconium-based UiO- amplification. Comparative catalytic studies with various UiO-MOFs used as crystalline sponges. Subsequent reaction of MOFs indicate different outcomes in terms of enantiomeric encapsulated Soai aldehyde with Zn(i-Pr)<sub>2</sub> vapour pro- moted excess, handedness distribution of the product and reaction absolute asymmetric synthesis of the corresponding alkanol. rate, when compared to pristine solid Soai aldehyde, while the ATR-IR and NMR confirm integration of aldehyde into the porous crystalline MOF remains highly stable to action of Zn(iPr)<sub>2</sub> material, and a similar localization of newly formed chiral vapour. This is an unprecedented example of absolute alkanol after reaction. Despite the confinement, asymmetric synthesis using MOFs.

## Introduction

Chirality remains an intriguing scientific topic. Biomolecules in nature exhibit overwhelming one-handedness, often called homochirality, such as L-amino acids and D-sugars. Asymmetric catalysis can lead to the synthesis of enantiomerically pure chiral products in areas such as fine-chemicals and pharmaceuticals with growing need in the last decades. The asymmetry can be introduced through a chiral auxiliary or a chiral catalyst.<sup>[1]</sup> In contrast with asymmetric catalysis, in which the structures of catalyst and product are different, in asymmetric autocatalysis a chiral product acts as chiral catalyst for its own production.<sup>[2]</sup> The Soai reaction remains a remarkable example of amplifying asymmetric autocatalysis.<sup>[3,4]</sup> The addition of Zn(i-Pr)<sub>2</sub> to a rigid pyrimidine-5-carbaldehydes such as **1** in toluene provides alkanols **2** with increasing ee.<sup>[5]</sup> Furthermore, it showed to be prone to amplification of ee despite the absence of the corresponding alcohol **2**, but in presence of various chiral factors<sup>[6]</sup> and, even more strikingly, in absence of any chiral substance.<sup>[7]</sup> Recently, asymmetric amplification of such autocatalysts was realized under heterogenous phase, via a heteroge-

neous vapour-solid interaction, by reaction of *iPr<sub>2</sub>Zn vapor on achiral solid aldehyde*.<sup>[8]</sup> The synthesis of optically active compounds from achiral precursors has been defined as absolute asymmetric synthesis.<sup>[9]</sup>

In search for a validate mechanism of the remarkable asymmetric amplification efforts have been made using advanced techniques such as microcalorimetry,<sup>[10]</sup> NMR analysis<sup>[11]</sup> and DFT calculations.<sup>[12]</sup> These analyses revealed the presence of dimers, tetramers and even higher-level aggregates in the reaction cycle. Combinatory studies of NMR and DFT techniques<sup>[13,14]</sup> and XRD analysis of crystals<sup>[15]</sup> added support for these findings (Figure 1). Gridnev *et al.* have computationally quantified the abundance of the species in the reaction pool.<sup>[13]</sup> Dimers were proposed as the resting state of the catalyst, while tetramers were found as the active catalytic species. An alternative mechanism involves hemiacetal complexes, first observed as transient intermediates,<sup>[16]</sup> then by formation of subsequent derivatives under heterogenous conditions<sup>[8b]</sup> and further by *in situ* mass spectroscopic investigations.<sup>[17]</sup> Nevertheless, as proposed by Brown *et al.*,<sup>[11c]</sup> once the reaction provides a tiny enantiomeric imbalance in the products, the ee can easily be propagated and amplified by the oligomerization of the reaction species.<sup>[18]</sup> Under homogeneous conditions, the dimers and tetramers involved in the reaction mechanism can diffuse in solution, propagate and even associate into indefinite polymers. In more recent investigations, Denmark *et al.* report on the function of the pyridyl- and pyrimidyl-moiety in the NMR studies revealing a tetrameric structure, also described as a cube escape model.<sup>[19]</sup>

Furthermore, the process is amenable to spontaneous molecular symmetry breaking under heterogeneous conditions by reaction of *iPr<sub>2</sub>Zn vapor-phase on solid aldehyde 1*.<sup>[20]</sup> Thus, in absence of solvent and with limited dynamic freedom the assembly and propagation of the reaction intermediates remains possible and allows for amplification in a constrained solid state. Therefore, it is relevant to probe confinement effects

[a] G. Rotunno, G. Kaur, Dr. A. Lazzarini, Dr. C. Buono, Prof. Dr. M. Amedjkouh  
Department of Chemistry

University of Oslo  
P.O. Box 1033, Blindern, 0315 Oslo (Norway)

[b] G. Rotunno, G. Kaur, Dr. A. Lazzarini, Dr. C. Buono, Prof. Dr. M. Amedjkouh  
Center for Materials Science and Nanotechnology (SMN)

Faculty of Mathematics and Natural Sciences  
University of Oslo

P.O. Box 1126, Blindern, 0318 Oslo (Norway) E-mail: mamou@kjemi.uio.no

Supporting information for this article is available on the WWW under <https://doi.org/10.1002/asia.202100419>

© 2021 The Authors. Chemistry - An Asian Journal published by Wiley-VCH GmbH. This is an open access article under the terms of the Creative Commons Attribution Non-Commercial License, which permits use, distribution and reproduction in any medium, provided the original work is properly cited and is not used for commercial purposes.

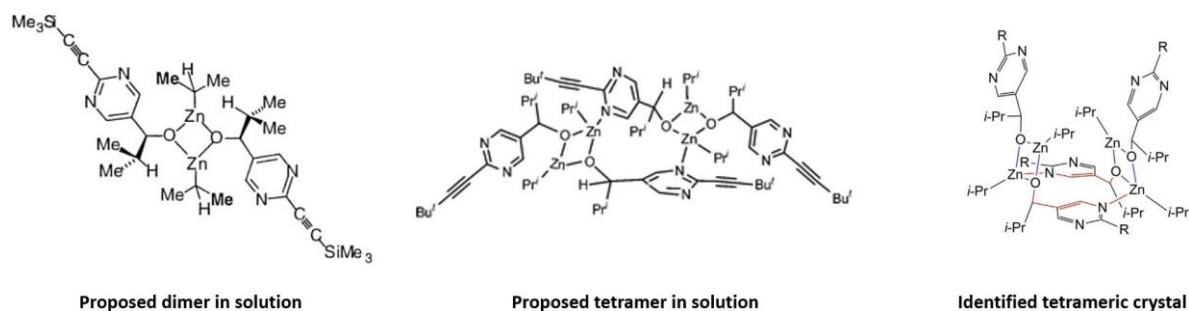


Figure 1. Selection of proposed or isolated reaction intermediates.

on the formation of the autocatalytic species and the extent of linker functionalities because of the need to transport typically amplification if possible. Metal-Organic Frameworks (MOFs) very large organic substrates and products. This effect could provide an adequate environment as crystalline sponge for significantly influence the final conversion and enantiopurity of guest inclusion for such heterogenous asymmetric catalysis and Soai alcohol 2 in the reaction.

perform asymmetric reactions in a pocket-like confined space. Because of the spontaneous symmetry breaking in the Soai MOFs are porous crystalline materials, consisting of a 2D or 3D reaction, there was no need of a chiral MOF as asymmetric network, with metal containing nodes known as secondary inductor/catalyst for our studies. The materials of our choice building units (SBUs) linked by multidentate organic ligands were UiO-type MOFs, namely UiO-66 and UiO-67, consisting of a (linkers) by strong chemical bonds.<sup>[21]</sup> They emerged as metal cluster of 6 Zr(IV) ions arranged in an octahedron and, respectively, the organic linkers terephthalic acid ( $H_2bdc$ ) and biphenyl-4,4'-dicarboxylic acid ( $H_2bpdc$ ) (Figure 2). To the best of our knowledge, this is the first example of absolute asymmetric autocatalysis performed within “achiral” MOF.

In the last decade, researchers have applied a variety of synthetic strategies to build chiral MOFs for asymmetric catalysis and a large number of MOF-catalysed organic reactions have been reported.<sup>[22]</sup> Herein, we present our study of the confinement of aldehyde 1 within the framework of MOFs functioning as nanocontainers/reactors. Consequently, the oligomerization is subject to mesoporosity of the framework, which enforces limited propagation of the reaction intermediates through channel openings. To this end, it is imperative to probe MOFs with various open channels and

## Inclusion

### Preliminary DFT calculations

Periodic DFT calculations have been performed in order to predict the position in which Soai aldehyde 1 would preferentially be allocated inside UiO-67 and UiO-66 (Figure 3). Firstly,

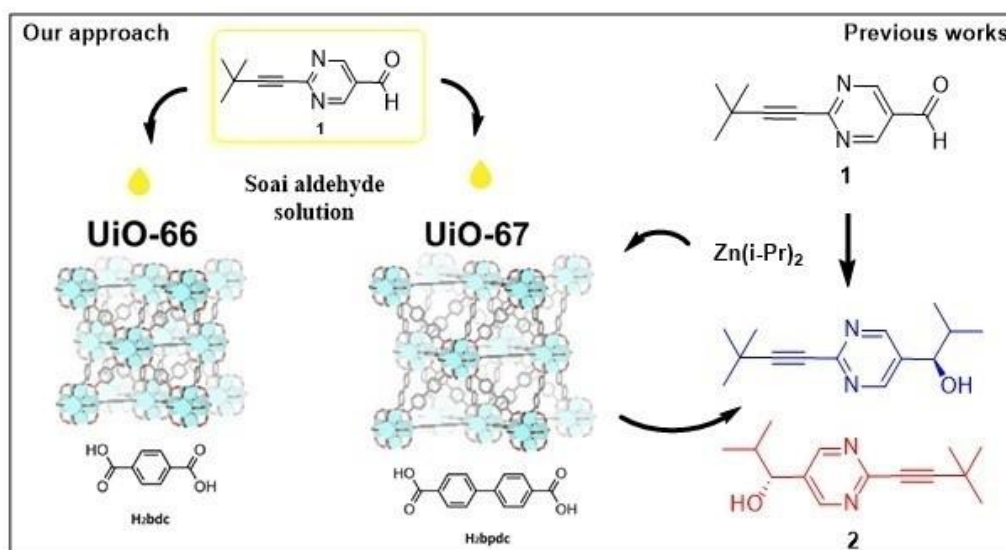


Figure 2. Schematic outline of guest inclusion in UiO-MOFs.



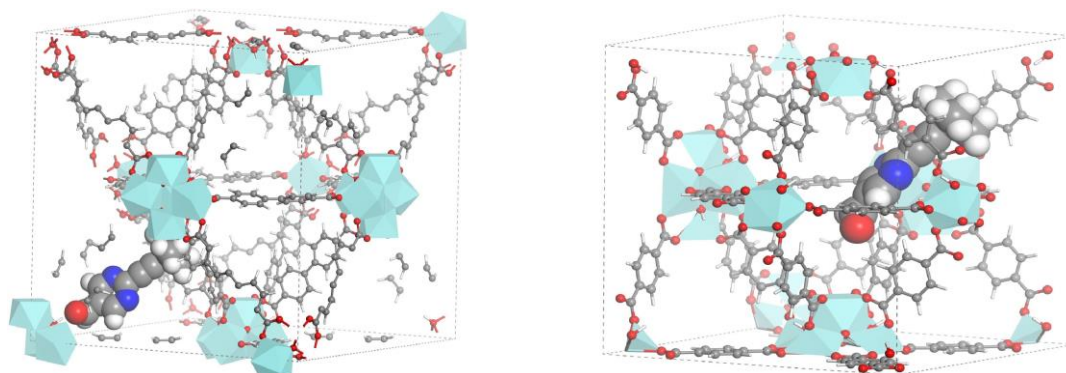


Figure 3. Periodic DFT calculations of **1** in cavities of UiO-67 (left) and UiO-66 (right).

comparing the structures of **1** and the linkers of the two MOFs, the size of the aldehyde (10.5 Å) was found slightly smaller than the size of the biphenyl dicarboxylate linker of UiO-67, while terephthalic acid linkers of UiO-66 were almost half the size of the aldehyde. (See SI). The octahedral cages of the MOFs have been calculated being 16 Å for UiO-67 and 11 Å for UiO-66.<sup>[23]</sup>

In UiO-67, the optimized structure shows **1** physisorbed in the octahedral cage of the framework, with the formation of an H-bond between the hydrogen of the hydrated cornerstone of the MOF cluster and the oxygen of the carbonyl group of the aldehyde. In the UiO-66 the cavity of the MOF is too small for the allocation of aldehyde **1** in the same position as in UiO-67. The most stable structure predicts the aldehyde inside the cavity establishing only weak van der Waals interactions with the organic linkers.

### The inclusion process

The inclusion of Soai aldehyde **1** has been performed by soaking sample of MOF powder in a toluene solution of **1** (Figure 2). We carried out tests with varying the ratio between aldehyde and MOF (0.5:1, 1:1, 2:1), which led to the optimized ratio in weight between MOF and aldehyde **1** being 1:2 to provide better HPLC analysis. The solution evaporated at r.t.: the slow evaporation of the solvent gradually concentrates the guest, which diffuses by capillary absorption and crystallizes inside the pores of the host.<sup>[24]</sup> After complete evaporation, the acetone and oven-dried at 140 °C. The washing process is a key MOF powder was washed and filtered under vacuum with step that removes the excess of **1** present on the surface of the MOF, unbound to the framework. High Performance Liquid Chromatography (HPLC) analyses of the leakage of aldehyde **1** from an unwashed MOF sample showed the presence of **1** in solution already after few minutes. Samples analysed at later times indicated that the area of the aldehyde peak of **1** remained almost unchanged, due to the considerably higher amount of **1** present on the surface and immediately released in solution compared to the amount leaked from the inside of the MOF. On the other hand, the concentration of **1** in a washed MOF sample slowly increased over time, proving

extraction of **1** from the MOF into the solution, with a significant diminution of the weakly coordinated aldehyde on the MOF surface (Figure 4-a).

### Quantification of the aldehyde in the different materials

In order to estimate the amount of aldehyde **1** included in the materials, two methods have been employed: leakage experiments followed by HPLC analysis and MOF digestion followed by NMR analysis. In the first method, the intensity of the absorption, and so the area of the aldehyde peak in the chromatogram, is proportional to its concentration in the liquid sample (Beer-Lambert law). However, it has been used only as an indirect method for a rough qualitative estimation, because the concentration will only represent the amount of aldehyde leaked from the MOF into the solution and not the amount present in the powder sample.

The second method is the MOF digestion by a media followed by NMR analyses of the resulting solution. The media dissolves the organic components of the MOF (linkers and aldehyde) while the inorganic portions precipitate as inorganic salts. NMR analysis allows to correlate the aldehyde signals with the signals coming from the linkers (Figure 4-c). This method can be considered a direct quantification of the amount of aldehyde in the material. With Zr-based MOFs, a basic digestion with NaOH in D<sub>2</sub>O is normally employed. In our case, the Soai aldehyde **1** was found insoluble in the basic media. Instead, an acidic solution of 1% v/v D<sub>3</sub>PO<sub>4</sub> in DMSO-d<sub>6</sub> was used as digestion media.

When analyses on the same materials have been made with the two methods, they have shown similar trends in the amount of aldehyde included (Figure 4-b). For instance, the inclusion process has been performed in MOFs with different linkers: pristine UiO-67, UiO-67 bpy<sub>10%</sub>, UiO-67 binaphtyl and UiO-66 (See SI). UiO-67 bpy<sub>10%</sub> was the UiO-MOF in which the highest amount of aldehyde **1** was allocated. On the other hand, UiO-66 was the one with the lowest amount of guest inclusion. Interestingly UiO-67 binaphtyl, characterized by a much hindered cage, was found able to allocate a slightly higher amount of Soai aldehyde compared to UiO-67. This

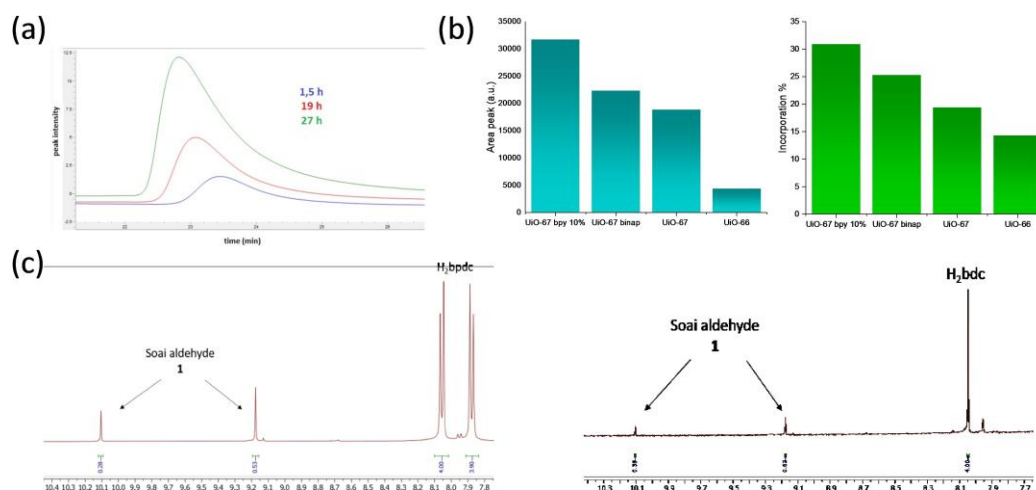


**Figure 4.** (a) Leakage experiments from washed UiO-67. (b) HPLC (left) and NMR (right) dual quantification of **1** in different UiO-MOFs. (c)  $^1\text{H}$ NMR of digested UiO-67 (left) and UiO-66 (right) in acidic solution of 1%  $\text{D}_3\text{PO}_4$  in  $\text{DMSO-d}_6$ .

could be explained by  $\pi$ - $\pi$  interactions between the naphthyl rings of the linker and the pyrimidine rings of aldehyde **1**.

them. Again, the results are in agreement with the DFT calculations.

### Analyses on the MOF materials after inclusion of Soai aldehyde **1**

It was crucial to obtain a crystalline material after the inclusion step. In amorphous MOFs Soai aldehyde **1** would probably have been allocated in only certain areas of the MOF framework. Consequently, in such a MOF it is difficult to exploit the confinement effect and to evaluate the influence of the framework on the reactions. PXRD (Powder X-Ray Diffraction) analysis of the MOF with included Soai aldehyde showed no loss in crystallinity compared to the starting material (See SI).

ATR-IR analysis (Attenuated Total Reflectance Infrared Spectroscopy) was performed on the materials. A series of diagnostic signals indicate the presence of aldehyde **1** in the framework of UiO-67 (red line of Figure 5-a). The signal at  $1700\text{ cm}^{-1}$  can be attributed to the stretching of the carbonyl group of the Soai aldehyde **1**, furthermore the peak around  $2200\text{ cm}^{-1}$  can be attributed to the C—N stretching of the aromatic ring while the C—H stretching of the tertbutyl/isopropyl groups can be observed below  $3000\text{ cm}^{-1}$ . Interestingly, the O H stretching of the hydroxyl groups of the clusters below  $3700\text{ cm}^{-1}$  in the pristine material are perturbed in the UiO-67 after inclusion. This is a possible confirmation of the interaction with **1** predicted by the DFT calculations. The ATR-IR analyses have also been performed on a sample of UiO-66 before and after the inclusion (Figure 5-b). The previously discussed signals of the aldehyde in the framework are present in UiO-66 after the inclusion treatment (blue line). Moreover, aldehyde **1** seems to be allocated in a different position in the framework of UiO-66 compared to UiO-67. This can be supported by the hydroxyl groups of the clusters not being perturbed in the sample after inclusion, meaning that the aldehyde is not interacting with

### Vapour phase reaction set-ups

Recently, we have reported two set-ups to perform vapour-phase reactions.<sup>[8b]</sup> These set-ups have been employed for the experiments described in the next section. In the first set-up, the Soai reagent (pristine **1** or included in the MOFs) is placed on the top of a cylindrical glass support, arranged inside a glass vial. In the second set-up, three cylindrical glass supports containing the reagent were located in a bigger vial, in an attempt to secure that the conditions of the gas phase reaction were the same in all the samples. In both cases,  $\text{Zn}(\text{i-Pr})_2$  solution in toluene is added on the bottom under inert atmosphere and the vial is immediately sealed (See SI, Section 1). The first set-up was employed for the experiments of Table 2, while the second set-up for all the other reported experiments.

## Results and Discussion

### Preliminary results

All reactions were conducted at room temperature, and stopped after 24 hours if not specified otherwise, with reaction conditions varying in concentration of substrate, nature and size of the MOF and potentially relevant chiral trigger alkanol **2**. Firstly, our interest has been focused on the reactivity of the Soai aldehyde **1** in three different materials. We began our studies with a set of gas phase reactions with pristine Soai aldehyde **1**, unwashed UiO-67 with included **1** and washed UiO-67 with included **1** respectively. Under these different conditions, subjecting aldehyde **1** to reaction with  $\text{iPr}_2\text{Zn}$  vapour allowed symmetry breaking by absolute asymmetric alkylation

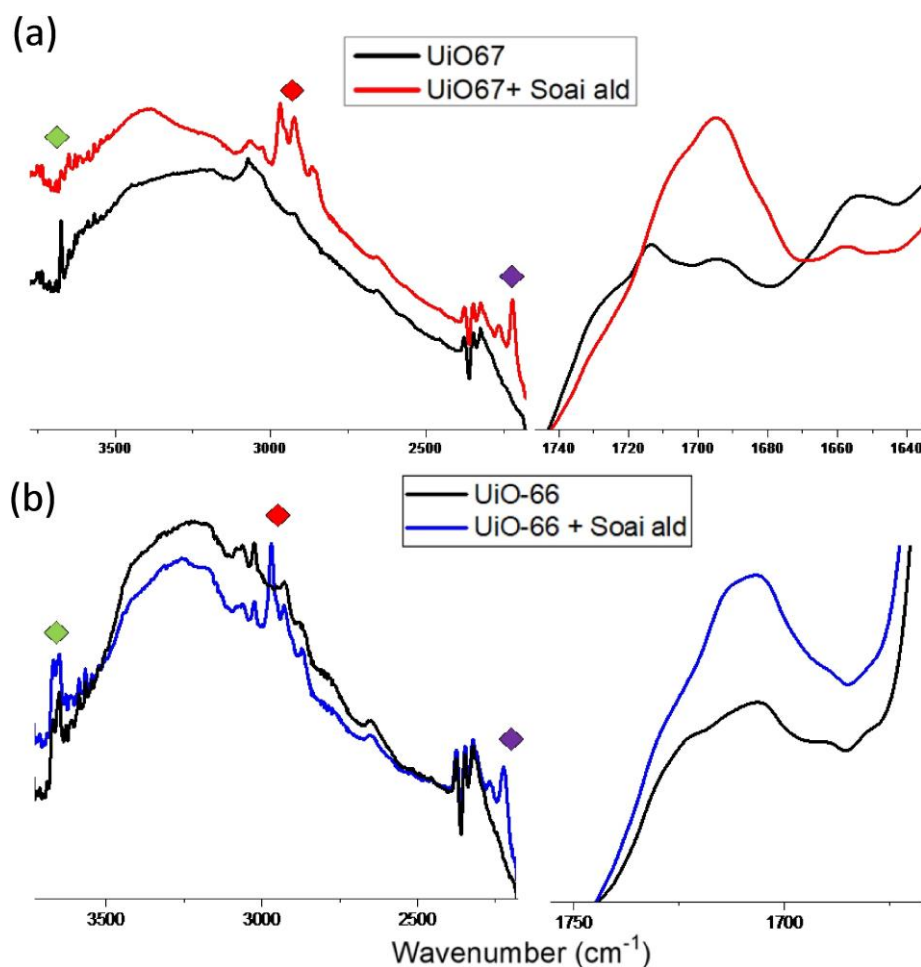


**Figure 5.** ATR-IR of UiO-66 and UiO-66 after inclusion of aldehyde 1. On the left, stretching of the hydroxyl groups (in green), stretching of the *tert*butyl/ isopropyl groups (in red), stretching of the C—N of the ring (in purple). On the right, stretching of the carbonyl group.

to afford alkanol 2. This observation was expected for pristine scale, to Zn(*i*-Pr)<sub>2</sub> vapors. The results shown in Table 1 reveal substrate 1, based on previous literature, although in the comparable conversions and final ee% obtained after reaction. On present experiment a remarkable 88% ee is reached. However, the basis of these observations, it was reasonable to think that this amplification is affected by the confinement conditions in the MOF. In terms of conversion, the washed MOF sample provided a slightly lower conversion compared to the other two samples. In contrast, the final ee% of the unwashed MOF was more similar to the pristine Soai powder, even with an opposite handedness of the product (*S*)-2 in 70% ee, whereas the washed MOF sample yielded a lower amplification of (*R*)-2 with 38% ee (Table 1). The results in Table 1 are in line with those obtained with the leakage experiments in washed vs. unwashed UiO-67. In the unwashed sample the Soai aldehyde 1 is confined in the framework but at the same time an excess of aldehyde 1 is also present on the surface of the MOF. The latter corresponds to surface confinement which reacts in a similar way to the pristine powder of 1. In contrast, after several washes there is little or no Soai aldehyde present on the surface and the UiO-67 MOF contains only confined 1. Thus, the conversion of Soai aldehyde 1 into Soai alcohol 2 takes place only within the pores of the MOF. A second series of experiments has been performed exposing the same substrate, washed UiO-67, but in different

scale, to Zn(*i*-Pr)<sub>2</sub> vapors. The results shown in Table 1 reveal comparable conversions and final ee% obtained after reaction. On the basis of these observations, it was reasonable to think that instead of the amount of MOF powder with included 1, the different ratio of 1 in the MOF could play a crucial role in the reaction outcome. However, as shown in in table 1, similar results were obtained in terms of conversion and amplification. UiO-67 with different loadings of included aldehyde 1 have been obtained and tested to the reaction. The amount of aldehyde 1, confined in MOF, has been evaluated by NMR analysis. Even different amounts of aldehyde 1 in the framework seem to not play a role in the final outcome of the reaction. This suggests that such low loadings are not significant to make a difference in the reaction outcome, even if the MOFs has different concentrations of aldehyde 1. Probably similar experiments with MOFs at higher inclusion of aldehyde 1 (3% or 100%) would give different results, but the difficulty to reach such high inclusion percentages makes it problematic to prove the assumption.

To better understand what could influence the outcome of the reaction in terms of handedness and conversion, a mixture of Soai aldehyde 1 and Soai alcohol 2 has been included in three samples of UiO-67. The initial solution for the inclusion

**Table 1.** Variations of reaction conditions.

Entry <sup>[a]</sup>	Initial reaction conditions		5-Pyridyl Alkanol 2 Configuration	ee [%] <sup>[b] [c]</sup>	Conv. [%]
1	Sample Form for 1	Pristine	<i>R</i>	88	99
2		Unwashed UiO-67	<i>S</i>	70	98
3		Washed UiO-67	<i>S</i>	38	82
4	Load of UiO-67 including 1 <sup>[d]</sup>	1.5 mg	<i>R</i>	43	95
5		3 mg	<i>R</i>	43	91
6		6 mg	<i>R</i>	46	88
7	Inclusion level of 1 in UiO-67 <sup>[e]</sup>	2.5%	<i>R</i>	28	69
8		10.5%	<i>R</i>	22	70
9		11%	<i>R</i>	23	72
10	Chiral trigger <sup>[f]</sup>	( <i>R</i> )-2 15% ee	<i>R</i>	50	81
11		( <i>S</i> )-2 50% ee	<i>S</i>	39	80
12		( <i>R</i> )-2 96% ee	<i>R</i>	69	84

[a] A typical procedure for vapour on solid alkylation is described in the Supporting information. [b] Determined on crude product. [c] The ee was determined using HPLC employing a chiral stationary phase. [d] Vapour phase reaction on different amount of washed UiO-67. [e] UiO-67 with different load of 1 determined by NMR. [f] Alkanol trigger 2 and aldehyde 1 were mixed together before inclusion into MOF.

had an aldehyde:alcohol ratio of 1:0,2, but in two out of three samples the ratio of the included species was found lower. The samples have then been tested to vapour phase reaction and the results are shown in Table 1.

The alcohol included was able to direct the handedness of the new formed alcohol, but the amplification of *ee* was seen only in the first case. The amount of alcohol 2 in the framework is lower compared to aldehyde 1, and it can be speculated that it won't be present in all MOF crystals and all framework cavities. There will be reaction cycles in certain crystals whose outcome in terms of handedness of alcohol 2 will be dictated by the presence of the already included alcohol, and "competing" reaction cycles that will develop under absolute conditions (without alcohol 2) with a random distribution of enantiomers for the product. The result of this multi-site reaction system, enhanced by the diffusion problems of the reaction intermediates, is that the presence of the reaction catalyst is almost uninfluential.

### Kinetic plots of the gas phase reactions

Three samples consisting of pristine Soai aldehyde, Soai aldehyde included in UiO-67 and Soai aldehyde included in UiO-66 have been placed in several glass vials, the addition of the Zn(i-Pr)<sub>2</sub> solution has been performed at the same time and the reaction has been stopped at fixed time intervals. Conversion and *ee* amplification obtained in the three different samples have been measured with HPLC and plotted in Figure 6-a and Figure 6-b. These show that after reaction initiates, conversion is more significant in pristine and confined Soai 1 in UiO-67 to reach 80%, while reaction in UiO-66 levels off at 40% conversion. While symmetry breaking remains a random event, amplification of 2 up to 80% *ee* is favoured by abundance of starting substrate 1 at the expense of confined reactions, ranging between 34-40% *ee*.

In the same way the kinetic profile of the reaction has been compared in pristine Soai aldehyde, Soai aldehyde included in UiO-67 and Soai aldehyde included in UiO-67 bpy<sub>10%</sub>. (Figure 6-c

and Figure 6-d). The kinetic plot of the conversion demonstrates an initial higher rate for the reaction confined in both the UiO-67 in respect to the pristine Soai aldehyde. The observed reactivity may find explanation in the ability to capture and diffuse vapors of Zn(i-Pr)<sub>2</sub> within the cavities of the solid framework, which is dependent of the size of the MOF and may influence its availability to react with aldehyde. Moreover, introduction of the bipyridine linker in the UiO-67 bpy<sub>10%</sub> provides an additional coordination site for the organozinc reagent, which allows a controlled diffusion as compared to UiO-67. Even small cavities of the UiO-66 are able to allocate the oligomers of the catalytic cycle, although with lower conversions. Another significant aspect for the reactivity is related to the boundary conditions of supply of aldehyde, i. e., available amount of 1 considered in terms of concentration in the solid, that can impact the ability to form different oligomers, both in nature and size. Thus, with deficient aldehyde 1 short oligomers may also be autocatalytically active with high rate but lower enantioselectivity. In contrast, a higher concentration of aldehyde is in favour of higher and more enantioselective oligomers resulting in higher enantiopurity of alkanol.<sup>[25]</sup> However, mobility between the cavities of the solid can induce dissociation of such large entities into shorter aggregates to pass through the openings, such as in UiO-66. The level of amplification was always found lower in the MOFs as compared to the pristine aldehyde 1, a consequence of the limited space available for the reaction to propagate due to the confinement in the framework. However, sampling at early conversion rates of the reactions in MOF did not provide measurable traces of alkanol 2. Therefore, the typical sigmoidal shape usually observed in the case of the Soai reaction could not be reproduced. Perhaps most important, is that in all cases, amplification keeps pace after symmetry breaking, but with less significant increments throughout the process, in contrast to the exponential amplification of typical Soai reaction.

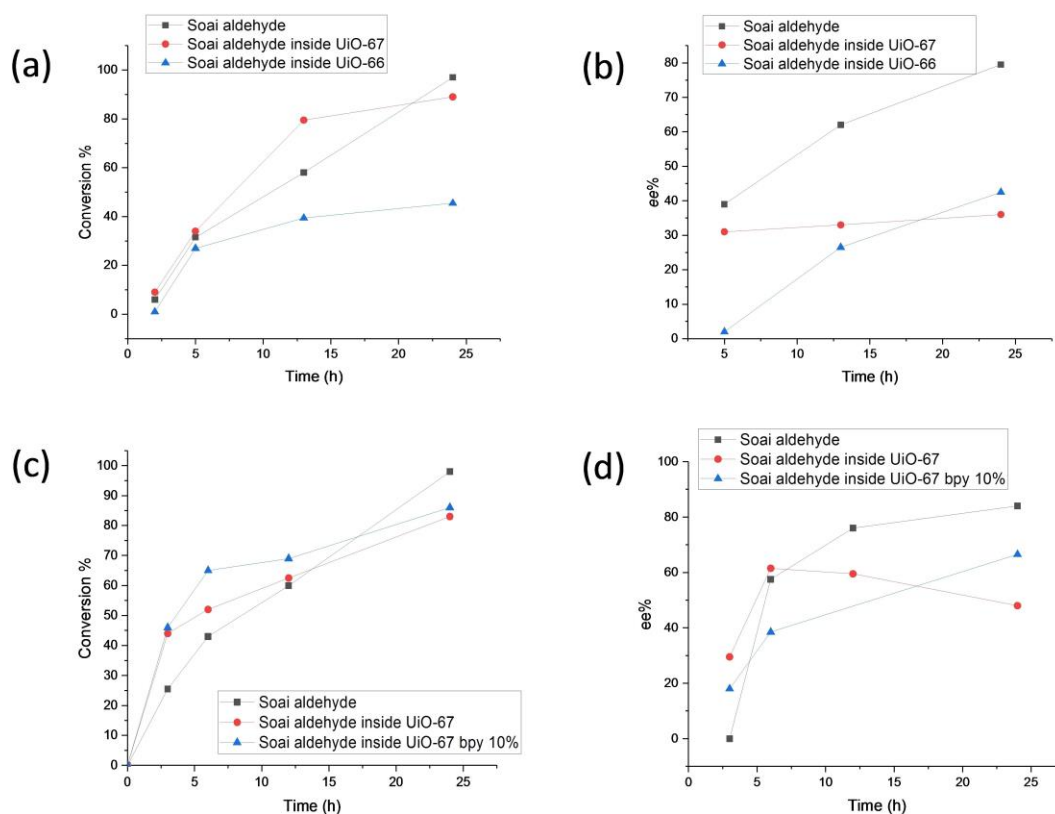


**Figure 6.** Effect of MOF size on conversion (a) and ee amplification (b) over time; Effect of chemical structure of MOF on conversion (c) and ee amplification (d) over time.

### Screening of different UiOMOFs

To make sure the symmetry breaking in MOFs follows a random event and allows for absolute asymmetric synthesis, we conducted the exposure experiments by using MOFs and Zn(i-Pr)<sub>2</sub> different origins. Thus, a number of inclusion forms of aldehyde 1 were screened for the vapour phase reactions with three different Zn(i-Pr)<sub>2</sub> batches. The zinc solutions were added at the same time and the reactions stopped for every run after 7 days. The results are shown in Table 2 below.

In absence of chiral inductor, alkylation of aldehyde 1 in UiO MOFs provide enantiomers of the alcohol 2 at random, a characteristic feature of an Absolute Asymmetric Synthesis. The low amplification level of ee in MOFs compared to the pristine

Soai aldehyde can only result from the confinement effect of the framework of the MOF: such a constraint allows for limited diffusion of the oligomeric species involved in the autocatalytic cycles. Thus, autocatalysis is probably confined to several reaction compartments, and the final observed ee consists of a sum of the total autocatalytic cycles occurring in multiple local sites of the MOF. In contrast, in the pristine Soai all equivalents of aldehyde 1 are part of a continuum allowing for a same autocatalytic cycle. The rising ee may be reflecting the local chirality in UiO-MOF series. Considering the 15 reactions performed in Table 2, five yielded (S)-2, while the other ten yielded (R)-2. This could lead to think of a *pro-R* orientation of the Soai aldehyde included in the MOF. Based on the recent report from Soai *et al.*, and despite the presence of a

**Table 2.** Screening of different UiO MOFs to the gas phase reaction.

Entry	Soaireagent	%	Zinc batch 1	Zinc batch 2	Zinc batch 3
1	Pristine	Conv.	99	99	99
		ee	93 (S)	92 (R)	94 (R)
2	UiO-67	Conv.	93	93	92
		ee	23 (R)	30 (R)	14 (S)
3	UiO-67 bpy <sub>10%</sub>	Conv.	81	86	89
		ee	19 (R)	26 (S)	48 (R)
4	UiO-67 binaphthyl	Conv.	80	72	82
		ee	21 (R)	43 (S)	28 (R)
5	UiO-66	Conv.	55	51	43
		ee	32 (R)	35 (R)	16 (S)



preferential location for the aldehyde in UiO-MOFs, aldehyde **1** is randomly distributed within the framework in a disordered manner.<sup>[8a]</sup> Even if (*R*)-**2** may seem to prevail, this could be just due to the small number of experiments performed.

### Analyses on the materials after the vapour-phase reactions

Two samples of pristine UiO-67 bpy<sub>10%</sub> and UiO-67 bpy<sub>10%</sub> with included aldehyde **1** were subjected to the vapour phase reaction. Figure 7-a depicts the Capillary X-ray diffraction (C-XRD) pattern of both the material which resembles the C-XRD of pristine MOF. This shows that both materials maintain crystallinity after reaction. The Zr cluster (Zr<sub>6</sub>O<sub>6</sub>(bpdC)<sub>6</sub>) contains μ<sub>3</sub>-OH. This site may provide an additional anchoring point for Zn(iPr)<sub>2</sub> during the vapour phase reaction (Figure 8).<sup>[26]</sup> Closer analyses at the XRD diffractograms did not show any interaction between zinc reagents and the clusters. Moreover, Soai has shown that the presence of additives containing hydroxyl moieties does not interfere with the autocatalytic process and the asymmetric amplification.<sup>[27]</sup>

ATR-IR analysis has also been carried out on the MOF samples after reaction. Confronting the spectra of the three materials in Figure 7-b, the C=O stretching of the carbonyl group of aldehyde **1** at 1700 cm<sup>-1</sup>, (totally absent in the parent material), almost disappears in the UiO-67 after vapour phase

reaction. Although diagnostic signals of the alcohol group of **2** are not possible to detect (hidden by peaks of the carboxylate linkers), other signals, common to both **1** and **2** are visible: the C—H stretching of the terbutyl/isopropyl groups below 3000 cm<sup>-1</sup> and the C—N stretching of the ring at 2200 cm<sup>-1</sup>. The stretching of the O—H groups above 3500 cm<sup>-1</sup>, present in the pristine material and perturbed in the material after the inclusion, is still perturbed after the vapour phase reaction. This hints that alcohol **2** is still allocated on the cluster. The ATR-IR analysis alone indicates that a similar molecule to aldehyde **1** is present in the material, and they complement nicely the results obtained through other techniques and described above.

### Conclusions

The present study shows that, despite the confined environment of a crystalline sponge, active autocatalytic species still can form in the Soai reaction and symmetry breaking with amplification is observed. Thus, under heterogenous conditions and in absence of chiral polarization, absolute asymmetric synthesis promotes formation of Soai alkanol **2** by reaction of Zn(iPr)<sub>2</sub> vapor with aldehyde **1** encapsulated in UiO-MOF series. In contrast to traditional asymmetric synthesis, and given that all MOFs used in these experiments are “achiral”, the present reaction set-up exemplifies a closed system far from equilibrium reaching a stable non-stationary phase. Somehow, reactions

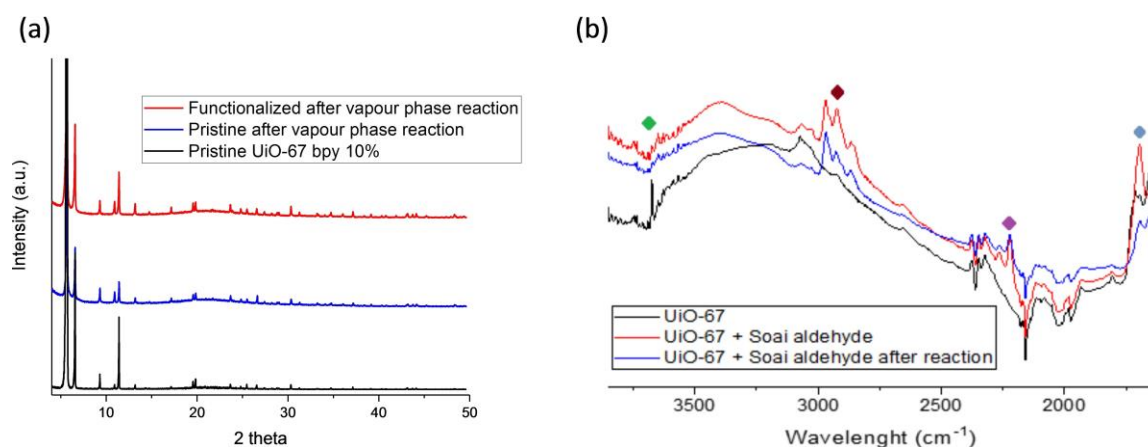


**Figure 7.** (a) XRD analysis on the MOFs. (b) IR analysis on the UiO-67 after vapour phase reaction showing stretching of the: hydroxyl groups (green), terbutyl group (red), C—N in pyrimidine ring (purple), carbonyl group (blue).

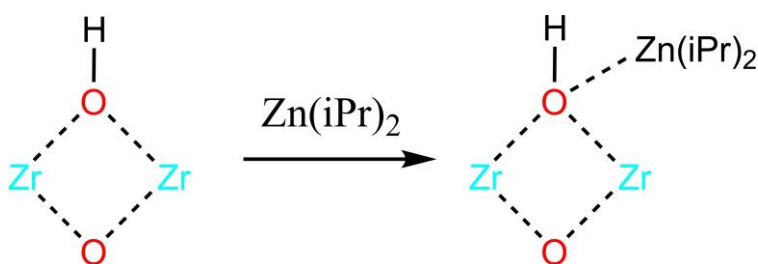


**Figure 8.** Possible interaction between Zn(i-Pr)<sub>2</sub> and the Zr—O moiety of the MOF cluster.

conducted in the UiO-67 MOF were faster than in smaller UiO-66 or in pristine materials. In contrast to pristine solid 1, moderate amplification of *ee* was observed for reactions conducted in UiO-MOFs as confinement restricts diffusion of chiral active oligomers of Zn-2 within the solid. Also, the boundary conditions in supply of reactants causes formation of different aggregates with different autocatalytic performances resulting in changing reaction rates and *ee*. ATR-IR data localize aldehyde 1 in close proximity to the Zr-cluster, in agreement with predicted coordination by DFT calculations, which is confirmed by similar localization of product 2 after reaction. Also, the crystallinity of the MOF is well preserved after vapour phase reaction with Zn(iPr)<sub>2</sub>. To our knowledge this is the first example of symmetry breaking for autocatalytic amplification in such confined environment.

## Conflict of Interest

The authors declare no conflict of interest.

**Keywords:** UiO-MOF · Autocatalysis · Symmetry breaking · Amplification · Chirality

- [1] a) K. Mislow, *Collect. Czech. Chem. Commun.* **2003**, *68*, 849-864; b) M. Bolli, R. Micura, A. Eschenmoser, *Chem. Biol.* **1997**, *4*, 309-320; c) B. L. Feringa, R. A. van Delden, *Angew. Chem. Int. Ed.* **1999**, *38*, 3419-3438; d) S. Pizzarello, A. L. Weber, *Science (Washington, DC, U. S.)* **2004**, *303*, 1151; e) I. Weissbuch, M. Lahav, *Chem. Rev. (Washington, DC, U. S.)* **2011**, *111*, 3236-3267; f) J. S. Siegel, *Chirality* **1998**, *10*, 24-27; g) J. M. Ribo, C. Blanco, J. Crusats, Z. El-Hachemi, D. Hochberg, A. Moyano, *Chem. Eur. J.* **2014**, *20*, 17250-17271.
- [2] a) A. J. Bissette, S. P. Fletcher, *Angew. Chem. Int. Ed.* **2013**, *52*, 12800-12826; *Angew. Chem.* **2013**, *125*, 13034-13061; b) D. G. Blackmond, *Chem. Rev.* **2020**, *120*, 4831-4847.
- [3] F. C. Frank, *Biochim. Biophys. Acta* **1953**, *11*, 459-463.
- [4] K. Soai, T. Shibata, H. Morioka, K. Choji, *Nature* **1995**, *378*, 767-768.
- [5] a) I. Sato, H. Urabe, S. Ishiguro, T. Shibata, K. Soai, *Angew. Chem. Int. Ed.* **2003**, *42*, 315-317; *Angew. Chem.* **2003**, *115*, 329-331; b) T. Shibata, S. Yonekubo, K. Soai, *Angew. Chem. Int. Ed.* **1999**, *38*, 659-661; *Angew. Chem.* **1999**, *111*, 746-748.
- [6] a) K. Soai, T. Kawasaki, A. Matsumoto, *Acc. Chem. Res.* **2014**, *47*, 3643-3654; b) K. Soai, T. Kawasaki, A. Matsumoto, *Tetrahedron* **2018**, *74*, 1973-1990.
- [7] a) D. A. Singleton, L. K. Vo, *Org. Lett.* **2003**, *5*, 4337-4339; b) K. Soai, I. Sato, T. Shibata, S. Komiya, M. Hayashi, Y. Matsueda, H. Imamura, T. Hayase, H. Morioka, H. Tabira, J. Yamamoto, Y. Kowata, *Tetrahedron: Asymmetry* **2003**, *14*, 185-188.
- [8] a) Y. Kaimori, Y. Hiyoshi, T. Kawasaki, A. Matsumoto, K. Soai, *Chem. Commun.* **2019**, *55*, 5223-5226; b) G. Rotunno, D. Petersen, M. Amedjokouh, *ChemSystemsChem* **2020**, *2*, e1900060.
- [9] a) B. L. Feringa, R. A. van Delden, *Angew. Chem. Int. Ed.* **1999**, *38*, 3418-3438; *Angew. Chem.* **1999**, *111*, 3624-3645; b) K. Mislow, *Collect. Czech. Chem. Commun.* **2003**, *68*, 849.
- [10] a) D. G. Blackmond, C. R. McMillan, S. Ramdeehul, A. Schorm, J. M. Brown, *J. Am. Chem. Soc.* **2001**, *123*, 10103-10104; b) F. G. Buono, D. G. Blackmond, *J. Am. Chem. Soc.* **2003**, *125*, 8978-8979.
- [11] a) I. D. Gridnev, J. M. Serafimov, J. M. Brown, *Angew. Chem. Int. Ed.* **2004**, *43*, 4884-4887; *Angew. Chem.* **2004**, *116*, 4992-4995; b) I. D. Gridnev, J. M. Brown, *Proc. Natl. Acad. Sci. USA* **2004**, *101*, 5727; c) J. Klanker-mayer, I. D. Gridnev, J. M. Brown, *Chem. Commun.* **2007**, 3151-3153; d) I. D. Gridnev, J. M. Serafimov, H. Quiney, J. M. Brown, *Org. Biomol. Chem.* **2003**, *1*, 3811-3819.
- [12] M. E. Noble-Terán, J.-M. Cruz, J.-C. Micheau, T. Buhse, *ChemCatChem* **2018**, *10*, 642-648.
- [13] I. D. Gridnev, A. K. Vorobiev, *ACS Catal.* **2012**, *2*, 2137-2149.
- [14] a) L. Schiaffino, G. Ercolani, *Angew. Chem. Int. Ed.* **2008**, *47*, 6832-6835; *Angew. Chem.* **2008**, *120*, 6938-6941; b) L. Schiaffino, G. Ercolani, *Chemistry* **2010**, *16*, 3147-3156; c) G. Ercolani, L. Schiaffino, *J. Org. Chem.* **2011**, *76*, 2619-2626.
- [15] A. Matsumoto, T. Abe, A. Hara, T. Tobita, T. Sasagawa, T. Kawasaki, K. Soai, *Angew. Chem. Int. Ed.* **2015**, *54*, 15218-15221; *Angew. Chem.* **2015**, *127*, 15433-15436.
- [16] T. Gehring, M. Quaranta, B. Odell, D. G. Blackmond, J. M. Brown, *Angew. Chem. Int. Ed.* **2012**, *51*, 9539-9542, S9539/S9539-9541.
- [17] O. Trapp, S. Lamour, F. Maier, A. F. Siegle, K. Zawatzky, B. F. Straub, *Chem. - Eur. J.* **2020**, *26*, 15871-15880.
- [18] a) E. Doka, G. Lente, *J. Am. Chem. Soc.* **2011**, *133*, 17878-17881; b) O. Fulop, B. Barabas, *J. Math. Chem.* **2016**, *54*, 10-17; c) B. Barabas, R. Kurdi, C. Zucchi, G. Palyi, *Chirality* **2018**, *30*, 913-922; d) B. Barabas, J. Toth, G. Palyi, *J. Math. Chem.* **2010**, *48*, 457-489; e) D. G. Blackmond, *Tetrahedron: Asymmetry* **2006**, *17*, 584-589; f) J.-C. Micheau, C. Coudret, J.-M. Cruz, T. Buhse, *Phys. Chem. Chem. Phys.* **2012**, *14*, 13239-13248.
- [19] S. V. Athavale, A. Simon, K. N. Houk, S. E. Denmark, *Nat. Chem.* **2020**, *12*, 412-423.
- [20] a) Y. Kaimori, Y. Hiyoshi, T. Kawasaki, A. Matsumoto, K. Soai, *Chem. Commun.* **2019**, *55*, 5223-5226; b) T. Buhse, J.-M. Cruz, M. E. Noble-Terán, D. Hochberg, J. M. Ribó, J. Crusats, J.-C. Micheau, *Chem. Rev.* **2021**, *121*, 2147-2229.
- [21] R. Batten Stuart, R. Champness Neil, X.-M. Chen, J. Garcia-Martinez, S. Kitagawa, L. Öhrström, M. O'Keefe, M. Paik Suh, J. Reedijk in *Terminology of metal-organic frameworks and coordination polymers (IUPAC Recommendations 2013)*, Vol. **85** **2013**, p. 1715.
- [22] a) A. Gheorghie, M. A. Tepaske, S. Tanase, *Inorg. Chem. Front.* **2018**, *5*, 1512-1523; b) X. Li, J. Wu, C. He, Q. Meng, C. Duan, *Small* **2019**, *15*, 1804770; c) S. Bhattacharjee, I. M. Khan, X. Li, Q.-L. Zhu, X.-T. Wu, *Catalysts* **2018**, *8*; d) A. V. Artem'ev, V. P. Fedin, *Russ. J. Org. Chem.* **2019**, *55*, 800-817; e) Y. Liu, W. Xuan, Y. Cui, *Adv. Mater.* **2010**, *22*, 4112-4135.
- [23] J. H. Cavka, S. Jakobsen, U. Olsbye, N. Guillou, C. Lamberti, S. Bordiga, K. P. Lillerud, *J. Am. Chem. Soc.* **2008**, *130*, 13850-13851.
- [24] a) L. M. Hayes, C. E. Knapp, K. Y. Nathoo, N. J. Press, D. A. Tocher, C. J. Carmalt, *Cryst. Growth Des.* **2016**, *16*, 3465-3472; b) M. Hoshino, A. Khutia, H. Xing, Y. Inokuma, M. Fujita, *IUCrJ* **2016**, *3*, 139-151; c) Y. Inokuma, S. Yoshioka, J. Ariyoshi, T. Arai, Y. Hitora, K. Takada, S. Matsunaga, K. Rissanen, M. Fujita, *Nature* **2013**, *495*, 461-466; d) J.-S. Qin, S. Yuan, A. Alsalmeh, H.-C. Zhou, *ACS Appl. Mater. Interfaces* **2017**, *9*, 33408-33412.
- [25] J. M. Brown, I. Gridnev, J. Klankermayer in *Asymmetric autocatalysis with organozinc complexes; Elucidation of the reaction pathway*, Vol. **284** (Ed. K. Soai), **2008**, pp. 35-65.
- [26] a) L. C. Gallington, I. S. Kim, W.-G. Liu, A. A. Yakovenko, A. E. Platero-Prats, Z. Li, T. C. Wang, J. T. Hupp, O. K. Farha, D. G. Truhlar, A. B. F. Martinson, K. W. Chapman, *J. Am. Chem. Soc.* **2016**, *138*, 13513-13516; b) I. S. Kim, J. Borycz, A. E. Platero-Prats, S. Tussupbayev, T. C. Wang, O. K. Farha, J. T. Hupp, L. Gagliardi, K. W. Chapman, C. J. Cramer, A. B. F. Martinson, *Chem. Mater.* **2015**, *27*, 4772-4778.
- [27] a) T. Kawasaki, Y. Wakushima, M. Asahina, K. Shiozawa, T. Kinoshita, F. Lutz, K. Soai, *Chem. Commun.* **2011**, *47*, 5277-5279; b) T. Shibata, H. Tarumi, T. Kawasaki, K. Soai, *Tetrahedron: Asymmetry* **2012**, *23*, 1023-1027.

Manuscript received: April 19, 2021  
 Revised manuscript received: June 30, 2021  
 Accepted manuscript online: July 11, 2021  
 Version of record online: July 21, 2021





## **Paper II**

*Absolute Autocatalytic Amplification under  
Heterogeneous Phase Conditions Involving Subsequent  
Hydride Transfer and a Hemiacetal Intermediate*



# Absolute Autocatalytic Amplification under Heterogenous Phase Conditions Involving Subsequent Hydride Transfer and a Hemiacetal Intermediate\*\*

Giuseppe Rotunno,<sup>[a, b]</sup> Dirk Petersen,<sup>[a]</sup> and Mohamed Amedjkouh<sup>\*[a, b]</sup>

**Abstract:** In contrast to the homogenous phase, absolute asymmetric amplification of pyridine alkanol is observed under heterogenous conditions. The reaction of  $i\text{Pr}_2\text{Zn}$  vapor on a solid powder of pyridine carbaldehyde induced autocatalytic amplification of chirality providing the alkanol product with an enantiopurity up to 90% ee. In this study, side products were identified and their formation is traced back to redox pathways involving hydride transfer, namely a chiral ester resulting most probably from a disproportionation of the starting aldehyde into a hemiacetal and subsequent hydride loss following a Claisen-Tishchenko mechanism. These observations provide new perspectives in the elucidation of the mechanism of amplification of chirality in the Soai reaction.

The origin of homochirality remains an intriguing scientific topic.<sup>[1]</sup> Although very few, recent work shows that enantioenrichment (*ee*) is achievable from achiral precursors without chiral catalysts, and reactants are obtained as single enantiomer crystals to be used in absolute asymmetric synthesis.<sup>[2]</sup> Not only chiral, but also achiral molecules can crystallize in chiral crystals: in these cases, the chirality of the crystal structure arises from a chiral packing of the molecule. Single phase homochirality without counter enantiomer nucleation may also be accessed through crystallization, although no chemical transformation occurs throughout the processes. Kondepudi's total spontaneous resolution and Viedma's attrition enhanced deracemization of  $\text{NaClO}_3$ ,<sup>[3]</sup> Viedma ripening was shown on an intrinsically chiral molecule, an amino acid derivative racemizing in solution in presence of a strong base. It was shown that circularly polarised light (CPL) induces crystal growth of a specific enantiomer by action of chiral side products.<sup>[4]</sup> By Viedma

ripening of organometallic complexes, six-coordinated  $\Delta$ - and  $\Lambda$ - $[\text{Co}(\text{bpy})_3]^{2+}$  cations and tetrahedral  $\Delta$ - and  $\Lambda$ - $[\text{Ag}(\text{PS})_2]^+$  cations (PS = (2-(methylthio)ethyl)-diphenylphosphine) were successfully obtained in enantiopure forms. The decisive stage showing spontaneous molecular symmetry breaking (SMSB) is the formation of the racemic conglomerate from the racemic mixture of enantiomers.<sup>[5]</sup> Enantioenrichment is also possible by selective crystallization or sublimation.<sup>[6]</sup>

To date, the Soai reaction offers the only example of an absolute asymmetric catalytic reaction in absence of chiral polarization in the alkylation of pyrimidinyl aldehyde **1** into alkanol **2**.<sup>[7]</sup> Frank envisioned an asymmetric autocatalytic model,<sup>[8]</sup> where one enantiomer catalyses its own production and at the same time inhibits the formation of its opposite enantiomer, giving rise to high asymmetric amplification from extremely low enantiopurity.<sup>[9]</sup> Thus, even classical statistical fluctuation in the enantiomeric ratio can lead to spontaneous asymmetric synthesis,<sup>[10]</sup> by virtue of non-linear relationship (NLE) of catalyst-product pair, in the form of a homochiral dimer species.<sup>[8,11]</sup> This is key to propagation of asymmetric amplification during the course of a reaction.<sup>[12]</sup> It was pointed out that the (+)-NLE must be working in parallel with autocatalysis to provide the autocatalytic amplification.<sup>[13]</sup> In addition, recently the Soai autocatalytic reaction system was tested to detect the energy imbalance that gives rise to directed symmetry breaking.<sup>[14]</sup>


We have recently reported on the combination of autocatalysis with remote amplification of chirality.<sup>[15]</sup> Notably, we introduced pyridinyl alkanols **4** as a new autocatalytic family and their amplification in parallel with pyrimidinyl alkanol **2**.<sup>[15c]</sup> Inspired by the work of Soai *et al.*, we hypothesized whether this combination would also function under heterogenous conditions in the alkylation of aldehydes **1** and **3** (Scheme 1). This work also discloses a new autocatalytic system with spontaneous molecular symmetry breaking with amplification of pyridinyl alkanol **4** operating under heterogenous conditions. Besides, we report on additional products, identified as ketone, alcohol, and esters. This work demonstrates that their formation is associated with episodes of hydride transfer involving a hemiacetal intermediate and may be key players in the amplification process.

Soai revealed the enantioface selective addition of  $i\text{Pr}_2\text{Zn}$  to pyrimidine-5-carbaldehyde **1**.<sup>[16]</sup> By selecting one enantiotopic crystal face, the chiral secondary alcohol **2** was formed with the absolute configuration corresponding to the two-dimensional chirality at the crystal surface. They could predict the absolute configuration of alcohol **2** from the parallelogram face shape.

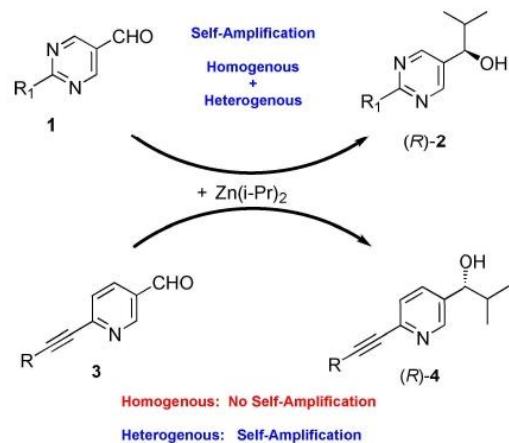
[a] G. Rotunno, D. Petersen, Prof. Dr. M. Amedjkouh  
Department of Chemistry  
University of Oslo  
Postbox 1033, Blindern  
0315 Oslo (Norway)  
E-mail: mamou@kjemi.uio.no

[b] G. Rotunno, Prof. Dr. M. Amedjkouh  
Centre for Materials Science and Nanotechnology (SMN)  
University of Oslo  
Postboks 1126 Blindern  
0316 Oslo (Norway)

[\*\*] A previous version of this manuscript has been deposited on a preprint server (DOI: 10.26434/chemrxiv.9619772.v1).

 Supporting information for this article is available on the WWW under <https://doi.org/10.1002/syst.201900060>





**Scheme 1.** Absolute asymmetric catalysis with pyridine and pyrimidine aldehydes

Furthermore, the ee value of product 2 could be enhanced to greater than 99.5% by asymmetric autocatalysis. An achiral pyrimidine-5-carbaldehyde that forms an achiral crystal (achiral space group  $P1$ ), with enantiotopic(001) and (00 $\bar{1}$ ) faces underwent enantioselective addition of  $iPr_2Zn$  to the single exposed enantiotopic surface to give highly enantiomerically enriched  $S$  and  $R$  secondary alcohols. The absolute configuration of the alcohol product correlated with the orientation of the prochiral aldehyde in the achiral crystal lattice. Just recently, this study was extended with an absolute asymmetric synthesis under kinetic control of vapor-solid phase of reaction of  $iPr_2Zn$  with aldehyde 1.<sup>[17]</sup>

Initially, we examined the behaviour of pyrimidine-5-carboxaldehyde 1 in presence of pyridine-3-carboxaldehyde 3 in a 1:1 stoichiometry. Five reactions with the setup of Figure 1a were initiated simultaneously and stopped at fixed times. The final sample afforded alcohol (R)-2 in 75% conversion and 81% ee, while alcohol (R)-4 was formed in 91% ee and 36% yield. Monitoring the progress of the reaction revealed a sudden formation of alkanol 2 with very high ee from the first sample, (Figure 2; dashed red lines), while the enantiopurity of 4 slowly increased over time, in agreement

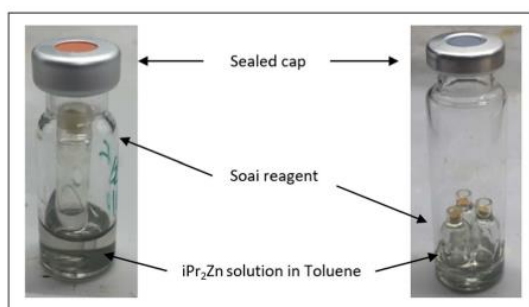


**Figure 1.** Vapour phase reaction setups. (a) Single sample; (b) Triplicate under the same  $iPr_2Zn$  atmosphere.

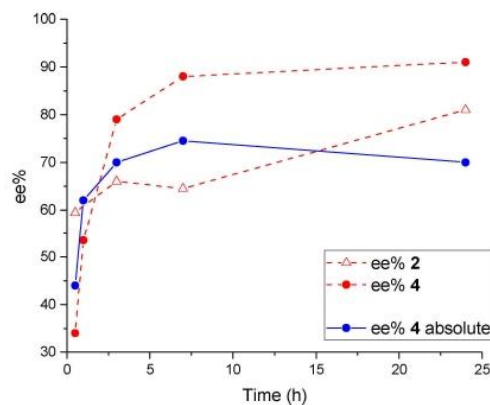


**Figure 2.** Progression of ee values vs. time: Of 2 and 4 under stoichiometric conditions (dashed red lines); of 4 under absolute conditions (solid blue line).

with our previous report on delayed amplification for alkanol 4 in solution (see Supporting Information Section 3).<sup>[15c]</sup> At a catalytic loading of 10 mol% of 1 in presence of pyrimidine-5-carboxaldehyde 3 and vapour of diisopropyl zinc, the same experiment provided quantitatively alkanol 2 with 95% ee, while alkanol 4 was isolated in 73% ee and 29% yield. Thus, absolute asymmetric synthesis of two distinct products is achieved by action of alkylating reagent vapor on solid substrate.

In previous work, addition of  $iPr_2Zn$  to aldehyde 3 in solution in toluene triggered autocatalysis and produced alkanol 4 as a racemate. Thus, no symmetry breaking by absolute asymmetric synthesis was observed for 4 under these conditions, as it is usually the case for the Soai reaction. A key question was whether heterogenous reaction conditions would provide settings for nucleation, by exposure of enantiotopic  $Re$  and  $Si$  faces, and thereby induce symmetry breaking in the alkylation of 3. This hypothesis was tested by conducting several sets of experiments under heterogeneous condition, by subjecting aldehyde 3 powder to vapor of  $iPr_2Zn$ . In absence of chiral trigger, the process operates as a spontaneous absolute asymmetric catalysis. Alkanol 4 was obtained with a final 75% ee and 21% conversion, as shown in Figure 2 (solid blue line), with a similar trend for evolution ee as in presence of 2 (see SI section 4).

Clearly, amplification of compound 4 under heterogenous conditions operates independently from the action of autocatalyst 2. When reactions are carried out in triplicates in the same container (Figure 1b), enantiomers of 4 are obtained at random as 2 times ( $R$ ) and once ( $S$ ) or the opposite, and often only ( $R$ ) as summarized in Figure 3. Thus, in presence of a same  $iPr_2Zn$  atmosphere, amplification of alkanol 4 is not subject to a chiral trigger as shown previously.

Closer analysis of crude material indicates the presence of ketone 5 and reduction alcohol 6. Furthermore, and perhaps more interesting formation of chiral ester 7 and achiral 8 is also observed (Scheme 2).

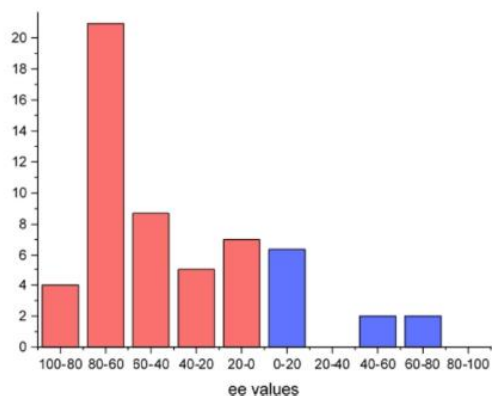
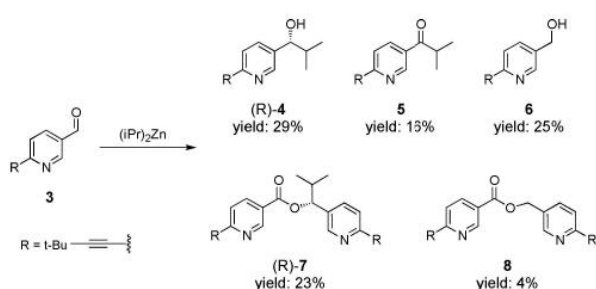
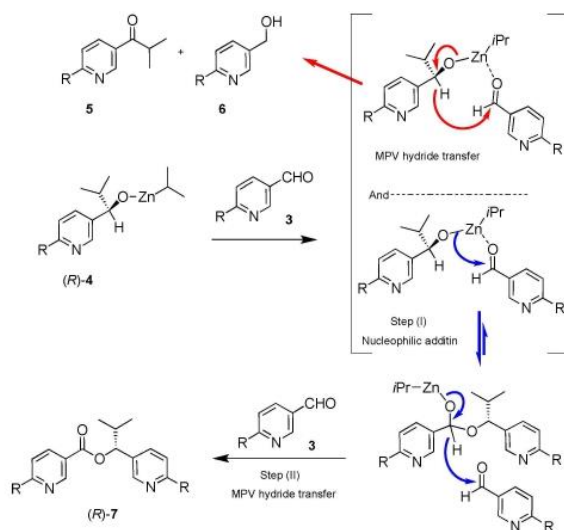


Figure 3. Frequency of ee values and distribution of enantiomers of 4.



Scheme 2. Products of the vapour solid reaction of 3 and  $i\text{Pr}_2\text{Zn}$ .

Compounds 5 and 6 could be formed by a Meerwein-Ponndorf-Verley oxidation of alkanol 4 and reduction of aldehyde 3 during amplification process (Scheme 3, Red arrows). On the other side, the only possible mechanism of formation of esters



Scheme 3. Suggested reaction mechanism for the formation of the reaction side products.

7 and 8 occurs through a Claisen-Tishchenko reaction following a Cannizzaro disproportionation mechanism (Scheme 3, Blue arrows).<sup>[18]</sup> The reaction pathway would involve key steps of the C–O bond formation and the hydride transfer which occur in the coordination sphere of the Zn metal as outlined in Scheme 3. The proposed mechanism starts in *step I* with a nucleophilic addition of the chiral Zn-4 alkoxide onto the carbonyl 3 to form a chiral Zn-hemiacetal. *Step II* can be viewed as analogous to the hydride transfer of the Meerwein-Ponndorf-Verley reaction of the Zn-hemiacetal intermediate to aldehyde 3 to produce chiral ester 7 and alkoxide Zn-6. The same reaction pathway involving Zn-6 would lead to formation of achiral ester 8.

Chiral hemiacetals have been observed in intramolecular condensation of Zn-alkoxides as a result of a monoalkylation of dialdehyde with  $\text{Et}_2\text{Zn}$ .<sup>[19]</sup> Further oxidation of hemiacetal would lead to the corresponding chiral ester.<sup>[20]</sup> More recent work revealed an intra- and intermolecular Claisen-Tishchenko catalysed by metallic zinc, although achiral.<sup>[21]</sup> The existence of Zn-hemiacetal has been described as transient intermediate in recent NMR studies, which suggested its association in a transition state in the Soai reaction.<sup>[22]</sup> This species, consisting of two alkoxides and one aldehyde, forms in the early stage of the amplification and last until complete consumption of aldehyde. Kinetic and DFT computations incorporating an acetal mechanism were also investigated lately.<sup>[23]</sup> The extent of formation of these side products is not yet understood but they are present in all runs above  $0^\circ\text{C}$ , and in nearly similar proportions. Although high amplification of 4 coincides with the absence of side products, their role in the reaction remains to be clarified.

Reaction at  $40^\circ\text{C}$  afforded compound 4 as racemate in 31% yield and 20% of ester 7 in 15% ee. The reaction also performs well at low temperatures. The highest amplification level is observed at  $0^\circ\text{C}$  after 20 h giving 20% of (R)-4 with 90% ee and only 9% of (R)-7 in 86% ee. An even slower reaction at  $-15^\circ\text{C}$  provided only alkanol 4 in 32% with 83% ee, after 3 days. Interestingly, none of the other side products is detected at this temperature. Thus, formation of ester 7 remains dependent of chiral alkanol 4 and is also function of temperature.

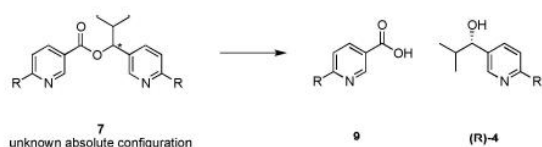
*Hypothesis:* Perhaps at higher temperature the vapor consists of a high proportion of toluene, which would dissolve most of the solid 3, making the reaction conditions likely homogenous, although we cannot determine this experimentally at this stage. Monitoring the reaction revealed a rapid onset of product optical activity at rt with 40% ee after 30 min to peak at 74% ee within 5 hours. At lower temperature of  $-15^\circ\text{C}$  a longer induction period shows a low 18% ee in the first 10 hours followed by a rapid increase up to 83% ee. This shows that  $i\text{Pr}_2\text{Zn}$  vapor reacts with solid 3 in small portions and limited toluene solvent. The overall process, accounts for the observed amplification by keeping a constant flow of  $i\text{Pr}_2\text{Zn}$  at low concentration throughout the reaction, but a much higher total concentration of both reagents than under homogenous conditions used in previous reports.

Moreover, in all cases HPLC on chiral stationary phase shows a constant trend in which absolute configuration of major enantiomer 7 follows that of 4. The absolute configuration of



ester **7** has been assigned to be the same as for alkanol **4**. For example, hydrolysis of ester (*R*)-**7** provided alcohol (*R*)-**4** (Scheme 4). This has also been shown for ester (*S*)-**7**.

To examine the correlation of the amplification of **4** and **7**, triplicate experiments with the reaction setup of Figure 1b, to a total of nine reactions, were performed and in all cases **4** and **7** were obtained with the same absolute configuration (*R*). Chiral amplification of **7** was often higher or comparable to that of **4** as shown in Table 1. Analysis over time shows a steady ee increase for chiral **7** while alkanol **4** terminates with a remarkably lower ee (Figure 4). This could reasonably be interpreted as an amplification of chiral **7** at the expense of alkanol **4** through a reversible hemiacetal formation step I in Scheme 3. Indeed, the hemiacetal forms as two diastereomers with a kinetically preferred intermediate for a hydride transfer converting into ester **7** (step II: thermodynamic sink), while the



Scheme 4. Hydrolysis of ester **7**.

**Table 1.** Absolute asymmetric synthesis of **4** and **7** by reaction of vapor  $i\text{Pr}_2\text{Zn}$  on solid **3**.

Entry <sup>[a]</sup>	ee ( <i>R</i> )- <b>4</b> <sup>[b]</sup>	ee ( <i>R</i> )- <b>7</b> <sup>[b]</sup>
1	48	72
2	53	65
3	62	83
4	55	54
5	47	25
6	63	79
7	67	81
8	50	57
9	49	66

[a] The 9 reactions of the triplicate series have been performed simultaneously using the same batch of **3** and  $i\text{Pr}_2\text{Zn}$ . [b] Determined using HPLC

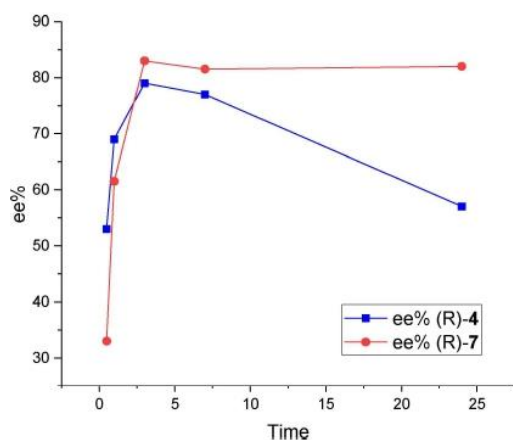


Figure 4. Asymmetric amplification of (*R*)-**4** (blue) and (*R*)-**7** (red) at RT.

other diastereomer reverts back to starting alkoxide Zn-**4** and aldehyde **3**.<sup>[24]</sup> It is not yet clear to which extent this hemiacetal intermediate can be implicated in the amplification process of **4** or even **7**. Yet, the Claisen-Tishchenko may represent a new chiral amplification process.

Finally, other alkylzinc reagents,  $\text{Et}_2\text{Zn}$  and  $\text{Me}_2\text{Zn}$  were employed as solutions in hexane, heptane and toluene. Upon exposure to vapor of  $\text{R}_2\text{Zn}$  reagents alkylation was observed in all cases. None of  $\text{Et}_2\text{Zn}$  or  $\text{Me}_2\text{Zn}$  did provide amplification, and all products were isolated as racemates. Interestingly, no side products were isolated with these reagents.

In conclusion, this paper broadens the scope of absolute asymmetric catalysis by an unprecedented phase alteration. We disclosed the realization of asymmetric amplification of pyridinyl alkanol **4** in heterogenous phase by the reaction of  $i\text{Pr}_2\text{Zn}$  vapor on solid aldehyde **3**. This is in striking contrast with the absence of absolute asymmetric catalysis of alkanol **4** under homogenous conditions in solution. One could assume that even in a mixture, different pathways remain possible for asymmetric amplification of **2** and **4**. Clearly, autocatalysis is in action as shown by monitoring the progress of ee over time. However, such absolute asymmetric catalysis is not observed for other zinc reagents and remains specific to  $i\text{Pr}_2\text{Zn}$ , adding more intrigue to this unique reactivity.

First observation of side products provides new insight into possible amplification process. Their formation rises through redox pathways involving hydride transfer, following mechanisms for MPV and Claisen-Tishchenko reactions (*vide supra*). Thus far, these remain undocumented for the Soai reaction under similar conditions. The selective formation of chiral ester **7** emerges as evidence of a subsequent reactivity of a chiral hemiacetal intermediate, which also have implications in the absolute asymmetric catalysis, and provides new perspectives for the mechanism elucidation of the Soai reaction.

Further studies are undertaken to examine the mechanism of their formation and its relation to amplification.

## Acknowledgements

This work was supported by the Research Council of Norway (TOPFORSK program 250795), the University of Oslo, and COST Action "Emergence and Evolution of Complex Chemical Systems" (CM 1304).

**Keywords:** amplification · asymmetric synthesis · autocatalysis · chirality · zinc

[1] a) K. Mislow, *Collect. Czech. Chem. Commun.* **2003**, *68*, 849–864; b) M. Bolli, R. Micura, A. Eschenmoser, *Chem. Biol.* **1997**, *4*, 309–320; c) B. L. Feringa, R. A. van Delden, *Angew. Chem. Int. Ed.* **1999**, *38*, 3419–3438; d) S. Pizzarello, A. L. Weber, *Science* **2004**, *303*, 1151; e) I. Weissbuch, M. Lahav, *Chem. Rev.* **2011**, *111*, 3236–3267; f) J. S. Siegel, *Chirality* **1998**, *10*, 24–27; g) J. M. Ribo, C. Blanco, J. Crusats, Z. El-Hachemi, D. Hochberg, A. Moyano, *Chem. Eur. J.* **2014**, *20*, 17250–17271.

[2] a) T. T. Mai, M. Branca, D. Gori, R. Guillot, C. Kouklovsky, V. Alezra, *Angew. Chem. Int. Ed.* **2012**, *51*, 4981–4984; b) S. Olsson, A. Lennartson, M. Hakansson, *Chem. Eur. J.* **2013**, *19*, 12415–12423; c) A. Lennartson, S.

- Olsson, J. Sundberg, M. Hakansson, *Angew. Chem. Int. Ed.* **2009**, *48*, 3137–3140.
- [3] a) D. K. Kondepudi, R. J. Kaufman, N. Singh, *Science* **1990**, *250*, 975–976; b) C. Viedma, *Phys. Rev. Lett.* **2005**, *94*.
- [4] a) W. L. Noorduin, T. Izumi, A. Millemaggi, M. Leeman, H. Meekes, W. J. P. Van Enckevort, R. M. Kellogg, B. Kaptein, E. Vlieg, D. G. Blackmond, *J. Am. Chem. Soc.* **2008**, *130*, 1158; b) W. L. Noorduin, A. A. C. Bode, M. van der Meijden, H. Meekes, A. F. van Etteger, W. J. P. van Enckevort, P. C. M. Christianen, B. Kaptein, R. M. Kellogg, T. Rasing, E. Vlieg, *Nat. Chem.* **2009**, *1*, 729–732.
- [5] a) P. M. Bjoremark, J. Jonsson, M. H. Hakansson, *Chem. Eur. J.* **2015**, *21*, 10630; b) P. M. Bjoremark, S. Olsson, T. Kokoli, M. Hakansson, *Chem. Eur. J.* **2015**, *21*, 8750–8753.
- [6] a) Y. Hayashi, M. Matsuzawa, J. Yamaguchi, S. Yonehara, Y. Matsumoto, M. Shoji, D. Hashizume, H. Koshino, *Angew. Chem. Int. Ed.* **2006**, *45*, 4593–4597; b) V. A. Soloshonok, H. Ueki, M. Yasumoto, S. Mekala, J. S. Hirschi, D. A. Singleton, *J. Am. Chem. Soc.* **2007**, *129*, 12112–12113.
- [7] a) K. Soai, T. Shibata, H. Morioka, K. Choji, *Nature* **1995**, *378*, 767–768; b) T. Shibata, S. Yonekubo, K. Soai, *Angew. Chem. Int. Ed.* **1999**, *38*, 659–661; c) I. Sato, H. Urabe, S. Ishiguro, T. Shibata, K. Soai, *Angew. Chem. Int. Ed.* **2003**, *42*, 315–317.
- [8] A. J. Bissette, S. P. Fletcher, *Angew. Chem. Int. Ed.* **2013**, *52*, 12800–12826.
- [9] F. C. Frank, *Biochim. Biophys. Acta* **1953**, *11*, 459–463.
- [10] a) K. Soai, I. Sato, T. Shibata, S. Komiyama, M. Hayashi, Y. Matsueda, H. Imamura, T. Hayase, H. Morioka, H. Tabira, J. Yamamoto, Y. Kowata, *Tetrahedron: Asymmetry* **2003**, *14*, 185–188; b) D. A. Singleton, L. K. Vo, *Org. Lett.* **2003**, *5*, 4337–4339; c) T. Kawasaki, K. Suzuki, M. Shimizu, K. Ishikawa, K. Soai, *Chirality* **2006**, *18*, 479–482.
- [11] a) D. G. Blackmond, *Proc. Mont. Acad. Sci.* **2004**, *101*, 5732–5736; b) J. M. Brown, I. Gridnev, J. Klankermayer, *Top. Curr. Chem.* **2008**, *284*, 35–65; c) I. D. Gridnev, A. K. Vorobiev, *ACS Catal.* **2012**, *2*, 2137–2149; d) T. Gehring, M. Quaranta, B. Odell, D. G. Blackmond, J. M. Brown, *Angew. Chem. Int. Ed.* **2012**, *51*, 9539–9542.
- [12] a) E. Doka, G. Lente, *J. Am. Chem. Soc.* **2011**, *133*, 17878–17881; b) O. Fulop, B. Barabas, *J. Math. Chem.* **2016**, *54*, 10–17; c) B. Barabas, R. Kurdi, C. Zucchi, G. Palyi, *Chirality* **2018**, *30*, 913–922; d) B. Barabas, J. Toth, G. Palyi, *J. Math. Chem.* **2010**, *48*, 457–489; e) D. G. Blackmond, *Tetrahedron: Asymmetry* **2006**, *17*, 584–589; f) J.-C. Micheau, C. Coudret, J.-M. Cruz, T. Buhse, *Phys. Chem. Chem. Phys.* **2012**, *14*, 13239–13248.
- [13] T. Satyanarayana, S. Abraham, H. B. Kagan, *Angew. Chem. Int. Ed.* **2009**, *48*, 456–494.
- [14] N. A. Hawbaker, D. G. Blackmond, *Nat. Chem.* **2019**, *11*, 957–962.
- [15] a) M. Funes-Maldonado, B. Sieng, M. Amedjkouh, *Eur. J. Org. Chem.* **2015**, 4081–4086; b) M. Funes-Maldonado, B. Sieng, M. Amedjkouh, *Org. Lett.* **2016**, *18*, 2536–2539; c) C. Romagnoli, B. Sieng, M. Amedjkouh, *Eur. J. Org. Chem.* **2015**, 4087–4092.
- [16] a) T. Kawasaki, S. Kamimura, A. Amihara, K. Suzuki, K. Soai, *Angew. Chem. Int. Ed.* **2011**, *50*, 6796–6798; b) K. Penzien, G. M. J. Schmidt, *Angew. Chem. Int. Ed.* **1969**, *8*, 608–609.
- [17] Y. Kaimori, Y. Hiyoshi, T. Kawasaki, A. Matsumoto, K. Soai, *Chem. Commun.* **2019**, 5223–5226.
- [18] a) L. Claisen, *Ber. Dtsch. Chem. Ges.* **1887**, *20*, 646–650; b) V. E. Tishchenko, *J. Russ. Phys. Chem. Soc.* **1906**, *38*, 355–418; c) V. E. Tishchenko, *J. Russ. Phys. Chem. Soc.* **1906**, *38*, 482–540; d) A. O. K. A. M. P. Koskinen, in *Organic Reactions*, Vol. 86, **2015**, pp. 105–410.
- [19] K. Soai, Y. Inoue, T. Takahashi, T. Shibata, *Tetrahedron* **1996**, *52*, 13355–13362.
- [20] M. Watanabe, N. Hashimoto, S. Araki, Y. Butsugan, *J. Org. Chem.* **1992**, *57*, 742–744.
- [21] M. Miyagawa, T. Akiyama, *Chem. Lett.* **2018**, *47*, 78–81.
- [22] T. Gehring, M. Quaranta, B. Odell, D. G. Blackmond, J. M. Brown, *Angew. Chem. Int. Ed.* **2012**, *51*, 9539–9542.
- [23] I. D. Gridnev, A. K. Vorobiev, *B Chem Soc Jpn* **2015**, *88*, 333–340.
- [24] a) D. Drahoňovský, J.-M. Lehn, *J. Org. Chem.* **2009**, *74*, 8428–8432; b) L. You, J. S. Berman, E. V. Anslyn, *Nat. Chem.* **2011**, *3*, 943–948.

Manuscript received: August 15, 2019

Version of record online: February 5, 2020





# **Appendix I**

## References



- [1] K. Soai, T. Shibata, H. Morioka and K. Choji, *Nature* **1995**, *378*, 767-768.
- [2] E. V. D. D. A. Anslyn, *Modern Physical Organic Chemistry* University Science Books, **2006**, p.
- [3] R. S. Cahn, C. Ingold and V. Prelog, *Angewandte Chemie International Edition in English* **1966**, *5*, 385-415.
- [4] Y. Noma and Y. Asakawa in *3.19 - Biotransformation of Monoterpenoids*, Eds.: H.-W. Liu and L. Mander), Elsevier, Oxford, **2010**, pp. 669-801.
- [5] H. H. K. Butchko, Frank N., *Comments on Toxicology*, *3*, (4), 253-78 **1989**.
- [6] W. H. Brooks, W. C. Guida and K. G. Daniel, *Current topics in medicinal chemistry* **2011**, *11*, 760-770.
- [7] a) H. U. Blaser, *Chemical Reviews* **1992**, *92*, 935-952; b) S. Hanessian, *Accounts of Chemical Research* **1979**, *12*, 159-165.
- [8] A. J. Bissette and S. P. Fletcher, *Angewandte Chemie International Edition* **2013**, *52*, 12800-12826.
- [9] G. N. Lewis, *Proc. Am. Acad. Arts Sci.* **1905**, *40*, 719 – 733.
- [10] I. Weissbuch and M. Lahav, *Chemical Reviews* **2011**, *111*, 3236-3267.
- [11] B. Rubinov, N. Wagner, M. Matmor, O. Regev, N. Ashkenasy and G. Ashkenasy, *ACS Nano* **2012**, *6*, 7893-7901.
- [12] L. C. D. Nichela, F. G. Einschlag, *Appl. Catal. B* **2008**, *82*, 11 – 18.
- [13] C. R. Butlerow, *Hebd. Seances Acad. Sci.* **1861**, 145.
- [14] a) T. Mukaiyama, K. Soai, T. Sato, H. Shimizu and K. Suzuki, *Journal of the American Chemical Society* **1979**, *101*, 1455-1460; b) N. Oguni and T. Omi, *Tetrahedron Letters* **1984**, *25*, 2823-2824; c) M. Kitamura, S. Suga, K. Kawai and R. Noyori, *Journal of the American Chemical Society* **1986**, *108*, 6071-6072; d) H. H. K. Soai, S. Niwa, *Heterocycles* **1989**, *29*, 2065.
- [15] K. Soai, S. Niwa and H. Hori, *Journal of the Chemical Society, Chemical Communications* **1990**, 982-983.
- [16] a) T. H. K. Soai, C. Shimada, K. Isobe, *Tetrahedron: Asymmetry* **1994**, *5* 789-792; b) K. Soai, T. Hayase and K. Takai, *Tetrahedron: Asymmetry* **1995**, *6*, 637-638; c) T. Shibata, K. Choji, H. Morioka, T. Hayase and K. Soai, *Chemical Communications* **1996**, 751-752; d) M. H. Shibata T, Tanji S, Hayase T, Kodaka Y, Soai K. , *Tetrahedron Lett* **1996**, *37*, 8783-8786.
- [17] a) T. Shibata, H. Morioka, T. Hayase, K. Choji and K. Soai, *Journal of the American Chemical Society* **1996**, *118*, 471-472; b) T. Shibata, S. Yonekubo and K. Soai, *Angewandte Chemie International Edition* **1999**, *38*, 659-661.
- [18] T. Shibata, T. Hayase, J. Yamamoto and K. Soai, *Tetrahedron: Asymmetry* **1997**, *8*, 1717-1719.
- [19] I. Sato, H. Urabe, S. Ishiguro, T. Shibata and K. Soai, *Angewandte Chemie International Edition* **2003**, *42*, 315-317.
- [20] T. Gehring, M. Busch, M. Schlageter and D. Weingand, *Chirality* **2010**, *22*, E173-E182.
- [21] J. Klankermayer, I. D. Gridnev and J. M. Brown, *Chemical Communications* **2007**, 3151-3153.
- [22] F. C. Frank, *Biochimica et Biophysica Acta* **1953**, *11*, 459-463.
- [23] D. R. F. H. B. Kagan, *Topics in Stereochemistry*, **1999**, p.
- [24] C. Puchot, O. Samuel, E. Dunach, S. Zhao, C. Agami and H. B. Kagan, *Journal of the American Chemical Society* **1986**, *108*, 2353-2357.
- [25] a) C. G. H. B. Kagan, *Angew. Chem.* **1998**, *110*, 3088 – 3127; b) C. G. H. B. Kagan, *Angew. Chem. Int. Ed.* **1998**, *37* 2922 – 2959; c) T. Satyanarayana, S. Abraham and H. B. Kagan, *Angewandte Chemie International Edition* **2009**, *48*, 456-494.
- [26] D. Guillaneux, S.-H. Zhao, O. Samuel, D. Rainford and H. B. Kagan, *Journal of the American Chemical Society* **1994**, *116*, 9430-9439.
- [27] N. Oguni, Y. Matsuda and T. Kaneko, *Journal of the American Chemical Society* **1988**, *110*, 7877-7878.
- [28] a) M. Yamakawa and R. Noyori, *Journal of the American Chemical Society* **1995**, *117*, 6327-6335; b) M. Kitamura, S. Suga, M. Niwa and R. Noyori, *Journal of the American Chemical Society* **1995**, *117*, 4832-4842; c) M. Kitamura, M. Yamakawa, H. Oka, S. Suga and R. Noyori, *Chemistry – A European Journal* **1996**, *2*, 1173-1181; d) M. Kitamura, S. Suga, H. Oka and R. Noyori, *Journal of the American*

- Chemical Society* **1998**, *120*, 9800-9809; e) M. Kitamura, H. Oka and R. Noyori, *Tetrahedron* **1999**, *55*, 3605-3614; f) R. Noyori, S. Suga, H. Oka and M. Kitamura, *The Chemical Record* **2001**, *1*, 85-100.
- [29] D. G. Blackmond, C. R. McMillan, S. Ramdeehul, A. Schorm and J. M. Brown, *Journal of the American Chemical Society* **2001**, *123*, 10103-10104.
- [30] D. G. Blackmond, *Tetrahedron: Asymmetry* **2006**, *17*, 584-589.
- [31] F. G. Buono and D. G. Blackmond, *Journal of the American Chemical Society* **2003**, *125*, 8978-8979.
- [32] I. D. Gridnev, J. M. Serafimov and J. M. Brown, *Angewandte Chemie International Edition* **2004**, *43*, 4884-4887.
- [33] L. Pu and H.-B. Yu, *Chemical Reviews* **2001**, *101*, 757-824.
- [34] X. Jiang, J. C. Bollinger and D. Lee, *Journal of the American Chemical Society* **2005**, *127*, 15678-15679.
- [35] M. Quaranta, T. Gehring, B. Odell, J. M. Brown and D. G. Blackmond, *Journal of the American Chemical Society* **2010**, *132*, 15104-15107.
- [36] I. D. Gridnev and A. K. Vorobiev, *ACS Catalysis* **2012**, *2*, 2137-2149.
- [37] A. Matsumoto, T. Abe, A. Hara, T. Tobita, T. Sasagawa, T. Kawasaki and K. Soai, *Angewandte Chemie International Edition* **2015**, *54*, 15218-15221.
- [38] O. Trapp, S. Lamour, F. Maier, A. F. Siegle, K. Zawatzky and B. F. Straub, *Chemistry – A European Journal* **2020**, *26*, 15871-15880.
- [39] I. Sato, H. Urabe, S. Ishii, S. Tanji and K. Soai, *Organic Letters* **2001**, *3*, 3851-3854.
- [40] M. Funes-Maldonado, B. Sieng and M. Amedjkouh, *European Journal of Organic Chemistry* **2015**, *2015*, 4081-4086.
- [41] C. Romagnoli, B. Sieng and M. Amedjkouh, *European Journal of Organic Chemistry* **2015**, *2015*, 4087-4092.
- [42] C. Romagnoli, B. Sieng and M. Amedjkouh, *Chirality* **2020**, *32*, 1143-1151.
- [43] a) W. Fuß, *Colloids and Surfaces B: Biointerfaces* **2009**, *74*, 498-503; b) W. A. Bonner, *Origins of life and evolution of the biosphere* **1991**, *21*, 59-111; c) I. G. d. V. V. V. Kuz'min, *Soviet Physics Uspekhi* **1989** *32*.
- [44] a) W. A. Bonner, E. Rubenstein and G. S. Brown, *Origins of life and evolution of the biosphere* **1999**, *29*, 329-332; b) Y. Inoue, *Chemical Reviews* **1992**, *92*, 741-770; c) B. L. Feringa and R. A. van Delden, *Angewandte Chemie International Edition* **1999**, *38*, 3418-3438.
- [45] a) R. M. Hazen and D. S. Sholl, *Nature Materials* **2003**, *2*, 367-374; b) K. Soai, S. Osanai, K. Kadowaki, S. Yonekubo, T. Shibata and I. Sato, *Journal of the American Chemical Society* **1999**, *121*, 11235-11236.
- [46] a) T. Matsuura and H. Koshima, *Journal of Photochemistry and Photobiology C: Photochemistry Reviews* **2005**, *6*, 7-24; b) M. Sakamoto, *Chemistry – A European Journal* **1997**, *3*, 684-689.
- [47] K. Mislow, *Collect Czech Chem Commun.* **2003**, *68*, 849.
- [48] J. A. Le Bel, *Bull. Soc. Chim. Fr* **1874**, *22*, 337-347.
- [49] J. H. van't Hoff, *Archives Néerlandaises des Sciences exactes et naturelles* **1874**, *9*, 445-454.
- [50] a) A. Cotton, *C. R. Hebd. Seanc. Acad. Sci. Paris* **1895**, *120*, 989; b) A. Cotton, *C. R. Hebd. Seanc. Acad. Sci. Paris* **1895**, *120*, 1044.
- [51] a) W. Kuhn, *Trans. Faraday Soc.* **1930** *26*, 293; b) W. Kuhn and E. Knopf, *Z. Phys. Chem., Abt. B* **1930**, *7*, 292.
- [52] a) Y. Inoue, *Chemical Reviews* **1992**, *92*, 741-770; b) B. L. Feringa and R. A. v. Delden, *Angew. Chem., Int. Ed.* **1999**, *38*, 3418-3438.
- [53] a) G. Balavoine, A. Moradpour and H. B. Kagan, *J. Am. Chem. Soc.* **1974**, *96*, 5152; b) H. B. Kagan and J. C. Fiaud, *Top. Stereochem.* **1988**, *18* 249.
- [54] a) K. Adachi, K. Naemura and M. Nakazaki, *Tetrahedron Lett.* **1968** 5467; b) J. F. Nicoud, C. Eskenazi and H. B. Kagan, *J. Org. Chem.* **1977** *42* 4270.

- [55] T. Fukue, M. Tamura, R. Kandori, N. Kusakabe, J. H. Hough, J. Bailey, D. C. B. Whittet, P. W. Lucas, Y. Nakajima and J. Hashimoto, *Origins Life Evol. Biosphere* **2010** 335.
- [56] S. Pizzarello and T. L. Groy, *Geochimica et Cosmochimica Acta* **2011**, 75 645–656.
- [57] a) J. J. Flores, W. A. Bonner and G. A. Massey, *Journal of the American Chemical Society* **1977**, 99, 3622-3625; b) U. J. Meierhenrich, L. Nahon, C. Alcaraz, J. H. Bredehöft, S. V. Hoffmann, B. Barbier and A. Brack, *Angewandte Chemie International Edition* **2005**, 44, 5630-5634; c) C. Meinert, P. Cassam-Chenai, N. C. Jones, L. Nahon, S. V. Hoffmann and U. J. Meierhenrich, *Origins of Life and Evolution of Biospheres* **2015**, 45, 149-161.
- [58] K. L. Stevenson and J. F. Verkieck, *J. Am. Chem. Soc.* **1968**, 90, 2974.
- [59] K. Hayashi and M. Irie, *Chem. Abstr.* **1978**, 89 6151j.
- [60] M. Suarez and G. B. Schuster, *J. Am. Chem. Soc.* **1995**, 117, 6732-6738.
- [61] a) A. Moradpour, J. F. Nicoud, G. Balavoine, H. Kagan and G. Tsoucaris, *J. Am. Chem. Soc.* **1971**, 93, 2353-2354; b) H. Kagan, A. Moradpour, J. F. Nicoud, G. Balavoine, R. H. Martin and J. P. Cosyn, *Tetrahedron Lett.* **1971**, 27 2479-2482.
- [62] a) W. J. Bernstein, M. Calvin and O. Buchardt, *J. Am. Chem. Soc.* **1972** 94, 494-497;; b) W. J. Bernstein and M. Calvin, *Tetrahedron Lett.* **1972** 22, 2195-2198; c) W. J. Bernstein, M. Calvin and O. Buchardt, *J. Am. Chem. Soc.* **1973**, 95, 527-532.
- [63] L. Pasteur, *Ann. Chim. Phys.* **1848**, 24, 442.
- [64] K. S. H. Murakami, N. Hirayama, R. Tamura *Novel Optical Resolution Technologies*, Springer, Berlin,, **2007**, p.
- [65] G. Levilain and G. Coquerel, *CrystEngComm* **2010**, 12, 1983-1992.
- [66] L.-C. Sögütöglu, R. R. E. Steendam, H. Meekes, E. Vlieg and F. P. J. T. Rutjes, *Chemical Society Reviews* **2015**, 44, 6723-6732.
- [67] D. K. Kondepudi, R. J. Kaufman and N. Singh, *Science* **1990**, 250, 975.
- [68] a) E. Havinga, *Chem. Wekbl.* **1941**, 642; b) E. Havinga, *Biochim. Biophys. Acta* **1954**, 171.
- [69] D. G. Blackmond, *Cold Spring Harbor Perspectives in Biology* **2010**, 2.
- [70] C. Viedma, *Physical Review Letters* **2005**, 94, 065504.
- [71] W. L. Noorduin, T. Izumi, A. Millemaggi, M. Leeman, H. Meekes, W. J. P. Van Enckevort, R. M. Kellogg, B. Kaptein, E. Vlieg and D. G. Blackmond, *Journal of the American Chemical Society* **2008**, 130, 1158-1159.
- [72] W. L. Noorduin, A. A. C. Bode, M. van der Meijden, H. Meekes, A. F. van Etteger, W. J. P. van Enckevort, P. C. M. Christianen, B. Kaptein, R. M. Kellogg, T. Rasing and E. Vlieg, *Nature Chemistry* **2009**, 1, 729-732.
- [73] K. Suwannasang, A. E. Flood, C. Rougeot and G. Coquerel, *Crystal Growth & Design* **2013**, 13, 3498-3504.
- [74] M. Iggländ, M. P. Fernández-Ronco, R. Senn, J. Kluge and M. Mazzotti, *Chemical Engineering Science* **2014**, 111, 106-111.
- [75] G. An, P. Yan, J. Sun, Y. Li, X. Yao and G. Li, *CrystEngComm* **2015**, 17, 4421-4433.
- [76] L. Addadi, Z. Berkovitch-Yellin, I. Weissbuch, J. van Mil, L. J. W. Shimon, M. Lahav and L. Leiserowitz, *Angewandte Chemie International Edition in English* **1985**, 24, 466-485.
- [77] J. L. Purvis, *Chem. Abstr.* **1957**, 51, 13910i.
- [78] B. S. Green and L. Heller, *Science* **1974**, 185, 525.
- [79] K. Penzien and G. M. J. Schmidt, *Angewandte Chemie International Edition in English* **1969**, 8, 608-609.
- [80] a) D. A. Singleton and L. K. Vo, *Organic Letters* **2003**, 5, 4337-4339; b) K. Soai, I. Sato, T. Shibata, S. Komiya, M. Hayashi, Y. Matsueda, H. Imamura, T. Hayase, H. Morioka, H. Tabira, J. Yamamoto and Y. Kowata, *Tetrahedron: Asymmetry* **2003**, 14, 185-188.
- [81] T. Kawasaki, M. Sato, S. Ishiguro, T. Saito, Y. Morishita, I. Sato, H. Nishino, Y. Inoue and K. Soai, *Journal of the American Chemical Society* **2005**, 127, 3274-3275.
- [82] H. Shindo, Y. Shirota, K. Niki, T. Kawasaki, K. Suzuki, Y. Araki, A. Matsumoto and K. Soai, *Angewandte Chemie International Edition* **2013**, 52, 9135-9138.

- [83] a) H. Mineki, T. Hanasaki, A. Matsumoto, T. Kawasaki and K. Soai, *Chemical Communications* **2012**, 48, 10538-10540; b) T. Kawasaki, T. Sasagawa, K. Shiozawa, M. Uchida, K. Suzuki and K. Soai, *Organic Letters* **2011**, 13, 2361-2363; c) T. Kawasaki and K. Soai, *Israel Journal of Chemistry* **2012**, 52, 582-590.
- [84] a) I. Sato, D. Omiya, T. Saito and K. Soai, *Journal of the American Chemical Society* **2000**, 122, 11739-11740; b) T. Kawasaki, Y. Matsumura, T. Tsutsumi, K. Suzuki, M. Ito and K. Soai, *Science* **2009**, 324, 492; c) T. Kawasaki, Y. Okano, E. Suzuki, S. Takano, S. Oji and K. Soai, *Angewandte Chemie International Edition* **2011**, 50, 8131-8133; d) A. Matsumoto, H. Ozaki, S. Harada, K. Tada, T. Ayugase, H. Ozawa, T. Kawasaki and K. Soai, *Angewandte Chemie International Edition* **2016**, 55, 15183-15183.
- [85] A. Matsumoto, Y. Kaimori, M. Uchida, H. Omori, T. Kawasaki and K. Soai, *Angewandte Chemie International Edition* **2017**, 56, 545-548.
- [86] T. Kawasaki, S. Kamimura, A. Amihara, K. Suzuki and K. Soai, *Angewandte Chemie International Edition* **2011**, 50, 6796-6798.
- [87] Y. Kaimori, Y. Hiyoshi, T. Kawasaki, A. Matsumoto and K. Soai, *Chemical Communications* **2019**, 55, 5223-5226.
- [88] W. C. Zeise, *Mag. Pharm.* **1830**, 35 105.
- [89] D. W. Breck, *Zeolite Molecular Sieves: Structure, Chemistry, and Use*, Wiley-Interscience, New York, **1974**, p.
- [90] H. Furukawa, K. E. Cordova, M. O'Keeffe and O. M. Yaghi, *Science* **2013**, 341, 1230444.
- [91] M. Eddaoudi, D. B. Moler, H. Li, B. Chen, T. M. Reineke, M. O'Keeffe and O. M. Yaghi, *Accounts of Chemical Research* **2001**, 34, 319-330.
- [92] a) S. S. Y. Chui, S. M. F. Lo, J. P. H. Charmant, A. G. Orpen and I. D. Williams, *Science* **1999**, 283, 1148; b) M. Eddaoudi, H. Li, T. Reineke, M. Fehr, D. Kelley, T. L. Groy and O. M. Yaghi, *Topics in Catalysis* **1999**, 9, 105-111; c) H. Li, M. Eddaoudi, M. O'Keeffe and O. M. Yaghi, *Nature* **1999**, 402, 276.
- [93] J. H. Cavka, S. Jakobsen, U. Olsbye, N. Guillou, C. Lamberti, S. Bordiga and K. P. Lillerud, *Journal of the American Chemical Society* **2008**, 130, 13850-13851.
- [94] S. Biswas, J. Zhang, Z. Li, Y.-Y. Liu, M. Grzywa, L. Sun, D. Volkmer and P. Van Der Voort, *Dalton Transactions* **2013**, 42, 4730-4737.
- [95] V. Guillerme, F. Ragon, M. Dan-Hardi, T. Devic, M. Vishnuvarthan, B. Campo, A. Vimont, G. Clet, Q. Yang, G. Maurin, G. Férey, A. Vittadini, S. Gross and C. Serre, *Angewandte Chemie International Edition* **2012**, 51, 9267-9271.
- [96] H. Furukawa, F. Gándara, Y.-B. Zhang, J. Jiang, W. L. Queen, M. R. Hudson and O. M. Yaghi, *Journal of the American Chemical Society* **2014**, 136, 4369-4381.
- [97] D. Feng, Z.-Y. Gu, J.-R. Li, H.-L. Jiang, Z. Wei and H.-C. Zhou, *Angewandte Chemie International Edition* **2012**, 51, 10307-10310.
- [98] a) L. Ma, C. Abney and W. Lin, *Chemical Society Reviews* **2009**, 38, 1248-1256; b) M. Yoon, R. Srirambalaji and K. Kim, *Chemical Reviews* **2012**, 112, 1196-1231.
- [99] a) L. J. Murray, M. Dincă and J. R. Long, *Chemical Society Reviews* **2009**, 38, 1294-1314; b) S. Ma and H.-C. Zhou, *Chemical Communications* **2010**, 46, 44-53; c) J. An and N. L. Rosi, *Journal of the American Chemical Society* **2010**, 132, 5578-5579.
- [100] a) J.-R. Li, R. J. Kuppler and H.-C. Zhou, *Chemical Society Reviews* **2009**, 38, 1477-1504; b) L. Pan, D. H. Olson, L. R. Ciemnomolonski, R. Heddy and J. Li, *Angewandte Chemie International Edition* **2006**, 45, 616-619; c) S. Keskin, T. M. van Heest and D. S. Sholl, *ChemSusChem* **2010**, 3, 879-891; d) W. Liang, C. J. Coghlan, F. Ragon, M. Rubio-Martinez, D. M. D'Alessandro and R. Babarao, *Dalton Transactions* **2016**, 45, 4496-4500.
- [101] a) M. Alvaro, E. Carbonell, B. Ferrer, F. X. Llabrés i Xamena and H. Garcia, *Chemistry – A European Journal* **2007**, 13, 5106-5112; b) M. G. Campbell, D. Sheberla, S. F. Liu, T. M. Swager and M. Dincă, *Angewandte Chemie International Edition* **2015**, 54, 4349-4352; c) L. E. Kreno, K. Leong, O. K. Farha, M. Allendorf, R. P. Van Duyne and J. T. Hupp, *Chemical Reviews* **2012**, 112, 1105-1125; d) K. M. Choi, H. M. Jeong, J. H. Park, Y.-B. Zhang, J. K. Kang and O. M. Yaghi, *ACS Nano* **2014**, 8, 7451-7457; e) D. Sheberla, J. C. Bachman, J. S. Elias, C.-J. Sun, Y. Shao-Horn and M. Dincă, *Nature Materials* **2016**, 16, 220.

- [102] R. C. Huxford, J. Della Rocca and W. Lin, *Current Opinion in Chemical Biology* **2010**, *14*, 262-268.
- [103] a) Z. Wei, Z.-Y. Gu, R. K. Arvapally, Y.-P. Chen, R. N. McDougald, J. F. Ivy, A. A. Yakovenko, D. Feng, M. A. Omary and H.-C. Zhou, *Journal of the American Chemical Society* **2014**, *136*, 8269-8276; b) H.-L. Jiang, D. Feng, K. Wang, Z.-Y. Gu, Z. Wei, Y.-P. Chen and H.-C. Zhou, *Journal of the American Chemical Society* **2013**, *135*, 13934-13938.
- [104] a) Y. Inokuma, S. Yoshioka, J. Ariyoshi, T. Arai, Y. Hitora, K. Takada, S. Matsunaga, K. Rissanen and M. Fujita, *Nature* **2013**, *495*, 461-466; b) M. Hoshino, A. Khutia, H. Xing, Y. Inokuma and M. Fujita, *IUCrJ* **2016**, *3*, 139-151.
- [105] W. J. Gee, *Dalton Transactions* **2017**, *46*, 15979-15986.
- [106] K. Biradha and M. Fujita, *Angewandte Chemie International Edition* **2002**, *41*, 3392-3395.
- [107] T. Kawamichi, T. Haneda, M. Kawano and M. Fujita, *Nature* **2009**, *461*, 633-635.
- [108] Y. Inokuma, M. Kawano and M. Fujita, *Nature Chemistry* **2011**, *3*, 349-358.
- [109] J. V. Knichal, H. J. Shepherd, C. C. Wilson, P. R. Raithby, W. J. Gee and A. D. Burrows, *Angewandte Chemie International Edition* **2016**, *55*, 5943-5946.
- [110] T. Shibata, K. Choji, T. Hayase, Y. Aizu and K. Soai, *Chemical Communications* **1996**, 1235-1236.
- [111] a) S. V. Athavale, A. Simon, K. N. Houk and S. E. Denmark, *Journal of the American Chemical Society* **2020**, *142*, 18387-18406; b) S. V. Athavale, A. Simon, K. N. Houk and S. E. Denmark, *Nature Chemistry* **2020**, *12*, 412-423.
- [112] C. J. Welch, M. Biba and P. Sajonz, *Chirality* **2007**, *19*, 34-43.
- [113] R. Schmidt; and H. Meerwein, *Justus Liebigs Ann Chem* **1925**, 444.
- [114] V. E. Tishchenko, *J. Russ. Phys. Chem. Soc* **1906**, 38.
- [115] Y. Ogata and A. Kawasaki, *Tetrahedron* **1969**, *25*, 929-935.
- [116] J. Li, J. Shi, H. Han, Z. Guo, H. Tong, X. Wei, D. Liu and M. F. Lappert, *Organometallics* **2013**, *32*, 3721-3727.
- [117] M. Miyagawa and T. Akiyama, *Chemistry Letters* **2017**, *47*, 78-81.
- [118] H. Geng, X. Chen, J. Gui, Y. Zhang, Z. Shen, P. Qian, J. Chen, S. Zhang and W. Wang, *Nature Catalysis* **2019**, *2*, 1071-1077.
- [119] O. V. Maltsev, R. Rausch, Z.-J. Quan and L. Hintermann, *European Journal of Organic Chemistry* **2014**, *2014*, 7426-7432.



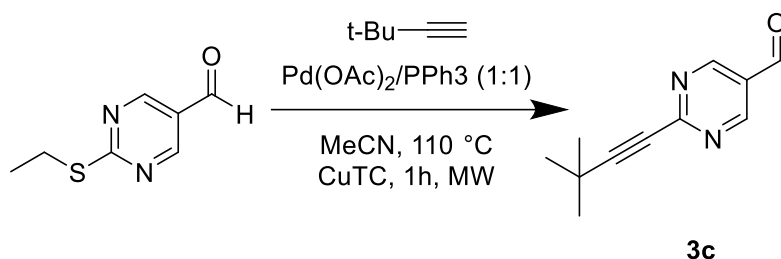


## **Appendix II**

**Additional supporting information for Chapter 2**



### Synthesis of Soai aldehyde 3c



The synthesis is based on a procedure by Hintermann *et al.* <sup>[119]</sup>

(a) *Preparation of catalyst solution:* Pd(OAc)<sub>2</sub> (0,092 g, 0,05 eq) and PPh<sub>3</sub> (0,1 g, 0,05 eq) were weighed into a dry glass vessel. The vessel was closed with a septum and flushed with argon. Dry MeCN (4 mL) was added and the mixture stirred at r.t. until a clear solution was obtained.

(b) *Catalytic coupling:* 2-Ethylsulphonyl-pyrimidine-5-carbaldehyde (1,34 g, 1 eq) and CuTC (2,5 g, 1,65 eq) were weighed into a microwave reaction glass. The vessel was closed with a septum, and flushed with argon. The catalyst solution (see above) was added via a syringe, followed by a solution of 3,3-dimethyl-1-butyne (1,7 mL, 1.7 mmol) in dry MeCN (8 mL). The vessel was closed with a septum suitable for microwave reactors and the reaction mixture subjected to microwave irradiation (110 °C, 1 h).

(c) *Workup and purification:* After cooling, a saturated solution of aq NH<sub>4</sub>Cl (6 mL) followed by EtOAc (25 mL) were added and the mixture filtered through celite to remove insoluble solids. The aqueous phase was extracted with EtOAc (2×25 mL). The combined organic phase was washed with 2 M NaOH and brine (2×20 mL), then dried over MgSO<sub>4</sub>. After filtration and evaporation, the residue was dried in high vacuum for complete removal of MeCN. Products were further purified by column chromatography on silica with Hex/EtOAc 80/20 as eluent to yield the NMR pure desired product (0.58 g, 38%).

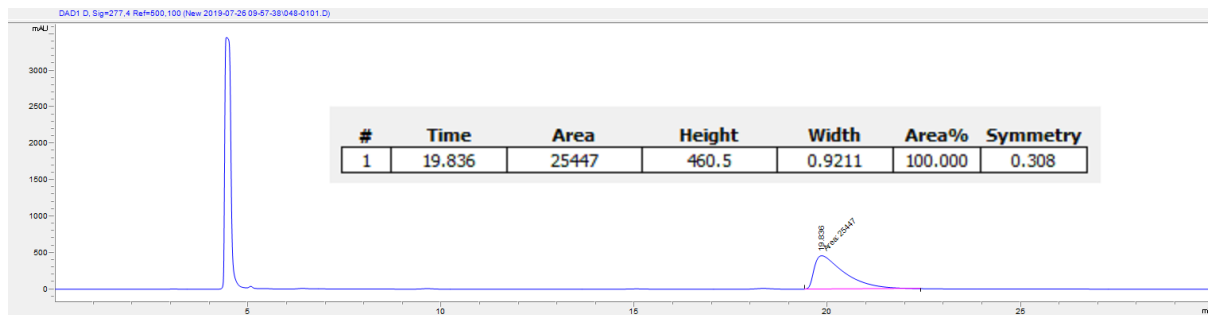
**<sup>1</sup>H NMR** (400 MHz, CDCl<sub>3</sub>): 10.14 (s, 1H), 9.13 (s, 2H), 1.42 (s, 9H)

**<sup>13</sup>C NMR:** (100 MHz, CDCl<sub>3</sub>): 188.4, 158.4, 156.5, 126.4, 103.3, 79.1, 30.4, 28.3 ppm

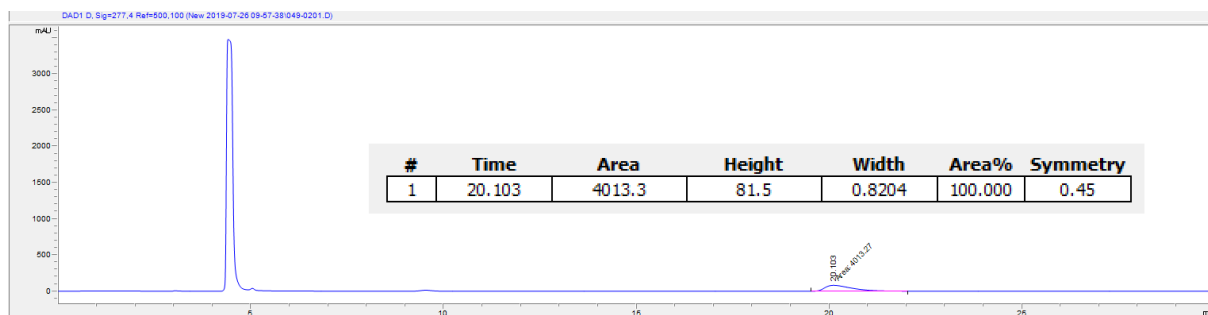
**HRMS (EI):** C<sub>11</sub>H<sub>12</sub>N<sub>2</sub>O calcd: 188.09496, found: 188.09509.

HPLC and NMR analysis from Table 2.1

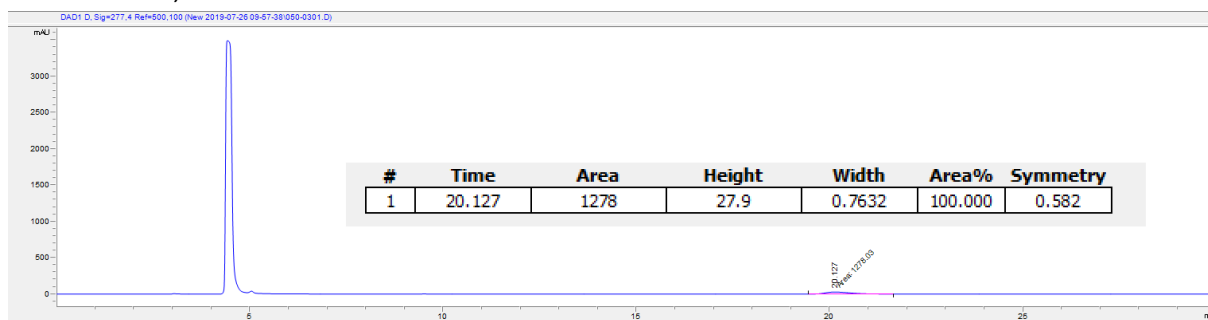
UiO-67 with 2:1 ratio



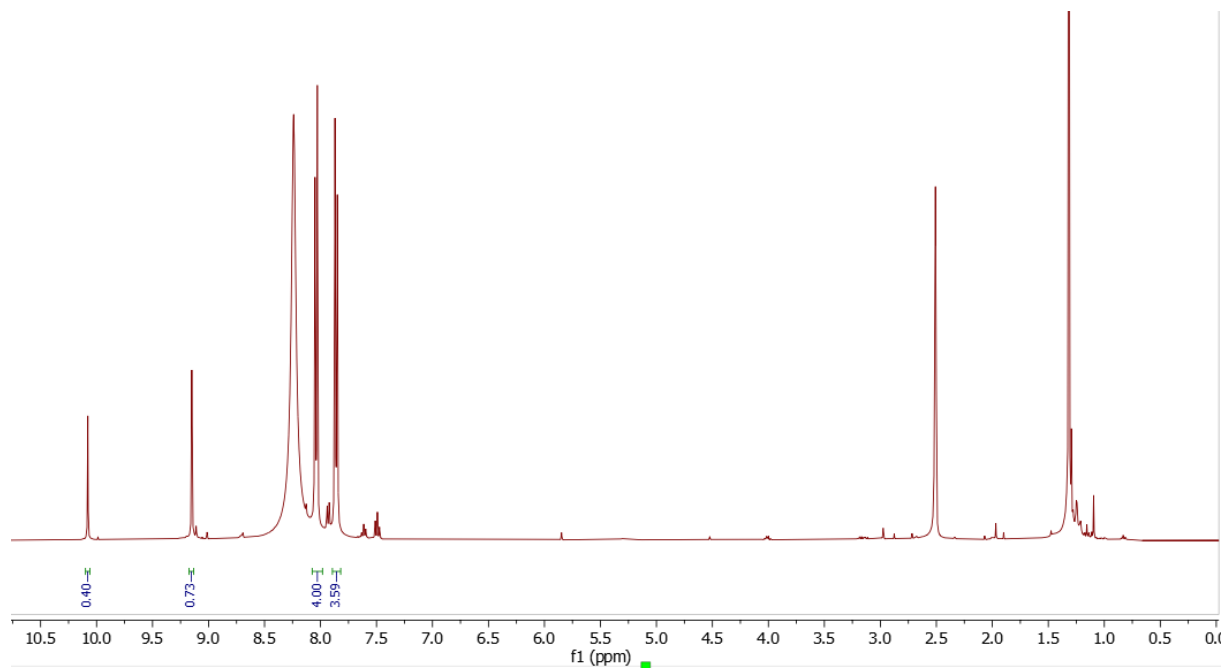
UiO-67 with 1:1 ratio



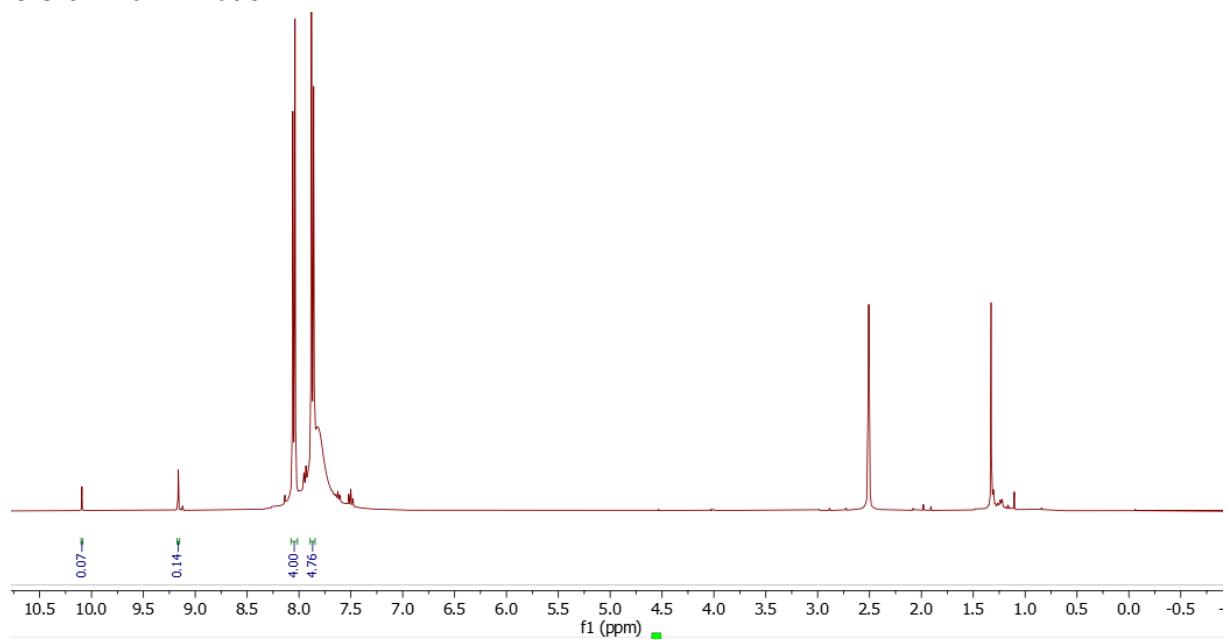
UiO-67 with 0,5:1 ratio



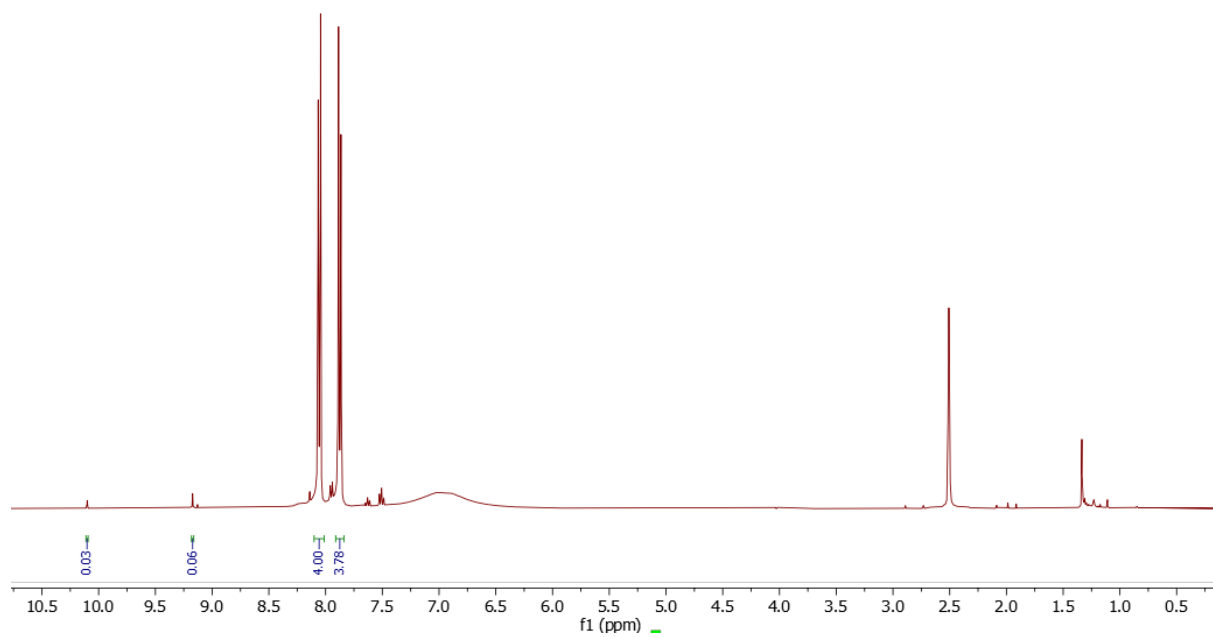
UiO-67 with 2:1 ratio



UiO-67 with 1:1 ratio



UiO-67 with 0,1:5 ratio



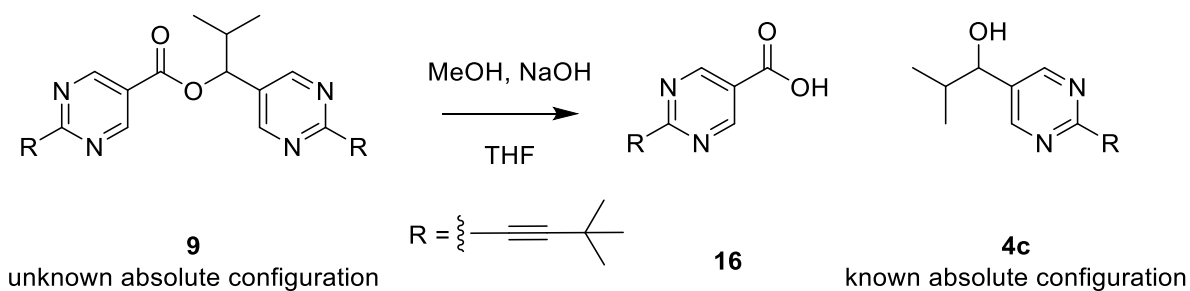
## **Appendix III**

**Additional supporting information for Chapter 3**





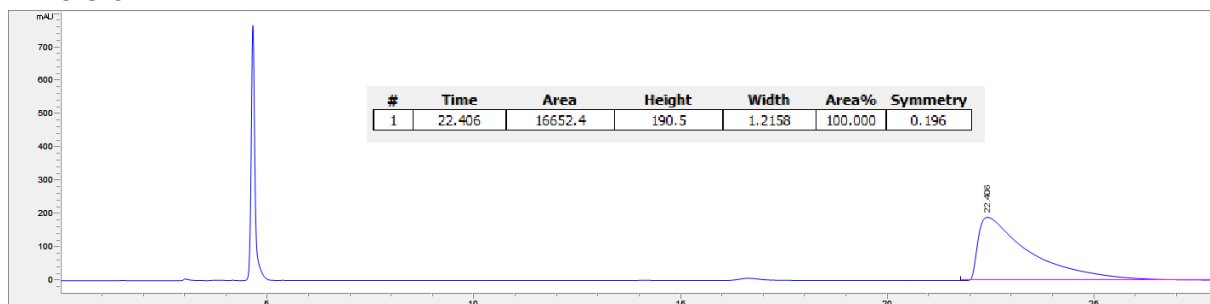
### Hydrolysis of ester **9**



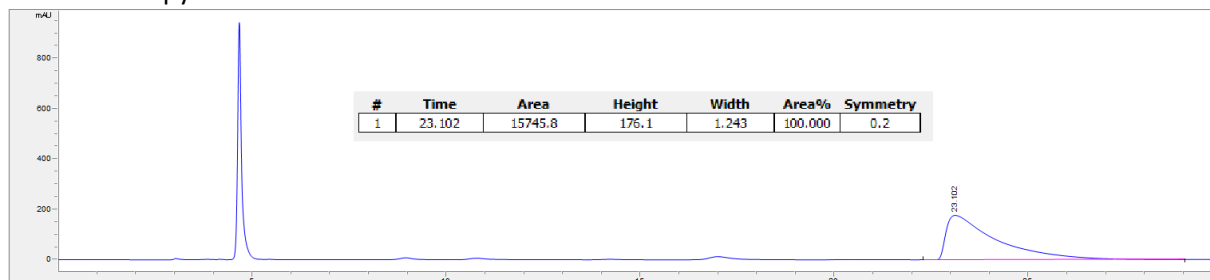
To a solution of dimethyl 1-(2-(3,3-dimethylbut-1-yn-1-yl)pyrimidin-5-yl)-2-methylpropyl 2-(3,3-dimethylbut-1-yn-1-yl)pyrimidine-5-carboxylate (**9**) (1eq, 15 mg, 0,036 mmol) in THF (0,4 ml) and MeOH (0,04 mL) a 3.0M aqueous NaOH solution (10 eq, 0,36 mL, 0,12 mL) was added, and the resulting mixture stirred at room temperature for 1 hour.

Figure 3.4

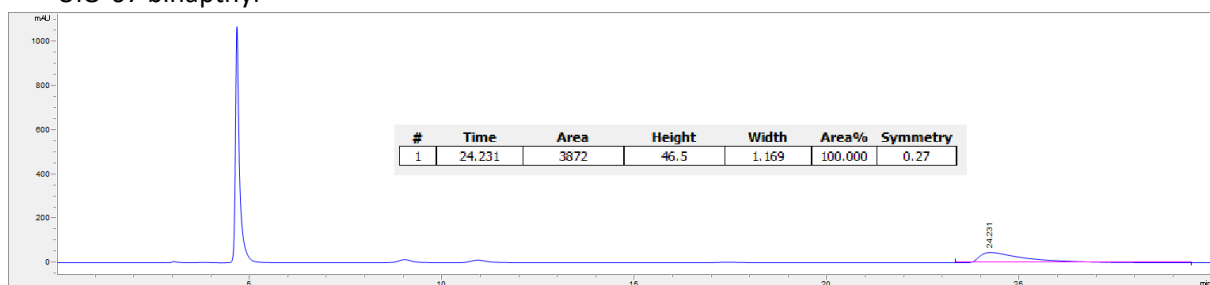
#### • UiO-67



#### • UiO-67 bpy 10%



#### • UiO-67 binaphthyl



• UiO-66

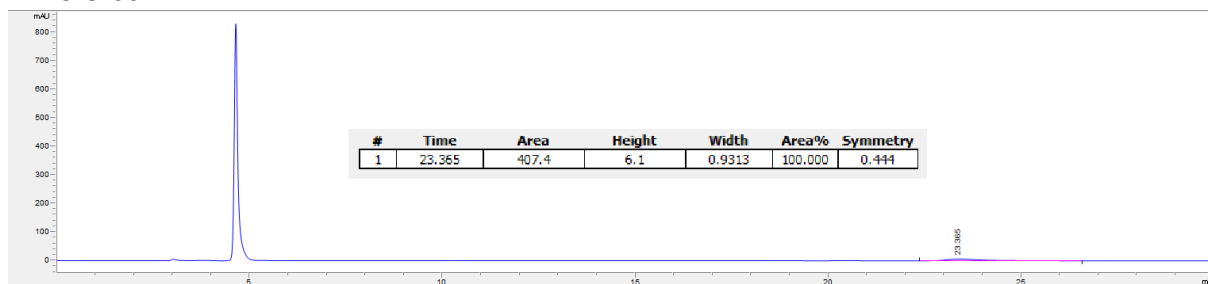
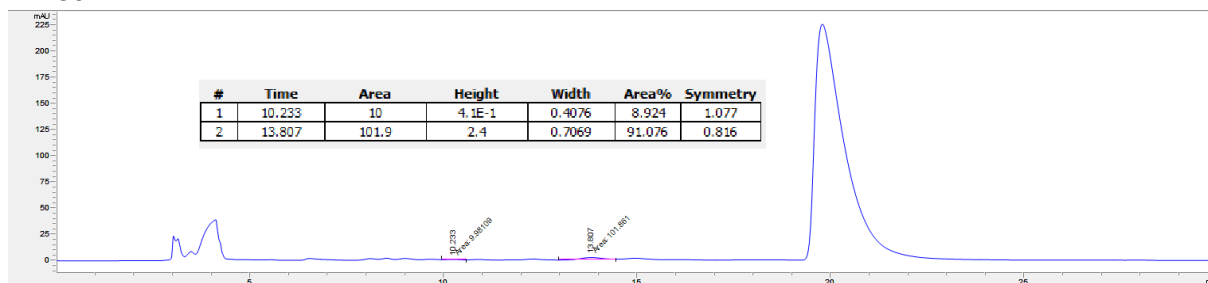
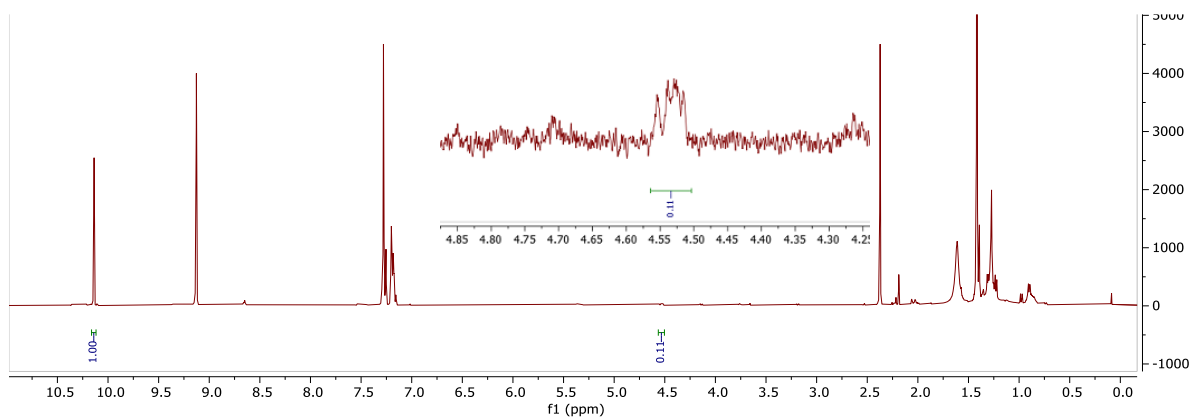
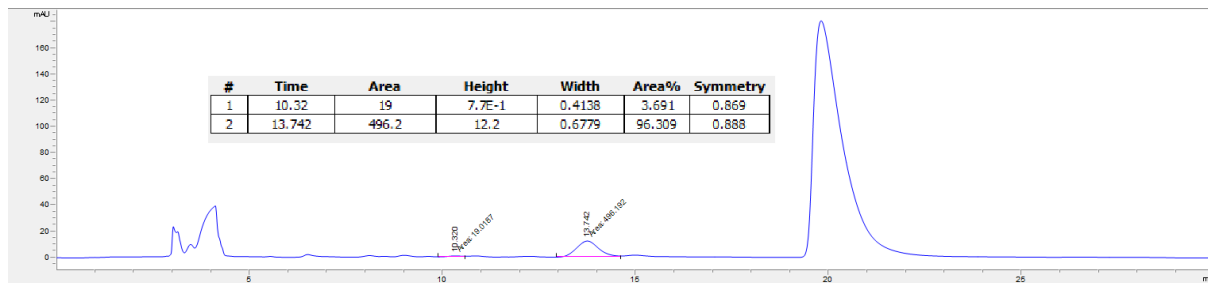


Figure 3.5

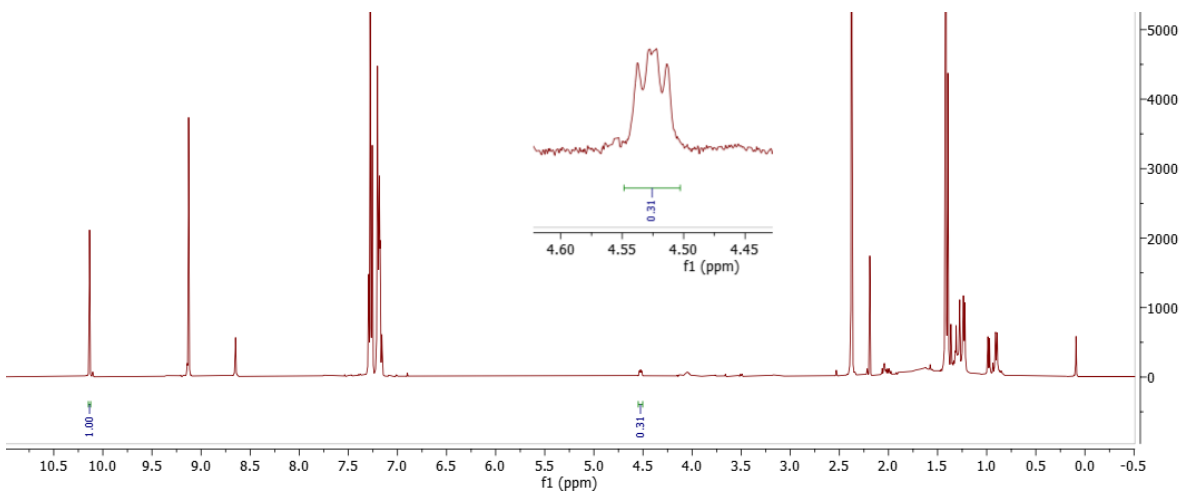
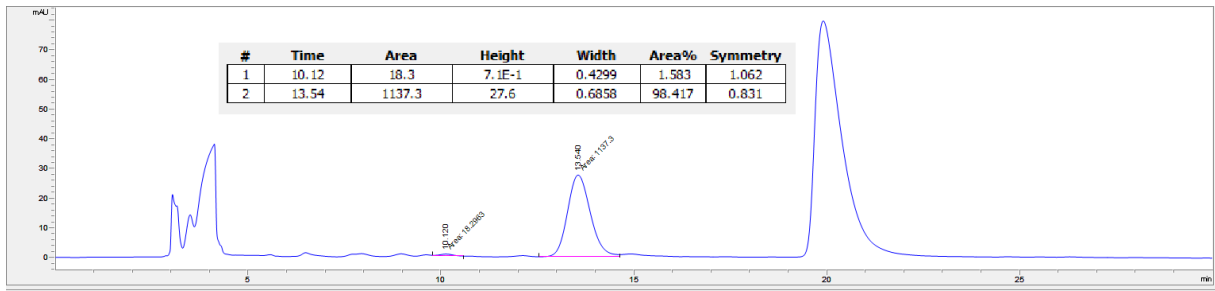
• 30 min



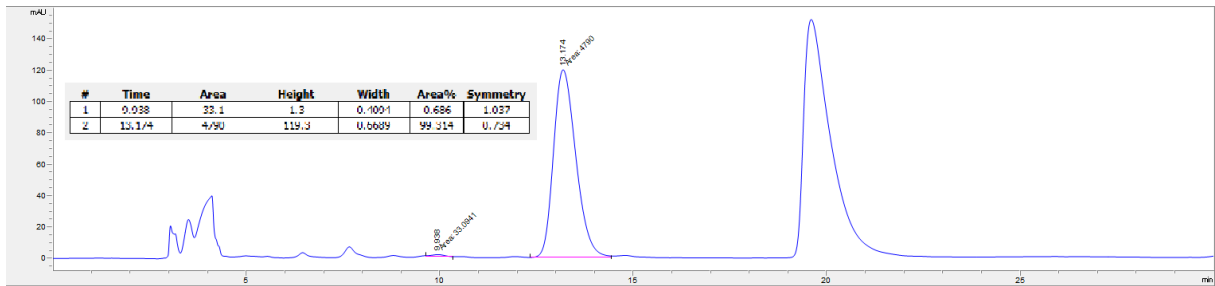
• 1 h

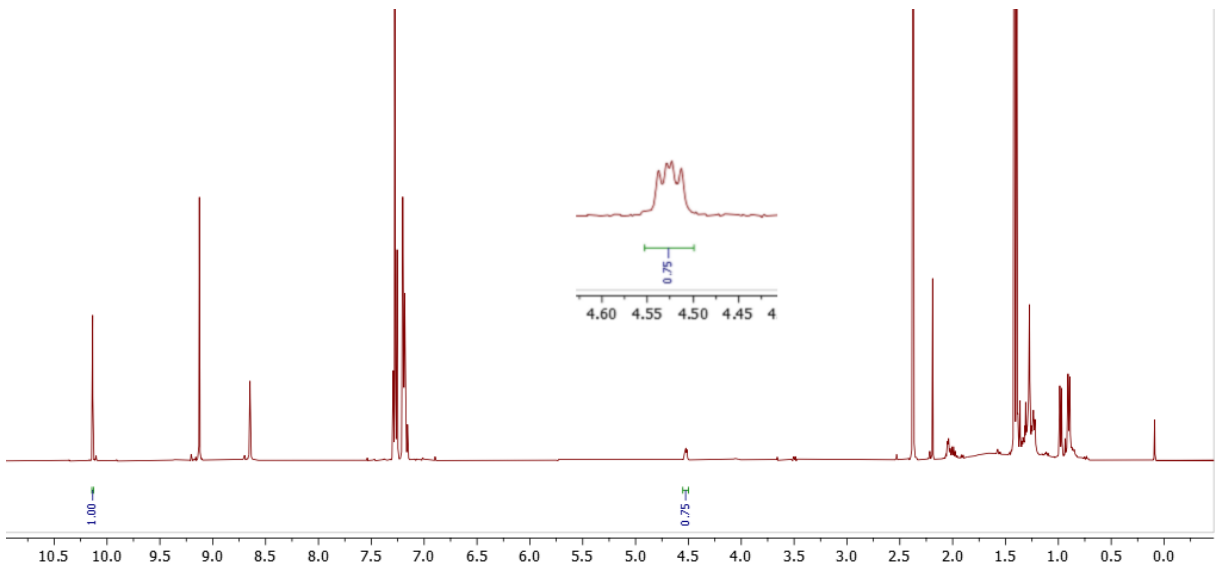


• 3 h



• 7 h





• 24 h

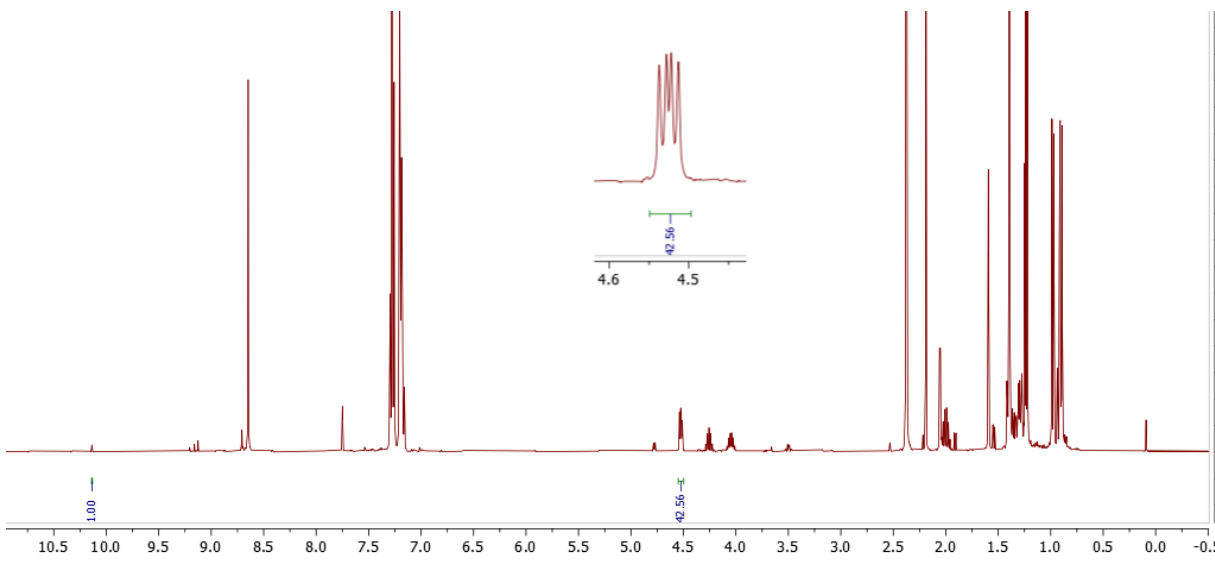
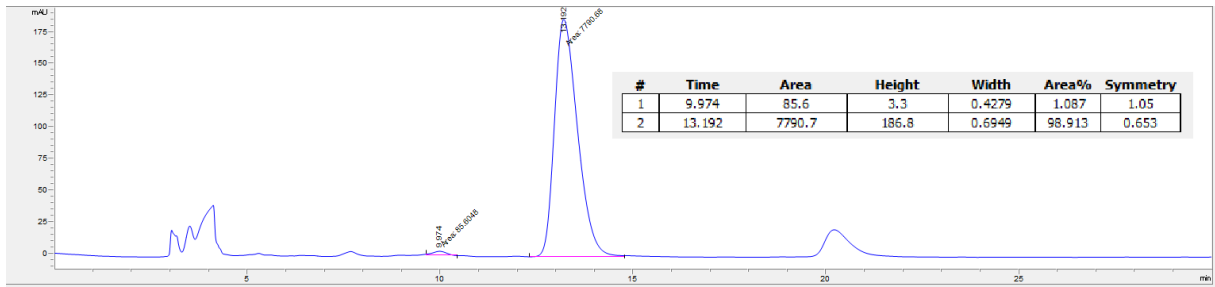
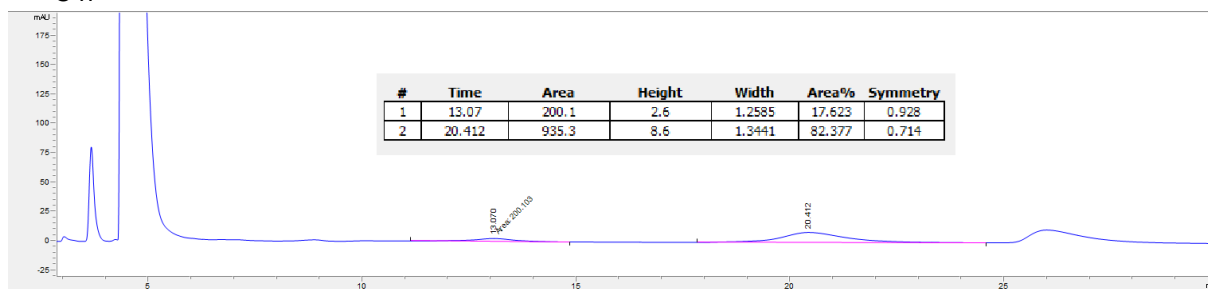
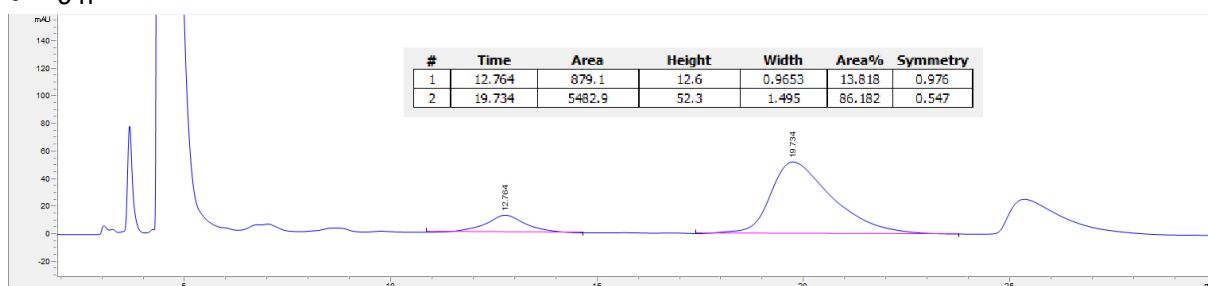


Figure 3.6

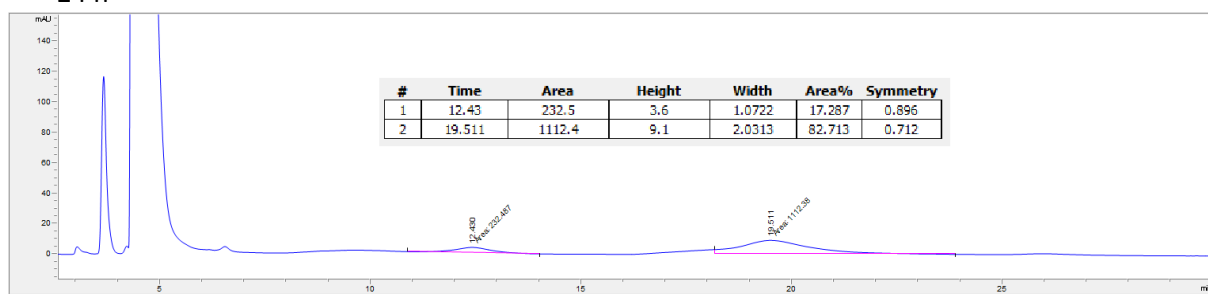
• 3 h



• 6 h



• 24 h



• 72 h

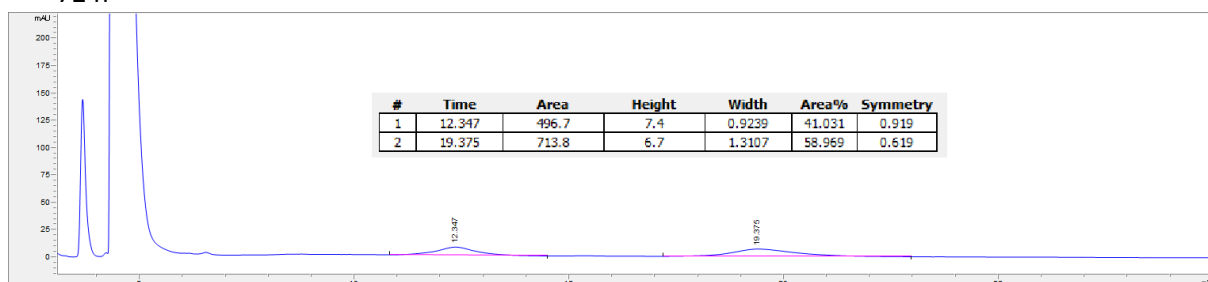
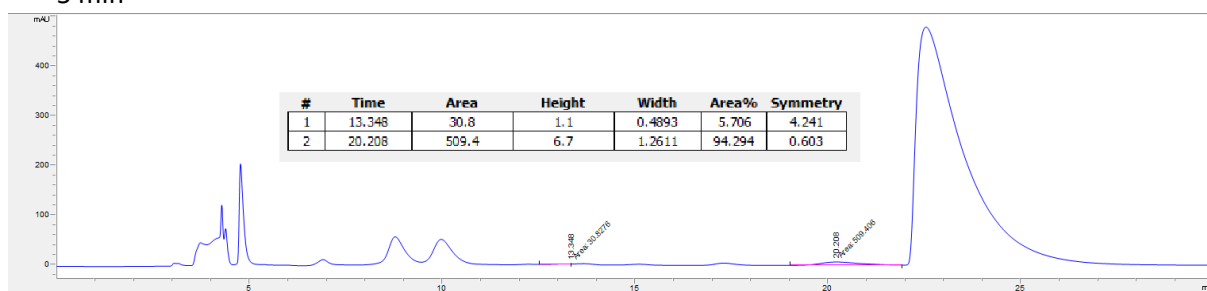
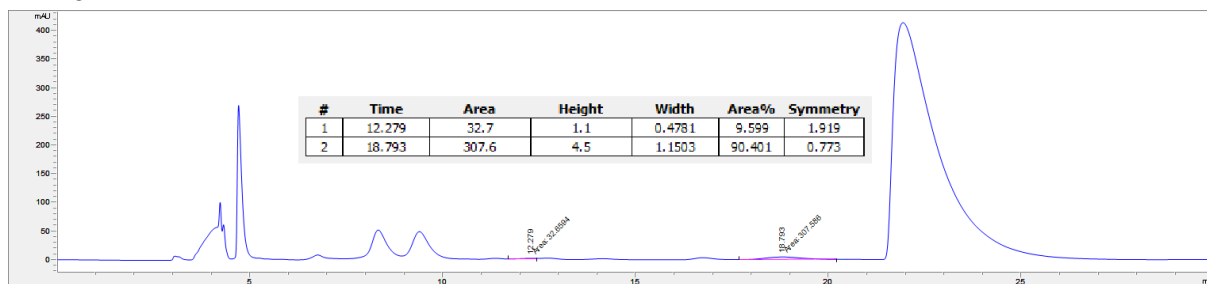


**Table 3.6**

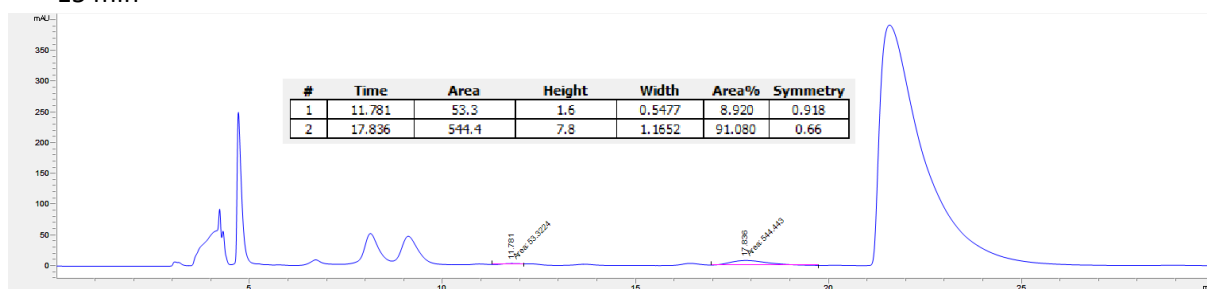
● 5 min



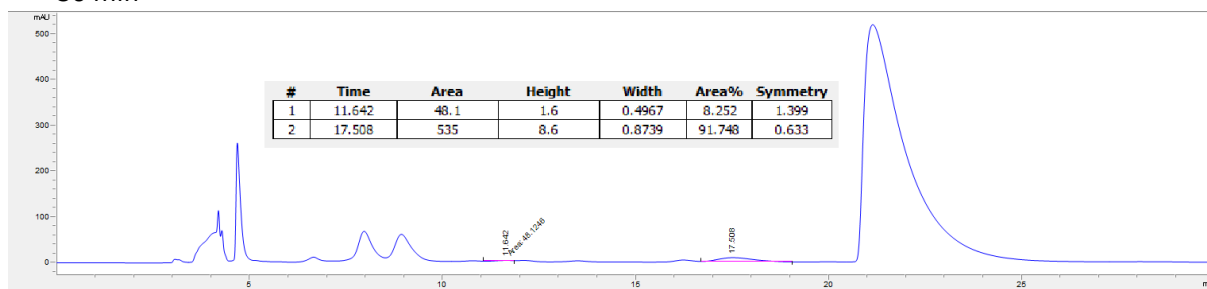
● 10 min



● 15 min



● 30 min



● 45 min

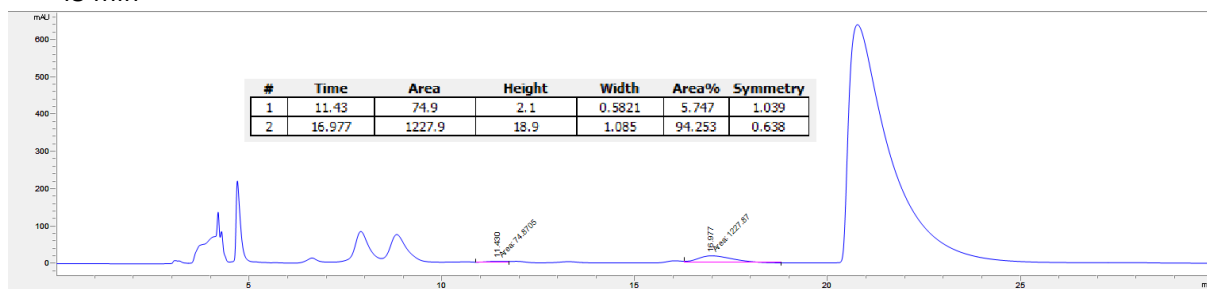
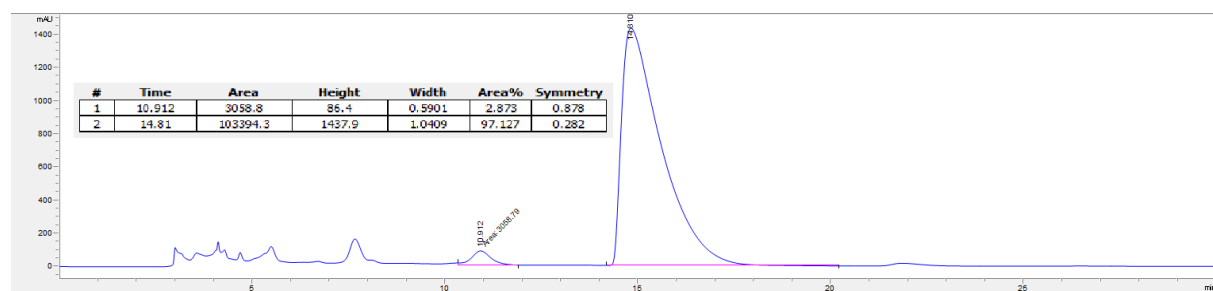
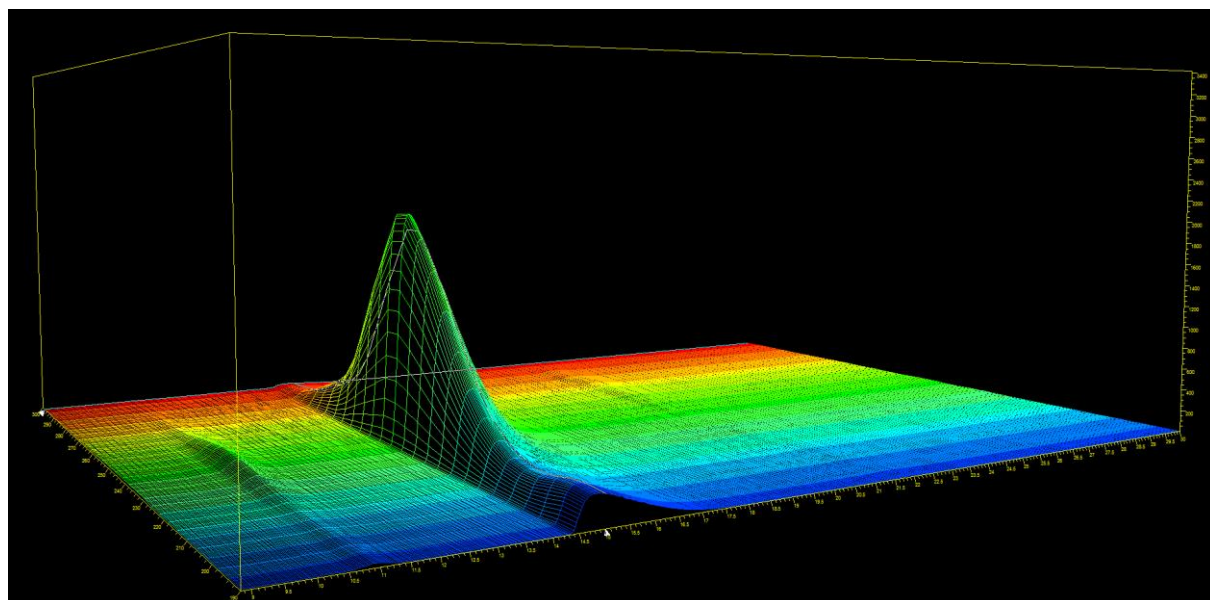
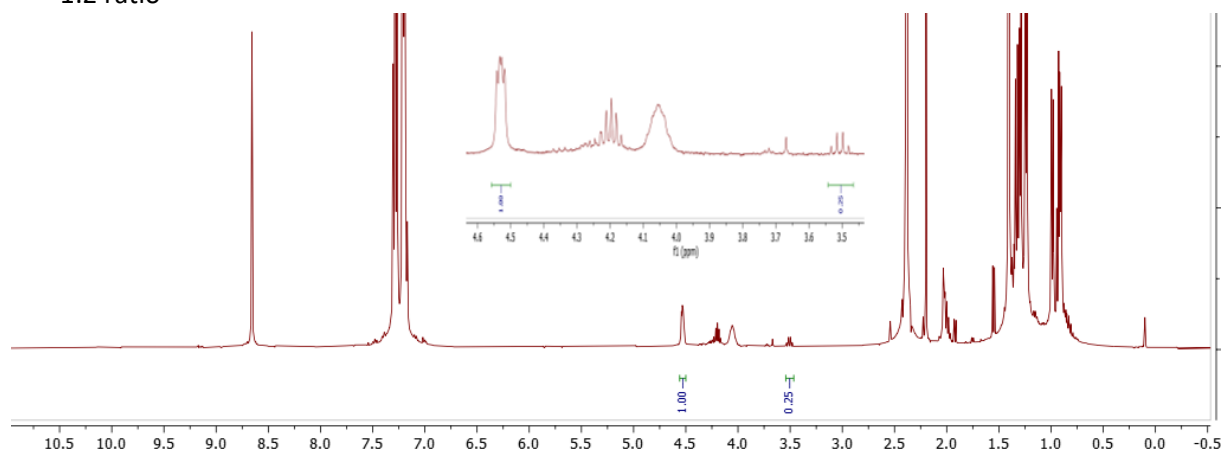
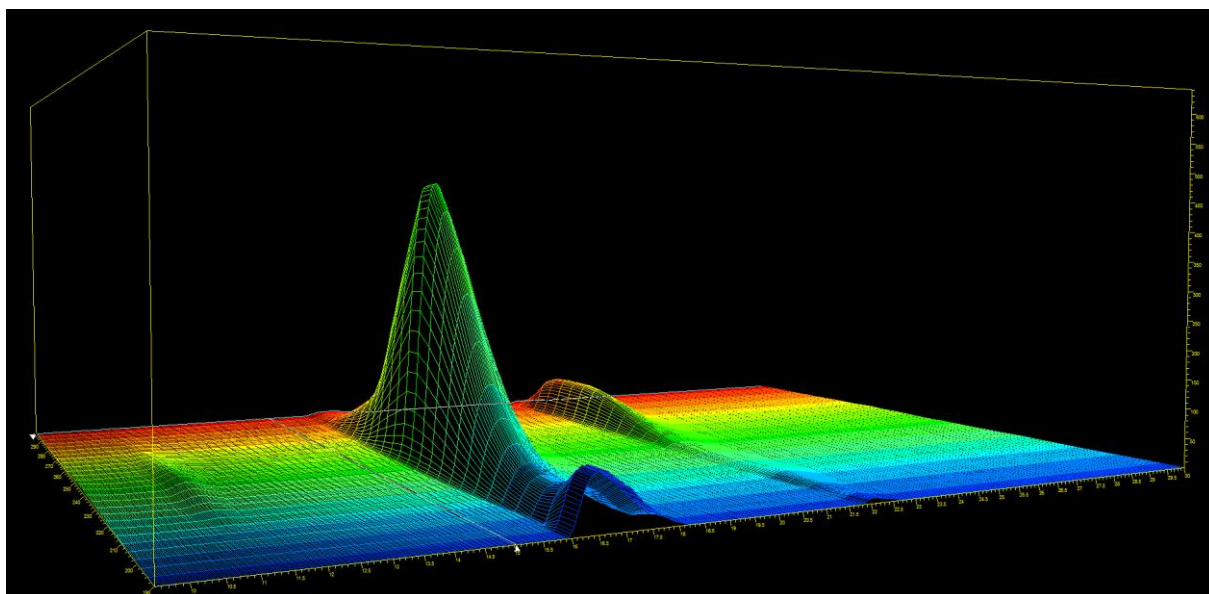
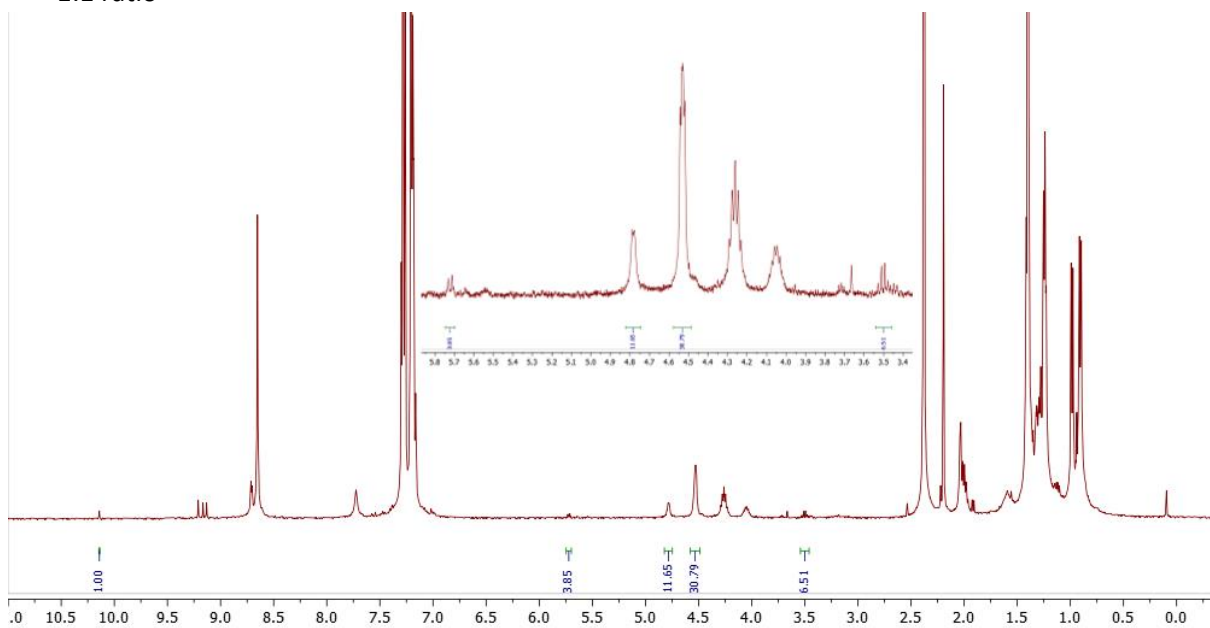


Table 3.7

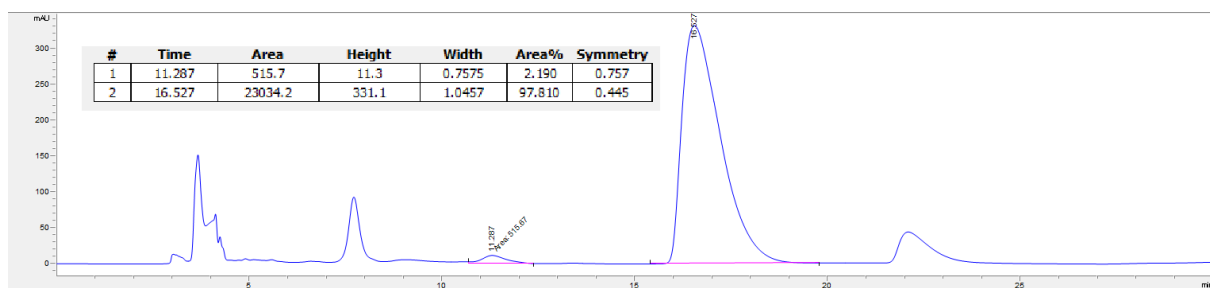
- 1:2 ratio



- 1:1 ratio

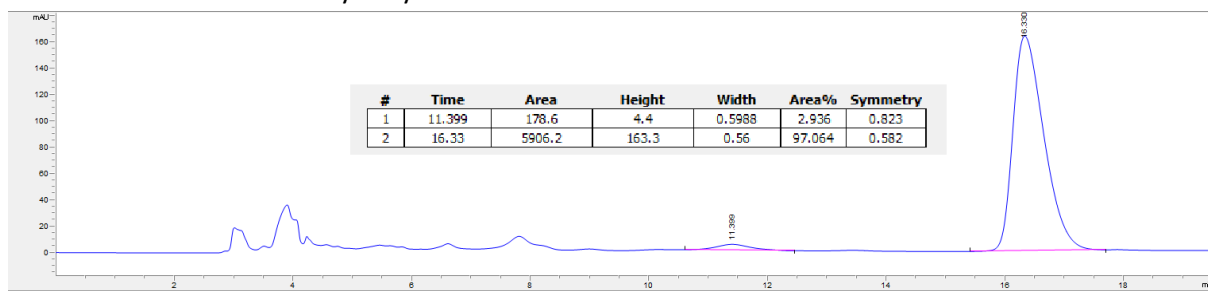


ee% 4c

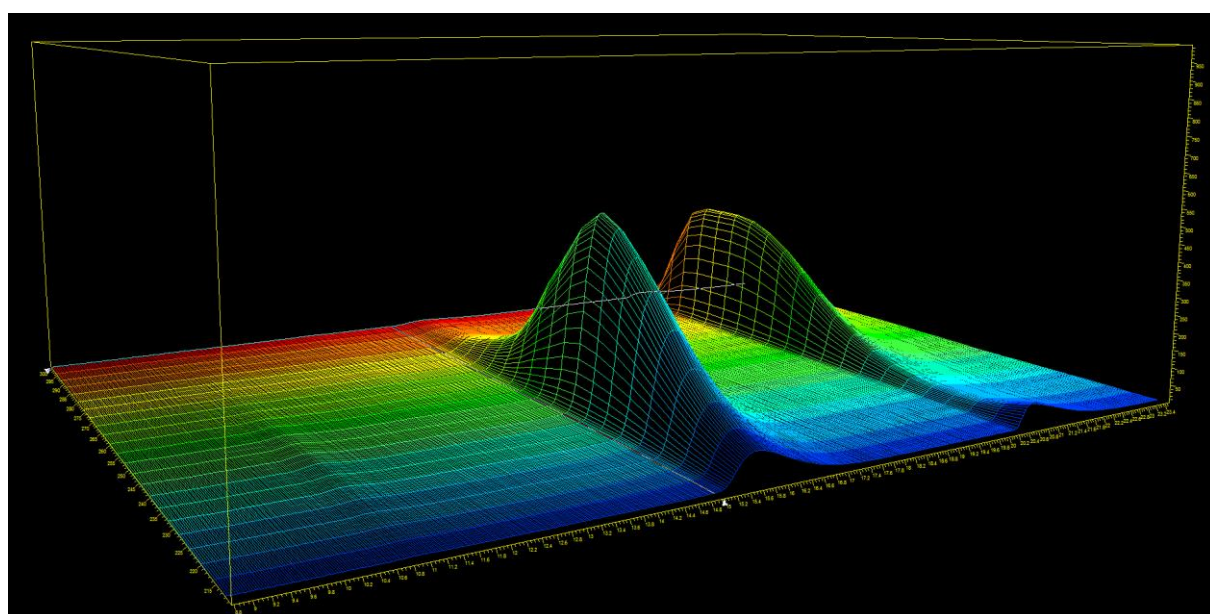
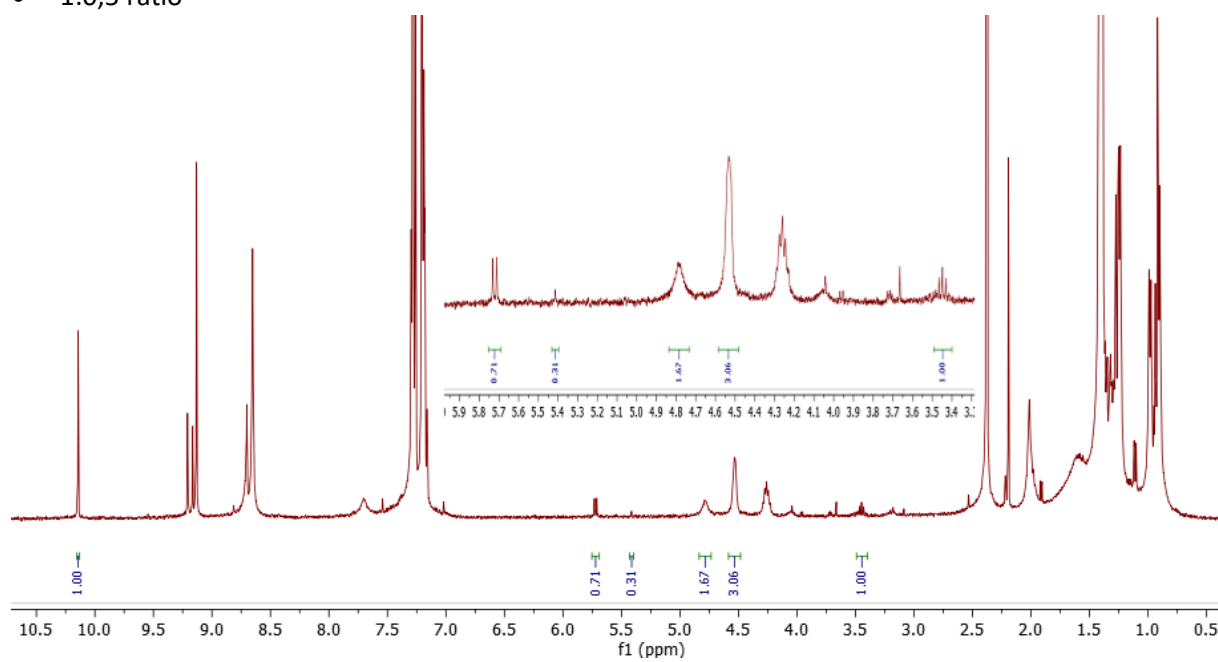




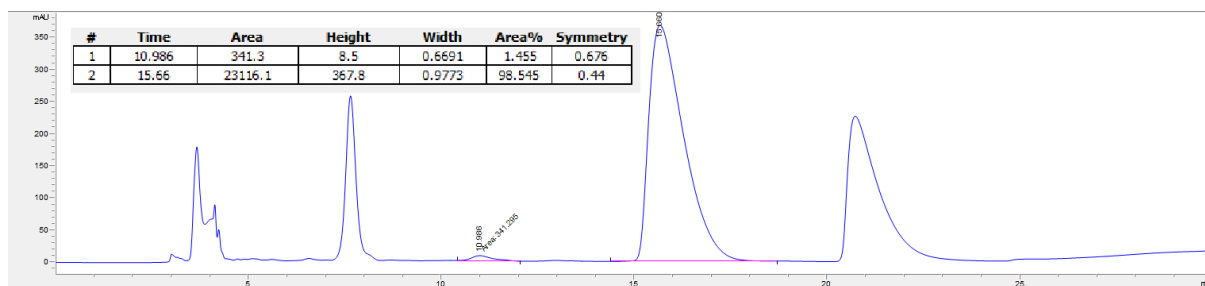
ee% **4c** obtained from the hydrolysis of **9**



• 1:0,5 ratio



ee% 4c



ee% 4c obtained from the hydrolysis of 9

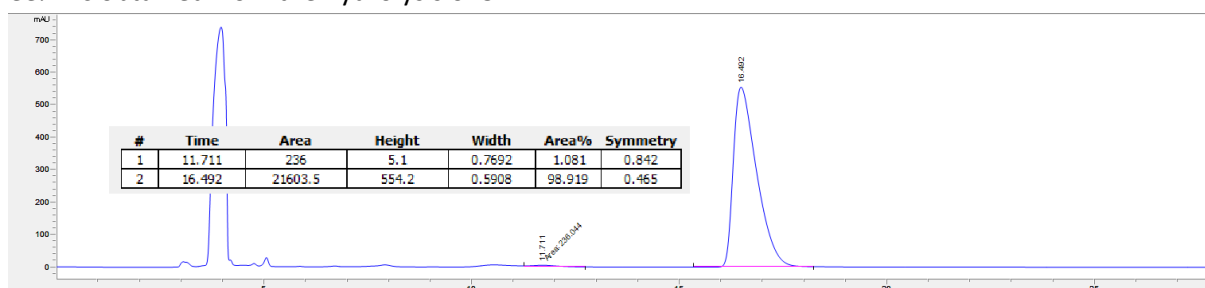
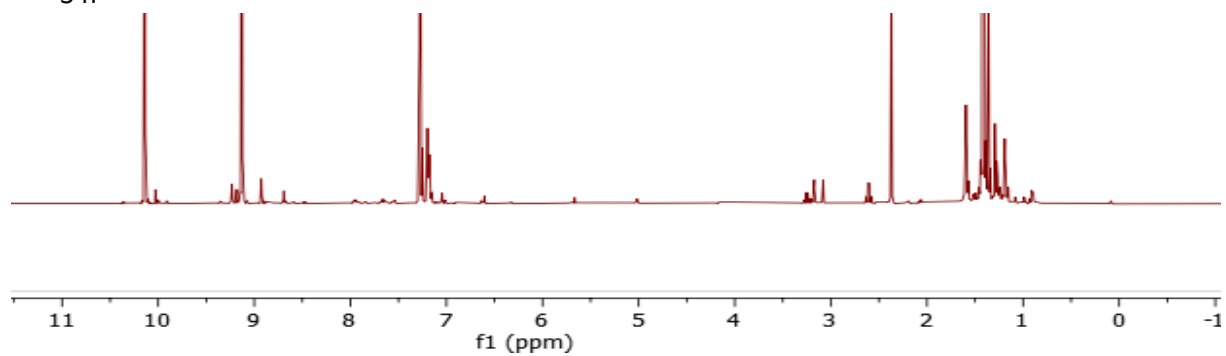
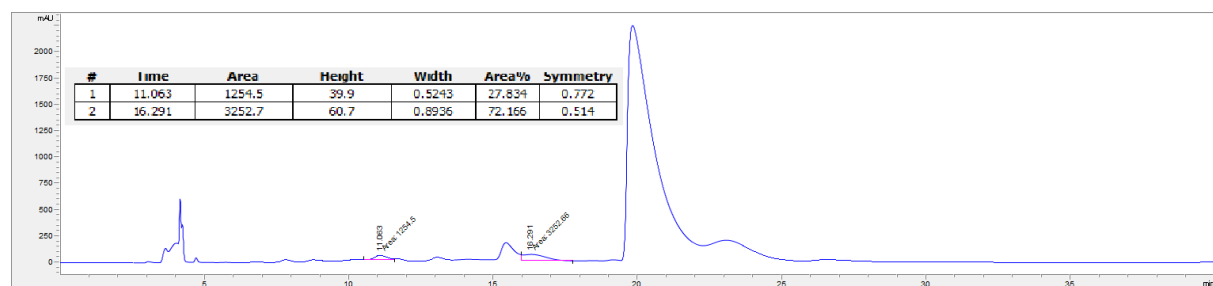
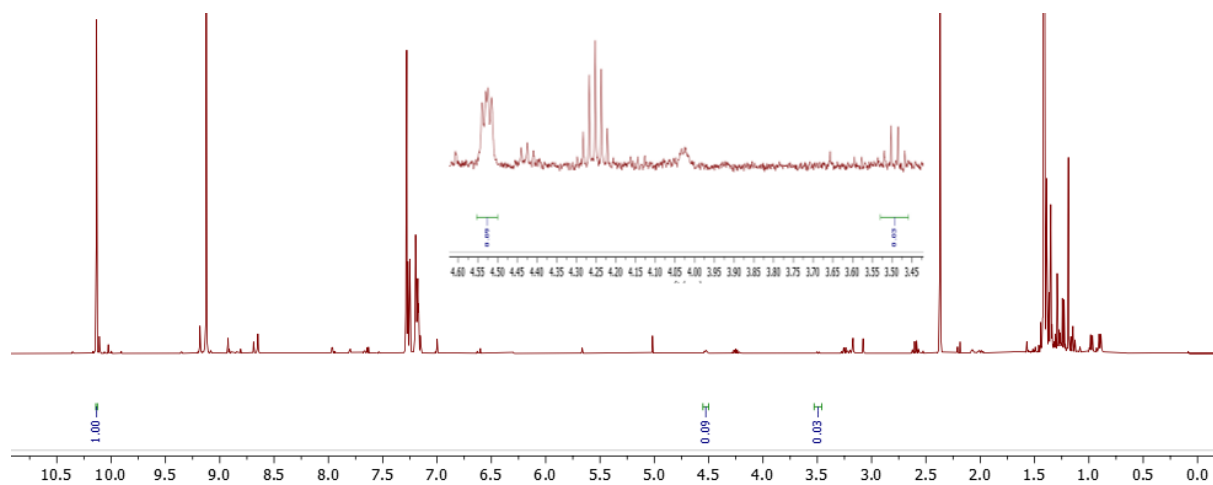


**Table 3.9**

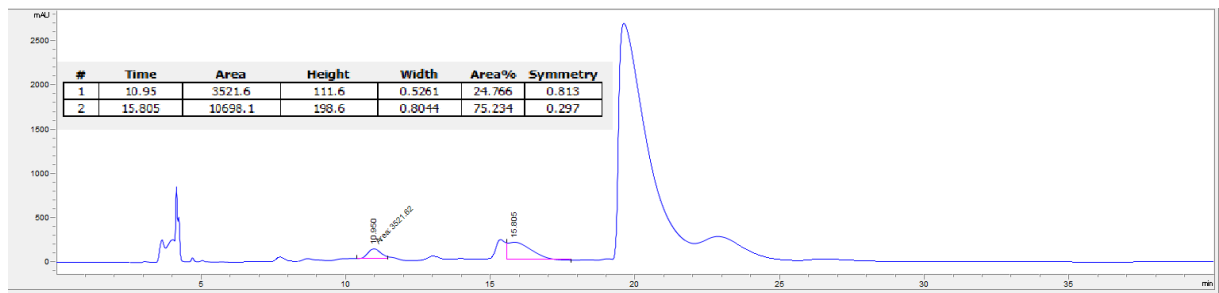
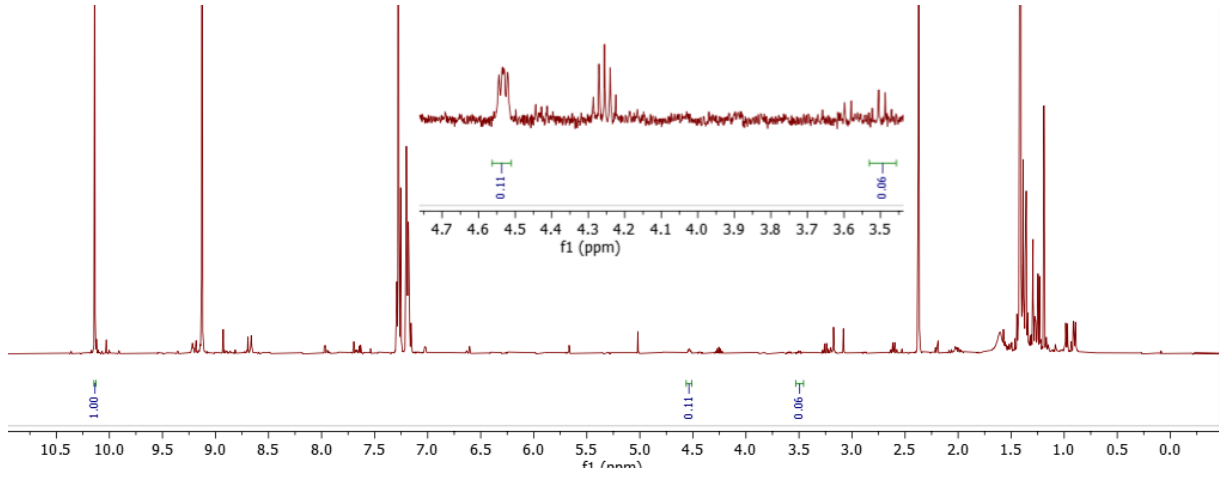
- 3 h



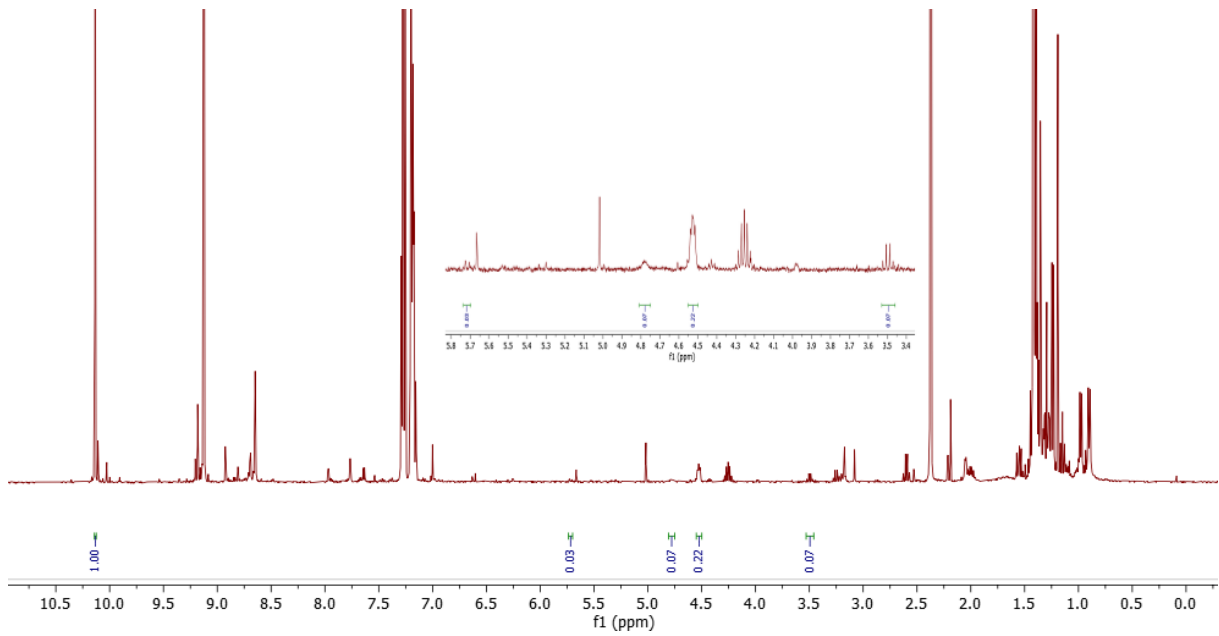
- 7 h

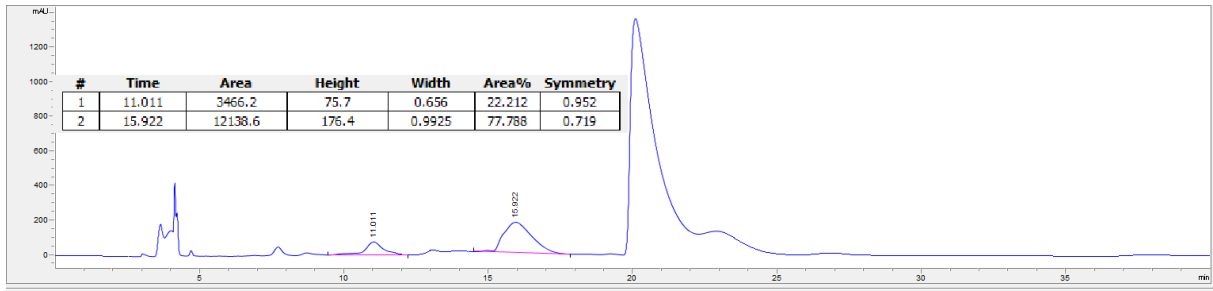


• 12 h



• 24 h

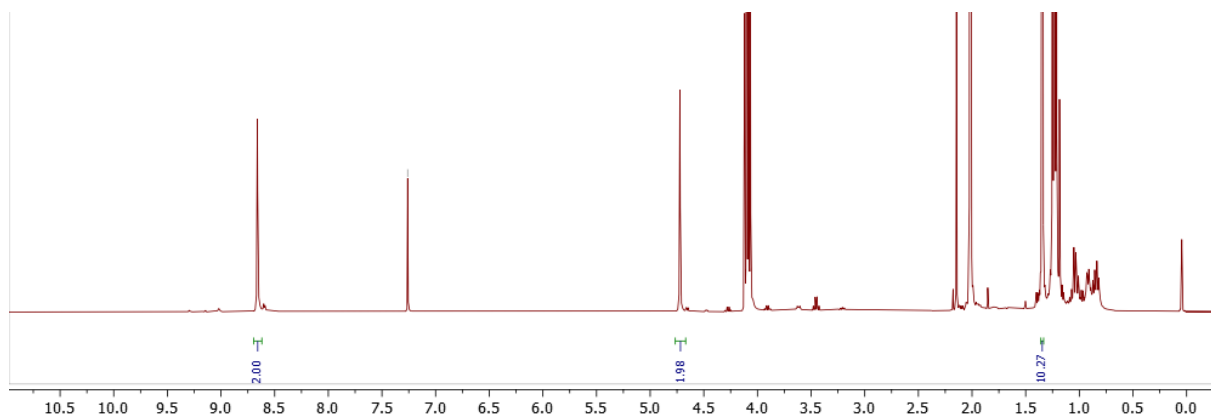
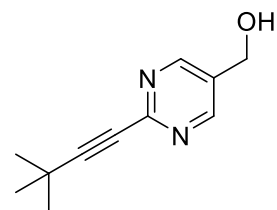




NMR spectra and HPLC chromatograms of isolated side products

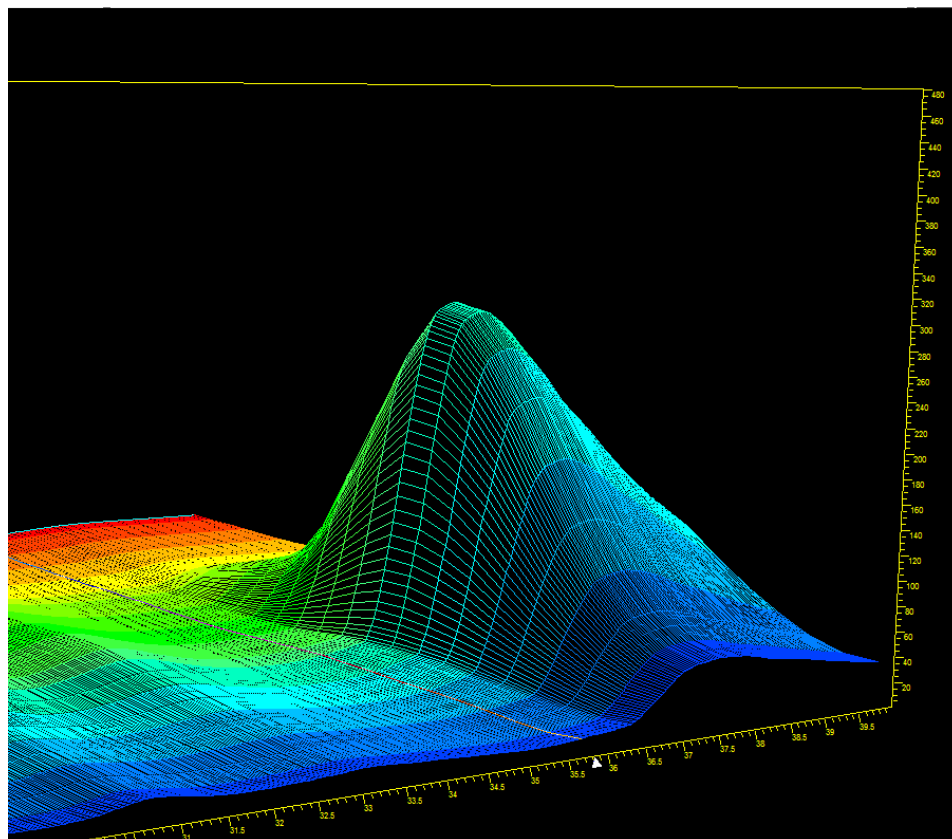
- (2-(3,3-dimethylbut-1-yn-1-yl)pyrimidin-5-yl)methanol (**7**)

$^1\text{H NMR}$  (400 MHz,  $\text{CDCl}_3$ ): 8.66 (s, 2H), 4.71 (s, 2H), 1.34 (s, 9H)

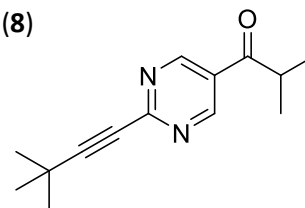


Chiaracel OD-H, hex/ipa 98/2, flow rate: 1,0 ml/min

$\lambda_{\text{max}}$ : 242 nm,  $t = 37,5$  min



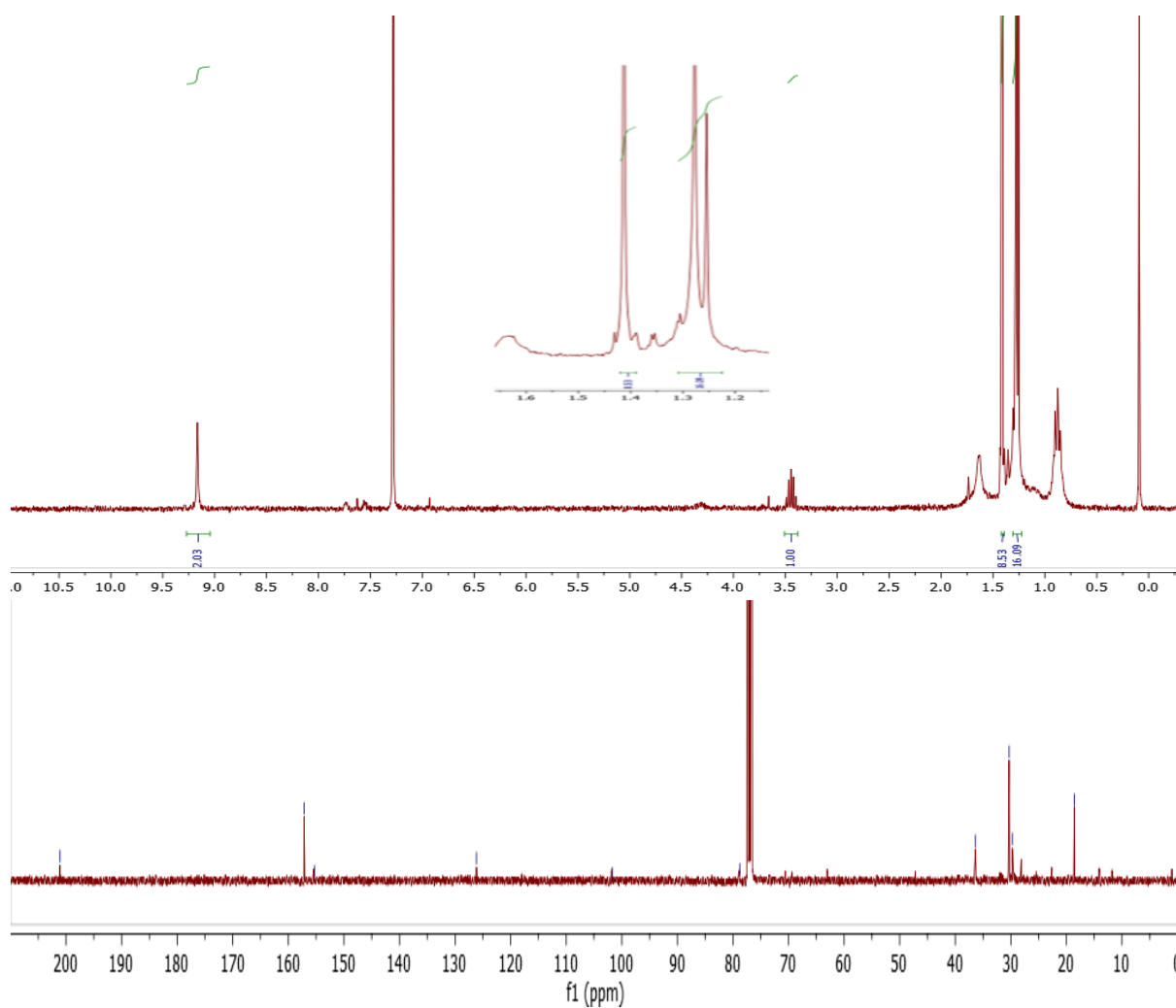
- 1-(2-(3,3-dimethylbut-1-yn-1-yl)pyrimidin-5-yl)-2-methylpropan-1-one (**8**)



$^1\text{H NMR}$  (400 MHz,  $\text{CDCl}_3$ ): 9.16 (s, 2H), 3.44 (m, 1H), 1.40 (s, 9H), 1.26 (d, 6H)

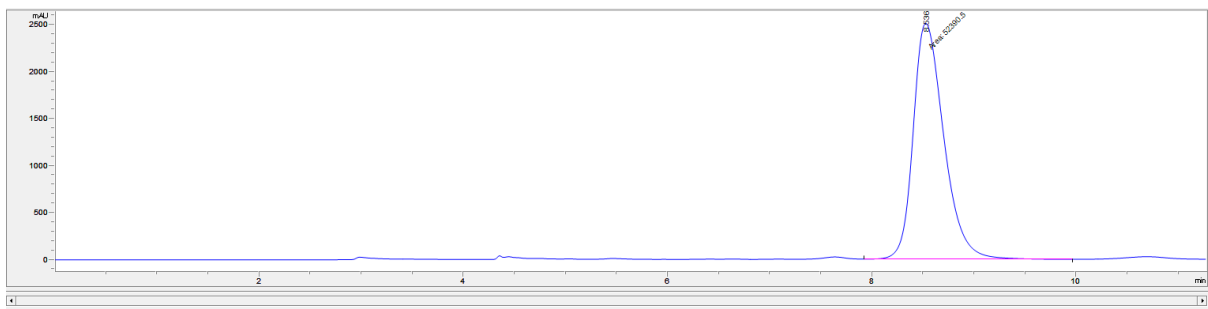
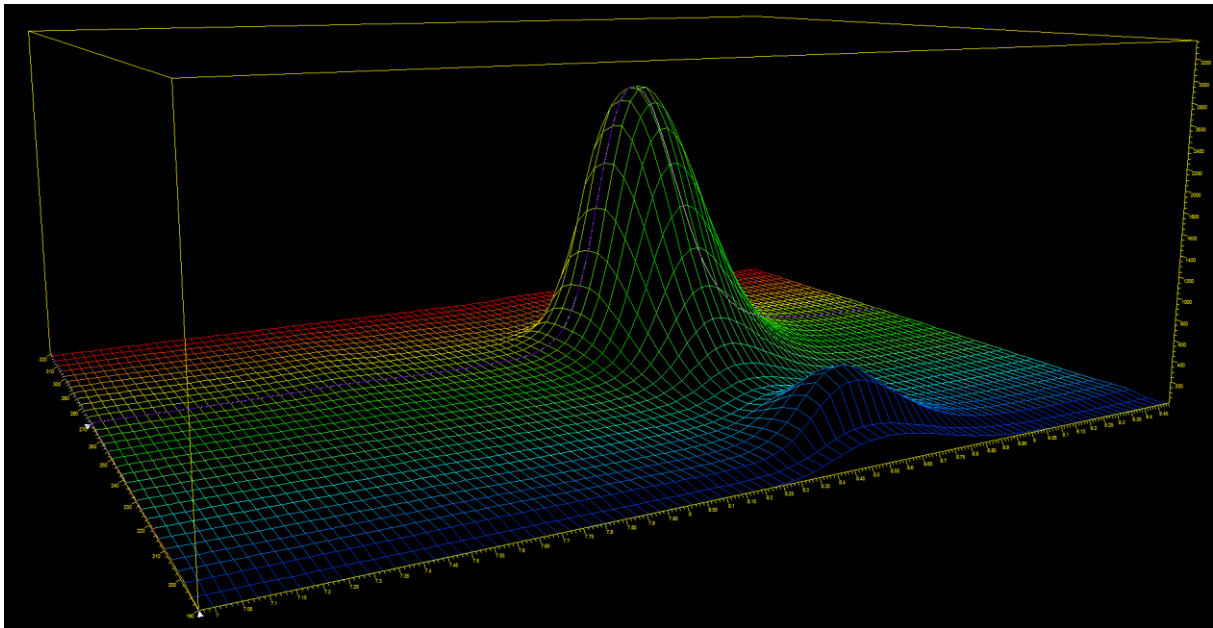
$^{13}\text{C NMR}$  (100 MHz,  $\text{CDCl}_3$ ): 201.07, 157.16, 155.44, 126.14, 101.80, 78.83, 36.35, 30.27, 29.69, 18.51

ESI for  $\text{C}_{14}\text{H}_{18}\text{N}_2\text{O}$ : 230,31 (calculated), 231,15 (found)



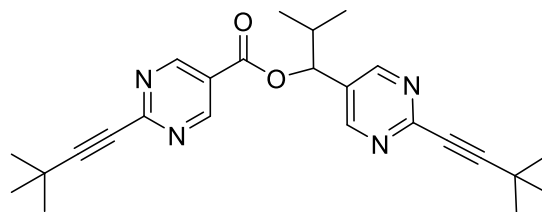
Chiaracel OD-H, hex/ipa 98/2, flow rate: 1,0 ml/min

$\lambda_{\text{max}}$ : 268 nm, t = 8,5 min



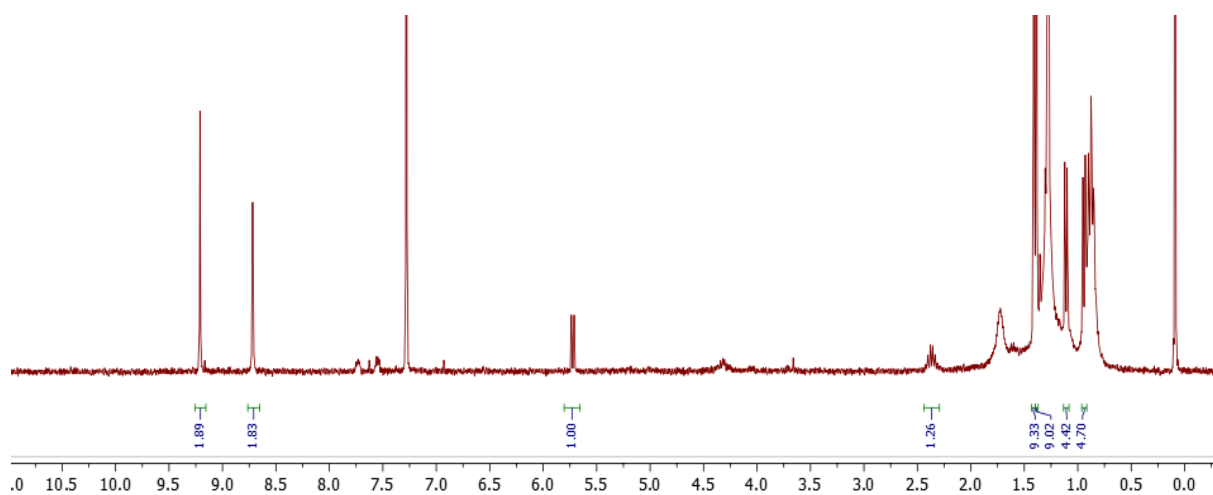


- 1-(2-(3,3-dimethylbut-1-yn-1-yl)pyrimidin-5-yl)-2-methylpropyl 2-(3,3-dimethylbut-1-yn-1-yl)pyrimidine-5-carboxylate (**9**)



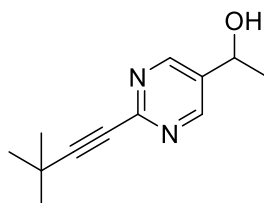
<sup>1</sup>H NMR (400 MHz, CDCl<sub>3</sub>): 9.20 (s, 2H), 8.70 (s, 2H), 5.71 (d, 1H), 2.35 (m, 1H), 1.41 (s, 9H), 1.38 (s, 9H), 1.10 (d, 3H), 0.93 (d, 3H)

HRMS for C<sub>25</sub>H<sub>30</sub>N<sub>4</sub>NaO<sub>2</sub> [M<sup>+</sup> + Na<sup>+</sup>]: 441.2261 (calculated), 441.2260 (found)



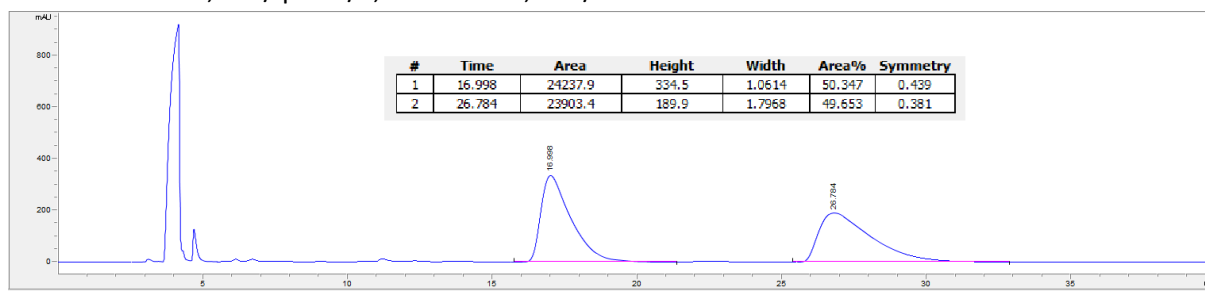
## Vapor phase reactions with different Zn(R)<sub>2</sub> compounds

- Reaction with Zn(Me)<sub>2</sub>

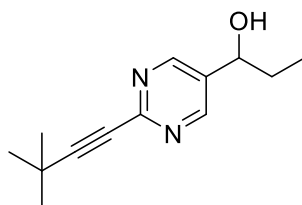


1-(2-(3,3-dimethylbut-1-yn-1-yl)  
pyrimidin-5-yl)ethan-1-ol

Chiaracel OD-H, hex/ipa 98/2, flow rate: 1,0 ml/min



- Reaction with Zn(Et)<sub>2</sub>



1-(2-(3,3-dimethylbut-1-yn-1-yl)  
pyrimidin-5-yl)propan-1-ol

Chiaracel OD-H, hex/ipa 98/2, flow rate: 1,0 ml/min

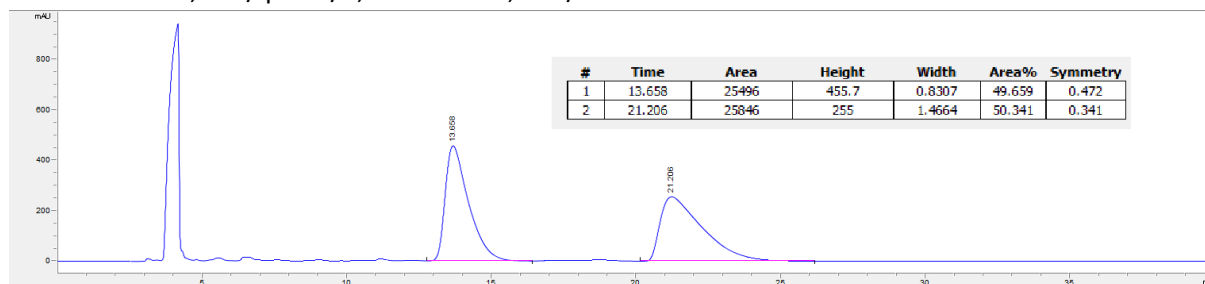
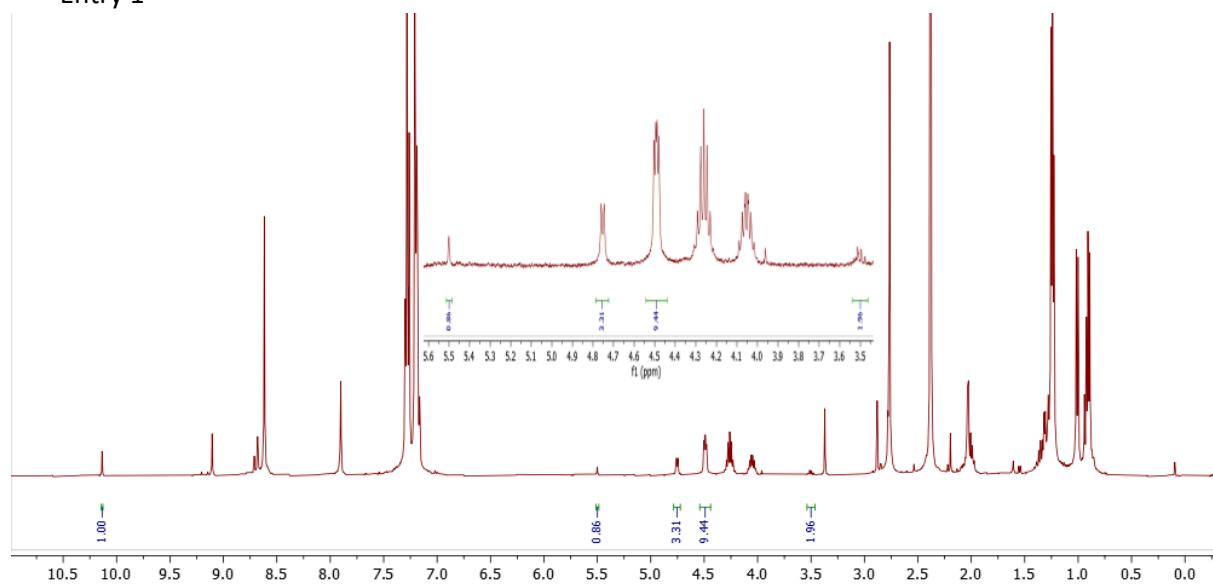
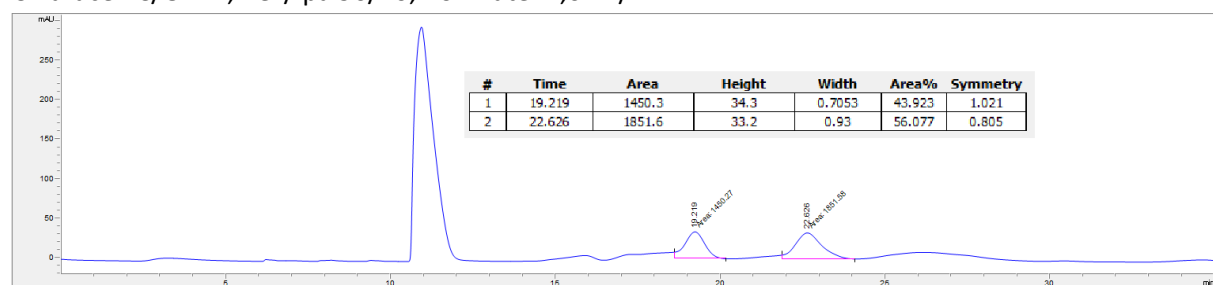


**Table 3.10**

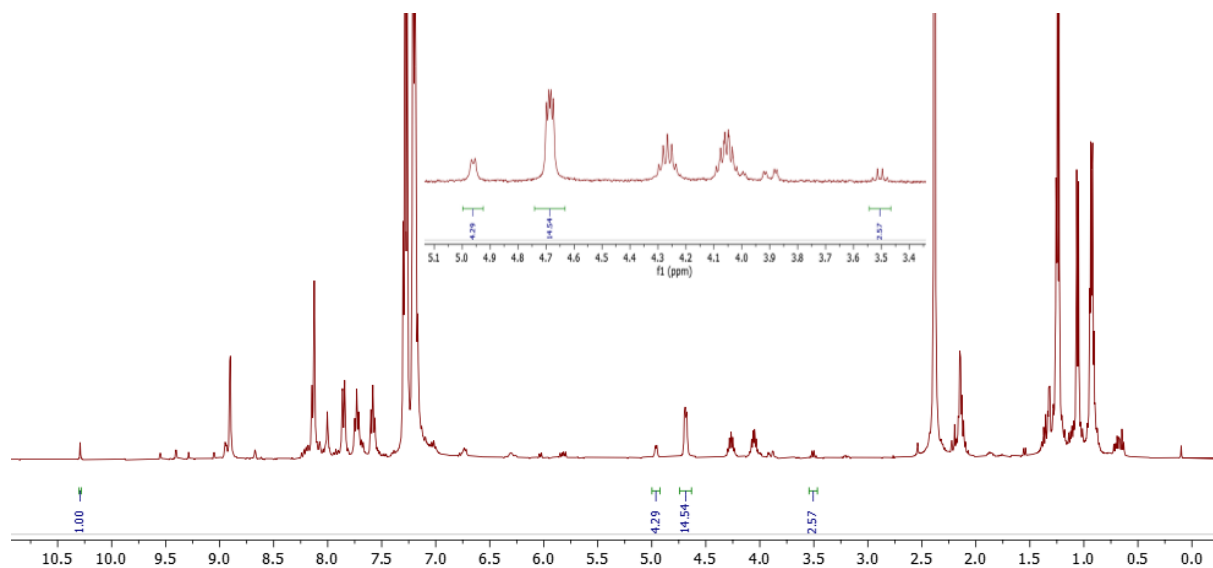
• **Entry 1**



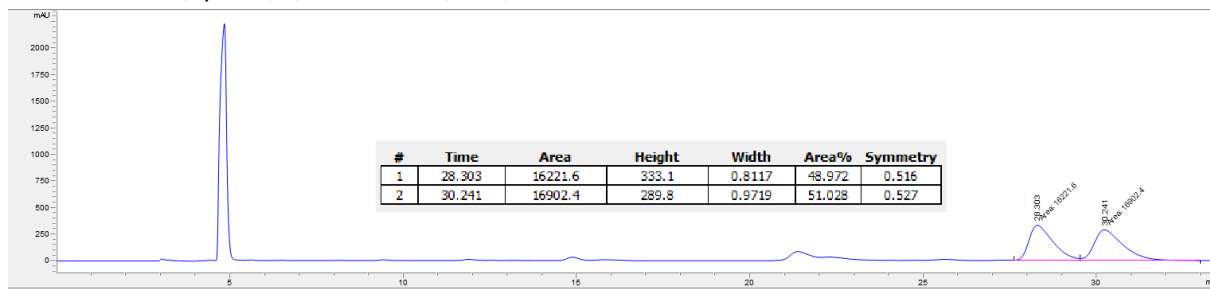
Chiaracel IC/OD-H, hex/ipa 90/10, flow rate: 1,0 ml/min



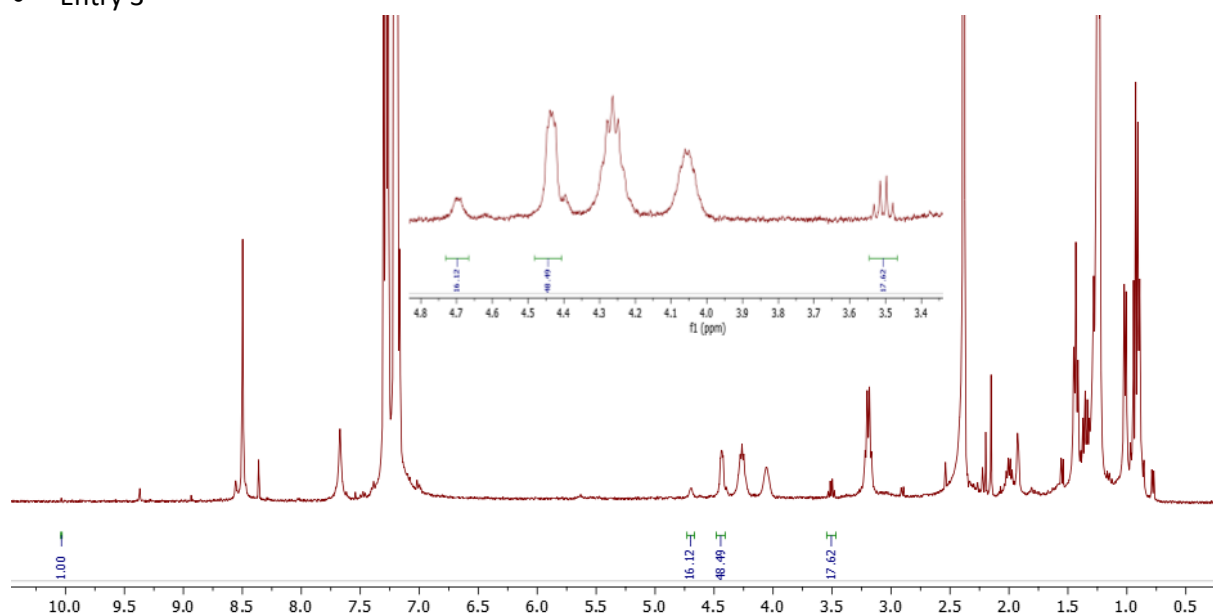
• **Entry 2**



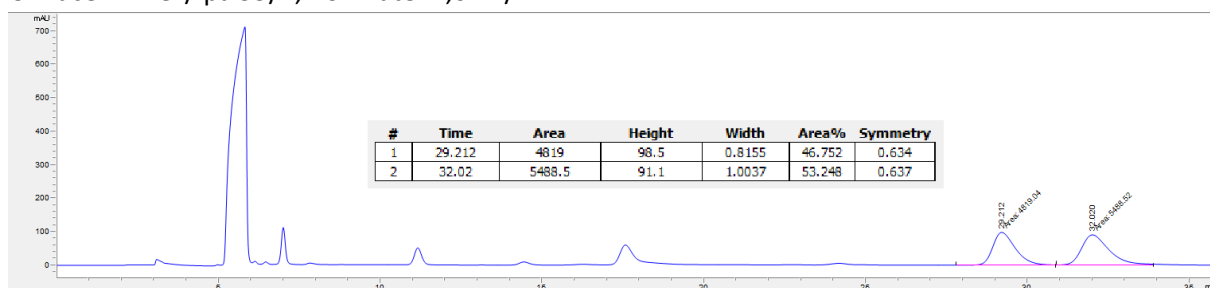
Chiracel IA hex/ipa 98/2, flow rate: 1,0 ml/min



• Entry 3



Chiracel IA hex/ipa 99/1, flow rate: 1,0 ml/min



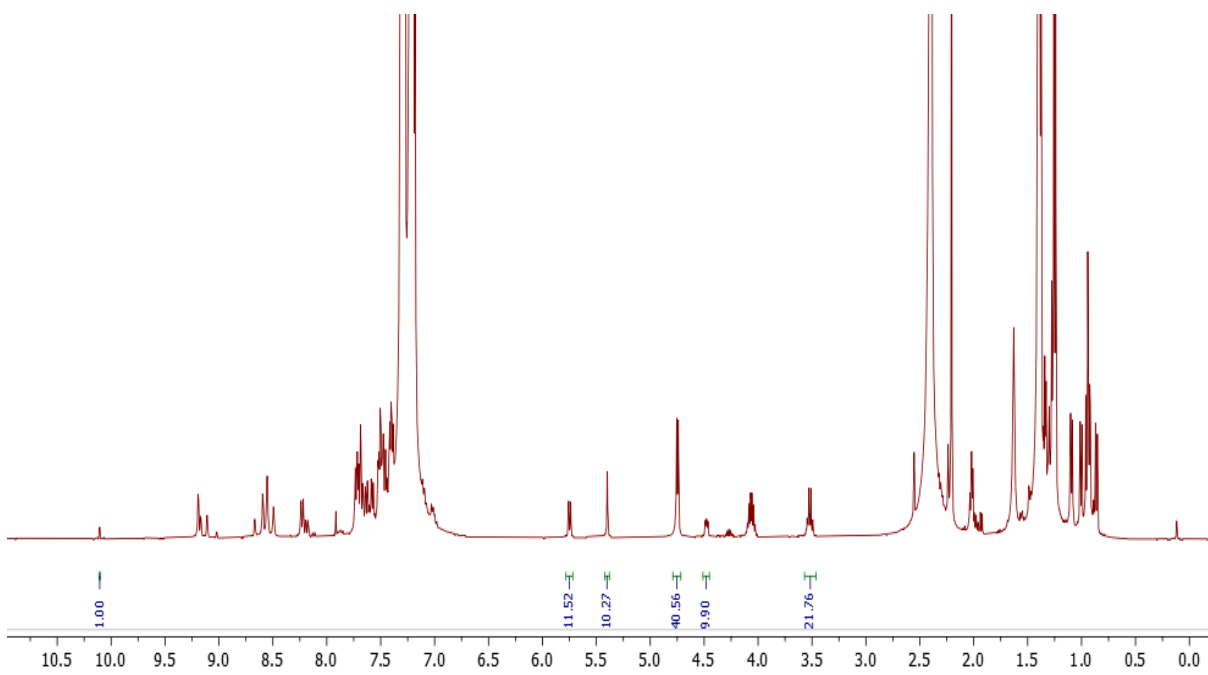
## **Appendix IV**

**Additional supporting information for Chapter 4**

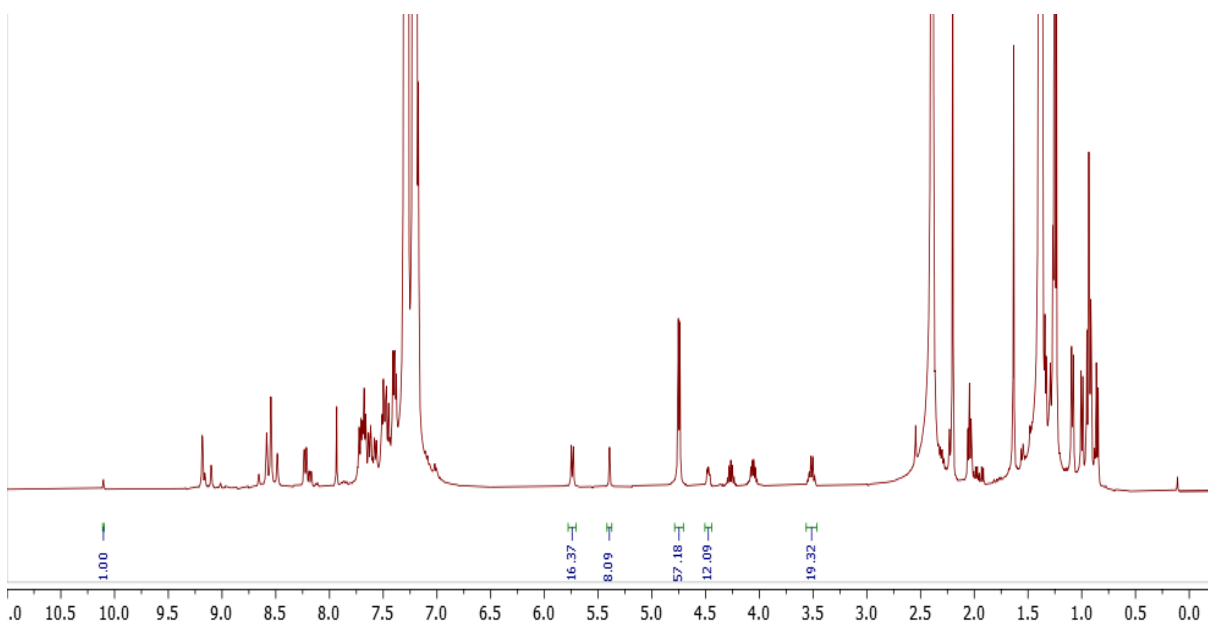


Figure 4.2

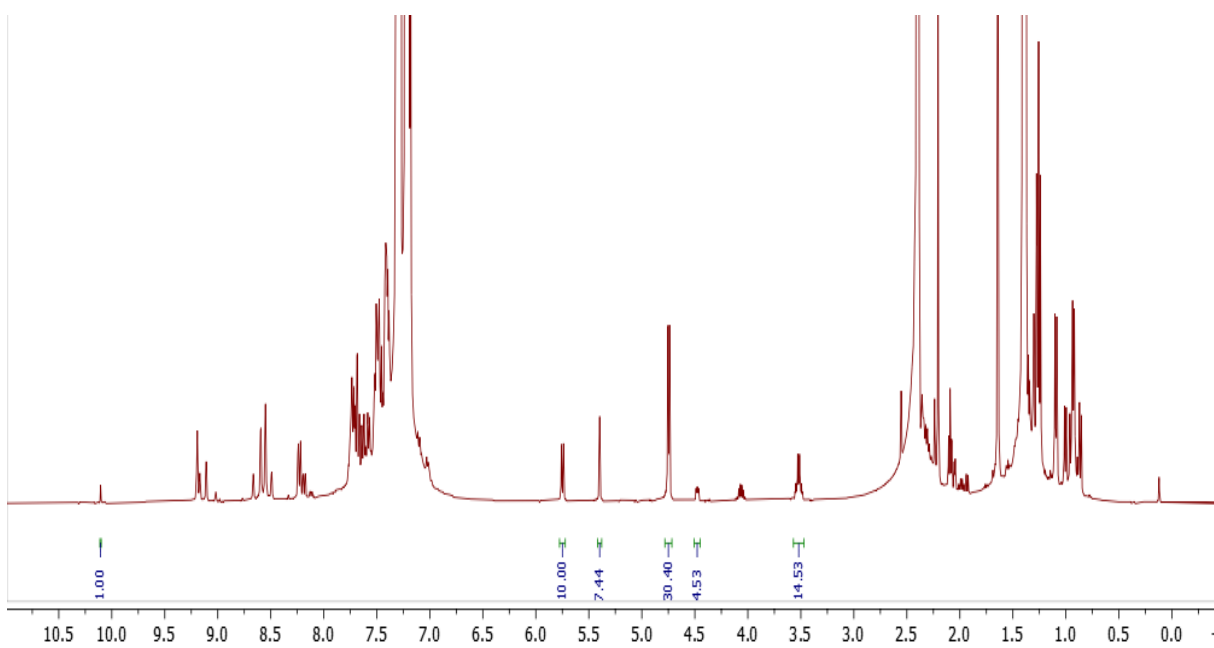
- 1:5 ratio



- 1:2 ratio



- 1:1 ratio



- 1:0.5 ratio

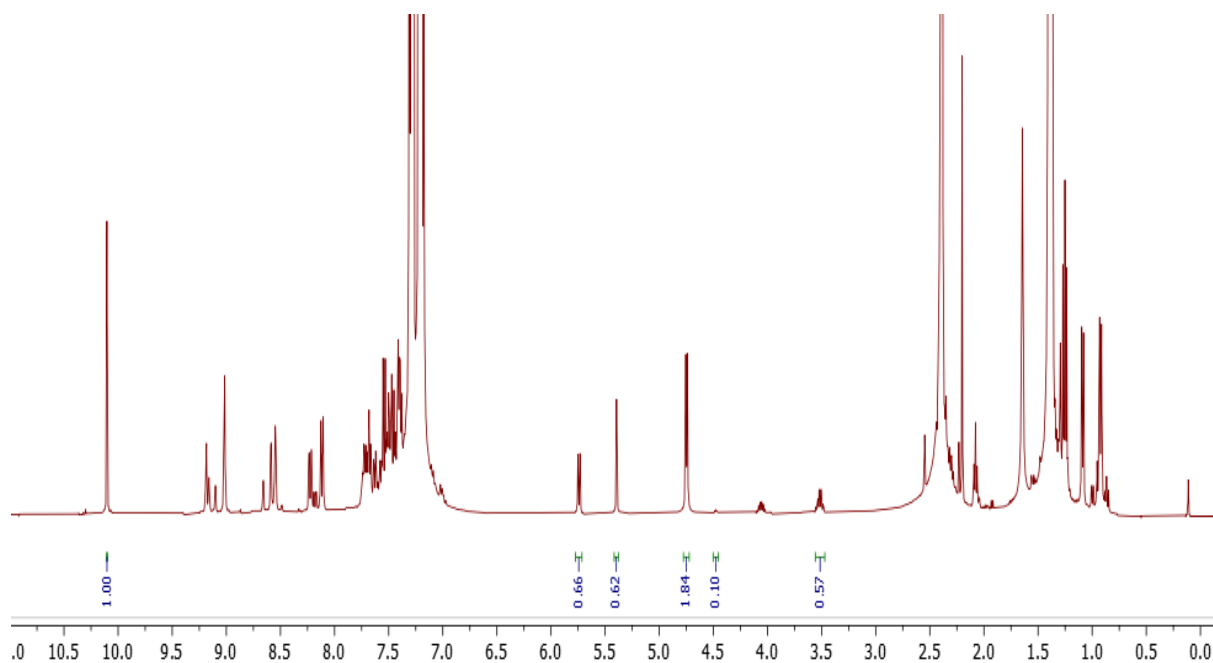


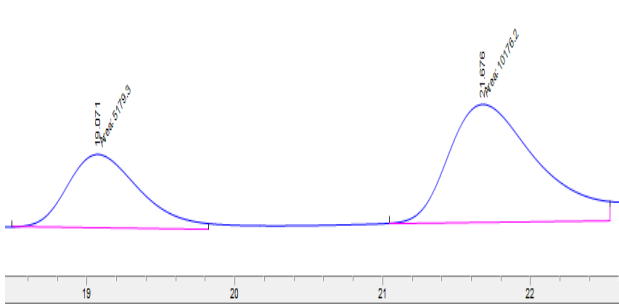


Table 4.6

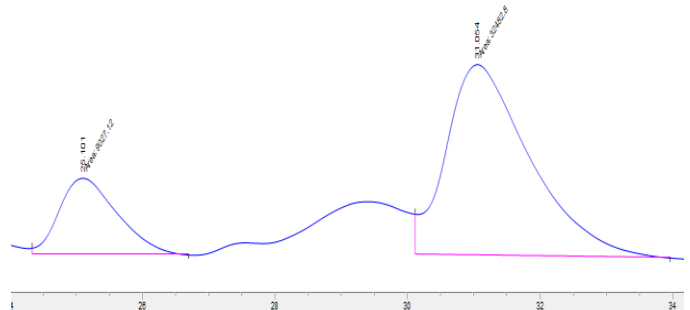
(R)-6a

(R)-13

- 1:5 ratio

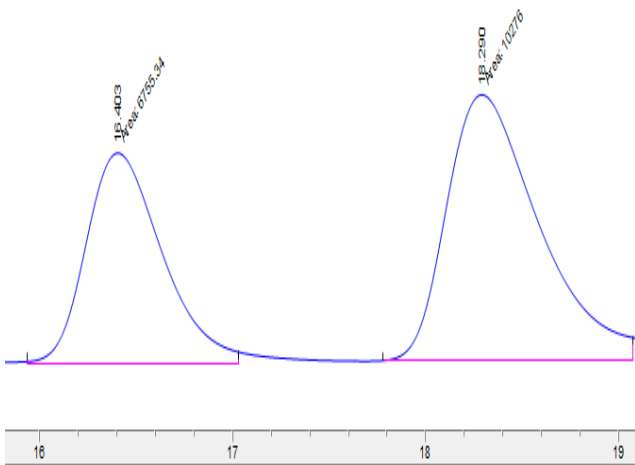


#	Time	Area	Height	Width	Area%	Symmetry
1	19.071	5179.3	150.3	0.5744	33.729	0.692
2	21.676	10176.2	240.7	0.7046	66.271	0.605

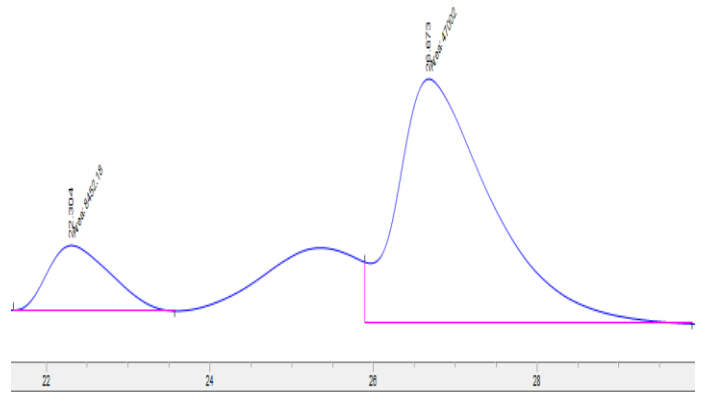


#	Time	Area	Height	Width	Area%	Symmetry
1	25.101	9027.1	147.4	1.021	21.747	0.678
2	31.054	32482.8	367.4	1.4736	78.253	0.582

- 1:2 ratio

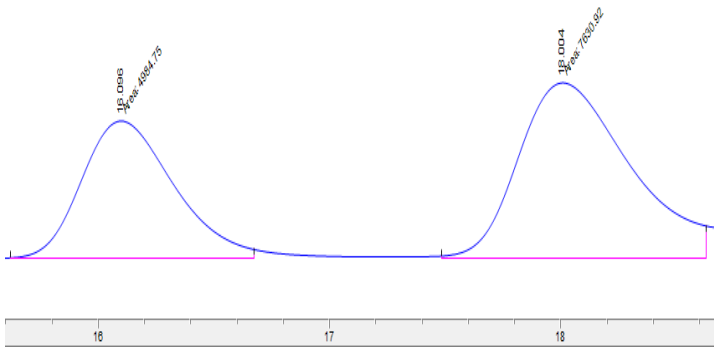


#	Time	Area	Height	Width	Area%	Symmetry
1	16.403	6755.3	245.8	0.458	39.664	0.704
2	18.29	10276	309.6	0.5532	60.336	0.602

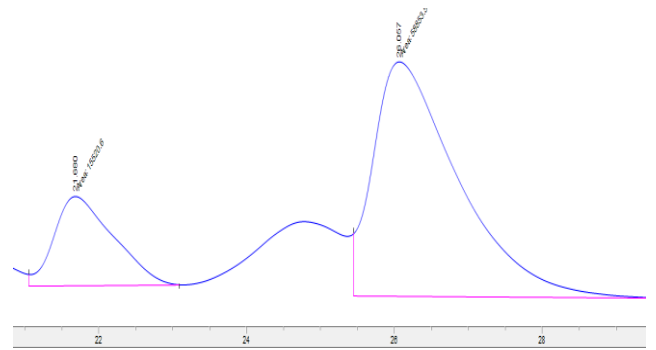


#	Time	Area	Height	Width	Area%	Symmetry
1	22.304	8452.2	157.7	0.8935	15.242	0.614
2	26.673	47002	584.5	1.3402	84.758	0.496

- 1:1 ratio

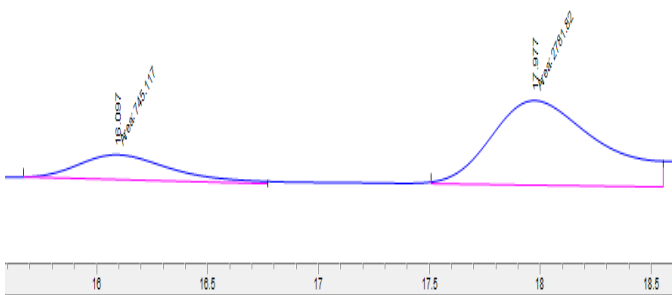


#	Time	Area	Height	Width	Area%	Symmetry
1	16.096	4984.8	178.7	0.4649	39.512	0.727
2	18.004	7630.9	227.2	0.5597	60.488	0.652

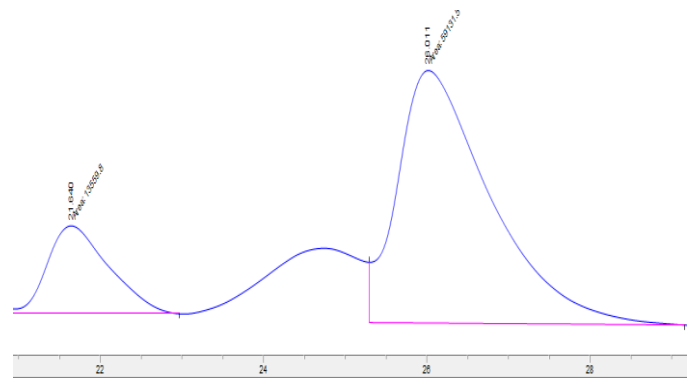


#	Time	Area	Height	Width	Area%	Symmetry
1	21.68	15520.6	278.4	0.9291	20.868	0.561
2	26.057	58853.5	729.7	1.3442	79.132	0.43

- 1:0.5



#	Time	Area	Height	Width	Area%	Symmetry
1	16.097	745.1	24.7	0.5037	21.126	0.705
2	17.977	2781.8	81.2	0.5711	78.874	0.636



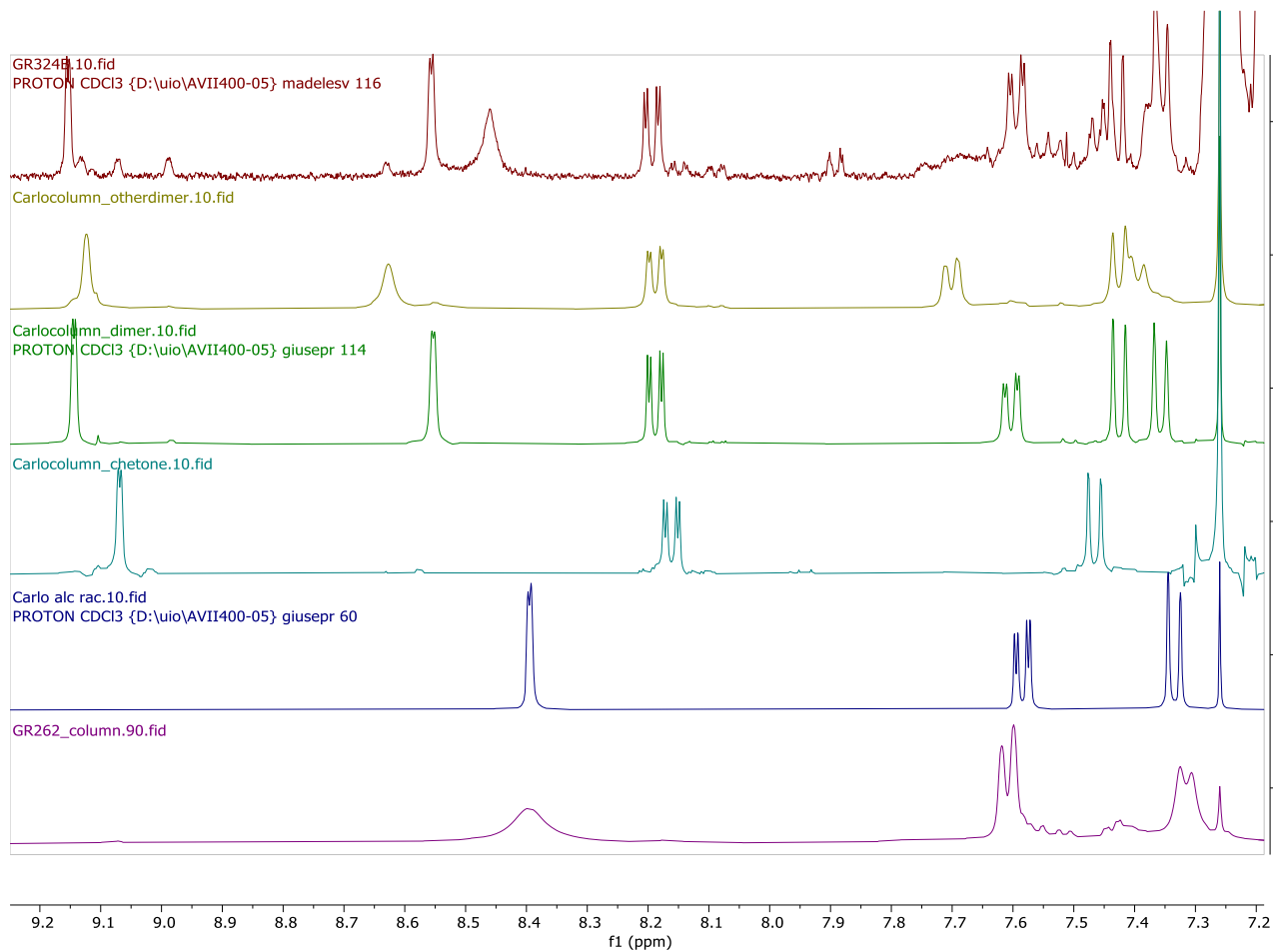
#	Time	Area	Height	Width	Area%	Symmetry
1	21.64	13559.8	258.4	0.8746	18.654	0.622
2	26.011	59131.5	745	1.3229	81.346	0.484

Results from Section 4.6

**REACTION:** Pyr ald-H + Pyr ald-D mixed together in 1:1 ratio and then vapour phase reaction with  $Zn(iPr)_2$

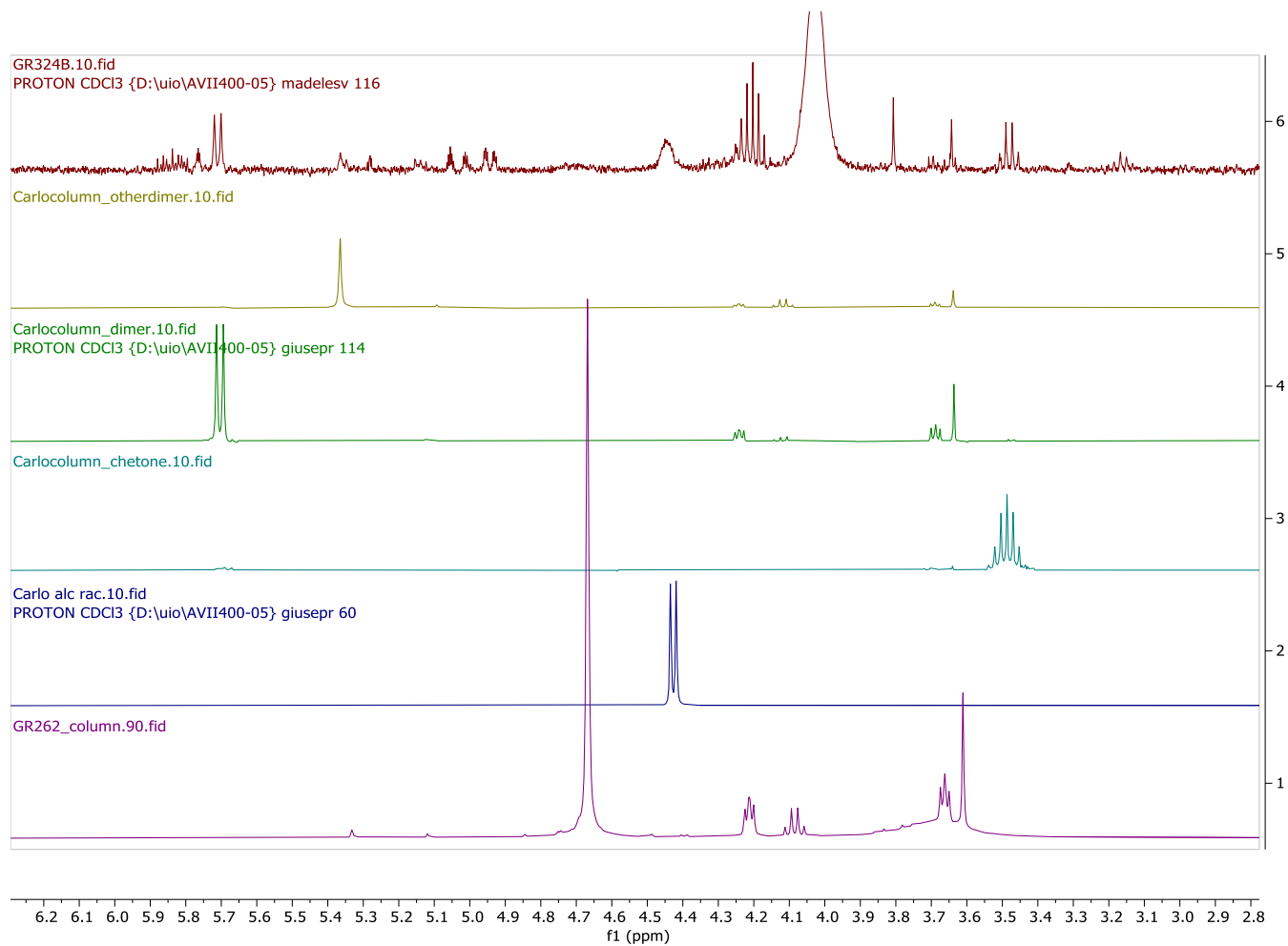
Zoom on the aromatic area of the crude and pure spectra of the products

Top to bottom: crude, ester 14, ester 13, ketone 12, alcohol 6a, alcohol 11

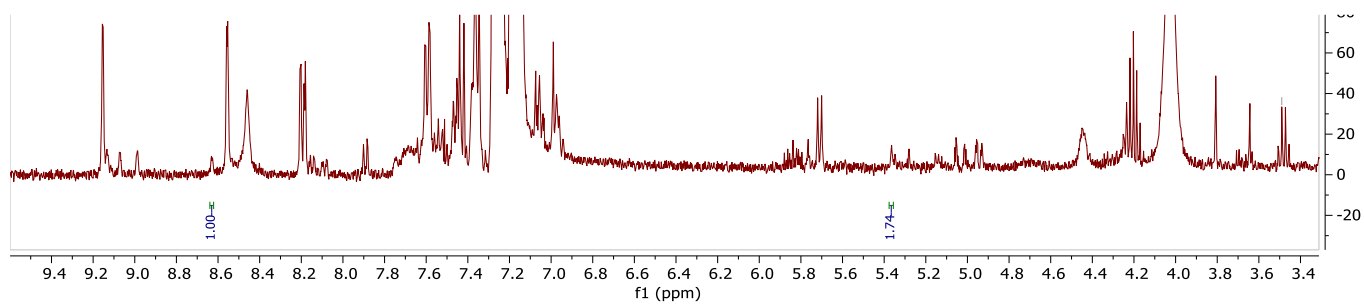


Zoom on the mid-field area of the crude and pure spectra of the products

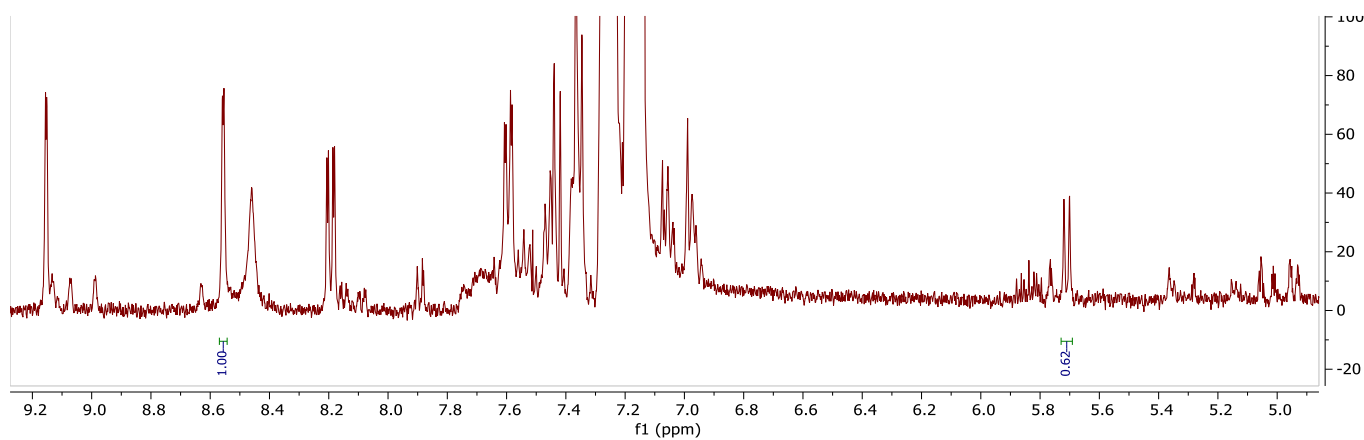
Top to bottom: crude, ester 14, ester 13, ketone 12, alcohol 6a, alcohol 11



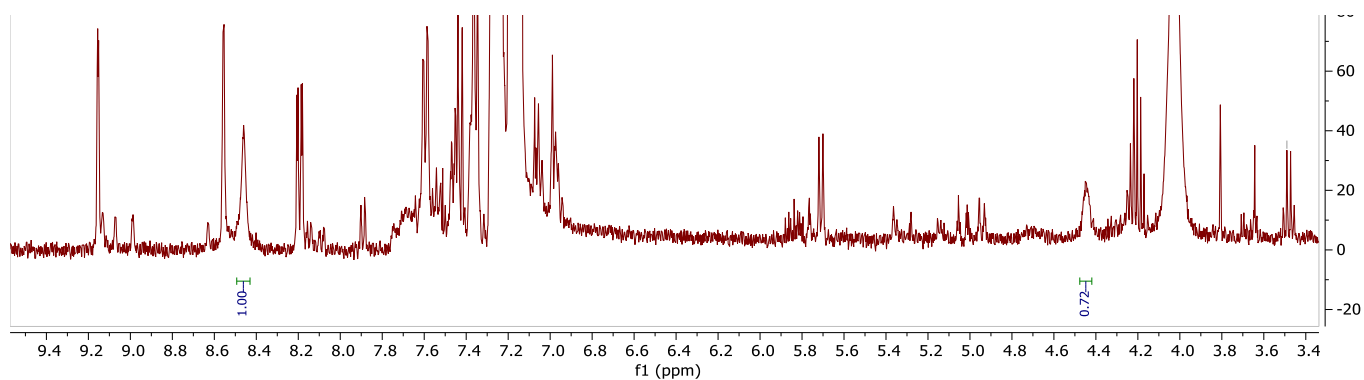
### Quantification of deuteration for ester **14**



### Quantification of deuteration for ester **13**



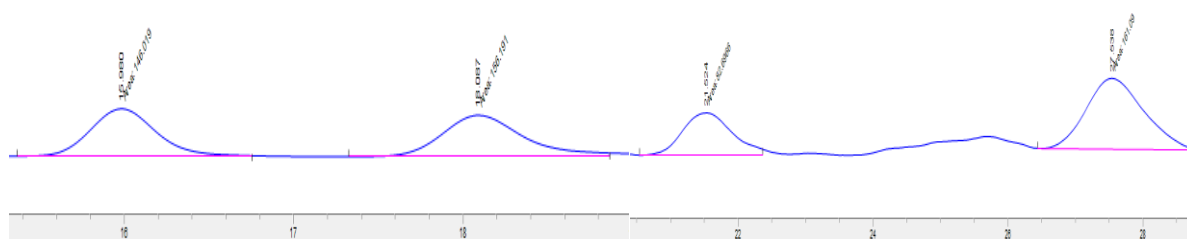
### Quantification of deuteration for alcohol **6a**



Results from Section 4.8

(R)-6a

(R)-13

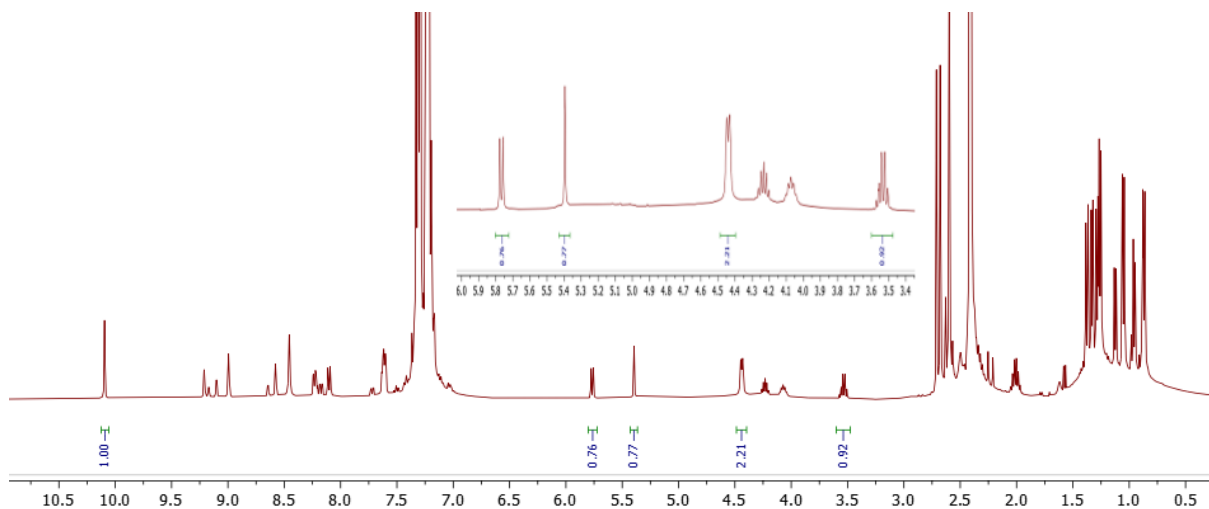


#	Time	Area	Height	Width	Area%	Symmetry
1	15.98	146	5.4	0.4516	48.317	0.878
2	18.087	156.2	4.7	0.5562	51.683	0.77

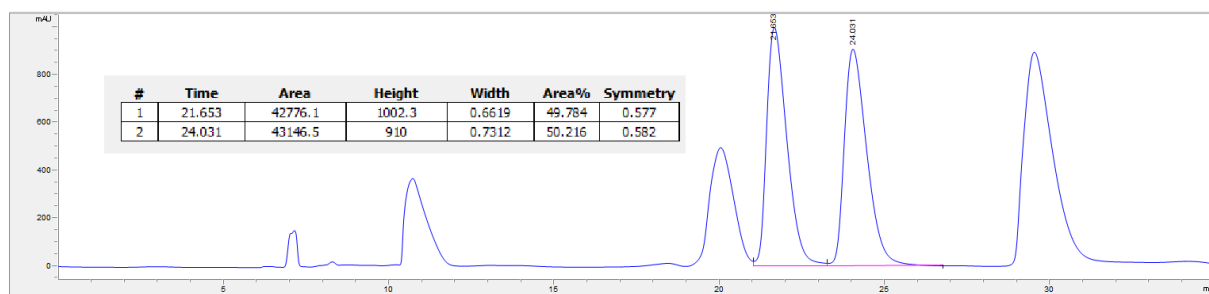
#	Time	Area	Height	Width	Area%	Symmetry
1	21.524	82.7	1.6	0.8609	33.922	0.907
2	27.538	161.1	2.7	1.0012	66.078	0.775

Table 4.7

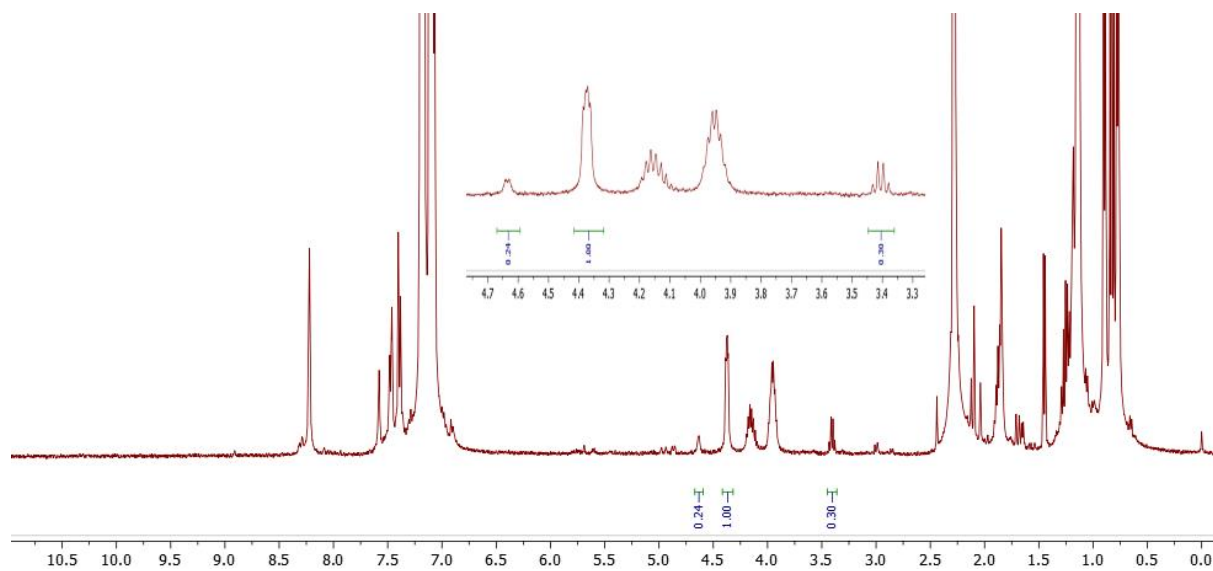
- Entry 1



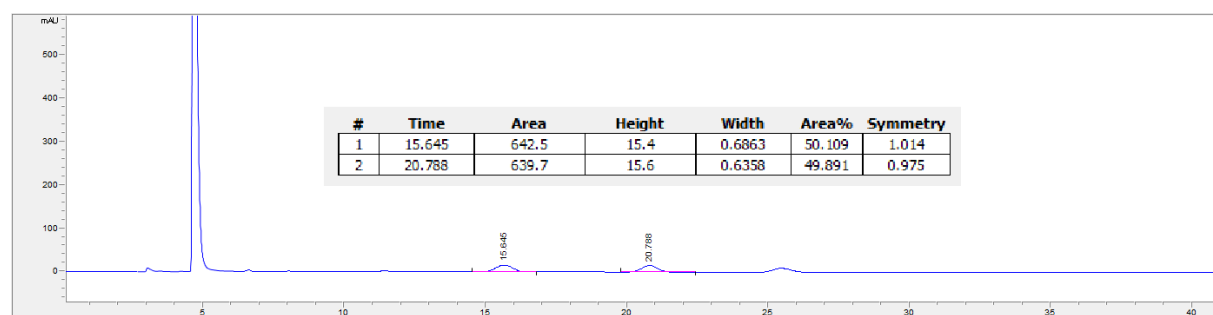
Chiralcel IC/OD-H hex/ipa 90/10, flow rate: 1,0 ml/min



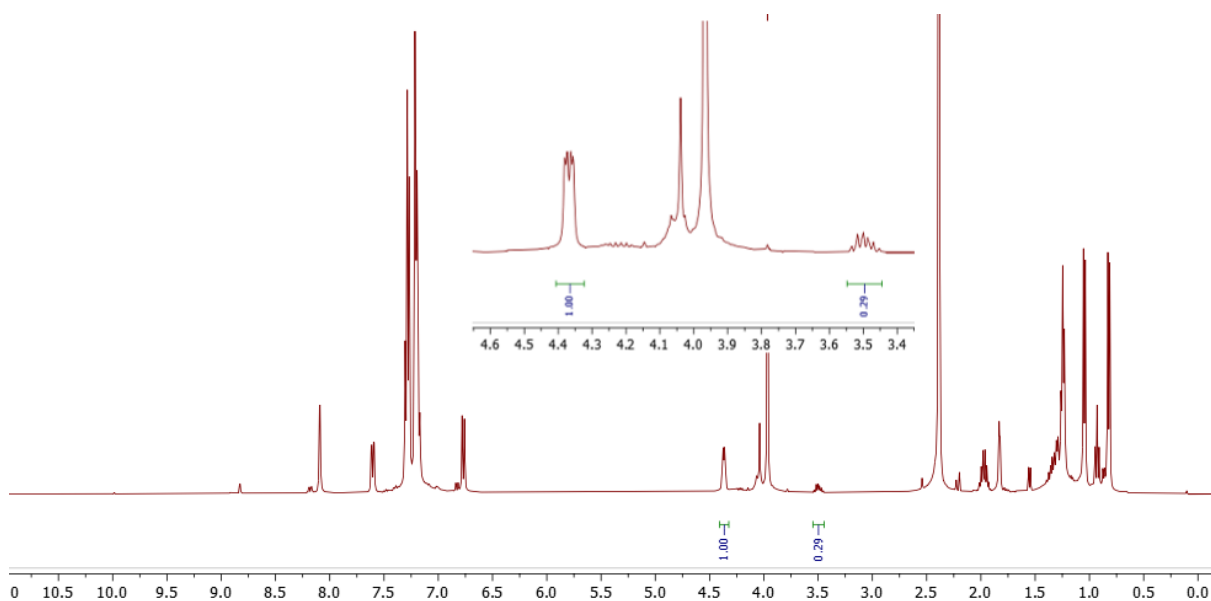
- Entry 2



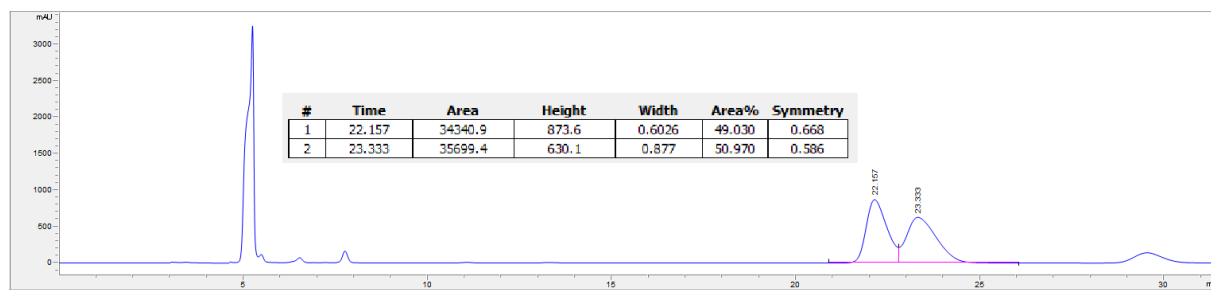
Chiralcel OD-H hex/ipa 98/2, flow rate: 1,0 ml/min



- Entry 3

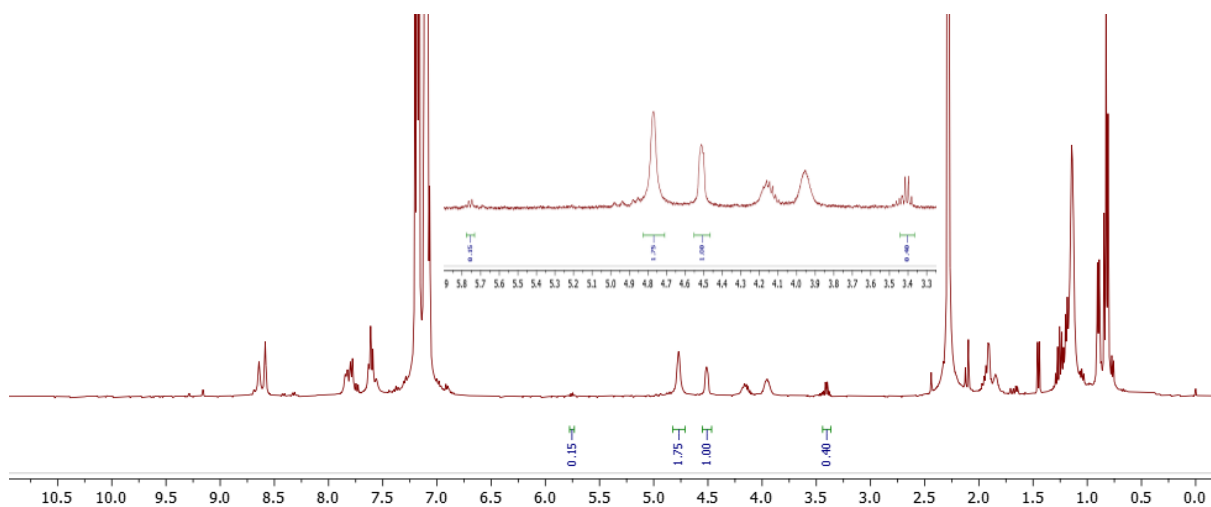


Chiralcel OD-H hex/ipa 99/1, flow rate: 1,0 ml/min

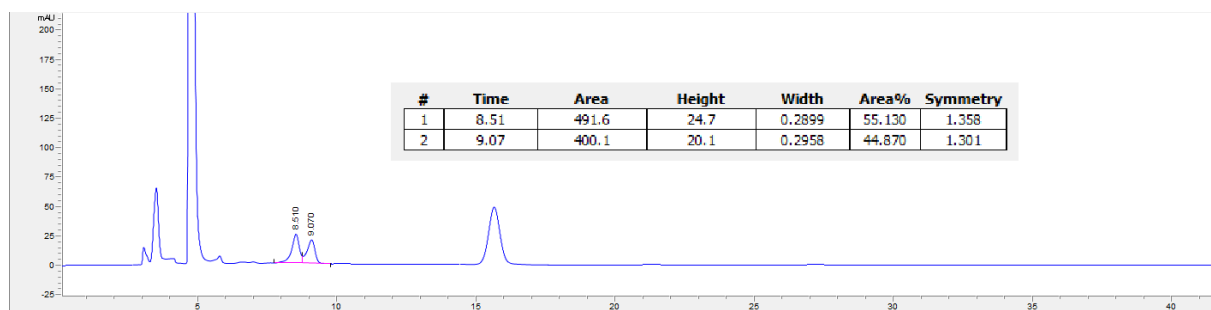




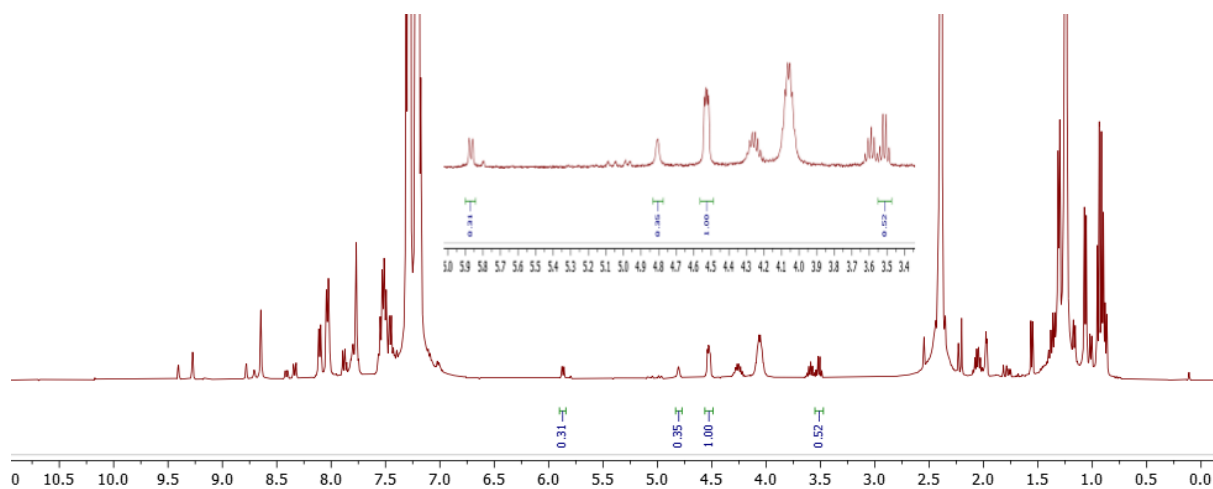
- Entry 4



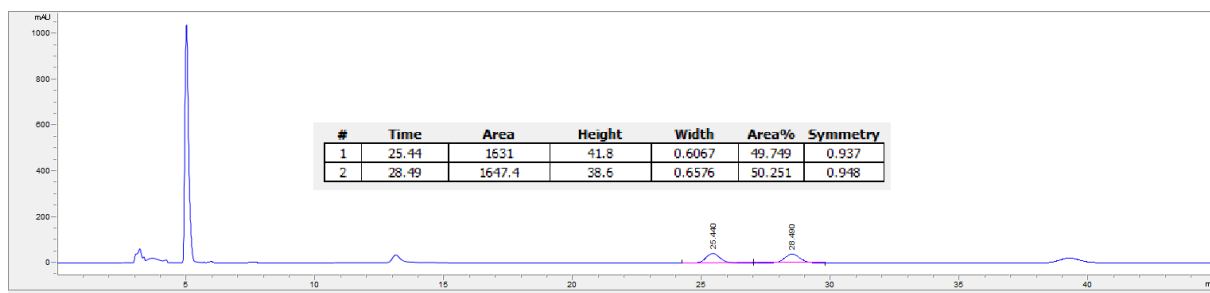
Chiralcel OD-H hex/ipa 98/2, flow rate: 1,0 ml/min



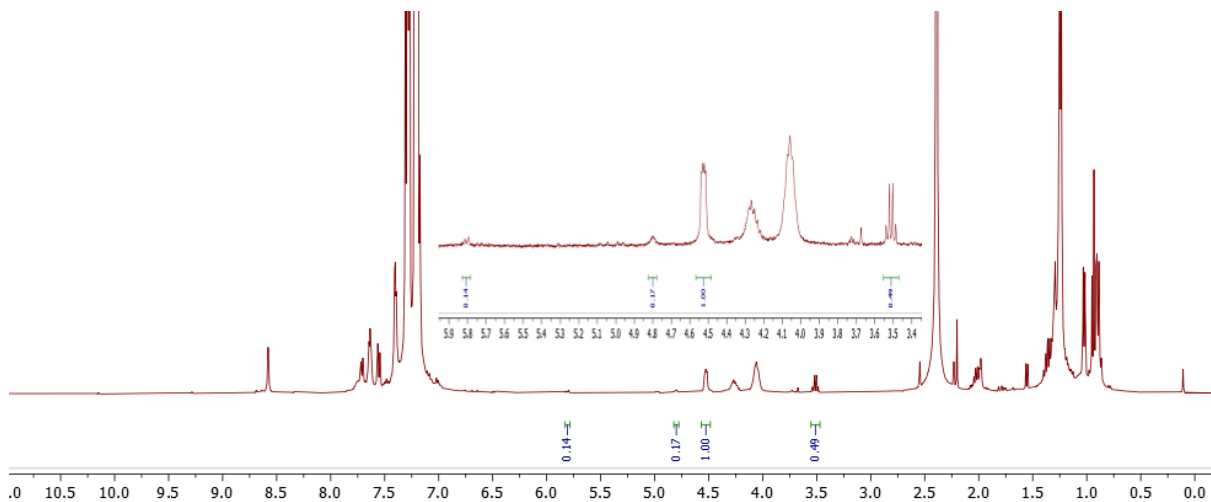
- Entry 5



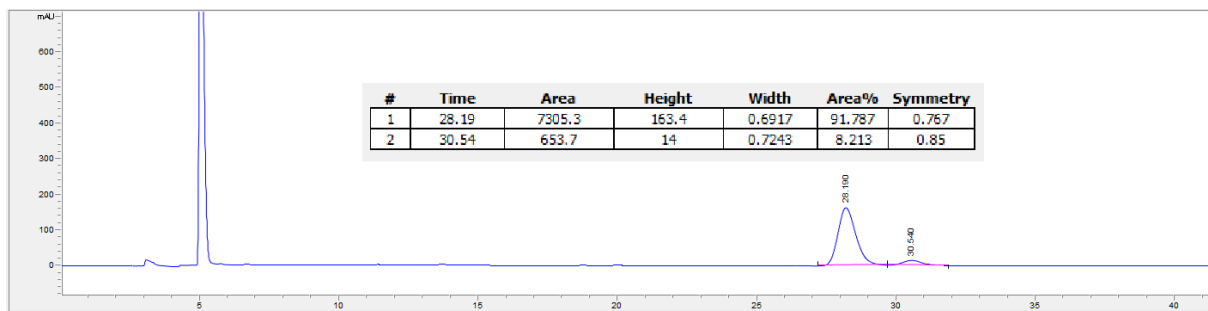
Chiralcel IA hex/ipa 98/2, flow rate: 1,0 ml/min



- Entry 6



Chiralcel IA hex/ipa 98/2, flow rate: 1,0 ml/min

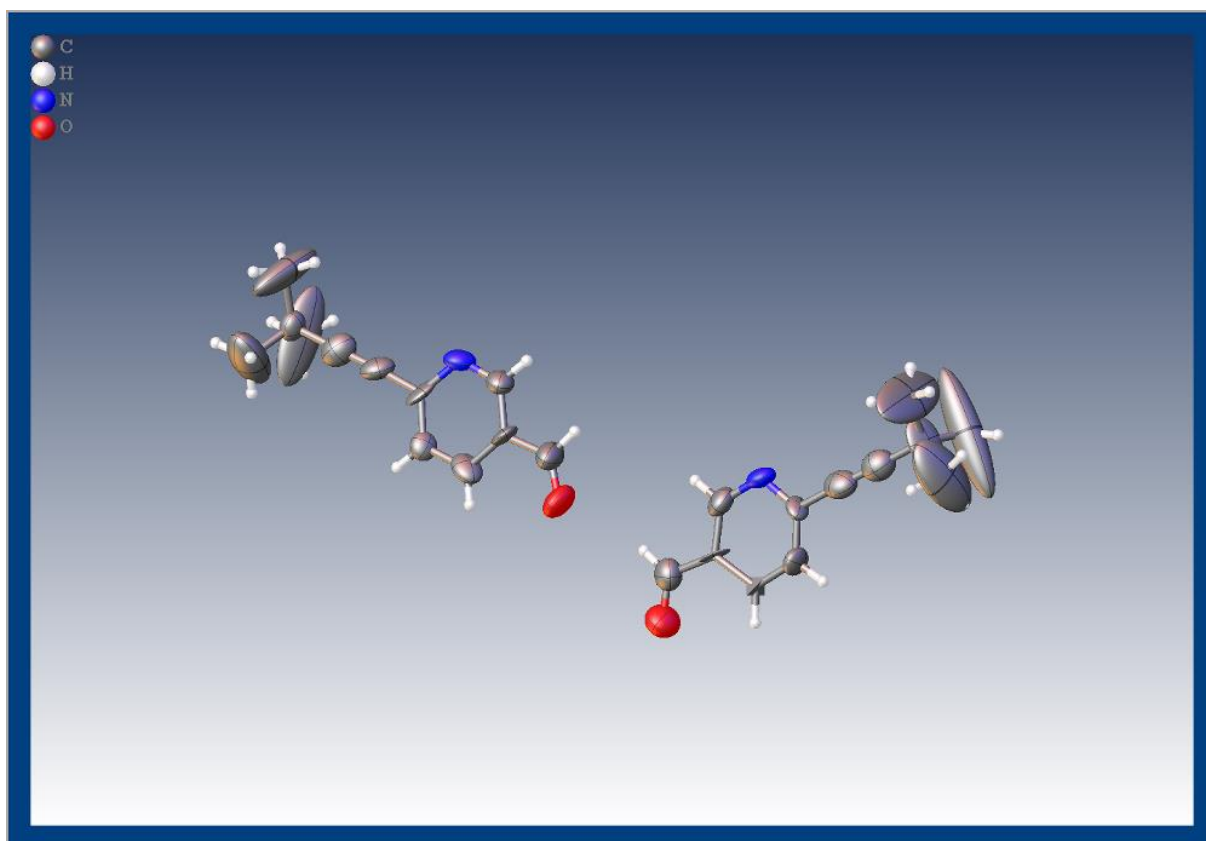


### Single crystal analysis on 5a

Single crystals of  $C_{12}H_{13}NO$  [**5a**] were obtained dissolving 1 mg of **5a** in 1 ml of DCM in a small glass vial, and putting the vial in a crystallization chamber filled with 10 ml of Pentane. The chamber was closed and solvents were allowed to diffuse during 7 days. A suitable crystal was selected and analysed on a 'Bruker D8 Venture' diffractometer. The crystal was kept at 299(2) K during data collection. Using Olex2 [1], the structure was solved with the XT [2] structure solution program using Intrinsic Phasing and refined with the ShelXL [3] refinement package using Least Squares minimisation.

1. Dolomanov, O.V., Bourhis, L.J., Gildea, R.J, Howard, J.A.K. & Puschmann, H. (2009), J. Appl. Cryst. 42, 339-341.
2. Sheldrick, G.M. (2015). Acta Cryst. A71, 3-8.
3. Sheldrick, G.M. (2015). Acta Cryst. C71, 3-8.

Crystal Data for  $C_{12}H_{13}NO$  (M = 187.23 g/mol): orthorhombic, space group Pca21 (no. 29), a = 17.26(2) Å, b = 6.114(8) Å, c = 22.06(3) Å, V = 2328(6) Å<sup>3</sup>, Z = 8, T = 299(2) K,  $\mu(\text{MoK}\alpha) = 0.068 \text{ mm}^{-1}$ , Dcalc = 1.068 g/cm<sup>3</sup>, 8987 reflections measured ( $4.72^\circ \leq 2\theta \leq 37.704^\circ$ ), 1826 unique ( $R_{\text{int}} = 0.0996$ ,  $R_{\text{sigma}} = 0.0762$ ) which were used in all calculations. The final  $R_1$  was 0.0861 ( $I > 2\sigma(I)$ ) and  $wR_2$  was 0.2533 (all data).



Empirical formula	C <sub>12</sub> H <sub>13</sub> NO
Formula weight	187.23
Temperature/K	299(2)
Crystal system	orthorhombic
Space group	Pca2 <sub>1</sub>
a/Å	17.26(2)
b/Å	6.114(8)
c/Å	22.06(3)
α/°	90
β/°	90
γ/°	90
Volume/Å <sup>3</sup>	2328(6)
Z	8
ρ <sub>calc</sub> /g/cm <sup>3</sup>	1.068
μ/mm <sup>-1</sup>	0.068
F(000)	800.0
Crystal size/mm <sup>3</sup>	0.350 × 0.250 × 0.220
Radiation	MoKα (λ = 0.71073)
2θ range for data collection/°	4.72 to 37.704
Index ranges	-15 ≤ h ≤ 15, -5 ≤ k ≤ 5, -20 ≤ l ≤ 19
Reflections collected	8987
Independent reflections	1826 [R <sub>int</sub> = 0.0996, R <sub>sigma</sub> = 0.0762]
Data/restraints/parameters	1826/13/260
Goodness-of-fit on F <sup>2</sup>	1.067
Final R indexes [I ≥ 2σ (I)]	R <sub>1</sub> = 0.0861, wR <sub>2</sub> = 0.2157
Final R indexes [all data]	R <sub>1</sub> = 0.1257, wR <sub>2</sub> = 0.2533
Largest diff. peak/hole / e Å <sup>-3</sup>	0.33/-0.25
Flack parameter	-7(10)

**Table 2 Fractional Atomic Coordinates (×10<sup>4</sup>) and Equivalent Isotropic Displacement Parameters (Å<sup>2</sup>×10<sup>3</sup>) for test\_a. U<sub>eq</sub> is defined as 1/3 of the trace of the orthogonalised U<sub>ij</sub> tensor.**

Atom	x	y	z	U(eq)
C4	-2158 (10)	-9850 (20)	-4249 (6)	35 (4)
N1	-1474 (11)	-6620 (20)	-3897 (7)	59 (4)
O1	-2923 (7)	-12580 (20)	-4675 (7)	104 (4)
C3	-1557 (13)	-11130 (20)	-4021 (8)	62 (5)
C2	-967 (10)	-10090 (40)	-3739 (9)	63 (5)
C1	-944 (10)	-7880 (30)	-3678 (8)	49 (4)

O2	-4448 (6)	-7600 (20)	-4680 (6)	98 (4)
N2	-5910 (11)	-1720 (20)	-5452 (7)	62 (4)
C5	-2065 (11)	-7620 (30)	-4184 (8)	64 (5)
C9	927 (13)	-5090 (50)	-2800 (10)	110 (9)
C18	-4582 (10)	-5700 (40)	-4786 (10)	89 (6)
C17	-5316 (10)	-2640 (30)	-5174 (8)	61 (5)
C16	-5252 (11)	-4860 (30)	-5094 (9)	67 (6)
C8	257 (14)	-6090 (30)	-3125 (10)	79 (6)
C7	-302 (14)	-6890 (30)	-3379 (9)	76 (6)
C14	-6446 (10)	-5300 (30)	-5632 (7)	54 (4)
C19	-7121 (13)	-2070 (30)	-5972 (9)	68 (5)
C13	-6484 (12)	-3080 (30)	-5673 (7)	58 (5)
C15	-5808 (12)	-6220 (30)	-5332 (8)	71 (5)
C20	-7691 (14)	-1290 (30)	-6239 (9)	81 (6)
C6	-2838 (10)	-10630 (40)	-4595 (8)	75 (5)
C21	-8370 (10)	-300 (30)	-6535 (8)	60 (5)
C24	-9016 (16)	-1610 (50)	-6291 (17)	210 (17)
C23	-8250 (20)	-730 (110)	-7173 (12)	310 (30)
C10	1550 (20)	-4790 (130)	-3158 (17)	490 (70)
C22	-8490 (20)	1910 (50)	-6299 (15)	250 (30)
C11	680 (20)	-3260 (60)	-2510 (30)	350 (40)
C12	1190 (20)	-6520 (80)	-2287 (17)	280 (30)

**Table 3 Anisotropic Displacement Parameters ( $\text{\AA}^2 \times 10^3$ ) for test\_a. The Anisotropic displacement factor exponent takes the form:  $-2\pi^2[h^2a^*U_{11}+2hka^*b^*U_{12}+\dots]$ .**

Atom	U <sub>11</sub>	U <sub>22</sub>	U <sub>33</sub>	U <sub>23</sub>	U <sub>13</sub>	U <sub>12</sub>
C4	66 (13)	14 (11)	26 (8)	9 (7)	5 (9)	24 (10)
N1	62 (11)	31 (8)	83 (10)	-2 (8)	-1 (9)	15 (9)
O1	90 (10)	76 (9)	147 (12)	-21 (9)	-26 (10)	-8 (8)
C3	84 (13)	2 (8)	99 (14)	-10 (10)	7 (12)	7 (12)
C2	46 (12)	55 (15)	86 (14)	12 (10)	-25 (12)	12 (10)
C1	37 (13)	43 (14)	66 (11)	-29 (10)	-9 (10)	-8 (11)
O2	73 (8)	75 (9)	147 (12)	-5 (9)	-31 (9)	31 (7)
N2	77 (13)	31 (9)	80 (10)	-10 (8)	-9 (9)	-4 (10)
C5	50 (13)	60 (15)	82 (13)	-9 (10)	-2 (11)	21 (11)
C9	97 (19)	170 (30)	63 (16)	-23 (14)	-45 (17)	-45 (17)
C18	59 (14)	58 (13)	149 (19)	-21 (15)	-25 (14)	7 (12)
C17	56 (13)	42 (13)	86 (14)	-15 (9)	-5 (11)	-2 (11)
C16	48 (13)	27 (12)	125 (17)	9 (11)	0 (12)	22 (11)
C8	83 (16)	73 (14)	80 (15)	1 (12)	5 (14)	9 (13)
C7	84 (17)	59 (13)	86 (15)	-9 (12)	18 (14)	11 (14)
C14	51 (13)	63 (15)	46 (10)	-11 (9)	-11 (10)	0 (10)
C19	88 (16)	38 (11)	77 (13)	-10 (10)	3 (12)	12 (12)
C13	64 (15)	47 (15)	65 (12)	-12 (10)	2 (11)	42 (12)

C15	70 (13)	66 (13)	77 (13)	-39 (11)	4 (11)	-20 (13)
C20	88 (17)	79 (15)	77 (14)	7 (12)	6 (13)	14 (13)
C6	55 (12)	78 (14)	92 (15)	-3 (13)	4 (13)	-1 (12)
C21	48 (11)	66 (12)	65 (14)	10 (9)	-7 (12)	8 (11)
C24	130 (20)	180 (30)	310 (50)	140 (30)	-50 (30)	-70 (20)
C23	160 (30)	700 (100)	70 (20)	-50 (30)	-70 (20)	170 (50)
C10	220 (40)	1120 (180)	130 (30)	-190 (60)	80 (40)	-400 (80)
C22	290 (50)	170 (30)	290 (40)	-120 (30)	-190 (40)	160 (30)
C11	290 (50)	180 (30)	580 (90)	-210 (50)	-320 (60)	40 (30)
C12	250 (40)	380 (60)	210 (30)	100 (40)	-160 (30)	-170 (50)

**Table 4 Bond Lengths for test\_a.**

Atom	Atom	Length/Å	Atom	Atom	Length/Å
C4	C5	1.38 (2)	C9	C8	1.49 (3)
C4	C3	1.40 (2)	C9	C12	1.50 (4)
C4	C6	1.48 (2)	C18	C16	1.44 (2)
N1	C1	1.29 (2)	C17	C16	1.38 (2)
N1	C5	1.35 (2)	C16	C15	1.37 (2)
O1	C6	1.21 (2)	C8	C7	1.22 (3)
C3	C2	1.35 (2)	C14	C13	1.36 (2)
C2	C1	1.36 (2)	C14	C15	1.40 (2)
C1	C7	1.42 (3)	C19	C20	1.24 (3)
O2	C18	1.21 (2)	C19	C13	1.42 (3)
N2	C17	1.32 (2)	C20	C21	1.47 (3)
N2	C13	1.38 (2)	C21	C23	1.45 (3)
C9	C11	1.36 (4)	C21	C22	1.46 (3)
C9	C10	1.35 (3)	C21	C24	1.48 (3)

**Table 5 Bond Angles for test\_a.**

Atom	Atom	Atom	Angle/°	Atom	Atom	Atom	Angle/°
C5	C4	C3	115.6 (17)	C17	C16	C15	119.7 (18)
C5	C4	C6	117.7 (17)	C17	C16	C18	118.6 (19)
C3	C4	C6	126.5 (15)	C15	C16	C18	121.7 (15)
C1	N1	C5	116.2 (14)	C7	C8	C9	178 (2)
C2	C3	C4	117.4 (13)	C8	C7	C1	178 (2)
C3	C2	C1	122.4 (16)	C13	C14	C15	118.1 (17)
N1	C1	C2	122.4 (16)	C20	C19	C13	176.9 (19)
N1	C1	C7	118.2 (18)	C14	C13	N2	122.7 (18)
C2	C1	C7	119.4 (19)	C14	C13	C19	120 (2)
C17	N2	C13	117.9 (14)	N2	C13	C19	117.3 (17)
N1	C5	C4	125.8 (16)	C16	C15	C14	118.8 (17)
C11	C9	C10	114 (4)	C19	C20	C21	177.7 (19)

C11	C9	C8	109(2)	O1	C6	C4	119.2(17)
C10	C9	C8	113(2)	C23	C21	C22	122(3)
C11	C9	C12	102(3)	C23	C21	C24	111(3)
C10	C9	C12	106(4)	C22	C21	C24	105(2)
C8	C9	C12	111(2)	C23	C21	C20	104.0(19)
O2	C18	C16	126.1(16)	C22	C21	C20	109.7(18)
N2	C17	C16	122.8(16)	C24	C21	C20	102.5(16)

**Table 6 Torsion Angles for test\_a.**

A	B	C	D	Angle/°	A	B	C	D	Angle/°
C5	C4	C3	C2	3(2)	N2	C17	C16	C18	179.9(18)
C6	C4	C3	C2	177.1(14)	O2	C18	C16	C17	180(2)
C4	C3	C2	C1	0(3)	O2	C18	C16	C15	-3(3)
C5	N1	C1	C2	1(2)	C15	C14	C13	N2	2(2)
C5	N1	C1	C7	179.0(14)	C15	C14	C13	C19	-179.9(14)
C3	C2	C1	N1	-2(3)	C17	N2	C13	C14	-2(2)
C3	C2	C1	C7	-179.6(17)	C17	N2	C13	C19	-180.0(15)
C1	N1	C5	C4	2(3)	C17	C16	C15	C14	-2(3)
C3	C4	C5	N1	-4(2)	C18	C16	C15	C14	-179.5(15)
C6	C4	C5	N1	-178.4(15)	C13	C14	C15	C16	0(3)
C13	N2	C17	C16	-1(3)	C5	C4	C6	O1	177.9(16)
N2	C17	C16	C15	3(3)	C3	C4	C6	O1	4(2)

**Table 7 Hydrogen Atom Coordinates ( $\text{\AA} \times 10^4$ ) and Isotropic Displacement Parameters ( $\text{\AA}^2 \times 10^3$ ) for test\_a.**

Atom	x	y	z	U(eq)
H3	-1561.5	-12647.56	-4061.14	74
H2	-562.59	-10919.97	-3581.73	75
H5	-2444.15	-6724.28	-4353.42	77
H18	-4216.74	-4684.89	-4655.74	106
H17	-4924.41	-1738.99	-5026.2	74
H14	-6831.54	-6177.9	-5797.17	64
H15	-5761.58	-7734.19	-5294.42	85
H6	-3195.77	-9637.13	-4750.09	90
H24A	-8968.65	-3093.84	-6429.28	315
H24B	-9498.83	-1011.98	-6428.73	315
H24C	-9000.57	-1581.42	-5855.91	315
H23A	-7750.95	-195.92	-7293.17	467
H23B	-8645.4	-14.45	-7405.22	467
H23C	-8275.16	-2282.16	-7243.64	467
H10A	1933.76	-5893.49	-3071.44	736
H10B	1772.18	-3370.38	-3080.61	736



H10C	1402.77	-4885.44	-3575.77	736
H22A	-8919.81	1909.98	-6022.18	372
H22B	-8599.67	2891.63	-6629.05	372
H22C	-8032.41	2393.61	-6091.5	372
H11A	667.31	-2064.63	-2790.12	528
H11B	1037.64	-2922.92	-2186.38	528
H11C	176.79	-3505.64	-2344.91	528
H12A	750.19	-7302.79	-2127.67	423
H12B	1408.2	-5625.48	-1973.4	423
H12C	1567.54	-7536.68	-2430.52	423